THE CITY UNIVERSITY

Department of Civil Engineering

INVESTIGATION OF SHELL AND AXISYMMETRIC SHELL STRUCTURES

- by -

Robert Llewellyn Nelson

B.Sc.(Hons), M.Inst.P., C.Eng., M.I.E.E., M.I.E.R.E.

A thesis submitted to

THE CITY UNIVERSITY

for the degree of Doctor of Philosophy

January 1978

To

Ryan, Dana and

'Muffy'

PREFACE

The author is with the Central Electricity Research Laboratories (C.E.R.L.) Leatherhead, of the Central Electricity Generating Board (C.E.G.B.)

In October 1974 he was registered with The City University to undertake research leading eventually to the Degree of Doctor of Philosophy.

The author's research was carried out during the registration period and has also been reported in the following C.E.G.B. Publications:-

1. Nelson, R.L., VACTIL: a program to analyse the natural frequencies and mode shapes of cooling towers whilst explicitly including the effects of leg supports and foundation elasticity, C.E.G.B. pub. No. RD/L/P 10/76.

2. Nelson, R.L., and Hellewell, J.S.,* Vibration tests on a 1/250th scale model of Didcot cooling tower, C.E.G.B. pub. No. RD/L/N 112/76.

   (The first author was a supervisor to the second author who was a pre-university vacation trainee. The first author was a co-worker during the project; also he commissioned the apparatus, planned the experiment and wrote the paper.)

3. Nelson, R.Ll., Stress matrix for a doubly curved shell finite element, C.E.G.B. pub. No. RD/L/N 113/76

4. Nelson, R.Ll., A new algorithm to program the element matrices of doubly curved shell finite elements, C.E.G.B. pub. No. RD/L/N 139/77

5. Nelson, R.Ll., Free vibration analysis of cooling towers with leg-supports by a finite element method, C.E.G.B. pub. No. RD/L/R 1935

6. Nelson, R.Ll., Proposals for improved doubly curved shell finite elements, C.E.G.B. pub. No. RD/L/N 140/77

7. Nelson, R.Ll., RESAP: a program to calculate the resonant stresses, frequencies and mode shapes of axisymmetric structures, C.E.G.B. pub. No. RD/L/P 9/77.

8. Nelson, R.Ll., VACTILo2: a program to calculate the frequencies, mode shapes and stresses of shell structures, C.E.G.B. pub. No. RD/L/P /77.

9. Nelson, R.Ll., Calculation of stresses mode shapes and frequencies of shell structures using doubly-curved finite elements, C.E.G.B. pub. No. RD/L/N 187/77.

No part of this thesis, in whole or in part, has been submitted elsewhere for the award of a higher degree or qualification. Unless otherwise stated the work is the candidate's own.

CONTENTS

LIST OF FIGURES

LIST OF TABLES

ACKNOWLEDGEMENTS

I am grateful to Professor J.E. Gibson for accepting me as a research student, for supervising my research and for advising me during the last three years.

I am indebted to my empolyers the C.E.G.B. for allowing the research work conducted by me at their research laboratories at Leatherhead (C.E.R.L.) to be published as a thesis and for allowing me the typing and other facilities at C.E.R.L.. I am very grateful to Mr P.E. Winney for his continual support and encouragement throughout and for discussions on the experimental aspects of cooling tower work. I am also grateful to Dr D.L. Thomas for very useful theoretical discussions and for the useful ideas that consequently ensued.

For typing, I am especially grateful to the excellent and patient skills of the C.E.R.L. typing pool.

DECLARATION

I grant powers of discretion to the Librarian of The City University to allow the thesis to be copied in whole or in part without further reference to me. This permission covers only single copies made for study purposes, subject to normal conditions of acknowledgement.

R.Ll. Nelson

ABSTRACT

The primary objective of the research reported in this thesis was to develop a theoretical method capable of accurately analysing cooling towers with leg-supports. A finite element method was derived and using the technique theoretical results were obtained for a 1/250th scale model and the corresponding full-scale structure. An experimental investigation was also conducted on the model tower. The theoretical results obtained for the model and full-scale towers are compared with the experimental results obtained for both structures. It is shown that the finite element method derived yields the most accurate prediction to date, as far as the author is aware, of the free vibrational behaviour of cooling towers with leg supports.

The experimental investigation of a model cooling tower was conducted using a multi-point excitation system. An innovatory use was made of a helium-neon laser as a displacement transducer. This device is deemed to give excellent results provided a few simple precautions are taken. The experimental data obtained clearly show the important vibratory modes of the model cooling tower. Due to another worker the experimental data for the corresponding full-scale tower were also available. This experimental information serves as a foundation for confirming the validity of the theoretical technique.

A novel algorithm used to compute the stiffness and mass matrices of doubly curved shell finite elements has been derived and described in detail in this thesis. The algorithm lends itself readily to a structured modular programming approach and hence this technique with its attendant ease of program modification has been adopted. The theoretical flexibility of the algorithm is also high.

Thus, different finite elements stiffness and mass matrices can be conveniently formed with minimal changes to the computer code. The algorithm should find wide use in forming the element matrices of finite elements.

A new form of constraints is utilized by the finite element method reported herewith. These constraints can be employed for rotationally periodic structures and are invaluable in allowing the analysis of large complex structures (such as cooling towers with leg-supports) within the size restrictions imposed by the computing system.

Sophisticated doubly curved shell and axisymmetric finite elements have been employed in the work reported herein. Detailed improvements and modifications to the elements have been discussed. Stress matrices are derived for use with these elements. Stress analysis of several structures have been conducted using these elements and the results are shown to be in good agreement with published information.

NOTATION

The standard symbols used in the text are given below. Some duplication is unavoidable; however, the correct meaning of the symbol will then be made clear in the text. Any symbol not defined, particularly matrices, are defined in the text. Unless otherwise stated the symbols have the following meaning:-

A,B	Lamé parameters (in this text A = 1 and B = R)
E	Young's Modulus
G	Shear Modulus = $E/2(1+\rho)$
L	Length of the meridian of an element
M_α	Couple acting in the plane through the meridian and normal to middle-surface
M_β	Couple acting in the plane through the circumferential line and normal to the middle-surface
$M_{\alpha\beta}$	Twisting moment. Couples act in opposite senses in the plane along the meridian and normal to the middle-surface
M	Mass density
N_α	Direct stress in meridional direction
N_β	Direct stress in circumferential direction
$N_{\alpha\beta}$	Shear stress in the circumferential direction
N	Number of similar substructures constituting the whole periodic structure - i.e. number of representative substructures
R	Radius of revolution (shortest distance from axis-of-revolution to middle surface of shell wall - i.e. radius of a parallel circle)
S	Foundation elasticity in the vertical direction
Z	Distance along the axis-of-revolution
CQ	Angle subtended by the meridional edges of a substructure at the axis of symmetry

a,b,c, and d are suffices associated with the Hermite interpolation polynomials - see text

$e(\alpha,\beta,\gamma)$ Strain at any point (α,β,γ)

f Hermite interpolation polynomials in $\bar{s}$

g Hermite interpolation polynomials in $\bar{\theta}$

h Thickness of shell wall

$\bar{h}$ $= \frac{h^3}{12}$

m Number of meridional nodes, i.e. nodes along a meridian (nodal circles)

n Number of circumferential wave-lengths, also termed harmonic or circumferential wave number

p $= -\left(\frac{1}{r} - \frac{\sin\phi}{R}\right)$

$\bar{p}$ $= \left(\frac{1}{r} + \frac{\sin\phi}{R}\right)$

r Radius of curvature of meridian

$\underline{r}$ Position vector

s Distance along a meridian (in the text it is synonymous with α.)

$\bar{s}$ $= \frac{s}{L}$

u Displacement along the meridian (downwards)

v Displacement along the circumference (anti-clockwise)

w Displacement normal to the shell (outwards)

x,y,z Cartesian coordinates

α,β,γ Tri-orthogonal set of "right-hand" curvilinear coordinates

- α - direction along meridian of shell structure (in a downward direction)
- β - direction along circumference of shell structure
- γ - direction through thickness of shell structure (radially outwards)

$\delta(\alpha,\beta)$ Displacement at any point on the middle surface ($\gamma = 0$)

δ^e Displacements at the nodes

ε,χ Strain components at middle surface

ε_α - extension in the α-coordinate direction
ε_β - extension in the β-coordinate direction
$\varepsilon_{\alpha\beta}$ - shear strain in the $\alpha\beta$ plane
χ_α - change of curvature in α-coordinate direction
χ_β - change of curvature in β-coordinate direction
$\chi_{\alpha\beta}$ - twist in $\alpha\beta$ plane

θ Angle subtended by the arc of a parallel circle

(in this text θ is synonymous with β)

$\bar{\theta}$ $= \theta/\psi$

θ_o $= R \times \theta$

κ_1,κ_2 Principal curvatures ($\kappa_1 = \frac{1}{r}$ and $\kappa_2 = \frac{\sin\phi}{R}$)

ν $= \frac{(1 - \rho)}{2}$

ξ $= \frac{r}{h}$

ρ Poisson's Ratio

σ_α Stress component along meridian

σ_β Stress component along circumference

$\sigma_{\alpha\beta}$ Shear stress component

ϕ Angle the normal to the shell wall makes with the Z-axis

(axis of revolution)

χ (see ε)

Ψ Angle subtended by the parallel meridional edges of the

finite element at the Z-axis

CHAPTER ONE

INTRODUCTION

1. INTRODUCTION

The primary purpose for the research reported in this thesis was the urgent requirement for a theoretical technique to accurately analyse the dynamic behaviour of cooling towers. The accurate analysis of a cooling tower idealized as a shell of revolution (i.e. when discrete column or leg-supports are not included in the model of the structure - the base of the tower is then an extension of the shell surface) is not particularly difficult and can be undertaken by conventional techniques. For example, the resonant frequencies and mode shapes of a hyperboloidal cooling tower shell can be analysed by solving the differential equations of motion [1]. However, if the effects of leg-supports are to be included accurately in the analysis, conventional techniques cannot be employed satisfactorily. The cooling tower can no longer be regarded as an idealized axisymmetric structure. Methods involving this assumption usually result in unacceptable errors (as will be domonstrated later in the text). It could be stated that the accurate analysis of a cooling tower with leg-supports appears at first sight to be analogous to the satisfactory solution of a structural problem involving a mathematical discontinuity.

It is believed that the theoretical method derived in this thesis succeeds in accurately analysing the dynamic behaviour of cooling towers with leg-supports. The method is based on the finite element method. An excellent introduction to the subject is given by Rockey et al. [2]. The book by Desai and Abel [3] is also of note. A classical work on the subject is due to Zienkiewicz [4]. The finite element method is an approximate numerical technique which can be used to solve a wide range of problems of a relatively complex nature. It has gained wide-spread popularity over the past twenty years with the advent of high speed digital computers. However, an investigation into the behaviour of a very large or complex structural system using the

finite element method can often lead to the problem of the mathematical model having too many degrees-of-freedom (d.o.f.) to be handled completely by even modern digital computers. An alternative to simplifying the mathematical model - which would lead to unsatisfactory approximations in the results - is to divide the structure into a system of connected components or substructures. The behaviour of a substructure can then be studied if certain constraints are imposed on the structure such that the substructure behaves exactly as if it were a part of the whole structure. For rotationally periodic structures such constraints can be imposed; they are new to finite element analysis and will be discussed in Chapter 3. These constraints will be referred to as 'Complex Constraints' to distinguish them from the usual type of constraints encountered in finite element analysis. The analysis of a representative substructure using complex constraints can be regarded as analogous to the study of a representative section of a symmetrical structure where symmetry-boundary conditions are invoked so that the representative section is mathematically equivalent to the whole structure.

The substructuring approach has been used with the finite element technique to derive a method of analysing cooling towers with leg-supports. A large computer program entitled VACTIL has been written by the author [5] to generate the solution. The method yields the most accurate theoretical prediction to date, as far as the author is aware, of the free vibrational behaviour of cooling towers. (The program, VACTIL, is at present being used by the Design Department of the C.E.G.B.). Confidence in the results permits the prediction of the effects of other parameters such as Poisson's Ratio, foundation elasticity, etc., on the vibrational characteristics of cooling towers.

The experimental work reported in this thesis is for a 1/250th scale model cooling tower and was investigated by the author using a Manual/Automatic Multipoint Apparatus. The results obtained were of sufficient accuracy to allow a adequate description of the modes of vibration of the tower to be made. The accuracy of the results were due partly to the employment of a innovatory displacement measuring device based on a 5 mW helium-neon laser. The use of the laser to measure displacements proved to be highly satisfactory provided a few simple precautions were observed. The measurements were more speedily and accurately obtained, when compared with the use of other devices such as capacitance transducers.

In the work reported in this thesis doubly curved* shell finite elements (four-noded element which is a part of a shell of revolution bounded between a pair of parallel circles and a pair of parallel meridia - see Fig. 4.2) and axisymmetric (ring) elements were used to analyse cooling towers and other structures. The doubly curved shell finite elements used and discussed in this thesis are basically similar to that derived by Woodman and Severn [6] from proposals for plate and axisymmetric elements made by Schmit, Bogner and Fox [7]. The doubly curved elements referred to in this text employ complicated displacement functions. These elements are capable of high accuracy. Due to the comparatively large number of nodal degrees of freedom used the elements are sensitive to geometrical 'imperfections' in the structure. These imperfections can be intentional, or unintentional, as for example due

---

*That is curvature in two independent orthogonal directions as for example the surface of a hyperboloid. In this context a cylinder can be regarded as a doubly curved shell of revolution where the radius of the meridional curvature is considered to be infinite.

to small errors in the calculated geometrical properties. Hence, care must be exercised in the calculation of geometrical properties (see Chapter 6). A quadratic variation of strains across the thickness of the elements have been assumed in their derivation. This is thought to give a more accurate estimate of the bending stiffness than if linear variations of strains are assumed.

Finite element stress-displacement matrices are derived in Chapter 4 for use with these elements. The stresses predicted are shown to agree well with published literature in Chapter 11.

A novel algorithm to numerically evaluate the stiffness and mass matrices of the doubly curved finite elements was derived with the following goals:

(i) Error checking and program modification would be simple and also that a high degree of confidence could be placed in the resulting coding.

(ii) Allow the basic algorithm to be used, with as few changes as possible, for evaluating the element matrices of several different doubly curved finite elements.

It is believed these goals have been met. The derivation of the algorithm is presented in Chapter 5. The algorithm readily lends itself to a structured modular programming approach. The ease of modification of this algorithm gives the technique real flexibility. For example, it is simple to change the numerical scheme so that the elasticity matrix of say Novozhilov [8] is used in the calculation of the element matrices instead of Vlasov's [4]. Using a conventional programming approach such alterations would require considerable effort with an attendant risk of introducing mathematical or programming errors in the coding. These remarks apply equally well to changing the displacement functions used in the element matrices.

This chapter has attempted to introduce the reader to the scope of this thesis and underline the salient features of the work that is to be described in detail in the following chapter. The chapter that follows immediately presents the background to the present investigation and discusses previous attempts to analyse the static and dynamic behaviour of cooling towers. It will be seen that the theoretical predictions have not agreed very satisfactorily with experimental evidence. A significant part of the thesis will then be concerned with the description of a method that enables accurate analyses of cooling towers. The experimental investigation of a model cooling tower will be described and good correlation obtained between the experimental results and the values predicted by the theoretical method. Experimental results available for the corresponding full-scale structure will also be used in the correlative study. Difficulties encountered in the research programme will be described. Improvements and modifications to the finite elements used in this work will be discussed. The derivation of the stress-displacement matrix for use with the shell finite elements will be detailed. The stress analysis of several shell and axisymmetric shell structures will be presented and the results will be shown to be in good agreement with published data.

CHAPTER TWO

COOLING TOWERS - PREVIOUS WORK

2. COOLING TOWERS - PREVIOUS WORK

In this chapter some of the theoretical and experimental investigations of previous workers will be discussed. It is shown that the dynamic analyses of cooling towers with leg-supports have not yielded accurate results. Experimental results obtained for full-scale cooling towers and their corresponding models are also discussed and are shown to be in poor agreement.

2.1 Static Wind Loading

Martin and Scriven [10] were among the first investigators to analyse the membrane stresses of hyperboloidal cooling towers subjected to a constant wind pressure. Later Martin, Maddock and Scriven [11] calculated the displacements of the structure. Kalnins [12] presented a numerical technique which combined the advantages of direct integration and the finite difference method for the analysis of shells of revolution subjected to symmetrical and non-symmetrical loads. Albasiny and Martin [13] claimed that their analysis - a combination of the finite difference method and a technique of separation of variables - of a cooling tower under static load conditions yielded results that agreed well with those obtained by the complete bending theory, and also with measured loads on model towers in wind tunnel tests. It must be noted that the towers analysed were of uniform thickness with no leg-supports. Tottenham [14] also analysed the stresses in a hyperboloidal cooling tower of uniform thickness and with no leg-supports using a matrix progression method. He concluded that the forces predicted by simple membrane theory were very close to that calculated by complete bending analysis. These investigations show therefore that satisfactory stress analyses of hyperboloids can be performed using simple membrane theory. However, for actual cooling towers, where the thickness is not uniform and the structure is supported on leg-supports, this approach leads to

unsatisfactory approximations. The method of Gould and Seng-Lip [15] is noteworthy as they included leg-supports in their analysis. They concluded that hyperboloidal shells with leg-supports must have sufficient reinforcement at the shell/support boundary as the concentrated stresses which are generated by the discrete supports are not adequately resisted by the membrane action in the shell. They concluded that thickening of the shell near the base was necessary. Abu-Sitta [16] attempted to study the effects of the stress interaction at the shell/support boundary by imposing several different types of boundary conditions at the base of the tower. He treated the effect of leg-supports using two different methods. However, firm conclusions cannot be made from a study of his results.

The methods of analysis referred to above, which are based essentially on the differential equations of equilibrium, are representative of the work of many investigators. Most of these methods are severely restricted with respect to accurately representing the geometry and material properties of the shells (and hence of cooling towers). The theory developed by Kalnins [12] is probably among the better of these methods.

Graffin and Strome [18] were among the first workers to use finite elements to solve the problem of static wind loading. Following this work Percy, Pian and Klein and Navaratna [19] derived an axisymmetric (ring) finite element. The shape of the finite element used was that of a frustum of a cone. A computer program SABOR III was used to generate the solution. (The C.E.G.B. computer program BACTo2 [20] is essentially of the same form as SABOR III.) Later the Ferrybridge 'C' cooling tower under steady wind loading were analysed by Will and Coffin [21] using conical and circular cylindrical shell elements. The wind loadings were allowed to vary in both the circumferential and

meridional directions. (The wind loads were based on experimental results of wind tunnel tests on model cooling towers.) Both the analyses referred to above necessitate approximating the cooling tower geometry, as elements that have no meridional curvature are employed. Thus it is probable that 'physical singularities' which are not present in the actual structure are introduced at the element boundaries by the finite element analyses. Hence, it would not be unexpected if errors are introduced into the calculated (static) stresses. This hypothesis appears to be supported by results from the computer program BACTo2 [20]. It was observed by Pope [21] that in order to get the direct force along the meridional axis reasonably accurately a large number of conical-frusta elements are required. Another important observation regarding the two finite element methods referred to above is that axisymmetric elements are used. This leads to unavoidable assumptions when analysing non-axisymmetric structures such as cooling towers with leg-supports. In the program BACTo2 an effort has been made to model the leg-supports. However, due to the axisymmetric nature of the analysis all the leg-supports are modelled as an 'equivalent' conical frusta. One of the main difficulties created when a cooling tower is approximated by an 'equivalent' axisymmetric structure is that the errors introduced by this assumption are of an unquantifiable nature. We shall see in the following section that this is one of the assumptions that tend to colour the results obtained from theoretical analyses of vibrating cooling towers.

2.2 Dynamic Behaviour of Cooling Towers

Until 1965, a considerable degree of effort had been expended in analysing the problems of static wind loading on cooling towers. From experiments conducted by Bailey and Fidler [22] (also see Reference 23) on hyperboloidal shells it appeared that cooling towers

were reasonably safe against buckling instabilities under wind loading produced by wind speeds of below 200 miles per hour. Relatively little attention, however, was given to the solution of the dynamic response of cooling towers and the possible contribution of wind-induced vibrations to the instability of cooling towers tended to be regarded as of secondary importance.

In November 1965 gale force winds caused the collapse of three newly constructed cooling towers at Ferrybridge 'C' Power Station. Observers who were present at the collapse of one of these towers reported that there was a general ovalling and rippling below the throat followed by large movements over an area whose diameter was about half that of the tower. A few seconds later the tower collapsed. The large amplitude vibrations referred to had periods of several seconds. The report of the Committee of Inquiry of the C.E.G.B. [24] into the collapse of the towers emphasized the need for a more relaistic appraisal of wind loading, and a better representation of the fluctuating component in the structural analysis. Armitt [25] conducted an extensive experimental investigation to determine the mechanics of the collapse of the Ferrybridge towers. He observed the behaviour of model towers in a wind tunnel and reported that resonant stresses were partly responsible for the collapse. He concluded that resonant stresses could be a serious problem associated with some tower designs and that the single most important parameter appeared to be the lowest resonant frequency.

Several attempts, both experimental and theoretical have been made to determine the free vibration characteristics of cooling towers, especially since the C.E.G.B. report [24] was published. The first stage of such investigations is usually the determination of the lowest natural frequencies and coresponding mode shapes of the

towers. Unfortunately, it will be seen in this review that the natural frequencies of full-scale cooling towers have not been accurately predicted. Hence predicted mode shapes and stresses, which are more difficult to calculate, must be suspect.

Except in the case of relatively simple geometries such as cylinders, conical and spherical shapes, etc., comparatively little effort has been expended in analysing vibrating shells of revolution. Kalnins [17] has described a method of solution for obtaining the eigenvalues and eigenvectors of general shells of revolution. His method is based on the classical linear bending theory of shells derived by Reissner [26]. The method is analogous to the Myklestad-Prohl [27,28] method for beams and is therefore a trial and error method. A prior knowledge of the approximate frequency of the required solution is necessary for economical application of the method. For each trial frequency a determinant is evaluated. When the determinant changes sign an interpolated value of the natural frequency is obtained and considered to be the solution.

The resonant frequency of axisymmetric structures can be obtained using the method of Percy et al. [19] and Webster [29]. Webster's method using a ring finite element appears to be reasonably efficient whereas the method of Percy et al. suffers from using coincal elements, and thus a large number of elements are required to obtain an accurate solution for structures that have meridional curvature.

Hashish [30] analysed the free vibration of hyperboloidal cooling tower using a modified finite difference method and compared the results with measured values. The theoretical values were observed to be significantly lower than the experimental values.

Neal [31] experimentally and theoretically determined the lowest two natural frequencies for a hyperboloidal shell supported by four pairs of inclined columns. The second lowest frequency, predicted by both techniques, agreed to within about 18%. The lowest frequency agreed to within about 1.5%. He experimentally determined the resonant frequencies of the same shell but supported by fourty pairs of support columns. (In full-scale cooling towers, the usual practice is to employ a large number of pairs of leg-supports; fourty is a typical number.) However, he did not then theoretically analyse the structure. No firm conclusions can be made from the results of Neal's investigation.

Woodman and Severn [6] used a doubly curved shell finite to analyse an idealized (i.e. constant thickness was assumed and no attempt was made to model the leg-supports) model of the Ferrybridge 'C' cooling tower. Note that as a shell finite element was used, no prior assumption was made that the structure was axisymmetric. This was a noteworthy departure from the usual practice of using axisymmetric elements. The theoretical results were compared to the experimental results of Williams [33,34]. Unfortunately very poor agreement was obtained. This may have been due in part to insufficient core-storage of the computer not allowing the use of a sufficient number of elements for satisfactory convergence.

It is now interesting to compare some experimental and theoretical results for an idealized cooling tower model. Williams [33] carried out frequency response tests on a 1/576th scale nickel model of Ferrybridge cooling tower. The model had no legs and was of uniform thickness. In Fig. 2.1 theoretical and experimental results are superimposed on those obtained by Williams [33]. These are (a) Kalnin's solution [17] for variable thickness using the program SHEL [35],

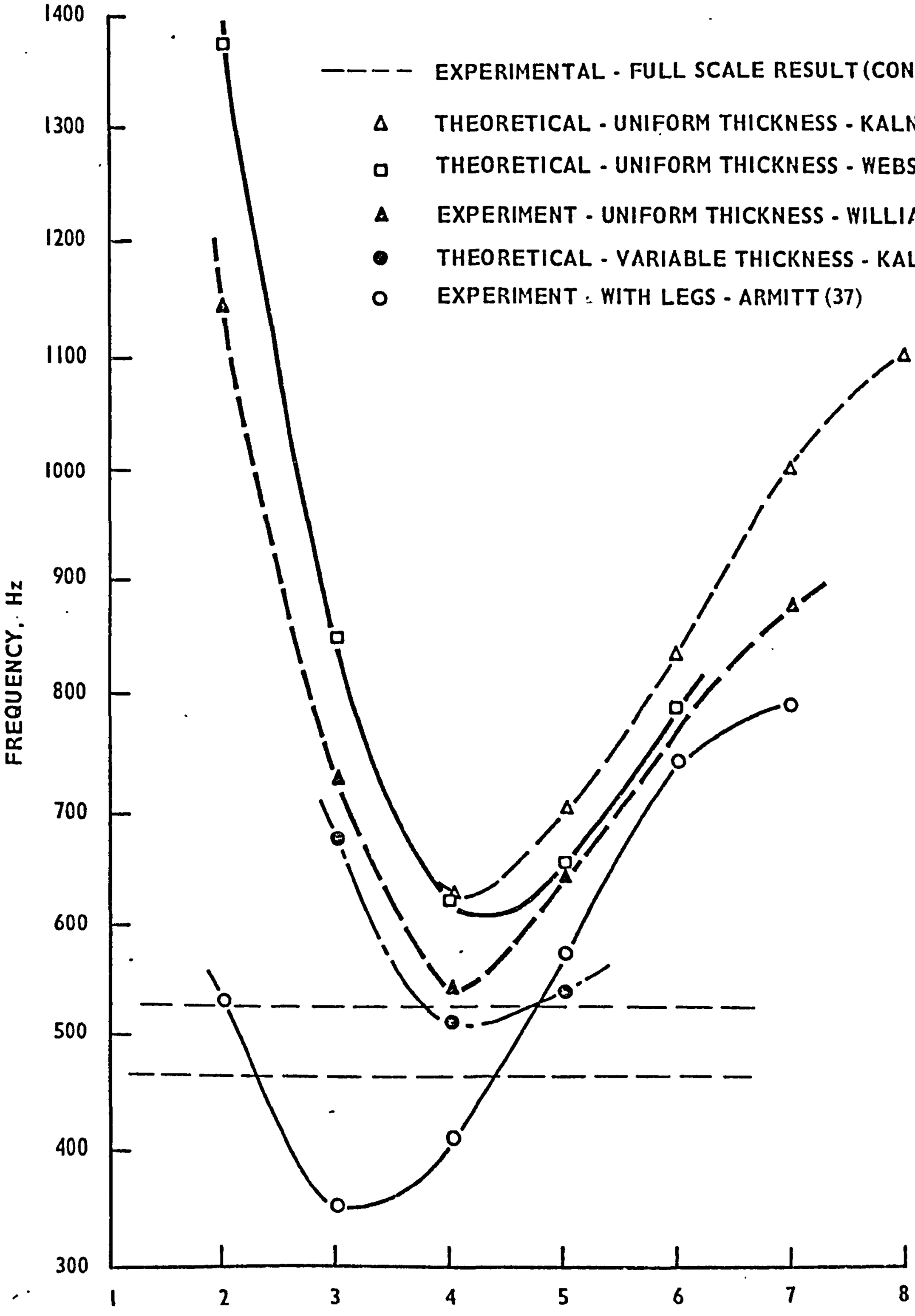

FIG.2.1 COMPARISON OF NATURAL FREQUENCIES OF FERRYBRIDGE 'C' COOLING TOWER MODEL ($^1/_{576}$TH NICKEL MODEL)

(b) Webster's solution for uniform thickness [29] using the program NOTTo2 [36], (c) Armitt's experimental results [37] for a model where the leg-supports and variable thickness were modelled accurately. (The two lowest resonant frequencies of the full-scale tower were also measured during a perfunctory experimental investigation. The frequencies were converted to the model values using the formula given in Section 8.3 and are depicted in the figure as two 'dashed' lines as the m and n values were not measured.) It is seen that generally indifferent agreement is obtained between the experimental and theoretical results. For the relatively simple case with constant thickness and no legs, the error at the lowest frequency (which for a cooling tower is arguably one of the most important parameters from a design viewpoint) is about 10%.

For the more complex situation, therefore, when leg-supports are included in the analyses, the predicted values are probably of little relevance. This is emphasized in Fig. 2.1 where the frequency measured by Armitt [37] is significantly lower than the experimental result for the idealized tower and the theoretically predicted values.

In order to establish conclusively that the poor correlation obtained for the Ferrybridge tower is representative of theoretical predictions for other tower designs, the results for several other model cooling towers are given in table 2.1. The models were made from 'Devcon' (see Chapter 7) and were 1/250th scale size. All the models had leg-supports. The computer programs SHEL [35] and NOTTo2 [36] were used to generate the solution. The numbers in parentheses given in the table are the number of circumferential wavelengths (n).

Table 2.1: Experimentally Measured and Theoretically Calculated Resonant Frequencies of Model Cooling Towers with Leg Supports

Model Cooling Tower	Natural Frequency (Hz)		
	Theoretical		Experiment [37]
	Kalnins [17]	Webster [36]	
Thorpe Marsh	185.3(3) 112.3(4) 180.2(5)	182.9(3) 151.2(4) 157.7(5)	93(3) 102(4) 125(4)
Drakelow 'C'	Not calculated	220.0(2) 140.5(3) - 106.7(4) 131.0(5)	53(2) 64(3) 72(-) 79(4) 118(5)
Hams Hall 'C'	Not calculated	140.1(3) 101.8(4) 129.6(5)	79(3) 103.5(4) 150.0(-)
Skelton Grange 'B'	Not calculated	224(2) 141.5(3) 143.4(4)	56(2) 66.5(3)
Ferrybridge 'C'	94.5(3) 71.0(4) 74.4(5)	117.8(3) 85.9(4) 93(5)	49(3) 57(4) 80(5)

The numbers in parentheses indicate the values of n: a dash means the value of n is uncertain.

Table 2.2: Comparison of Frequencies for 1/250th Scale Model and Full-Scale Cooling Tower at West Burton

Model Frequency (Hz)		Full Scale Frequency (Hz)
Measured	Extrapolation	Measured
66	0.61	0.41
78	0.72	0.61
103	0.95	0.81
112	1.96	-
128	1.19	0.96
143	1.33	1.06
160	1.48	1.20
180	1.67	1.42
213	1.98	1.58

Burrough, Jeary and Winney [39] were among the first workers to instrument a full-scale model in order to measure the structural resonances. They recorded the output of a number of accelerometers placed at strategic positions on the tower surface; power spectral densities were then obtained and an estimate of the probable and possible resonant frequencies were made. These frequencies are given in column 3 of table 2.2. The results for the corresponding 1/250th-scale model were obtained using the same technique and are presented in column one of table 2.2. In column two of the table the model frequencies have been extrapolated to the full-scale structure by means of equation 8.1 (see Chapter 8). There are difficulties in comparing the values given in columns two and three as the model shapes were not available for both the model and full-scale. Also (it could be argued) that there is some uncertainty in the material values assumed for the equation. It is interesting to note that when the tower was idealized as a uniform shell and the programs SHEL and NOTTo2 were used to calculate the lowest natural frequency, values of 145.8 Hz and 150.6 Hz, respectively, were obtained. (This compares to the lowest frequencies given in table 2.2 which are .66 Hz and .41 Hz. The latter figure when converted to an equivalent model frequency is 44 Hz.) The difficulties referred to above serve to illustrate the problems that are inherent in comparing the results obtained for model and full-scale structures.

In Section 2.1 it was seen that for the static analyses of cooling towers the theoretical proposals of Gould and Seng-Lip [15] and Abu-Sitta [16] are noteworthy as a rational attempt was made to incorporate the effects of leg-supports. Similarly, for dynamic analyses the finite element methods due to Deb Nath [40] and Young, Sun, Lo, Kayser and Bogdanoff [41] are of interest. In Reference 40 a doubly curved shell finite element was used in the dynamic analysis

and the effects of leg-supports were included by omitting parts of the shell at the base. The cooling tower chosen by Deb Nath for his calculations was the full-scale tower at Didcot (which is the same as that investigated herein - see Chapter 9). His values for the natural frequencies are at variance with the experimental values obtained by Winney [42,43] for the actual full-scale tower. In Reference 41 the resonant frequencies of the 'Paradise cooling tower' (U.S.A.) were calculated. Two types of finite elements were used: a three-dimensional beam finite element and an orthotrophic quadrilateral flat plate finite element orientated arbitrarily in three dimensional space. The former type were used to represent the leg-supports and the latter were used to model the hyperboloidal shell of revolution. The resonant frequencies calculated by this method have not been validated as experimental results were not available for a correlative study. However, it should be noted that the central processor unit (c.p.u.) time required by the 'CDC 6500' digital computer (used for the analysis) was 2124 seconds. The long c.p.u. time required is attributable to two reasons: (i) A flat plate was used to represent a doubly curved structure. Hence convergence of the element would be expected to be poor. (ii) As the whole tower, including leg-supports, was analysed, a large number of degrees of freedom would have been required.

2.3 Closure

A survey of previous analyses of cooling towers has been attempted. It has been observed that in general, poor correlation between experimental and theoretical results has been achieved. Two aspects of the theoretical analyses in general (that introduce unquantifiable errors) have been noted: i.e. (a) attempts have been made to model the cooling towers as idealized axisymmetric structures and (b) the discrete nature of the leg-supports at the base of the tower has not been modelled accurately.

Some of the problems encountered when comparing results for model and full-scale cooling towers have been discussed. The survey will serve as a background to the work discussed in this thesis.

CHAPTER THREE

SUBSTRUCTURING AND ROTATIONALLY PERIODIC STRUCTURES

3. SUBSTRUCTURING AND ROTATIONALLY PERIODIC STRUCTURES

This chapter reviews some of the work that has been reported regarding substructuring, periodic structures and periodic structures forming a closed ring. It is shown that a cooling tower can be regarded as a closed ring of identical periodic substructures and explains the basis for analysing the free undamped vibration of rotationally periodic structures by applying 'complex constraints' to the boundaries of only one representative substructure.

3.1 Substructures and the Displacement Mode in Periodic System

Przemieniecki [44] has presented a basis for analysing the static behaviour of structures using substructuring. Hurty [45] employed the technique for dynamic analysis. Summaries of some of the variations of Hurty's method are given by Hou [46] and in Reference 47. The substructuring method pre-supposes that the free vibrational behaviour of a large structural system can be determined by a knowledge of the component substructure. That is, the mode shapes of the complete structure are assumed to be a linear combination of the individual substructures. The substructuring method as applied by Holze and Boresi [48] can be applied to large or complex problems because only a subset of the structure mode shapes associated with the lowest frequencies are used to synthesize the system mode shapes. Note that the method described by Holze and Boresi [48] can be used for analysing systems that are composed of non-identical sub-structures, or alternatively identical substructures.

We shall now confine our discussion to systems consisting of identical substructures that are linked at identical junctions. A structural system with a regularly repeating section - a representative substructure - is referred to as periodic. When analysing a periodic system it is of obvious advantage both from a theoretical and computational

view-point to be able to use the repetitive nature of the structure to simplify the calculation.

The vibrational behaviour of periodic systems can be studied by considering the displacement mode as a wave propagating in the system [49]. The mathematics of wave propagation in periodic structures is well based in the literature. For example Brillouin [50] considers the problems that occur in solid state physics, electrical engineering and electronics. Mead and Sen Gupta [51] have applied wave propagation techniques to the study of the free and forced vibration of periodic skin-rib structures. Mead [52,53] has studied wave propagation and natural modes in mono- and multi-coupled systems with and without damping. The flexural motion of waves in beams and plates have been investigated by Heckl [54] and Cremer and Leilch [55]. In the papers referred to, exact harmonic solutions have been found for the equations of motion of the periodic system. The comparatively recent papers by Mead [56] and Abrahamson [57] are noteworthy because they underline the use of approximate numerical techniques such as the finite element method, to wave propagation in periodic systems. Orris and Petyt [49] analyse the vibrational behaviour of a periodic system by considering the displacement mode as a wave propagating in the system, and then by studying the wave's 'propagation constant'. They use the finite element technique to evaluate the 'phase constant' of the system. They show that when a system is vibrating in one of its free waves, there is a constant ratio between the amplitude of the motion in one substructure and that at the corresponding point in the adjacent substructure. The ratio of these amplitudes is equal to exp (μ), where μ is the complex propagation constant of the wave. For a purely imaginary μ, the corresponding vibration frequencies can be found by imposing constraints on the finite element equations of motion of a

single substructure. The constraints are of the form $[U_L] = [U_R] \exp(+\mu)$. $[U_L]$ and $[U_R]$ are the displacement vectors on the left- and right-hand boundaries, respectively. The resulting Hermitian eigenvalue problem can now be solved to obtain the resonant angular frequencies, ω, corresponding to μ; μ can have any purely imaginary value between $-i\pi$ and $+i\pi$.

3.2 Rotationally Periodic Structures

We shall now restrict our discussion of periodic structures to consider only those systems that form a closed ring. Rotational periodicity can also be termed rotational symmetry or cyclic symmetry. (A comprehensive treatment of symmetry is given by Weyl [58].) In this text a rotationally periodic structure will be regarded as follows:- a structure made up of identical segments and symmetrically arranged about an axis-of-revolution. Thus, if the geometry of the structure is defined for any radial or axial position at some angle θ, it will be identical at an angle $(\theta + n \times \frac{2\pi}{N})$ where both n and N are integers. N is structure dependent (e.g. the number of identical substructures that constitute the rotationally periodic structure). n is any integer less than N. Note that an axisymmetric structure can be regarded as a rotationally periodic structure where the periodicity tends to infinity; i.e. $N \to \infty$.

MacNeal, Harder and Mason [59] have developed a method of simplifying the analysis of rotationally periodic structures and have incorporated the technique in the finite element computer program NASTRAN which can be used for static stress analysis, steady state heat transfer analysis, and vibration analysis. The key operation in the method is the transformation of the degrees of freedom of the structure into uncoupled symmetrical components.

Thomas [60] developed the method of Orris and Petyt [49]

further. Whereas Orris and Petyt considered infinitely long 'chains' Thomas used the technique for studying rotationally periodic structures consisting of a finite number, say N, of identical substructures forming a closed ring. Thomas regards any normal mode of vibration as a wave propagating round the structure where the wave undergoes a phase change, ψ, between adjacent substructures. Using this approach to calculate the natural frequencies and normal mode shapes of a rotationally periodic structure, the treatment is as follows. The mass and stiffness matrices of one representative substructure are computed and required degrees of freedom (d.o.f.) constrained by the standard methods [4]. The unconstrained d.o.f. on one boundary (say, left-hand) of the substructure are constrained so that all the displacements corresponding to these d.o.f. have the same amplitude as the corresponding displacements on the right-hand boundary, but have the prescribed phase difference of ψ.

This can be expressed in complex arithmetic as

$$[U_L] = [U_R]\exp(+ i\psi) \qquad \ldots(3.1)$$

where $[U_L]$ and $[U_R]$ are the complex displacement vectors on the left- and right-hand boundaries respectively. (Note that the d.o.f. associated with the displacements in equation (3.1) are referred to as a 'boundary' d.o.f. and are distinct from those 'internal' d.o.f. not associated with the substructure boundaries.)

The method of Thomas [60] referred to above is similar to that described by MacNeal, Harder and Mason [59]. However, MacNeal et al use real arithmetic in their method whereas Thomas uses complex arithmetic. The use of complex arithmetic simplifies the equations required to define the technique as it is not necessary to consider sine and cosine components of displacement separately. There are other advantages of the method outlined by Thomas in Reference 60 and

detailed in a later paper [61]. Some of these advantages are:- (a) Rotationally periodic as well as not quite rotationally periodic structures (i.e. with small perturbations) can be analysed. (b) The treatment can be generalised so that each substructure can be mechanically connected to any number of substructures, so long as the connections are rotationally periodic. (c) The method is not confined for use with finite elements but can be used in any matrix analysis of structures that are linearly elastic. (d) The method is not confined to vibration. It can be used in other structural eigenvalue problems such as buckling.

We shall therefore adopt the method of Thomas for use in the investigation of cooling towers. We shall regard a cooling tower on leg-supports as a number of identical substructures joined together to form a closed ring. The cooling tower at Didcot Power Station which is analysed in this thesis can be divided into forty such substructures, each consisting of a $2\pi/40$ (i.e. $N = 40$) sector of shell, and one "V" shaped pair of legs (see Fig. 3.1).

For convenience of expression the process of applying constraints to U_L of the form described in equation (3.1) will be referred to as 'applying complex constraints'. It is now pertinent to examine the possible values of the phase angle ψ. In order to ensure continuity of displacements between the first and last substructure of a rotationally periodic structure with N identical substructures, $N\psi$ should be a multiple of 2π. That is, ψ can only take the discrete values

$$0, \left(\frac{2\pi}{N}\right) \times 1 , \left(\frac{2\pi}{N}\right) \times 2 \ldots\ldots \left(\frac{2\pi}{N}\right) \times z .$$

z is an integer that takes the value $\left(\frac{N}{2} + 1\right)$ or $\left(\frac{N+1}{2}\right)$ depending on whether N is even or odd, respectively. If $\psi = \frac{2\pi}{N} \times n$, where $0 \leq n \leq z$,

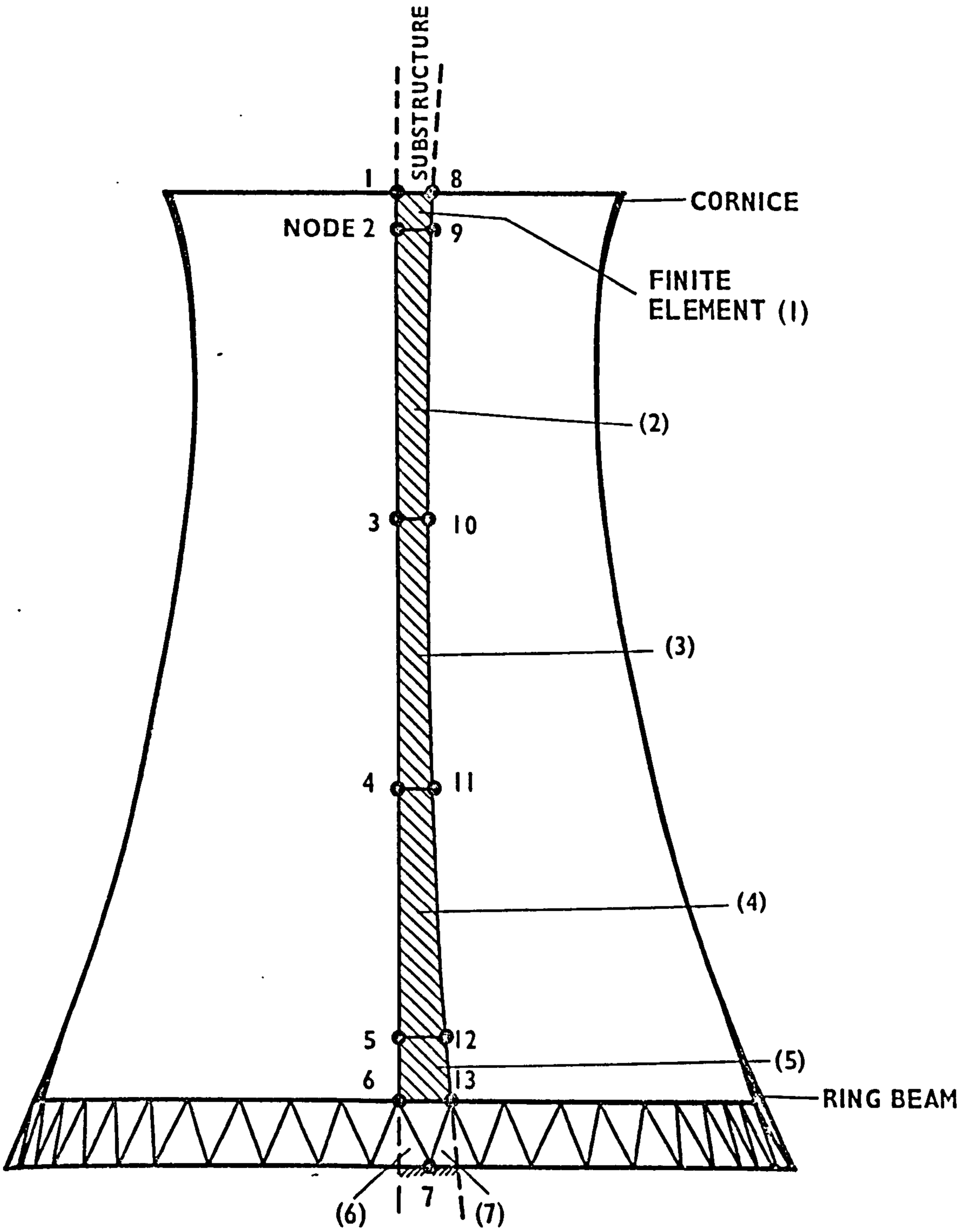

FIG.3.1 TYPICAL FINITE ELEMENT REPRESENTATION OF COOLING TOWER WITH LEG-SUPPORTS

(Angle Subtended at Axis-of-Revolution by Substructure is 9^0)

n is the harmonic circumferential wave number.

The numerical technique by which complex constraints are applied in the program VACTIL [5] will now be outlined. It will be seen that the technique can be easily applied to a free vibration problem using finite elements.

From a computational view-point the displacements that are complex-constrained can be regarded as undergoing a transformation (as for example a coordinate transformation). Let the displacements before the application of complex constraints be a complex vector U_p of order j and let it be U_Q after the application of complex constraints. Let the kth component of the vector U_p be denoted as U_p^k. (Similarly for U_Q.....) Now let complex constraints be applied so that the kth component of U_p is equal in amplitude to that of the kth component of the vector U_Q but differs by the phase angle ψ ($= \frac{2\pi}{N} \times n$). (For convenience of explanation we have assumed that only one component of U_p is complex-constrained.) Thus, the displacements can be equated as

$$\left.\begin{aligned} U_p^1 &= U_Q^1 \\ U_p^2 &= U_Q^2 \\ &\vdots \quad \vdots \\ U_p^k &= U_Q^k \times \exp(+i\psi) \\ &\vdots \quad \vdots \\ U_p^j &= U_Q^j \end{aligned}\right\} \qquad \ldots(3.3)$$

In matrix form equation (3.3) is

$$[U_p] = [T][U_Q] \qquad \ldots(3.4)$$

where the matrix [T] contains terms in zero (mostly), unity and one term in exp ($i\psi$). In practice many d.o.f. are complex-constrained. The

treatment is the same except that the matrix $[T]$ contains as many terms of exp $(i\psi)$ as there are constraints.

Now let K_s be the stiffness matrix of the representative substructure before the application of complex constraints. (Note that the conventional type of finite element constraint can be applied to K_s, if required.) Let K be the corresponding matrix after complex constraints have been applied. K is Hermitian-complex. Then

$$K = [T]^T [K_s][T] \qquad ...(3.5)$$

(with $(\ )^T$ standing for transpose of a matrix).

The equation (3.5) can be regarded as having been obtained from equation (3.4) by a treatment similar to that used for the transformation of geometrical coordinates (see Reference 4, page 10).

The numerical evaluation of equation (3.5) in the author's finite element computer program VACTIL [5] is performed in double precision complex arithmetic. When K_s is large, as is usually the case, a technique such as described for the transformation of geometrical coordinates in Chapter 6 must be employed to minimize computer core requirements.

The treatment for the mass matrix of the representative sub-structure, M_s, is the same as for K_s. The natural frequencies and mode shapes of the complete structure, for any given value of n, are obtained by solving the eigenvalue equation

$$(\underline{K} - \omega^2 \underline{M})\ \underline{x} = 0\ . \qquad ...(3.6)$$

$\underline{K}$ and $\underline{M}$ are the mass and stiffness matrices of a single substructure, subjected to the complex constraints described above, and are complex Hermitian matrixes. $\underline{x}$ is the vector of nodal displacements of the substructure; note that the eigenvectors are complex. The constrained

matrices $\underline{K}$ and $\underline{M}$ must be formed separately for each value of ψ considered; that is, for each value of n. The eigenvalues of the constrained substructure are identical to the eigenvalues of the full structure [60]. $\underline{x}$ can be used to generate the corresponding eigenvectors of the full structure. A detailed description of the mathematical basis of the technique is given in Reference 61.

3.3 Computer Time and Storage

One important advantage in using complex constraints is that only a representative substructure is analysed in preference to the whole structure. Thus both computer time and region requirements are reduced. Moreover, using a conventional finite element method and non-axisymmetric finite elements the number of circumferential nodes*, n, cannot be requested a priori. However, when using complex constraints the value of n is selected by choice of ψ.

It is useful to obtain an approximate estimate of the saving in computer c.p.u. time and computer storage (or region size) obtained by using complex constraints.

Let t be the ratio of the c.p.u. time taken to solve the eigenvalue equation for the whole structure to the corresponding time taken for a representative substructure. let C be the ratio of the computer region taken to analyse the whole structure to the corresponding region size required to analyse a representative substructure.

Many eigenvalue solution subroutines require a c.p.u. time that is proportional to the number of d.o.f. cubed. Also remembering that when complex arithmetic is used, each numerical multiplication

---

*There have been references to "non-classical" mode shapes in the literature [40,33]. The value of n to be ascribed to a particular mode shape will be discussed in a later section.

takes about four times longer than when real arithmetic is used, it can easily be shown that t is approximately equal to $N^3/(2N + 4)$ for extracting all the eigenvalues.

Storage requirements for an analysis are primarily dependent on the size of the overall (global) matrices and is proportional to the number of d.o.f. squared. Thus C is roughly $\frac{1}{2} N^2$.

For a cooling tower with forty representative substructures (i.e. N = 40) t = 761 and C = 800. These figures demonstrate that when analysing complex structures that are rotationally periodic the analysis of only one representative structure is either (a) essential to enable the problem to be solved without exceeding the restrictions imposed by the computing system or (b) greatly reduces the computer time and storage required.

3.4 Closure

The finite element analysis of a complex structure is facilitated if the system can be regarded as composed of component substructures. If the system is periodic the displacement mode can be regarded as a propagating wave and described by a complex propagation constant. If the structure is composed of identical substructures then the analysis can be greatly simplified by the use of complex constraints on one representative substructure.

CHAPTER FOUR

STRESS-DISPLACEMENT MATRICES FOR DOUBLY CURVED FINITE ELEMENTS

4. STRESS-DISPLACEMENT MATRICES FOR DOUBLY CURVED FINITE ELEMENTS

4.1 Introduction

The purpose of this chapter is to derive stress-displacement matrices (often referred to simply as stress matrices) for use with doubly curved shell finite elements. For convenience of explanation the specific case of the doubly curved shell finite element proposed in Reference 40 is considered. However, the derivation can easily be adapted to enable the derivation of the stress matrices of other doubly curved elements. By way of illustration the stress matrix of an axisymmetric element is also derived.

As the method of finite elements is well known - an explosive expansion of the subject has taken place in the last decade - an introduction to the subject will not be given in this thesis. (For a comprehensive introduction to the subject see References 2, 3 and 4.) However, some of the basic principles used in the derivation of a finite element will be detailed in this chapter.

The stiffness matrix for the doubly curved shell finite element is presented in Reference 40 in explicit rather than implicit form - only the expression for the strain energy is given explicitly [40, page 100]. Thus, in order to derive the finite element stress matrix it is also necessary to obtain equations that are common to the derivation of the stiffness matrix. Also to enable some of the equations used in the analysis to be verified, an expression for the element strain energy is obtained and seen to be equal to that given in Reference 40.

4.2 Geometry of a Shell of Revolution

In this section the geometry of a shell of revolution will be briefly discussed. Equations will be developed which will be of

use in the derivation of the stress matrices and which are also required for computing important geometrical properties (such as $\sin\phi/R$).

A smooth surface can be defined in the Cartesian coordinate system (x,y,z,). However, such a system does not lend itself readily to the geometry of a shell sector. Any point on the surface can be defined uniquely as follows:

$$\left.\begin{aligned} x &= F_1\ (\alpha,\beta) \\ y &= F_2\ (\alpha,\beta) \\ z &= F_3\ (\alpha,\beta) \end{aligned}\right\} \qquad \ldots(4.1)$$

The parameters α and β are defined as curvilinear coordinates. F_1, F_2 and F_3 are continuous and single-valued functions of α and β and exist in their simplest form for an orthogonal system of curvilinear coordinates. As an added benefit the directions of the principal radii of curvature are mutally perpendicular.

Equations (4.1) can be written in vector form, thus,

$$\underline{r} = \underline{r}\ (\alpha,\beta)$$

If $d\underline{s}$ is the vector joining the two coordinates (α,β) and $(\overline{\alpha+d\alpha},\ \overline{\beta+d\beta})$, then

$$d\underline{s} = \frac{d\underline{r}}{\partial\alpha}\ d\alpha + \frac{d\underline{r}}{\partial\beta}\ d\beta$$

The dot (scalar) product of $d\underline{s}$ with itself is:

$$(d\underline{s}).\ (d\underline{s}) = ds^2 = (A^2\ d\alpha^2 + B^2 d\beta^2)$$

(As the coordinate system is orthogonal the dot product of the two vectors $\frac{\partial \underline{r}}{\partial \alpha}$ and $\frac{\partial \underline{r}}{\partial \beta}$ is zero.) Here $A^2 = \left(\frac{\partial \underline{r}}{\partial \alpha}\right) \cdot \left(\frac{\partial \underline{r}}{\partial \alpha}\right)$ and $B^2 = \left(\frac{\partial \underline{r}}{\partial \beta}\right) \cdot \left(\frac{\partial \underline{r}}{\partial \beta}\right)$

When only one of the curvilinear coordinates α or β is varied in any particular operation the above equation gives

$$ds_\alpha = A d\alpha \qquad \ldots(4.2a)$$

$$ds_\beta = B d\beta \qquad \ldots(4.2b)$$

(ds_α is the increase in arc length along the coordinate line α for an increase in this curvilinear coordinate by $d\alpha$). A and B are usually known as the Lamé parameters and define (see below) the directional characteristics of the coordinate lines α and β, respectively.

As shells composed of only one material are to be analysed, the surface joining the loci of points equidistant from both walls of the shell will be defined as the reference surface. The concept of a reference surface is very useful, as will be seen. Consider the reference surface of a general shell of revolution, as given in Fig. 41. Let r (QA in Fig. 4.1) be the radius of curvature of the meridian (first principal radius of curvature) and R (OA in Fig. 4.1) be the radius of the parallel circle, i.e. the circle with its plane normal to the axis of revolution, Z-axis. The normals to the points at A and B intersect at Q. Let QA make an angle ϕ with the Z-axis.

Let θ be specified as the curvilinear coordinate β. For a unit increase in θ, i.e. $d\theta = 1$, ds_β will be the incremental length in this coordinate direction, i.e. $ds_\beta = B \times 1$ from equation (4.2b). However ds_β is also identical with the arc of a parallel circle and can be expressed as $ds_\beta = R d\theta$. By comparison with equation (4.2b),

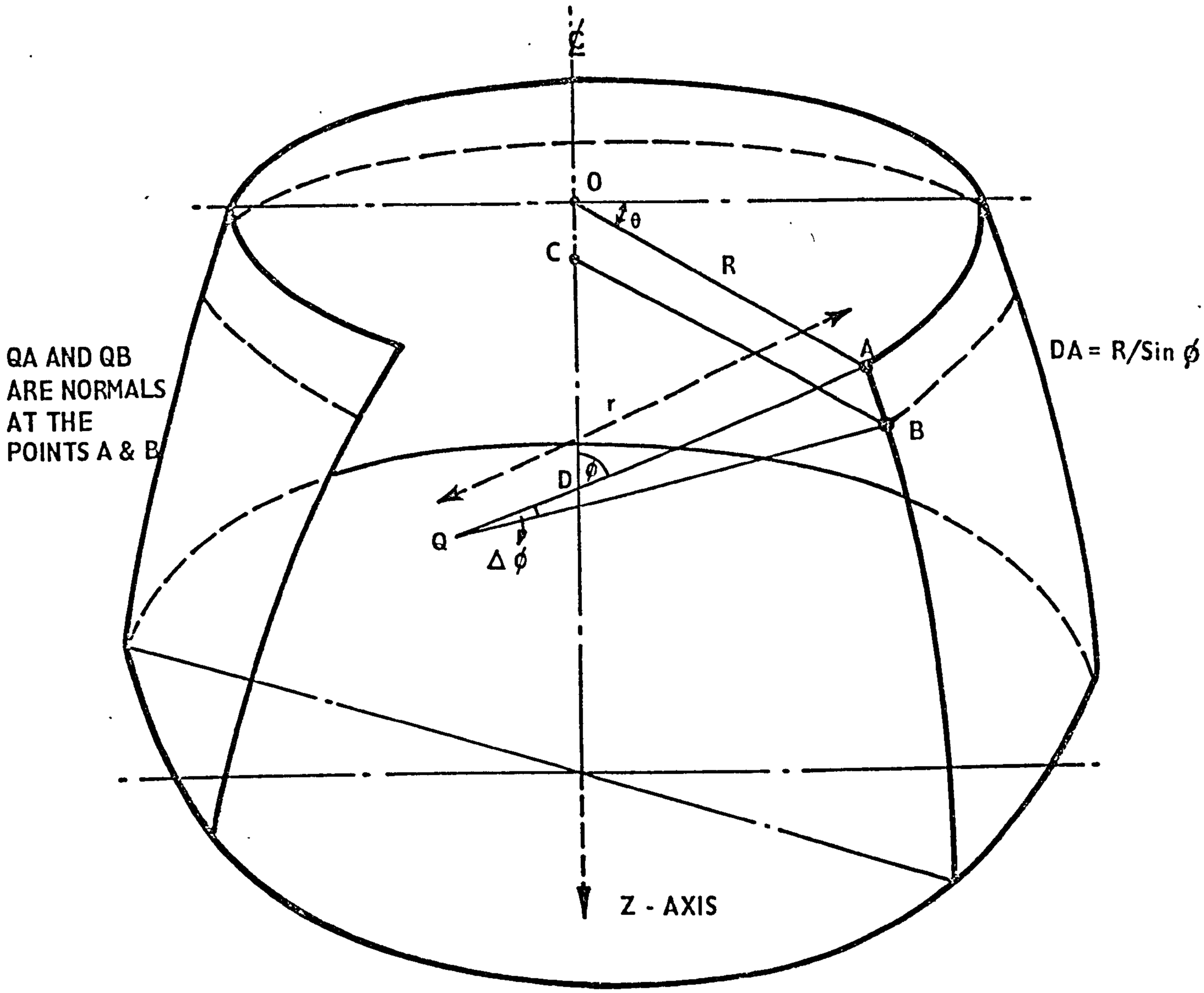

FIG.4.1 MIDDLE SURFACE OF SHELL OF REVOLUTION

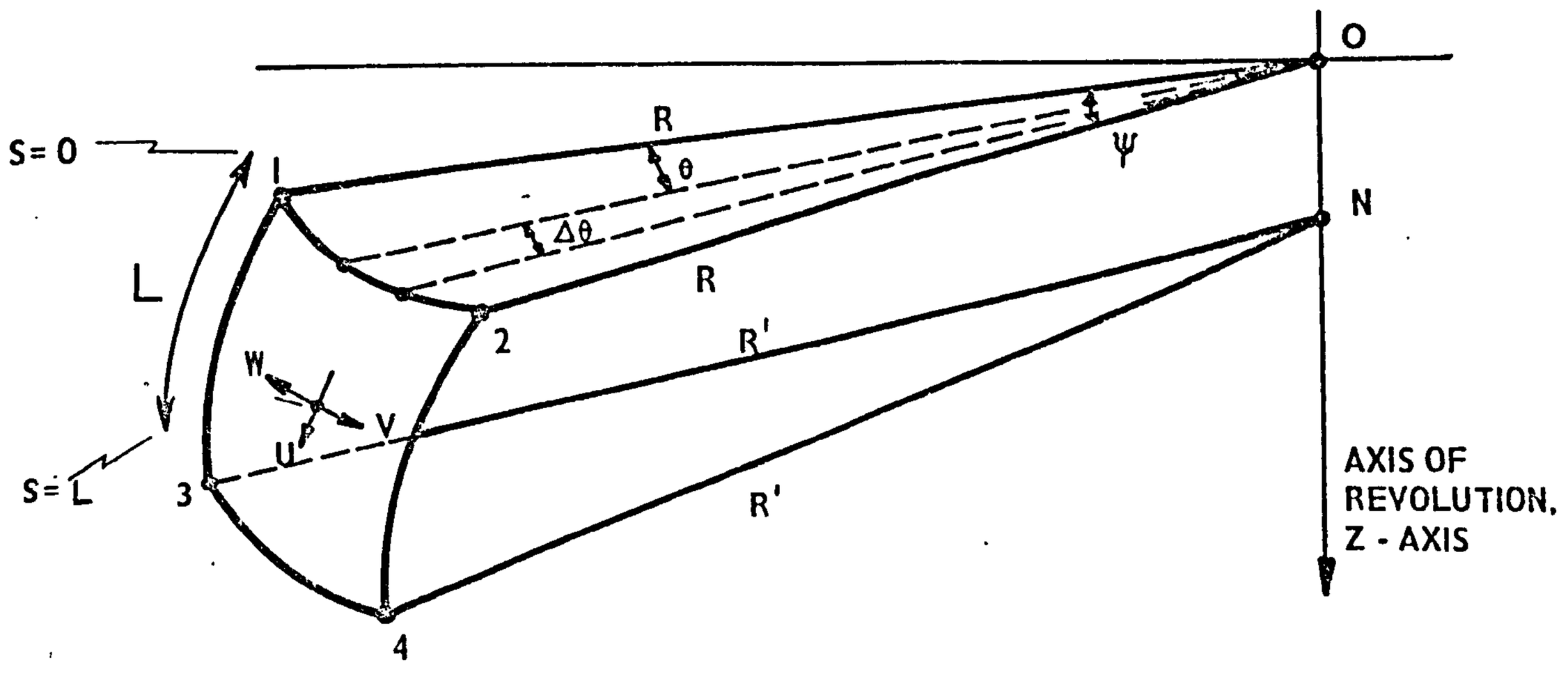

FIG.4.2 SHELL ELEMENT

therefore, B = R. If the length along the meridian is chosen as the other curvilinear coordinate α, then A is unity.

i.e.

$$\left.\begin{aligned} A &= 1 \\ B &= R \end{aligned}\right\} \qquad \ldots(4.2c)$$

Hence, the Lamé parameters have been obtained for the special case where the meridional arc length, s, and the angle defining the arc of a parallel circle, θ, are adopted as the curvilinear coordinates. (To complete the triad of "right-hand" orthogonal axes, a third axis γ normal to the reference surface is defined, and is declared zero at the reference surface.) This choice is not arbitrary; the attendant simplifications obtained in the geometrical expressions used in the derivation of the stiffness matrix are manifold.

Now r is the principal radius of curvature associated with the distance along a meridian s (or α). The second principal radius of curvature associated with θ (or β) is $(R/\sin\phi)$. Expressed as curvatures,

$$\kappa_1 = \frac{1}{r} \qquad \ldots(4.3a)$$

and

$$\kappa_2 = \frac{\sin\phi}{R} \qquad \ldots(4.3b)$$

From Fig. 4.1, for small AB

$$\frac{\{(CB - OA) = \Delta R\}}{\{AB = r\Delta\phi\}} = \cos\phi \text{ and in the limit } \frac{\partial R}{\partial \phi} = r\cos\phi \qquad \ldots(4.3c)$$

Now $r\Delta\phi = AB = \Delta s$ and in the limit $\frac{\partial\phi}{\partial s} = \frac{1}{r}$.

Hence (using equation (4.3c)) $\frac{\partial R}{\partial s} = \cos\phi$ $\qquad \ldots(4.4a)$

and $$\frac{\partial^2 R}{\partial s^2} = -\sin\phi\,\frac{\partial\phi}{\partial s} = -\frac{\sin\phi}{r} \qquad \ldots(4.4b)$$

It is readily shown [8, page 43] that the elemental volume of the segment of a shell bounded by two parallel circles, meridional sections and surfaces parallel to the reference surface, say d(vol), is given by the expression

$$d(vol) = AB(1 + \gamma\kappa_1)(1 + \gamma\kappa_2)d\gamma\, d\alpha\, d\beta$$

Substituting from equations (4.2) and (4.3),

$$d(vol) = R\left[1 + \left(\frac{1}{r} + \frac{\sin\phi}{R}\right) + \frac{1}{r}\,\frac{\sin\phi}{R}\,\gamma^2\right] \times d\gamma\, d\theta\, ds \qquad \ldots(4.5)$$

From the geometrical definition of the shell three parameters are evaluated numerically; i.e. $\frac{\partial R}{\partial Z}$, $\frac{\partial^2 R}{\partial Z^2}$ and $\frac{\partial^3 R}{\partial Z^3}$. (Here Z is the distance along the axis-of-revolution.) These parameters must be used to evaluate other important geometrical properties. For example, the meridional length (L) is obtained as follows:

$$\Delta L^2 = (\Delta Z^2 + \Delta R^2)\ ,$$

from consideration of Fig. 4.1.

Thus

$$L = \int_o^L \Delta L = \int \left[1 + \left(\frac{\partial R}{\partial Z}\right)^2\right]^{\frac{1}{2}} dZ \qquad \ldots(4.5b)$$

Cos ϕ is similarly obtained:

$$\cos\phi = \Delta R/\Delta L = \left(\frac{\partial R}{\partial Z}\right) \Big/ \left[1 + \left(\frac{\partial R}{\partial Z}\right)^2\right]^{\frac{1}{2}} \qquad \ldots(4.5c)$$

An expression for the important parameter (1/r) is obtained as follows:-

As $r\Delta\phi = \Delta L$ and $\Delta L = \Delta Z/\sin\phi$

$$\frac{\partial\phi}{\partial Z} = \left(\frac{1}{r}\right)/\sin\phi \qquad \ldots(4.5d)$$

Also as $\sin\phi = \frac{\partial Z}{\partial s}$ and $\frac{\partial^2 R}{\partial s^2} = -\frac{\sin\phi}{r}$ we get

$$\frac{1}{\partial s}\left(\frac{\partial R}{\partial Z}\sin\phi\right) = -\sin\phi/r \ .$$

With elementary manipulations, and remembering to use equation (4.5d) we get,

$$\left(\frac{1}{r}\right) = -\sin^3\phi \times \left(\frac{\partial^2 R}{\partial Z^2}\right) \qquad \ldots(4.5e)$$

The important geometrical parameter $\frac{1}{r} \times \frac{\partial r}{\partial s}$ {see equation (4.9b)} is obtained frcm equation (4.5e) and is:-

$$\frac{1}{r}\left(\frac{\partial r}{\partial s}\right) = \cos\phi\left[3 \times \frac{1}{1 + \left(\frac{\partial R}{\partial Z}\right)^2} \times \left(\frac{\partial^2 R}{\partial Z^2}\right) \times \left(\frac{\partial R}{\partial Z}\right) - \frac{\left(\partial^3 R/\partial Z^3\right)}{\left(\partial^2 R/\partial Z^2\right)}\right] \Bigg/ \left(\frac{\partial R}{\partial Z}\right) \qquad \ldots(4.5f)$$

The above completes the basic geometrical information required for the section and chapters that follow.

4.3 Basic Assumptions of Thin Shell Theory

A shell is defined as a body bounded by two curved surfaces where the distance between the surfaces is small in comparison to the other dimensions. In this thesis it will be assumed that the shell is formed from a material that is homogenous, isotropic and linearly elastic.

A shell is defined to be thin when the ratio (ξ) of the first principal radius of curvature (r) to its thickness (h) is large in comparison to unity. Kraus [62] advocates that $\xi \geq 10$ and Novozhilov [8] that $\xi \geq 20$. In practice, shells of engineering interest (e.g. cooling towers) have ξ values that lie in the range 50 to 1000.

Several important assumptions are made in the theory of thin elastic shells. These assumptions are known variously as either Love's Postulates or Kirchhoff's Hypotheses, and are stated as follows:

(i) The deflections of the shell are small.

(ii) The straight fibres of a plane (within the shell wall) normal to the reference surface before deformation remain so after deformation and do not change their length.

(iii) The normal stresses acting on planes parallel to the reference surface can be neglected in comparison with other stresses.

That these assumptions are valid in many practical situations is clear from the immense quantity of established work involving thin shells and based on the above. Also, Novozhilov and Finnkel'Shtein [63]

formally discuss the implications of these assumptions and conclude that the errors are of the order $\left(\frac{1}{\xi}\right)$.

4.4 Stress-Strain Relationships for General and Thence Thin Shells

Let us now consider Hook's Law for a homogeneous, isotropic, linearly elastic medium. Let $\sigma_{\alpha\alpha}$, $\sigma_{\beta\beta}$ and $\sigma_{\gamma\gamma}$ be the normal stresses acting on three mutually perpendicular faces of an element cut from the elastic body. (The first suffix gives the direction of the stress, and the second the direction of the normal to the plane on which the stress acts.) Let $e_{\alpha\alpha}$, $e_{\beta\beta}$ and $e_{\gamma\gamma}$ be the corresponding strains induced in the body. Let $\sigma_{\alpha\beta}$, $\sigma_{\beta\gamma}$ and $\sigma_{\gamma\alpha}$ be the shear stresses on these faces with $e_{\alpha\beta}$, $e_{\beta\gamma}$ and $e_{\gamma\alpha}$ the attendant strain components (or shear deformation). The relation between the stresses and strains can be given in matrix form as

$$\left[\sigma(\alpha,\beta,\gamma)\right] = \left[D_1\right]\left[e(\alpha,\beta,\gamma)\right] \qquad \ldots(4.6a)$$

D_1 is often termed the "Elasticity Matrix". (However, it must be noted that there are various forms of the Elasticity Matrix, as will be seen in this chapter, and that expressions given in the literature involving this term must be interpreted with care.) The terms of this matrix are readily available from the standard theory of properties of materials. (For example, see Hearmon [64], pages 65 to 67.)

For a thin shell the terms of the constitutive matrices given in equation 4.6a can be significantly simplified. Returning to Kirchhoff's Hypotheses, (ii) implies that deformation of a thin shell as a three-dimensional body takes place without the shearing

deformations $e_{\gamma\alpha}$, $e_{\beta\gamma}$ and without strain $e_{\gamma\gamma}$ through the thickness of the shell.

i.e. $$e_{\gamma\alpha} = e_{\beta\gamma} = e_{\gamma\gamma} = 0$$

For linearly elastic, homogeneous materials the shear strain components are directly proportional to the corresponding stress components. Thus as $e_{\beta\gamma} = \frac{\sigma_{\beta\gamma}}{G}$ and $e_{\gamma\alpha} = \frac{\sigma_{\gamma\alpha}}{G}$, where G is the Shear Modulus $(= \frac{1}{2(1+\rho)})$, the shear stress components $\sigma_{\beta\gamma}$ and $\sigma_{\gamma\alpha}$ vanish. Note that $e_{\gamma\gamma} = \partial/\partial\gamma\{w(\alpha,\beta,\gamma)\}$ where $w(\alpha,\beta,\gamma)$ is the displacement normal to any surface within the thickness of the shell for γ = constant. Therefore, $e_{\gamma\gamma}$ is deemed to be zero this displacement will be independent of the value of γ. That is, the normal displacement of the reference (or middle) surface will be equal to the normal displacement at any point within the shell on a common normal.

Finally, application of Kirchhoff's third hypothesis allows $\sigma_{\gamma\gamma}$ to be declared zero. (Even in the case of a pressure vessel it is said [65] that the stresses in the thickness direction, $\sigma_{\gamma\gamma}$, are very small in relation to meridional stresses, $\sigma_{\alpha\alpha}$, or circumferential stresses, $\sigma_{\beta\beta}$, that are induced by the pressure.) It is now possible to present the stress-strain relationship for thin elastic shells. This is a re-formulation of the general relationship expressed by equation (4.6a)

$$\begin{bmatrix} \sigma_{\alpha\alpha} \\ \alpha_{\beta\beta} \\ \sigma_{\alpha\beta} \end{bmatrix} = \frac{E}{(1-\rho^2)} \begin{bmatrix} 1 & \rho & 0 \\ \rho & 1 & 0 \\ 0 & 0 & \frac{1-\rho}{2} \end{bmatrix} \begin{bmatrix} e_{\alpha\alpha} \\ e_{\beta\beta} \\ e_{\alpha\beta} \end{bmatrix} \qquad \ldots(4.6b)$$

i.e.

$$[\sigma(\alpha,\beta,\gamma)] = [D_2][e(\alpha,\beta,\gamma)] \qquad \ldots(4.7)$$

where E is Young's Modulus and ρ is Poisson's Ratio.

4.5 The Stiffness Matrix for a Double-Curvature, Shell Finite Element

4.5.1 Relation between strain and nodal displacements

In the previous section the stress and strain components were shown to exist only in the $\alpha\beta$ plane for thin shells of revolution (equation (4.7)). The study of the three-dimensional continuum can now be satisfactorily reduced to the analysis of the two-dimensional reference surface.

It can be shown that the deformation of the reference surface can be completely determined by six strain components (see Novozhilov [8] pages 26 and 27). Let ε_α, ε_β be the extensions of a point (α,β) on the reference surface in the directions of α and β, respectively. Similarly, let χ_α and χ_β be 'rotations' in these directions. Let $\varepsilon_{\alpha\beta}$ be the shear strain and $\chi_{\alpha\beta}$ the twist. Thus, considering a small element on the middle surface, ε_α, ε_β and $\varepsilon_{\alpha\beta}$ characterize the variations of its dimensions whilst χ_α, χ_β and $\chi_{\alpha\beta}$ characterize its distortion.

It is now necessary to relate the strains at the middle surface to the strains at any point in the material. For a general shell, the relevent equations have been derived by Vlasov [9, page 249, equations 7.8]. Substituting for κ_1 κ_2, A and B gives:

$$e_{\alpha\alpha} = \varepsilon_\alpha + \chi_\alpha \gamma + (-\kappa_1 \chi_\alpha)\gamma^2 + \sum_{n=3}^{\infty} \chi_{\alpha n} \gamma^n$$

$$e_{\beta\beta} = \varepsilon_\beta + \chi_\alpha{}^1 \gamma + (-\kappa_2 \chi_\beta)\gamma^2 + \sum_{n=3}^{\infty} \chi_{\beta n} \gamma^n \qquad \ldots(4.8a)$$

and $$e_{\alpha\beta} = \varepsilon_{\alpha\beta} + \chi_{\alpha\beta}\gamma + (\tfrac{1}{2}p^2 \varepsilon_{\alpha\beta} - \tfrac{1}{2}\bar{p}\chi_{\alpha\beta})\gamma^2 + \sum_{n=3}^{\infty} \chi_{\alpha\beta n} \gamma^n$$

where $\chi_{\alpha n}$, $\chi_{\beta n}$ and $\chi_{\alpha\beta n}$ are defined by Vlasov, pages 249-251. p and $\bar{p}$ are defined later. (Note that $-\frac{h}{2} \leq \gamma \leq +\frac{h}{2}$, where h is the thickness of the shell wall.) For thin shells Love [121] assumes a linear variation of $[\varepsilon(\alpha,\beta,\gamma)]$ with γ. Several other authors also neglect the terms of order γ^2 or higher. However, Vlasov [9, page 262] argues that this contradicts a basic assumption (i.e. (ii) in Section 4.3) of thin shell theory. On the other hand, it must be noted that Novozhilov [8, page 53], while accepting that these contradictions do exist, strongly suggests that the mathematical inaccuracies so generated are still of the order of $\frac{1}{\xi}$. On consideration, for the present purpose we assume a quadratic variation of the strain across the thickness of the shell wall. The following matrix equation is then obtained from equation (4.8a):

$$\begin{bmatrix} e_{\alpha\alpha} \\ e_{\beta\beta} \\ e_{\alpha\beta} \end{bmatrix} = \begin{bmatrix} 1 & 0 & 0 & \gamma(1 - \frac{\gamma}{r}) & 0 & 0 \\ 0 & 1 & 0 & 0 & \gamma(1 - \frac{\sin\phi}{R}\gamma) & 0 \\ 0 & 0 & (1 + \frac{1}{2}p^2\gamma^2) & 0 & 0 & \gamma(1 - \frac{1}{2}\bar{p}\gamma) \end{bmatrix}$$

$$\times \begin{bmatrix} \varepsilon_\alpha & \varepsilon_\beta & \varepsilon_{\alpha\beta} & \chi_\alpha & \chi_\beta & \chi_{\alpha\beta} \end{bmatrix}^T \qquad \ldots(4.8b)$$

(where the superscript T denotes the transpose of the particular matrix)

or

$$\left[\, e(\alpha\ \beta\ \gamma)\right] = \left[\, \gamma\,\right]\left[\, \varepsilon(\alpha,\beta\ (,\gamma=0)\,)\right] \qquad \ldots(4.8c)$$

Here, $p = -\left(\frac{1}{r} - \frac{\sin\phi}{R}\right)$ and $\bar{p} = \left(\frac{1}{r} + \frac{\sin\phi}{R}\right)$.

Continuing our analysis of the reference surface it is now desired to relate the strains to the displacements at the middle surface. This relation is obtained from Valsov [9, page 250, equations (7.11)]. Remembering to substitute for A, B, κ_1 and κ_2 we get:

$$\left[\, \varepsilon(\alpha,\beta)\right] = \left[\, B_1\,\right]\left[\, \delta(\alpha,\beta\ (,\gamma=0)\,)\right] \qquad \ldots(4.9a)$$

where

$$\left[\, B_1\,\right] = \begin{bmatrix} \frac{1}{L}\frac{\partial}{\partial\bar{s}} & 0 & \frac{1}{r} \\ \frac{\cos\phi}{R} & \frac{1}{R\Psi}\frac{\partial}{\partial\bar{\theta}} & \frac{\sin\phi}{R} \\ \frac{1}{R\Psi}\frac{\partial}{\partial\bar{\theta}} & \frac{1}{L}\frac{\partial}{\partial\bar{s}} - \frac{\cos\phi}{R} & 0 \\ \left(\frac{-\partial r}{Lr^2\,\partial\bar{s}}\right) & 0 & -\left(\frac{1}{r^2} + \frac{1}{L^2}\frac{\partial^2}{\partial\bar{s}^2}\right) \\ -\frac{p\cos\phi}{R} & 0 & -\left(\frac{\sin^2\phi}{R^2} + \frac{\cos\phi}{LR}\frac{\partial}{\partial\bar{s}} + \frac{1}{\Psi^2R^2}\frac{\partial^2}{\partial\bar{\theta}^2}\right) \\ -\frac{p}{\Psi R}\frac{\partial}{\partial\bar{\theta}} & p\left(\frac{1}{L}\frac{\partial}{\partial\bar{s}} - \frac{\cos\phi}{R}\right) & 2\left(\frac{\cos\phi}{\Psi R^2}\frac{\partial}{\partial\bar{\theta}} - \frac{1}{\Psi RL}\frac{\partial^2}{\partial\bar{\theta}\partial\bar{s}}\right) \end{bmatrix} \qquad \ldots(4.9b)$$

and $[\delta(\alpha,\beta)] = [u\ v\ w]^T$. u, v and w are the orthogonal displacements along the coordinate axes α,β,γ (see Fig. 4.2). With reference to the doubly curved shell finite element shown in Fig. 4.2, the bar sign signifies normalization with respect to the element dimensions. That is, $\bar{s} = \frac{s}{L}$ and $\bar{\theta} = \frac{\theta}{\Psi}$. L is the length of the meridian (see Fig. 4.2) and Ψ is the angle subtended by the parallel meridians of the element considered. (Note that $\frac{1}{L}\frac{\partial}{\partial \bar{s}} = \frac{\partial}{\partial s}$ and $\frac{1}{\Psi}\frac{\partial}{\partial \bar{\theta}} = \frac{\partial}{\partial \theta}$.)

4.5.2 Displacement function

The displacements at any point on the middle surface must now be related to the variables (displacements) at the nodes of the finite element (e.g. 1, 2, 3 and 4 in Fig. 4.2). That is, an equation of the form

$$[\delta(\sigma,\beta)] = [P][\delta^e] \qquad \ldots(4.10)$$

is required where $[\delta^e]$ is the nodal displacement vector. The matrix $[P]$ is obtained using the following arguments.

It is assumed that each of the three displacements, i.e. $u(\alpha,\beta) = u(s,\theta) = u$, say, v and w, can be written as the products of one-dimensional, cubic interpolation polynomials and undetermined displacements at the nodes of the elements. For u the expression is:

$$u = \sum_{i=1}^{i_m} \left\{ f_a g_b (u_i) + L\, f_{(a+1)}\, g_b \left(\frac{\partial u}{\partial s}\right)_i + R\Psi f_a\, g_{(b+1)} \left(\frac{\partial u}{\partial \theta_o}\right)_i + LR\Psi f_{(a+1)}\, g_{(b+1)} \left(\frac{\partial^2 u}{\partial s \partial \theta_o}\right) \right\} \qquad \ldots(4.11)$$

Here, $\theta_o = R \times \theta$.

If there are four nodes (i.e. $i_m = 4$), then

$a = 1$ when $i = 1$ or 2

$= 3$ when $i = 3$ or 4

and $b = 1$ when $i = 1$ or 3

$= 3$ when $i = 2$ or 4.

Also, $f_1(\bar{s}) = f_1$ (say) $= 1 - 3\bar{s}^2 + 2\bar{s}^3$. Similarly $g_1(\bar{\theta}) = g_1$ (say) $= 1 - 3\bar{\theta}^2 + 2\bar{\theta}^3$

$$f_2 = \bar{s} - 2\bar{s}^2 + \bar{s}^3 \qquad g_2 = \bar{\theta} - 2\bar{\theta}^2 + \bar{\theta}^3$$

$$f_3 = 3\bar{s}^2 - 2\bar{s}^3 \qquad g_3 = 3\bar{\theta}^2 - 2\bar{\theta}^3$$

$$f_4 = -\bar{s}^2 + \bar{s}^3 \qquad g_4 = -\bar{\theta}^2 + \bar{\theta}^3.$$

The accuracy, and usefulness, of the above displacement function has been verified by several authors [66, 40, 6, 67]. Thus, several important requisites, like for example, the continuity of displacements and slopes between adjacent elements along an entire edge, are satisfied.

From equation (4.11) it is observed that there are 16 displacement terms in u for a finite element with four nodes. Thus, the three orthogonal displacements u, v and w give rise to 48 displacements or degrees of freedom at the nodes of the element:

$$A_j, \left(\frac{\partial A}{\partial s}\right)_j, \left(\frac{\partial A}{\partial \theta_o}\right)_j, \left(\frac{\partial^2 A}{\partial s \partial \theta_o}\right)_j$$

where j takes the values 1 to $i_m(=4)$ and A takes the notation u, v and w respectively for each value of j. Let these 48 displacements be denoted by the nodal displacement vector $[\delta^{\hat{e}}]$. Then,

$$\delta(\alpha,\beta) = \begin{bmatrix} [T_{11}] & [T_{12}] & [T_{13}] & [T_{14}] \\ [T_{21}] & [T_{22}] & [T_{23}] & [T_{24}] \\ [T_{31}] & [T_{32}] & [T_{33}] & [T_{34}] \end{bmatrix} \times [\delta^e] \qquad \ldots(4.12)$$

where the sub-matrices $[T_{ij}]$ are given by $[T_{1i}] = \left[[T_{mi}][O_8]\right]$, $T_{2i} = \left[[O_4][T_{mi}][O_4]\right]$ and $[T_{3i}] = \left[[O_8][T_{mi}]\right]$. Here $[O_4]$ and $[O_8]$ are zero row-matrices of order (1 × 4) and (1 × 8) respectively. From equation (4.11) $[T_{mi}] = [f_a g_b \; Lf_{(a+1)} gb \; R\Psi f_a g_{(b+1)} \; LR\Psi f_{(a+1)} g_{(b+1)}]$ where a and b vary, as in equation (4.11), with i.

Now comparing equation (4.12) with equation (4.10), it can be seen that $[P]$ in equation (4.10) is the matrix of order (3 × 48) given above in equation (4.12) (i.e. the matrix with terms in the sub-matrix $[T_{ij}]$).

4.5.3 Strain energy

Sufficient information has been derived in the previous sections to enable expressions for the strain energy and thence the stiffness matrix to be obtained.

When a material has been subjected to elastic deformation the forces that are responsible for the deformation process are negated by the ensuing internal stresses within the material. These internal stresses contribute to the total internal energy of the body; this contribution is referred to as an increase in the strain energy, U.

$$U = \int_{vol} U_o \; d(vol)$$

where U_o is the strain energy per unit volume. For a material that was unstressed before the deformation, $U_o = \int_{\sigma=0}^{\sigma} \int_{e=0}^{e} de.\, d\sigma$

For a linearly elastic material, the stress-strain characteristics are linear; hence,

$$U_o = \frac{1}{2}\, e.\sigma$$

Thus, for the present case, in matrix notation

$$U = \frac{1}{2} \int_{vol} \left[e(\alpha,\beta,\gamma) \right]^T \left[\sigma(\alpha,\beta,\gamma) \right] d(vol) \qquad \ldots(4.13)$$

From equation (4.7)

$$U = \frac{1}{2} \int_{vol} \left[e(\alpha,\beta,\gamma) \right]^T \left[D_2 \right] \left[e(\alpha,\beta,\gamma) \right] d(vol)$$

Substituting from equation (4.8c) for $\left[e(\alpha,\beta,\gamma) \right]$ and from equation (4.5) for d(vol), we obtain

$$U = \frac{1}{2} \int_{\bar{s}=0}^{1} \int_{\bar{\theta}=0}^{1} \left[\varepsilon(\alpha,\beta) \right]^T \left[D \right] \left[\varepsilon(\alpha,\beta) \right] d\bar{\theta}.d\bar{s} \quad \ldots(4.14a)$$

where

$$D = \int_{\gamma=-h/2}^{+h/2} R\{1 + \left(\frac{1}{r} + \frac{\sin\phi}{R} \right) + \frac{1}{r}\frac{\sin\phi}{R}\gamma^2\} \times \left[\gamma \right]^T \left[D_2 \right] \left[\gamma \right] d\gamma$$

$$\ldots(4.14b)$$

(Note the rule of matrix algebra where $(\left[x \right]\left[y \right])^T = \left[y \right]^T \left[x \right]^T$)

Now, substituting for $\left[\varepsilon(\alpha,\beta) \right]$ from equation (4.9a) we obtain

$$U = \frac{1}{2} \int\int \left[\delta(\alpha,\beta) \right]^T \left[B_1 \right]^T \left[D \right] \left[B_1 \right] \left[\delta(\alpha,\beta) \right] d\bar{\theta}\, d\bar{s}$$

As shown earlier, equation (4.10), $\left[\delta(\alpha,\beta) \right] = \left[P \right] \left[\delta^e \right]$, and

hence,

$$U = \frac{1}{2} \int \int [\delta^e]^T [P]^T [B_1]^T [D][B_1][P][\delta^e] \, d\bar{\theta} \, d\bar{s}$$

Now let $[B] = [B_1][P]$, ...(4.14c)

which gives

$$U = \frac{1}{2} \int \int [\delta^e]^T [B]^T [D][B][\delta^e] \, d\bar{\theta} \, d\bar{s} \qquad \ldots(4.15)$$

Let $[K] = \int_{\bar{s}=0}^{1} \int_{\bar{\theta}=0}^{1} [B]^T [D][B] \, d\bar{\theta} \, d\bar{s}$ ...(4.16)

Then $U = \frac{1}{2} [\delta^e]^T [K][\delta^e]$ ...(4.17)

We now invoke the Principle of Virtual Work - "During any virtual displacement imposed on a body the total external work done by the externally applied nodal forces must be equal to the total internal work done by the stresses". Let the virtual displacements at the nodes be $[\delta^{el}]$ and $[F^e]$ the statically equivalent forces at the nodes. Then the external work done = $[\delta^{el}]^T[F^e]$. By the Principle of Virtual Work the internal work done is due to the actual stresses associated with the nodal displacements $[\delta^e]$, and the virtual strains associated with the virtual nodal displacements $[\delta^{el}]$.

Now, applying arguments similar to those used to obtain equation (4.17), it is seen that the internal work done is $[\delta^{el}]^T [K][\delta^e]$.

(Note that U_o is now equal to e.σ as the stress due to the actual displacements $[\delta^e]$ is constant, while the virtual strain is increased owing to the virtual displacements $[\delta^{el}]$.)

Thus, $[\delta^{el}]^T [F^e] = [\delta^{el}]^T [K][\delta^e]$

Premultiplying both sides by $[\delta^{el}]$ gives

$$[\delta^{el}][\delta^{el}]^T[F^e] = [\delta^{el}][\delta^{el}]^T [K][\delta^e]$$

The inverse of $([\delta^{el}][\delta^{el}]^T)$ exists as $[\delta^{el}]$ can be so chosen - the Virtual Work Principle must be valid for any system of applied displacements. Premultiplying both sides by this inverse gives

$$[F^e] = [K][\delta^e]$$

This is a generalisation of the familiar expression for Hook's Law in matrix form. $[K]$ is the stiffness matrix. By evaluating equation (4.14b) is can be shown that $[D]$ has the following form:-

$$[D] = \frac{E}{(1-\rho^2)} \begin{bmatrix} d_1 & & & & & \\ \rho d_1 & d_1 & & \text{symmetric terms} & & \\ 0 & 0 & d_2 & & & \\ d_4 & \rho d_4 & 0 & d_6 & & \\ \rho d_5 & d_5 & 0 & d_9 & d_8 & \\ 0 & 0 & d_3 & 0 & 0 & d_7 \end{bmatrix} \quad \ldots(4.18a)$$

where, neglecting h^4 in terms and terms of similar or smaller magnitude,

$$d_1 = R(h + \bar{h}\,\frac{\sin\phi}{Rr})$$

$$d_2 = R\nu\ (h + \bar{h}\{\frac{\sin\phi}{Rr} + p^2\})$$

where $\nu = \frac{1}{2}(1-\rho)$ and $\bar{h} = \frac{h^3}{12}$

$$d_3 = \frac{1}{2}\,\nu\,\bar{p}\,R\,\bar{h}$$

$$d_4 = \bar{h}\,\sin\phi$$

$$d_5 = \bar{h}\,\frac{R}{r}$$

$$d_6 = \bar{h}\,R$$

$$d_7 = \nu\,\bar{h}\,R$$

$$d_8 = \bar{h}\,R$$

$$d_9 = \rho\,\bar{h}\,R$$

...(4.18b)

The other matrix term in the expression for the stiffness matrix is $[B]$. $[B]$ is calculated from equation (4.15) where $[P]$ is obtained from (4.12) and $[B_1]$ from equation (4.9b). Whilst differentiating with respect to $\bar{s}$, when evaluating $[B]$, it must be remembered that R varies along s. Thus, for example,

$$\frac{\partial(Rf_1)}{\partial\bar{s}} = \left(f_1' + \frac{1}{R}\,f_1\,R'\right)\,R$$

where from equation (4.4a), $R' = \frac{\partial R}{\partial\bar{s}} = L\cos\phi$. Differentiation with respect to $\bar{\theta}$ is straightforward as R and L are not functions of θ.

At this state it is pertinent to note that by substituting for $[D]$ in equation (4.14a) from equation (4.18) is can be verified that the expression for the strain energy, U, is identical to

that obtained by Deb Nath [40, page 100, equation (A.1)]. (However, see Section 4.6.3 regarding U for the ring element.)

4.6 The Stress Matrix

4.6.1 Stress at any point

The equations set out in the previous sections now allow the 'stress matrix' to be obtained with relative ease. From equations (4.7), (4.8c), (4.9a), (4.10) and (4.15)

$$[\sigma(\alpha,\beta,\gamma)] = [D_2][\gamma][B_1][P][\delta^e]$$

$$= [D_3][B][\delta^e]$$

$$= [H_1][\delta^e] \qquad \ldots(4.19a)$$

where $[D_3] = [D_2][\gamma]$ $\ldots(4.19b)$

and $[H_1] \quad [D_3][B]$ $\ldots(4.19c)$

(Note that the displacement vector $[\delta^e]$ is in the 'local' curvilinear coordinate system of the shell element.)

$[H_1]$ is called the stress-displacement matrix or, simply, the stress matrix. $[B]$ in equation (4.19c) is evaluated as described in Section (4.5.3.). $[D_3]$ is obtained from equations (4.7) and (4.8b):

$$[D_3] = \frac{E}{(1-\rho^2)} \begin{bmatrix} 1 & \rho & 0 & \gamma\left(1-\frac{\gamma}{r}\right) & \gamma\rho\left(1-\frac{\sin\phi}{R}\gamma\right) & 0 \\ \rho & 1 & 0 & \gamma\rho\left(1-\frac{\gamma}{r}\right) & \gamma\left(1-\frac{\sin\phi}{R}\gamma\right) & 0 \\ 0 & 0 & \nu\left(1+\frac{1}{2}p^2\gamma^2\right) & 0 & 0 & \gamma\nu\left(1-\frac{1}{2}\bar{p}\gamma\right) \end{bmatrix}$$

$\ldots(4.19d)$

Thus the stress matrix $[H_1]$ of order (3 × 48) can be obtained and the stress components $\sigma_{\alpha\alpha}$, $\sigma_{\beta\beta}$ and $\sigma_{\alpha\beta}$ can be determined at any point (α,β,γ) on or within the shell wall.

4.6.2 Stress resultants and couples

Whilst it is useful to know the stress at any particular point in the wall of the shell it is often more practical to calculate the 'averaged' stress distribution in the shell. By integrating the stress components along a normal to the shell wall for γ varying from $-\frac{h}{2}$ to $+\frac{h}{2}$ a two-dimensional theory of stress can be presented. For convenience, it is possible to describe the action of the stress components over a unit value of arc of a parallel circle at the reference surface. Thus, for unit wall length in the circumferential direction the forces can be obtained. (This is similar to the treatment used in Beam Theory.) From elementary theory [68, page 73] it is known that a system of forces can be represented by statically equivalent resultants and couples. Using the above concepts it is now possible to define components of stress and moment that enable the 'averaged' stress behaviour of the shell to be described.

The arc length of a parallel circle for γ = constant subtending and angle $\Delta\theta$ at the Z-axis is equal to $\Delta\theta(R + \gamma) = \Delta\theta.R(1 + \frac{\gamma}{R})$. Defining $\Delta\theta$ such that unit arc length at the middle surface is obtained (i.e. $\Delta\theta.R = 1$) we get $(1 + \frac{\gamma}{R})$.

The stress resultants and couples of $\sigma_{\alpha\alpha}$ distributed over an α = constant face of the shell, for unit arc length of the reference surface, are given by

$$N_\alpha = \int_{\gamma=-\frac{h}{2}}^{+\frac{h}{2}} \sigma_{\alpha\alpha} \left(1 + \frac{\gamma}{R}\right) d\gamma$$

and

$$M_\alpha = \int \sigma_{\alpha\alpha} \left(1 + \frac{\gamma}{R}\right) \gamma \, d\gamma$$

Similar relationships apply for $\sigma_{\beta\beta}$ and $\sigma_{\alpha\beta}$. Thus, the three components of $\left[\, \sigma(\alpha,\beta,\gamma) \,\right]$ in equation (4.7) are given by six stress resultants and couples - N_α, N_β, $N_{\alpha\beta}$ and M_α, M_β, $M_{\alpha\beta}$, respectively. The directions of these components are indicated in Fig. 4.3.

In matrix notation, therefore,

$$\left[\, N \,\right] = \begin{bmatrix} N_\alpha \\ N_\beta \\ N_{\alpha\beta} \end{bmatrix} = \int_{\gamma = -\frac{h}{2}}^{+\frac{h}{2}} \left[\, \sigma(\alpha,\beta,\gamma) \,\right] \left(1 + \frac{\gamma}{R}\right) d\gamma$$

From equations (4.7), (4.8c) and (4.19b)

$$\left[\, N \,\right] = \int_{-h/2}^{+h/2} \left[\, D_3 \,\right] \left[\, \varepsilon(\alpha,\beta) \,\right] \left(1 + \frac{\gamma}{R}\right) d\gamma$$

Similarly,

$$\left[\, M \,\right] = \begin{bmatrix} M_\alpha \\ M_\beta \\ M_{\alpha\beta} \end{bmatrix} = \int_{-h/2}^{+h/2} \left[\, D_3 \,\right] \left[\, \varepsilon(\alpha,\beta) \,\right] \left(1 + \frac{\gamma}{R}\right) \gamma \quad d\gamma$$

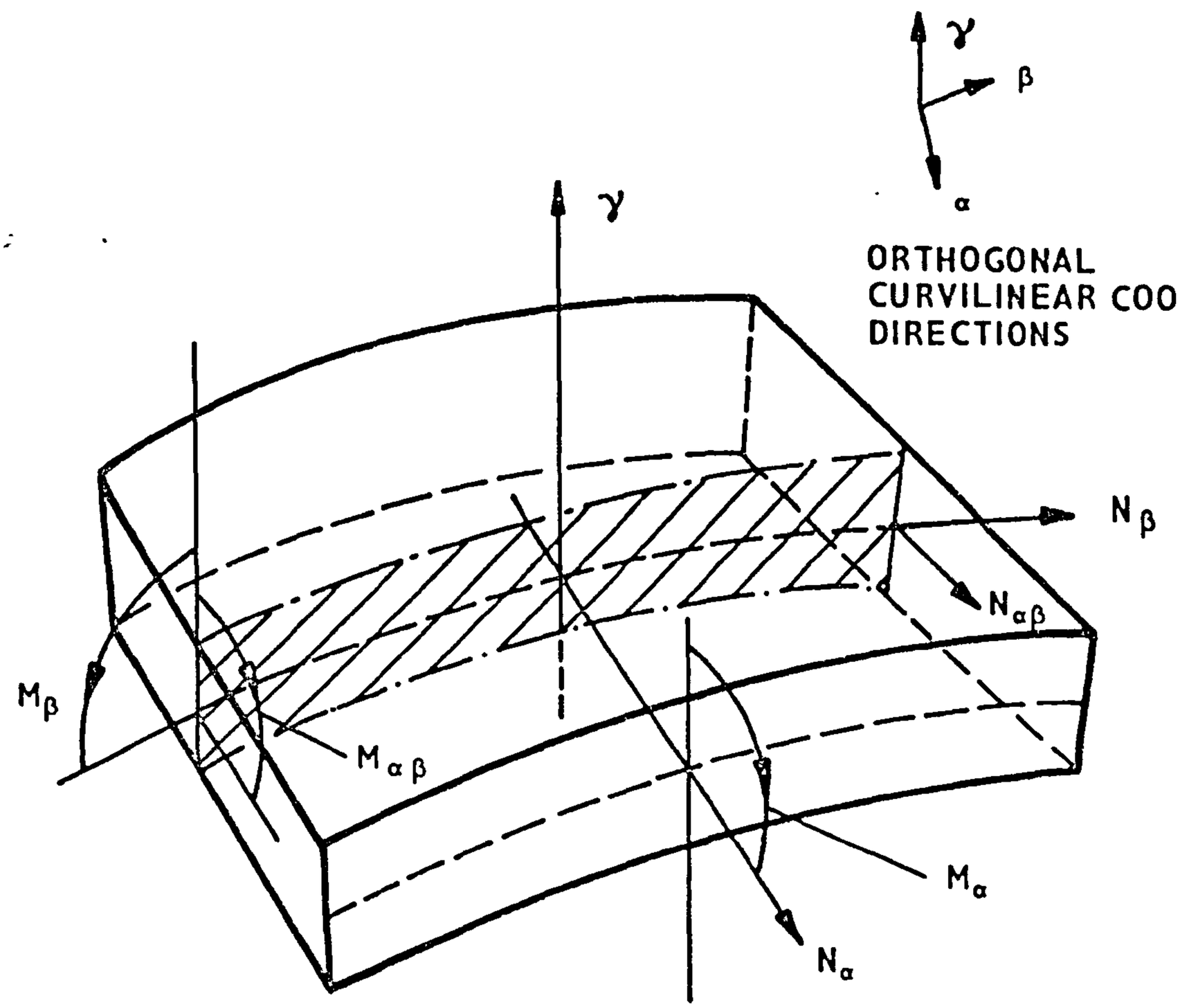

FIG. 4.3a STRESS-RESULTANTS AND MOMENTS

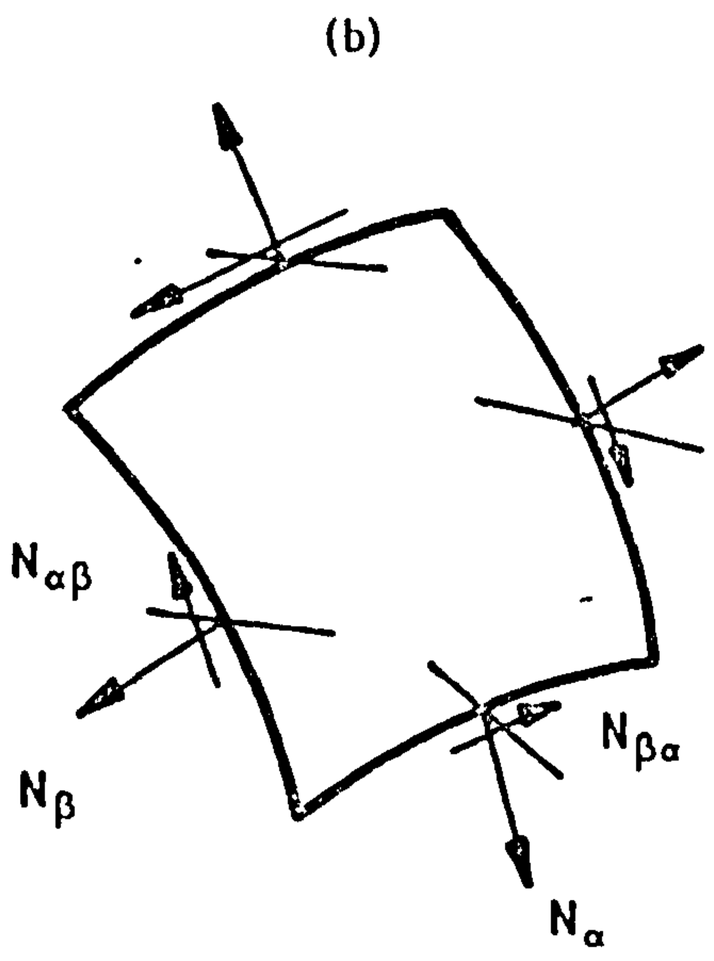

FIG. 4.3b DIRECT STRESS AND SHEARING ACTIONS

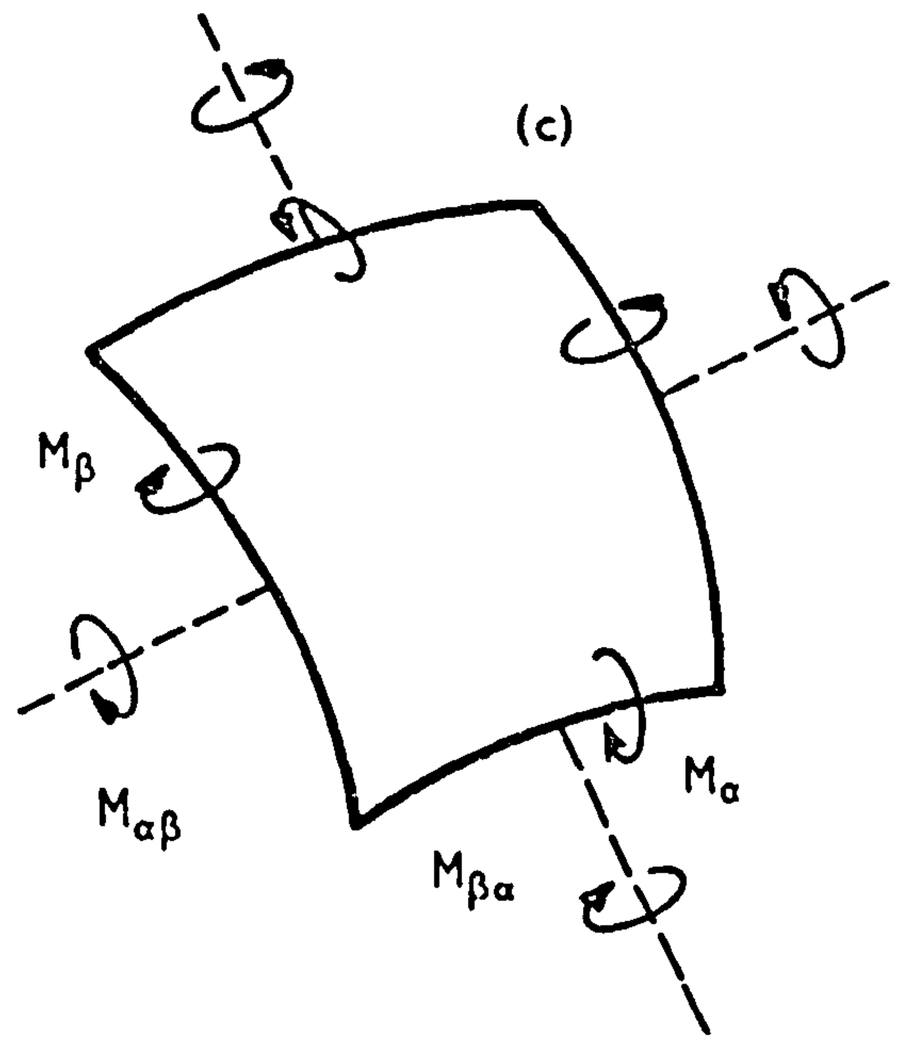

FIG. 4.3c COUPLES

Now integrating, and neglecting terms of order h^4 or smaller we can write

$$\left[N_m \right] = \begin{bmatrix} N \\ M \end{bmatrix} = \begin{bmatrix} N_\alpha \\ N_\beta \\ N_{\alpha\beta} \\ M_\alpha \\ M_\beta \\ M_{\alpha\beta} \end{bmatrix} = \begin{bmatrix} h & \rho h & 0 & \bar{h}\left(\frac{1}{R} - \frac{1}{r}\right) & \frac{\rho\bar{h}}{R}\left(1 - \sin\phi\right) & 0 \\ \rho h & h & 0 & \rho\bar{h}\left(\frac{1}{R} - \frac{1}{r}\right) & \frac{\bar{h}}{R}\left(1 - \sin\phi\right) & 0 \\ 0 & 0 & \nu\left(h + \frac{1}{2}p^2\bar{h}\right) & 0 & 0 & \nu\bar{h}\left(\frac{1}{R} - \frac{\bar{p}}{2}\right) \\ \frac{\bar{h}}{R} & \frac{\rho\bar{h}}{R} & 0 & \bar{h} & \rho\bar{h} & 0 \\ \frac{\rho\bar{h}}{R} & \frac{\bar{h}}{R} & 0 & \rho\bar{h} & \bar{h} & 0 \\ 0 & 0 & \frac{\nu\bar{h}}{R} & 0 & 0 & \nu\bar{h} \end{bmatrix}$$

$$\times \frac{E}{(1 - \rho^2)} \times \left[\varepsilon(\alpha,\beta) \right] \qquad \ldots(4.20a)$$

where $\bar{h} = \frac{h^3}{12}$

i.e. $$\left[N_m \right] = \left[D_4 \right]\left[\varepsilon(\alpha,\beta) \right] \qquad \ldots(4.20b)$$

As before. substituting for $\left[\varepsilon(\alpha,\beta) \right]$,

$$\left[N_m \right] = \left[D_4 \right]\left[B \right]\left[\delta^e \right]$$

i.e.

$$\left[N_m \right] = \left[H_2 \right]\left[\delta^e \right] \qquad \ldots(4.21)$$

Here $\left[H_2 \right]$ is the stress matrix of order (6 × 48) for obtaining the averaged force per unit length of arc in terms of stress resultants and couples. ($\left[D_4 \right]$) is readily obtained from equation (4.20a) and

$[B]$ is evaluated as described previously.) Hence, alternative forms of the stress matrix have been presented as $[H_1]$ and $[H_2]$.

4.6.3 Ring element

The stress matrix for the ring element [40] can be similarly derived. The ring element can be regarded as a special case of the shell element. The relevant differences are as follows:

(a) Ψ is now 2π. Hence numerical differentiation or integration with respect to $\bar{\theta}$ is not necessary.

(b) The nodes of the ring element are taken to be the parallel circles defining the element. Hence, the ring element has two nodes.

(c) The displacements along the parallel circles of the ring element are taken to be sinusoidal or cosinusoidal.

The matrices $[D_3]$ and $[D_4]$ (equations (4.19d) and (4.20b) are not functions of θ and are therefore identical for the ring element. However, $[B_1]$ in equation (4.9b) is a function of θ; hence, it differs (slightly) from the expression given in this text. The ring element has 24 degrees of freedom compared with the 48 degrees of freedom for the shell element. The displacement function is therefore simpler (also see item (c) above) and hence $[P]$ in equation (4.12) is different.

The expression for the strain energy, U, of the ring element can be calculated as indicated in Section 4.5.3, in order to verify the accuracy of the equations used. However, it must be noted that in the expression for the strain energy given by Deb Nath [40, equation (A1)] there is a typographical error. The third bracketed term should read:

$$\frac{h^3}{12}\left(\chi_s^2 + \chi_\theta^2 + 2\nu\,\chi_s\,\chi_\theta + \frac{1-\nu}{2}\,\chi_{s\theta}^2\right)$$

The derivation of the stress matrix of the ring element is as follows. (Where relevant, previous equation numbers, marked with a prime sign, will be used as this will illustrate the similarity between the two derivations.) The equation (4.19) can be written for the ring element as

$$[\sigma(\alpha,\beta,\gamma)] = [D_3][B][\delta^e] = [H_1][\delta^e] \qquad \ldots(4.19a')$$

where $[H_1]$ is the stress matrix.

The alternate form of the stress matrix enabling the stress resultants and couples to be calculated is given by

$$[N_m] = [D_4][B][\delta^e] = [H_2][\delta^e] \qquad \ldots(4.21')$$

For the ring element, $[D_3]$ and $[D_4]$ are given explicitly by equations (4.19d) and (4.20a).

From equation (4.10) an equation of the form

$$[\delta(\alpha,\beta)] = [P'][\delta^e] \qquad \ldots(4.10')$$

is obtained. If $[\delta^e]$, the nodal displacement vector, is re-arranged so that the nodal displacements are grouped according to genre and not according to node number, displacements of the following form will be obtained:-

$$u_1, \frac{\partial u_1}{\partial s}, \frac{\partial^2 u_1}{\partial s^2}, \frac{\partial^3 u_1}{\partial s^3}, u_2, \frac{\partial u_2}{\partial s} \quad \frac{\partial^2 u_2}{\partial s^2} \ldots\ldots \frac{\partial^3 w_4}{\partial s^3} \qquad \ldots(4.22)$$

Let this vector be $[\delta_g^e]$. That is, the orthogonal curvilinear displacements u, v and w in the middle surface of the element are given by

$$\begin{bmatrix} u \\ v \\ w \end{bmatrix} = \begin{bmatrix} u_o \cos n\theta \\ v_o \sin n\theta \\ w_o \cos n\theta \end{bmatrix} = \left[\delta(\alpha,\beta)\right]$$

Here the suffix 'o' denotes amplitude. (In equation (4.22) all the displacement variables are amplitudes. However, for typographical convenience, the 'o' is omitted.)

$$= \begin{bmatrix} \cos n\theta & 0 & 0 \\ 0 & \sin n\theta & 0 \\ 0 & 0 & \cos n\theta \end{bmatrix} \begin{bmatrix} [T] & [0] & [0] \\ [0] & [T] & [0] \\ [0] & [0] & [T] \end{bmatrix} \left[\delta_g^e\right] \quad \ldots(4.23)$$

i.e.

$$\left[\delta(\alpha,\beta)\right] = [A][P]\left[\delta_g^e\right]$$

where $[A]$ is the (3×3) matrix with trigonometric terms and $[P]$ is the (3×3) matrix diagonal in $[T]$ in equation (4.23), and where $[T] = [F_1 \quad LF_2 \quad L^2F_3 \quad L^3F_4 \quad F_5 \quad LF_6 \quad L^2F_7 \quad L^3F_8]$. (The nodal vector $[\delta^e]$ is calculated by the 'free vibration analysis' part of the program. $\left[\delta_g^e\right]$ is obtained merely by re-arranging $[\delta^2]$.)

Here,

$$\begin{bmatrix} F_1 \\ F_2 \\ F_3 \\ F_4 \\ F_5 \\ F_6 \\ F_7 \\ F_8 \end{bmatrix} = \begin{bmatrix} 1 & 0 & 0 & 0 & -35 & 84 & -70 & 20 \\ 0 & 1 & 0 & 0 & -20 & 45 & -36 & 10 \\ 0 & 0 & \frac{1}{2} & 0 & -5 & 10 & -7.5 & 2 \\ 0 & 0 & 0 & \frac{1}{6} & -\frac{2}{3} & 1 & -\frac{2}{3} & \frac{1}{6} \\ 0 & 0 & 0 & 0 & +35 & -84 & 70 & -20 \\ 0 & 0 & 0 & 0 & -15 & 39 & -34 & 10 \\ 0 & 0 & 0 & 0 & 2.5 & -7 & 6.5 & -2 \\ 0 & 0 & 0 & 0 & -\frac{1}{6} & 0.5 & -\frac{1}{2} & \frac{1}{6} \end{bmatrix} \times \begin{bmatrix} 1 \\ \bar{s} \\ \bar{s}^2 \\ \bar{s}^3 \\ \bar{s}^4 \\ \bar{s}^5 \\ \bar{s}^6 \\ \bar{s}^7 \end{bmatrix}$$

Now, from equation (4.14c),

$$[B] = [B_1][P]$$

$$= [B_1'][A][P]$$

where $[B_1']$ is given by:-

$$[B_1'] = \begin{bmatrix} \frac{1}{L}\frac{d}{d\bar{s}} & 0 & \frac{1}{r} \\ \frac{\cos\phi}{R} & \frac{n}{R} & \frac{\sin\phi}{R} \\ -\frac{n}{R} & \left(\frac{1}{L}\frac{d}{d\bar{s}} - \frac{\cos\phi}{R}\right) & 0 \\ -\frac{dr}{Lr^2\,d\bar{s}} & 0 & -\left(\frac{1}{r^2} + \frac{d^2}{L^2\,d\bar{s}^2}\right) \\ -\frac{p\cos\phi}{R} & 0 & -\left(\frac{\sin^2\phi}{R^2} + \frac{\cos\phi}{LR}\frac{d}{d\bar{s}} - \frac{n^2}{R^2}\right) \\ \frac{pn}{R} & p\left(\frac{1}{L}\frac{d}{d\bar{s}} - \frac{\cos\phi}{R}\right) & \frac{2n}{R}\left(-\frac{\cos\phi}{R} + \frac{1}{L}\frac{d}{d\bar{s}}\right) \end{bmatrix}$$

Hence, the alternate forms of the stress matrix are obtained by substituting in either equation (4.19a) (i.e. stress components) or

equation (4.21) (i.e. stress resultants).

4.7 Conclusions

1. The stress matrix for the double-curvature, shell finite element has been derived enabling the stress components at any point in the shell wall to be determined. An alternative form of the stress matrix is also presented that allows the 'averaged' value of stress per unit length of arc, in terms of stress resultants and couples, to be evaluated.

2. The information that has been presented will enable the stress matrices of other doubly curved elements to be derived. By way of illustration the stress matrix of a doubly curved ring finite element has also been derived.

3. The equations used in the derivation of the stress matrix yield an expression for the strain energy that is equal to that obtained previously. This suggests that the equations used in the analysis are correct.

CHAPTER FIVE

AN ALGORITHM FOR PROGRAMMING THE ELEMENT MATRICES OF DOUBLY CURVED FINITE ELEMENTS

1. AN ALGORITHM FOR PROGRAMMING THE ELEMENT MATRICES OF DOUBLY CURVED FINITE ELEMENTS

5.1 Introduction

Writing a computer routine to numerically evaluate the stiffness and mass matrices of doubly curved shell finite elements is a particularly difficult task when adopting a conventional programming approach. The coding is long and complicated and error checking of the routine by the original author or by a program maintenance engineer is extremely tedious. Some degree of uncertainty will, therefore, remain. Also, if it is desired to change the formulation of the element, for example to change the displacement function of the elasticity matrix used in the derivation, it is often more convenient to re-write the whole routine rather than attempt to change the coding.

The derivation of a algorithm for which it is thought that the above criticisms do not apply is presented in this chapter. The basis of the algorithm is that the apparently diverse and complicated matrix calculations are reduced to a few simple manipulations. The algorithm readily lends itself to a structured programming approach and hence this technique (with its attendant advantages of ease of modifying the coding and verifying the accuracy) has been adopted. Therefore, the whole procedure can be verified or modified with ease and a high degree of confidence can be placed in its execution. For ease of explanation the algorithm has been derived for use with the doubly curved shell finite element proposed in Reference 40. However, due to the modular, general nature of the basic technique it can also be readily adapted for use with other types of finite elements.

5.2 Brief Problem Description

The doubly-curved shell finite element [40] has four nodes with twelve degrees of freedom per node. It uses a complicated displacement function [67] and the strain is assumed to vary quadratically through the thickness of the element. The stiffness matrix of the finite element is, therefore, a complicated matrix of order (48 × 48).

The element stiffness matrix is obtained by numerically evaluating the final product of five matrices - see Fig. 5.1. These individual matrices contain terms which are differential operators and operands and the final products must be integrated in two dimensions. The algebraic manipulation involved in obtaining the 2,304 terms of the final matrix is tedious and it is, therefore, difficult to avoid introducing algebraic errors. Moreover, the computer coding required for numerically evaluating the final matrix reflects the complexity of the final expressions, and also has the possibility of containing coding anomalies.

5.3 Theroretical Framework and Computational Procedures

The stiffness matrix of an element can be written as:

$$K_E = \int_{\bar{\theta}=0}^{1} \int_{\bar{s}=0}^{1} [t_o][C][Z(\bar{s})][C]^T [t_o]^T \, d\bar{\theta}.d\bar{s} \quad ...(5.1)$$

The detailed terms included in the matrices are given in Fig. 5.1. The nomenclature used in Fig. 5.1 has been explained in Chapter 4. However, note that; $[t_o]$ is a matrix of order (48 × 3) and is given by equation (4.11) in Chapter 4, $[C]$ is a matrix of order (3 × 6) and is given by the transpose of $[B_1]$ given in equation (4.9b) in Chapter 4, $[Z(\bar{s})]$ is a matrix of order (6 × 6) and is

$$
\begin{bmatrix}
f_1 g_1 & O & O \\
L f_2 g_1 & O & O \\
R\Psi f_1 g_2 & O & O \\
L R\Psi f_2 g_2 & O & O \\
f_1 g_3 & O & O \\
L f_2 g_3 & O & O \\
R\Psi f_1 g_4 & O & O \\
L R\Psi f_2 g_4 & O & O \\
f_3 g_1 & O & O \\
L f_4 g_1 & O & O \\
R\Psi f_3 g_2 & O & O \\
L R\Psi f_4 g_2 & O & O \\
f_3 g_3 & O & O \\
L f_4 g_3 & O & O \\
R\Psi f_3 g_4 & O & O \\
L R\Psi f_4 g_4 & O & O \\
O & f_1 g_1 & O \\
O & L f_2 g_1 & O \\
O & R\Psi f_1 g_2 & O \\
O & L R\Psi f_2 g_2 & O \\
O & f_1 g_3 & O \\
O & L f_2 g_3 & O \\
O & R\Psi f_1 g_4 & O \\
O & L R\Psi f_2 g_4 & O \\
O & f_3 g_1 & O \\
O & L f_4 g_1 & O \\
O & R\Psi f_3 g_2 & O \\
O & L R\Psi f_4 g_2 & O \\
O & f_3 g_3 & O \\
O & L f_4 g_3 & O \\
O & R\Psi f_3 g_4 & O \\
O & L R\Psi f_4 g_4 & O \\
O & O & f_1 g_1 \\
O & O & L f_2 g_1 \\
O & O & R\Psi f_1 g_2 \\
O & O & L R\Psi f_2 g_2 \\
O & O & f_1 g_3 \\
O & O & L f_2 g_3 \\
O & O & R\Psi f_1 g_4 \\
O & O & L R\Psi f_2 g_4 \\
O & O & f_3 g_1 \\
O & O & L f_4 g_1 \\
O & O & R\Psi f_3 g_2 \\
O & O & L R\Psi f_4 g_2 \\
O & O & f_3 g_3 \\
O & O & L f_4 g_3 \\
O & O & R\Psi f_3 g_4 \\
O & O & L R\Psi f_4 g_4
\end{bmatrix}
\quad
\begin{matrix} 1 \\ \vdots \\ \bar{s}=0 \end{matrix}
\quad
\begin{matrix} 1 \\ \vdots \\ \bar{s}=0 \end{matrix}
$$

$$
[C] =
\begin{bmatrix}
\frac{1}{L}\times\frac{\partial}{\partial\bar{s}} & \frac{\cos\phi}{R} & \left(\frac{1}{R\Psi}\times\frac{\partial}{\partial\bar{\theta}}\right) & \frac{-\partial r}{Lr^2\partial\bar{s}} & \frac{-p\cos\phi}{R}\left(\frac{-p}{\Psi R}\times\frac{\partial}{\partial\bar{\theta}}\right) \\
O & \left(\frac{1}{R\Psi}\times\frac{\partial}{\partial\bar{\theta}}\right) & \left(\frac{1}{L}\frac{\partial}{\partial\bar{s}}-\frac{\cos\phi}{R}\right) & O & O \quad p\left(\frac{1}{L}\frac{\partial}{\partial\bar{s}}-\frac{\cos\phi}{R}\right)' \\
\frac{1}{r} & \frac{\sin\phi}{R} & O & \left(-\frac{1}{r^2}-\frac{\partial^2}{L^2\partial\bar{s}^2}\right) & \left(-\frac{\sin^2\phi}{R^2}-\frac{\cos\phi}{LR}\frac{\partial}{\partial\bar{s}}-(\Psi^2R^2)^{-1}\frac{\partial^2}{\partial\bar{\theta}^2}\right) \quad 2\left(\frac{\cos\phi}{\Psi R^2}\frac{\partial}{\partial\bar{\theta}}-\frac{\partial^2}{\Psi RL\partial\bar{\theta}\partial\bar{s}}\right)
\end{bmatrix}
$$

$$
[Z] =
\begin{bmatrix}
z_{11} & z_{12} & O & z_{14} & z_{15} & O \\
z_{21} & z_{22} & O & z_{24} & z_{25} & O \\
O & O & z_{33} & O & O & z_{36} \\
z_{41} & z_{42} & O & z_{44} & z_{45} & O \\
z_{51} & z_{52} & O & z_{54} & z_{55} & O \\
O & O & z_{63} & O & O & z_{66}
\end{bmatrix}
$$

$$
[C]^T =
\begin{bmatrix}
\frac{1}{L}\frac{\partial}{\partial\bar{s}} & O & \frac{1}{r} \\
\frac{\cos\phi}{R} & \frac{1}{R\Psi}\frac{\partial}{\partial\bar{\theta}} & \frac{\sin\phi}{R} \\
\frac{1}{R\Psi}\frac{\partial}{\partial\bar{\theta}} & \left(\frac{1}{L}\frac{\partial}{\partial\bar{s}}-\frac{\cos\phi}{R}\right) & O \\
\left(\frac{-\partial r}{Lr^2\partial\bar{s}}\right) & O & -\left(\frac{1}{r^2}+\frac{1}{L^2}\frac{\partial^2}{\partial\bar{s}^2}\right) \\
-\frac{p\cos\phi}{R} & O & -\left(\frac{\sin^2\phi}{R^2}+\frac{\cos\phi}{LR}\frac{\partial}{\partial\bar{s}}+\frac{1}{\Psi^2R^2}\frac{\partial^2}{\partial\bar{\theta}^2}\right) \\
-\frac{p}{\Psi R}\frac{\partial}{\partial\bar{\theta}} & p\left(\frac{1}{L}\frac{\partial}{\partial\bar{\theta}}-\frac{\cos\phi}{R}\right) & 2\left(\frac{\cos\phi}{\Psi R^2}\frac{\partial}{\partial\bar{\theta}}-\frac{1}{\Psi RL}\frac{\partial^2}{\partial\bar{\theta}\partial\bar{s}}\right)
\end{bmatrix}
$$

$$
[t_o] = \begin{bmatrix} t_o \end{bmatrix}^T
$$

$$
\text{Element Stiffness Matrix, } K_e = \int_{\bar{s}=0}\int_{\bar{\theta}=0} [t_o][C][Z][C]^T[t_o]^T
$$

The polynomials $f_1, f_2 \cdots$ and $g_1, \cdots g_4$ are defined as :-

$f_1(\bar{s}) = 1 - 3\bar{s}^2 + 2\bar{s}^3$ $\qquad$ $g_1(\bar{\theta}) = 1 - 3\bar{\theta}^2 + 2\bar{\theta}^3$

$f_2(\bar{s}) = \bar{s} - 2\bar{s}^2 + \bar{s}^3$ $\qquad$ $g_2(\bar{\theta}) = \bar{\theta} - 2\bar{\theta}^2 + \bar{\theta}^3$

$f_3(\bar{s}) = 3\bar{s}^2 - 2\bar{s}^3$ $\qquad$ $g_3(\bar{\theta}) = 3\bar{\theta}^2 - 2\bar{\theta}^3$

$f_4(\bar{s}) = -\bar{s}^2 + \bar{s}^3$ $\qquad$ $g_4(\bar{\theta}) = -\bar{\theta}^2 + \bar{\theta}^3$

given by $[D]$, in equation (4.18a) of Chapter 4.

The individual terms constituting the matrices in equation (5.1) must be studied for a full appreciation of the difficulties involved in formulating a computer coded routine (therefore see Fig. 5.1). Note that it is tempting to multiply $[C][Z(\bar{s})][C]^T$ to obtain a matrix of order (3 × 3). This is incorrect as $[C]^T$ must first operate on $[t_o]^T$ and $[t_o]$ must first be operated on by $[C]$. That is, the equation given in Fig. 5.1 only implies the order or multiplication and not the order in which the differential operations are to be performed. Thus, $[t_o][C]$ must first be evaluated before the product is used to multiply $Z(\bar{s})$, and $[C]^T[t_o]^T$ must be evaluated before $[t_o][C][Z(\bar{s})]$ is allowed to operate on $[C]^T[t_o]^T$. (Note that $[t_o][C]$ is a strain-tensor.)

We now rewrite the equation (5.1) as:

$$K_E = \iint \begin{bmatrix} [t] & [o] & [o] \\ [o] & [t] & [o] \\ [o] & [o] & [t] \end{bmatrix} \times \begin{bmatrix} C_{11} & C_{12} \cdots C_{16} \\ C_{21} \cdots\cdots\cdots \\ C_{31} \cdots\cdots\cdots C_{36} \end{bmatrix} [Z(\bar{s})][C]^T[t_o]^T \, d\bar{\theta}. \qquad \ldots(5.2)$$

$[t]$ is a column vector of order (16 × 1) and is a sub-matrix of the matrix $[t_o]$.

Equation (5.2) can be re-written as

$$K_E = \iint \begin{bmatrix} b_{11} & b_{12} \cdots\cdots b_{16} \\ b_{21} \cdots\cdots\cdots\cdots\cdots \\ b_{31} \cdots\cdots\cdots\cdots\cdots \end{bmatrix} [Z(\bar{s})][C]^T[t_o]^T \, d\bar{s}.d\bar{\theta} \qquad \ldots(5.3a)$$

where $b_{ij} = [t][C_{ij}]$ ...(5.3b)

Note that the b_{ij} are now sub-matrices of order (16 × 1).

Equation (5.3) can be re-written as:

$$K_E = \iint [B][Z(\bar{s})][B]^T = \begin{bmatrix} k_{11} & k_{12} & k_{13} \\ k_{21} & k_{22} & k_{23} \\ k_{31} & k_{32} & k_{33} \end{bmatrix} \quad \ldots(5.4)$$

the matrix $[B]$ contains the sub-matrices b_{ij} and is of order (48 × 6).

Equation (5.4) can be expanded by elementary matrix manipulations, thus:

$$k_{11} = \iint (b_{11}\ z_{11}\ b_{11} + \ldots\ldots)\ d\bar{s}.d\bar{\theta}$$

The complete expressions for the symmetrical matrix K_E is given on the following page by equation (5.5):

$$k_{11} = \iint [\; (b_{11}\, z_{11}\, b_{11} + b_{12}\, z_{21}\, b_{11} + b_{14}\, z_{41}\, b_{11} + b_{15}\, z_{51}\, b_{11}) + (b_{11}\, z_{12}\, b_{12} + b_{12}\, z_{22}\, b_{12} + b_{14}\, z_{42}\, b_{12} + b_{15}\, z_{52}\, b_{12}) + (b_{13}\, z_{33}\, b_{13} + b_{16}\, z_{63}\, b_{13}) + (b_{11}\, z_{14}\, b_{14} + b_{12}\, z_{24}\, b_{14} + b_{14}\, z_{44}\, b_{14} + b_{15}\, z_{54}\, b_{14}) + (b_{11}\, z_{15}\, b_{15} + b_{12}\, z_{25}\, b_{15} + b_{14}\, z_{45}\, b_{15} + b_{15}\, z_{55}\, b_{15}) + (b_{13}\, z_{36}\, b_{16} + b_{16}\, z_{66}\, b_{16})] \; d\bar{s}.d\bar{\theta}$$

$$k_{22} = \iint [\; (b_{22}\, z_{22}\, b_{22}) + (b_{23}\, z_{33}\, b_{23} + b_{26}\, z_{63}\, b_{23}) + (b_{23}\, z_{36}\, b_{26} + b_{26}\, z_{66}\, b_{26})] \; d\bar{\theta}.d\bar{s}$$

$$k_{33} = \iint [\; (b_{31}\, z_{11}\, b_{31} + b_{32}\, z_{21}\, b_{31} + b_{34}\, z_{41}\, b_{31} + b_{35}\, z_{51}\, b_{31}) + (b_{31}\, z_{12}\, b_{32} + b_{32}\, z_{22}\, b_{32} + b_{34}\, z_{42}\, b_{32} + b_{35}\, z_{52}\, b_{32}) + (b_{31}\, z_{14}\, b_{34} + b_{32}\, z_{24}\, b_{34} + b_{34}\, z_{44}\, b_{34} + b_{35}\, z_{54}\, b_{34}) + (b_{31}\, z_{15}\, b_{35} + b_{32}\, z_{25}\, b_{35} + b_{34}\, z_{45}\, b_{35} + b_{35}\, z_{55}\, b_{35}) + (b_{36}\, z_{16}\, b_{36})] \; d\bar{\theta}.d\bar{s}$$

$$k_{21} = \iint [\; (b_{22}\, z_{21}\, b_{11}) + (b_{22}\, z_{22}\, b_{12}) + (b_{23}\, z_{33}\, b_{13} + b_{26}\, z_{63}\, b_{13}) + (b_{22}\, z_{24}\, b_{14}) + (b_{22}\, z_{25}\, b_{15}) + (b_{23}\, z_{36}\, b_{16} + b_{26}\, z_{66}\, b_{16})] \; d\bar{\theta}.d\bar{s}$$

$$k_{31} = \iint [\; (b_{31}\, z_{11}\, b_{11} + b_{32}\, z_{21}\, b_{11} + b_{34}\, z_{41}\, b_{11} + b_{35}\, z_{51}\, b_{11}) + (b_{31}\, z_{12}\, b_{12} + b_{32}\, z_{22}\, b_{12} + b_{34}\, z_{42}\, b_{12} + b_{35}\, z_{52}\, b_{12}) + (b_{36}\, z_{63}\, b_{13}) + (b_{31}\, z_{14}\, b_{14} + b_{32}\, z_{24}\, b_{14} + b_{34}\, z_{44}\, b_{14} + b_{35}\, z_{54}\, b_{14}) + (b_{31}\, z_{15}\, b_{15} + b_{32}\, z_{25}\, b_{15} + b_{34}\, z_{45}\, b_{15} + b_{35}\, z_{55}\, b_{15}) + (b_{36}\, z_{66}\, b_{16})] \; d\bar{\theta}.d\bar{s}$$

$$k_{32} = \iint [\; (b_{31}\, z_{12}\, b_{22} + b_{32}\, z_{22}\, b_{22} + b_{34}\, z_{42}\, b_{22} + b_{35}\, z_{52}\, b_{22}) + (b_{36}\, z_{63}\, b_{23}) + (b_{36}\, z_{66}\, b_{26})] \; d\bar{\theta}.d\bar{s}$$

...(5.5)

All the k-matrices have not been included in equation (5.5) as K_E is symmetrical and thus $k_{ij} = k_{ji}$. Also note that though each k-matrix is a summation of thirty-six matrix terms, some of the matrix terms are zero matrices (as the Z matrix in Fig. 5.1 contains zero terms), and hence only the non-zero matrix terms are entered in equation (5.5).

Each term of the stiffness matrix K_E can be written in terms of the ij^{th} term of the sub-matrix, $k_{m\ell}$ in the following form:

$$k^{ij}_{m\ell} = \int_{\bar{s}=0}^{1} \int_{\bar{\theta}=0}^{1} \sum_{\bar{k}=1}^{6} \sum_{\bar{h}=1}^{6} b^{i}_{m\bar{k}} \; z_{\bar{k}\bar{h}} \; b^{j}_{\bar{h}\ell} \; d\bar{s}.d\bar{\theta} \qquad \ldots(5.6)$$

where the m and ℓ suffices have the range 1 to 3 respectively (e.g. m, ℓ = 1, 3). For typographical convenience we omit the transpose sign for the 'ending b-terms'.

The suffices $\bar{k}$ and $\bar{h}$ range from 1 to 6. The column vector $b_{m\bar{k}}$ is defined by equation (5.3b). Thus, with reference to $b^{i}_{m\bar{k}}$ the suffices m and $\bar{k}$ denote the particular term of the matrix $[C]^{m\bar{k}}$ given in equation (5.3b) and the superscript i denotes the particular row of the column vector $[t]$.

Consider the term b^{i}_{mk}. Let it be written as

$$b^{i}_{mk} = H_{mk}.A_{mk}.t^{i}$$

The usual indicial notation where double sufficies are taken to mean summation is <u>not</u> being employed. Here, H_{mk} is a differential operator associated with the term C_{mk}, A_{mk} is the scalar associated with the differential operator, and t^{i} is a term

of the column matrix defined in equation (5.2); t^i is therefore the differential operand. For example consider the term $b^2_{16} = \frac{-p}{\psi R} \frac{\partial}{\partial \bar{\theta}} (Lf_2\, g_1)$; see Fig. 5.1. Here $H_{16} = \frac{\partial}{\partial \bar{\theta}}$, $A_{16} = -\frac{p}{\psi R}$ and $t^2 = Lf_2 g_1$.

We can now re-write equation (5.6) as:

$$K^{ij}_{m\ell} = \iint \sum_{\bar{k}=1}^{6} \sum_{\bar{h}=1}^{6} (H_{m\bar{k}}.A_{m\bar{k}}.t^i).(z_{\bar{k}\bar{h}}).(H_{\bar{h}\ell}.A_{\bar{h}\ell}.t^j)\, d\bar{s}.d\bar{\theta} \qquad ...(5.7)$$

Equation (5.7) is the mathematical basis for the method. The computational aspects of evaluating the terms of the equation will now be explained.

Consider t^i where i can take any value from 1 to 16. A particular value of i will give a term which is a product of the interpolation polynominals f and g (and other parameters). Also, consider the differential operator $H_{m\bar{k}}$ in equation (5.7). Computationally it is not possible to accord this variable an identity of its own. However, the quantity $(H_{m\bar{k}} t^i)$ can be considered as a computational variable. $H_{m\bar{k}}$ can be any one of six differential operators (see matrix C in Fig. 5.1)i.e. 'no differentiation', $\frac{\partial}{\partial \bar{s}}$, $\frac{\partial}{\partial \bar{\theta}}$, $\frac{\partial}{\partial \bar{s}^2}$, $\frac{\partial}{\partial \bar{\theta}^2}$ and $\frac{\partial^2}{(\partial \bar{\theta}\ \partial \bar{s})}$. Thus, in principle, it is necessary to prepare six one-dimensional arrays each of order 16. That is t, $\frac{\partial t}{\partial \bar{s}}$, $\frac{\partial}{\partial \bar{\theta}}$..... $\frac{\partial^2 t}{(\partial \bar{\theta}\ \partial \bar{s})}$. However, in practice it is advantagous to partition and simplify the vector t and then to perform the differentiation on the sub-matrices of this vector.

Let

$$[t] = \begin{bmatrix} \delta_1 \\ \delta_2 \\ \delta_3 \\ \delta_4 \end{bmatrix}$$ where each δ column vector is of order 4.

(Note that $[t]$ is the displacement function of the shell element. It has been sub-divided into four vectors as a four-noded element is being considered. In a general analysis, therefore, the vector $[t]$ can be sub-divided into as many nodes as are contained within the finite element.)

Now the $[\delta_1]$, $[\delta_2]$, $[\delta_3]$ and $[\delta_4]$ matrices can be written generally as:-

$$[\delta_n] = \begin{bmatrix} f_y \cdot g_{\lambda+1} \\ Lf_{y+1} \cdot g_{\lambda+1} \\ R\psi f_y \cdot g_{\lambda+2} \\ LR\psi f_{y+1} \cdot g_{\lambda+2} \end{bmatrix} \quad \ldots(5.8)$$

where λ is 0 if n is odd and 2 if n is even. y is 1 if n is less than 3 and 3 if n is greater than 2. {n varies from 1 to 4.}

$[\delta_n]$ can be simplified (from a purely computational view-point) as

$$[\delta_n] = (a.f_d.g_e) \quad \ldots(5.9)$$

The values of a, d and e vary with i (which is given in equation (5.7)) and are given in the following Table:

i	a	d	e
1	1	1	1
2	L	2	1
3	Rψ	1	2
4	LRψ	2	2
5	1	1	3
6	L	2	3
7	Rψ	1	4
8	LRψ	2	4
9	1	3	1
10	L	4	1
11	Rψ	3	2
12	LRψ	4	2
13	1	3	3
14	L	4	3
15	Rψ	3	4
16	LRψ	4	4

It is now necessary to differentiate analytically only the Hermite interpolation polynomials f_1, f_2, f_3, f_4 and $g_1 \ldots\ldots g_4$. The computer code can be used to assemble the differentiation of products of functions of $\bar{s}$, such as R, and the f-polynomials. Returning now to equation (5.7) it is necessary only to note the type of differential operation signified by $H_{\underline{mk}}$ at an early state of the computational procedure and to use this information to select the appropriate differentiated form of the f and g polynomials at a later stage. At the early stage it is also convenient to allow the computational procedure to select the appropriate values of $A_{\underline{mk}}$, $z_{\underline{kh}}$ and $A_{\underline{h\ell}}$. The possibility of 'human error' is thus reduced to a minimum.

The partitioning and simplification of the displacement function $[t]$ enables a corresponding increase in the theoretical flexibility of the procedure to be made. For example, if it is required to extend the generality of the shell element by allowing variation in the geometrical properties of the structure with the circumferential position ($\bar{\theta}$) this approach is invaluable.

The above deals with the differentiation of the terms of $k_{m\ell}^{ij}$. The integration procedure is explained by re-writing equation (5.7) as:

$$k_{m\ell}^{ij} = \int_{\bar{\theta}=o}^{1} G(\bar{\theta})\,d\bar{\theta} \int_{\bar{s}=0}^{1} F(\bar{s})\,d\bar{s}\,, \qquad \ldots(5.10)$$

where the terms which are functions of $\bar{s}$ and $\bar{\theta}$ are separated and written as $F(\bar{s})$ and $G(\bar{\theta})$ respectively. At the present the geometrical properties are assumed not to vary with $\bar{\theta}$ and therefore $G(\bar{\theta})$ is integrated analytically. However, as the geometrical properties are functions of $\bar{s}$, $F(\bar{s})$ has to be computed by a numerical method.

{Gaussian-Quadrature integration is used, Kronrod [69]. } When the geometrical properties are not functions of $\bar{s}$, as for a cylinder, $F(\bar{s})$ is evaluated analytically. The above procedure minimizes the errors in numerical integration and also reduces the computing time.

In order to get ideas fixed, consider the following examples.

In equation (5.7) let i = 2, j = 7, m = 1 and ℓ = 1 for $\bar{k} = 1$ and $\bar{h} = 1$.

i.e.

$$k_{11}^{27}\Big|_{\substack{\bar{k}=1\\ \bar{h}=1}} = \int_{\bar{s}=0}^{1}\int_{\bar{\theta}=0}^{1}\left(\frac{\partial}{\partial\bar{s}}\cdot\frac{1}{L}.Lf_2g_1\right)\left(z_{11}\right)\left(\frac{\partial}{\partial\bar{s}}\cdot\frac{1}{L}.R\psi f_1g_4\right)d\bar{s}.d\theta$$

z_{11} is given by equation (4.18b) in Chapter 4 and is:

$$= R\left(h + \frac{h^3}{12}\frac{\sin\phi}{Rr}\right)$$

i.e.

$$k_{11}^{27}\Big|_{\substack{\bar{k}=1\\ \bar{h}=1}} = \int_{\bar{\theta}=0}^{1} g_1g_4\, d\bar{\theta}\int_{\bar{s}=0}^{1} R\left(h + \frac{h^2}{12}\ \frac{\sin\phi}{Rr}\right)\left(\frac{R\psi}{L}\right)\left(\frac{\partial f_2}{\partial\bar{s}}.\frac{\partial f_1}{\partial\bar{s}}\right)\ d\bar{s}$$

and is in the form given in equation (5.10).

The sub-matrix $k_{m\ell}$ is obtained by repeating calculations similar to the above example many times. (Note that some of the matrix-terms of $k_{m\ell}$ are merely the transpose of other terms, or are symmetrical.)

The (whole) element stiffness matrix, K_E, is therefore assembled in the above fashion - i.e. by repeating a comparatively simple expression a very large number of times (about 1 million). Thus in principle, the validity of the calculation procedure is verified merely by very careful verification of the computer coding used for the basic manipulation.

The element mass matrix has not been considered in this chapter - it is very simple in comparison to the stiffness matrix, and can be programmed in a similar fashion to the above.

Finally note that for explanatory purposes only single or mono-operators have been considered. However, duo- or even tri-operators have to be oonsidered in the actual calculation. An example of the latter is:-

$$-\left(\frac{\sin^2\phi}{R^2} + \frac{\cos\phi}{LR}\,\frac{\partial}{\partial s} + \frac{1}{\psi^2 R^2}\cdot\frac{\partial}{\partial\theta^2}\right)$$

This leads to only a little more computing sophistication as the permutations of the differential operations and associated scalars have to be summed. Again this is a repetitive procedure involving the basic calculation referred to above. The summation is over four terms for duo-operators and nine terms for tri-operators. The derivation of the expression for duo-operators is given in the Appendix 5.1.

5.4 Discussion

The simplicity of the method has been demonstrated since the conception, implementation and preliminary testing of the computer coding required only eleven working days. A block diagram of the

subroutines used for the purpose is given in Fig. 5.2.

The above technique was then used to form the stiffness and mass matrices of the shell finite element. The present method gave excellent results thereby confirming a small but theoretically very significant error in the coding used previously to program the shell and stiffness matrices.

The 'anomaly' in the displacement function discussed in Appendix 12.1 was investigated successfully. This investigation highlighted a feature of the present method (i.e. theoretical flexibility) as changes to the displacement function were made by a few simple changes to the coding. A conventional programming approach would have resulted in complicated changes of coding format with the attendant risk of introducing errors. Similar ease in changing the coding is envisaged if other changes to the theoretical assumptions basic to the present finite element have to be made.

5.5 Conclusions

A new algorithm to evaluate the stiffness matrix of a doubly curved shell finite element has been derived and shown to be accurate and easy to implement. It has been shown that the apparent diverse and complicated matrix calculations required to obtain the stiffness matrix can be reduced to a basic numerical expression that is then repeated a large number of times. Error checking of the coding is simple. Because of the general modular nature of the numerical scheme theoretical changes to the finite element can be easily implemented. Moreover, adaption of the technique to other finite elements is straightforward.

R = very approximate REGION SIZE

Main calling routine

KFORM S = 130 R = 2·7K

Common blocks

1	C DATA	5
2	CMATRX	15
3	GAUS	0·6
4	DUTT	3·0
5	CUSE	15·8
6	STIF	37
7	TRAN	0·060
8	KMAUC	0·20
9	CKFORM	0·040
10	CPROC	0·004
11	CAP	12

K11 S = 40 R = 0·9K — **K22** S = 19 R = 0·5 — **K33** S = 35 R = 0·8 — **K21** S = 25 R = 0·6 — **K31** S = 30 R = 0·9 — **K32** S = 20 R = 0·5

Calling routines for individual sub-matrices. (Initializes the sufficies)

BZB S = 25 R = 0·9

Arranges calls to S/R's BB, ZVALS and KSUBT

BB S = 123 R = 2·0K

Initializes A_{mk} and A_{hl} Specifies whether mono- duo- or tri- operators

ZVALS

Initializes Z_{kh}

KSUBT S = 60 R = 1·6K

Copies transpose of a (16×16) matrix term, if required: COPIES the (16×16) matrix into stiffness matrix

S/R TZT obtains a 16 × 16 matrix term

TZT S = 20 R = 0·5

MULTIPLIES THE 8-vectors associated with b^{I}_{mk} and the 8-vectors associated with b^{J}_{hl}.

S/R DELTAI obtains a 4 × 4 matrix term

DELTAI S = 25 R = 0·6

PERFORMS MATRIX MULTIPLICATION OF A PAIR OF 8-vectors. SPECIFIES VALUES OF a, d and e.

S/R PROC obtains a 'final' single term

PROC S = 40 R = 0·8

ARRANGES PERMUTAT-IONS WHEN DUO- OR TRI-OPERATORS ARE PRESENT

GINTEG S = 20 R = 0·5

These two S/R's obtain the integrated value of the g-polynomials

GINTAX S = 40 R = 0·8

TWO S = 30 R = 0·8

OBTAINS INTEGRATED VALUES OF BOTH f and g functions and THEN MULTIPLIES THE PRODUCTS

PROCAX S = 40 R = 0·8

PROCESSES THE TERM $H_{mk}(a\ f_d)$

S/R 'TWO' INTEGRATES THE FUNCTION $\int G(\bar{e})\,d\bar{e} \int F(\bar{s})\,d\bar{s}$

Total Region Size (approx:) = 18½K bytes
Source Statements (") = 800

CHAPTER SIX

GEOMETRICAL ANALYSES

6. GEOMETRICAL ANALYSES

This chapter considers several analyses of a geometrical nature that are of importance in the analysis of cooling towers and allied structures.

6.1 Description of Meridian

Certain types of shells of revolution have meridional curvature that cannot be properly described by exact geometrical equations. For example, a nominally hyperboloidal cooling tower shell may have meridional curvature that is not truly hyperbolic, but which is more accurately described by a function such as a polynomial. Such a meridian is referred to as a 'general meridian'. It is best described by determining several points on the meridian and then using this information to obtain a function describing the curve. The points on the meridian can be defined in terms of their distance (R) from the axis-of-revolution (Z-axis), along a line perpendicular to it and the Z-coordinate of the point of intersection on the Z-axis. The function can be then used to calculate the geometrical parameters (e.g. $\frac{\sin \phi}{R}$ - see Section 4.2).

In the program VACTIL [5] either a polynomial or cubic spline function is used to define the meridian. Note that any method that does not allow a prior knowledge of the coordinates at the bottom of the shell of revolution is unacceptable. This is because the coordinates of the node common to the cooling tower shell and the leg-support must be specified as identical. Otherwise, there will be discontinuity of displacements at the common node because of the different displacements that would be predicted by the displacement functions of the finite elements used to model the shell and leg-supports.

We first consider the polynomial representation of the meridian. The radius of revolution, R, at any point on the meridian can be given as

$$R = A_o + A_1 z^1 + ... + A_{n-1} z^{n-1} \qquad ... (6.1)$$

where n is the number of R and Z pairs defining n points on the meridian. z is normalised with respect to the axial length of the meridian (i.e. $0 \leq z \leq 1$) and is defined as zero at the top of the meridian. For any value of the independent variable (z) R is obtained, given the coefficients of the polynomial (i.e. A_o, A_1, A_2....A_{n-1}). If h pairs of R and Z values are available, then in matrix form

$$[R] = \begin{bmatrix} 1 & z_1 & z_1^2 & z_1^3 & ..... & z_1^{n-1} \\ 1 & z_2 & z_2^2 & z_2^3 & ..... & z_2^{n-1} \\ \vdots & \vdots & \vdots & \vdots & & \vdots \\ 1 & z_n & z_n^2 & z_n^3 & ..... & z_n^{n-1} \end{bmatrix} \cdot \begin{bmatrix} A_o \\ A_1 \\ \vdots \\ A_{n-1} \end{bmatrix} \qquad ... (6.2)$$

where $[R]$ is a column vector of order n. We can write equation (6.2) as

$$[R] = [Q][A] \qquad ... (6.2b)$$

where Q is the matrix of order (n × n).

Therefore, the coefficients of the polynomial are given as

$$[A] = [Q]^{-1}[R] \qquad ... (6.2c)$$

The equations (6.2b) or (6.2c) can be solved to obtain the coefficients $[A]$. However, the matrix $[Q]$ is ill-conditioned. For a typical problem, with n = 12 (say), the determinant is of the order of 10^{-30}. Thus usual techniques [74] used to solve for $[A]$ in equations (6.2b) or (6.2c) may lead to incorrect solutions due to rounding-errors.

A simple technique can be derived that can minimize the rounding errors, if use is made of the special characteristics of $[Q]$. Consider the simple matrix equation:

$$\begin{bmatrix} 1 & z_1 & z_1^2 \\ 1 & z_2 & z_2^2 \\ 1 & z_3 & z_3^2 \end{bmatrix}^{-1} = (-1)^3 \begin{bmatrix} +z_2z_3 & -z_3z_2 & +z_1z_2 \\ -(z_2 + z_3) & +(z_3 + z_1) & -(z_1 + z_2) \\ +1 & -1 & +1 \end{bmatrix}$$

$$\times \begin{bmatrix} \frac{(-1)^1}{(z_1 - z_2)(z_1 - z_3)} & 0 & 0 \\ 0 & \frac{(-1)^2}{(z_2 - z_1)(z_2 - z_3)} & 0 \\ 0 & 0 & \frac{(-1)^3}{(z_3 - z_1)(z_3 - z_2)} \end{bmatrix} \quad \ldots (6.3)$$

The right-hand side of equation (6.3) is merely a factorization of the (3 × 3) matrix on the left-hand side of the equation. The factorization process is deduced by studying equation (6.3) and the following equation:-

$$(z_1 - z_2)(z_1 - z_3) = 1 \times z_1^2 - (z_2 + z_3) \times z_1^1 + (z_2z_3)$$

We can similarly factorize the matrix $[Q]^{-1}$ of order n, thus:-

$$
(-1)^n \begin{bmatrix}
(z_2z_3 \ldots z_n)(-1)^{1+1} & (z_3z_4 \ldots z_nz_1)(-1)^{1+2} & \ldots \\
\vdots & \vdots & \vdots \\
(z_2z_3z_4 + z_2z_3z_5 + \ldots)(-1)^{n-3+1} & (z_3z_4z_5 + z_3z_4z_6 + \ldots)(-1)^{n-3+2} & \ldots \\
(z_2z_3 + z_2z_4 + z_2z_5 + \ldots)(-1)^{n-2+1} & (z_3z_4 + z_3z_5 + z_3z_6 + \ldots)(-1)^{n-2+2} & \ldots \\
(z_2 + z_3 + z_4 + \ldots)(-1)^{n-1+1} & (z_3 + z_4 + z_5 + \ldots)(-1)^{n-1+2} & \ldots \\
1 \times (-1)^{n+1} & 1 \times (-1)^{n+2} & \ldots
\end{bmatrix}
$$

$$
\times \begin{bmatrix}
\dfrac{(-1)^1}{(z_1 - z_2)(z_1 - z_3)\ldots} & 0 & 0 & \ldots \\
0 & \dfrac{(-1)^2}{(z_2 - z_1)(z_2 - z_3)\ldots} & 0 & \ldots \\
0 & 0 & \ddots & \\
\vdots & \vdots & \dfrac{(-1)^n}{(z_n - z_1)(z_n - z_2)\ldots} & \ldots \\
0 & 0 & & \ldots
\end{bmatrix}
$$

... (6.4)

The relative merits of using the above technique is observed in Table 6.1. (It is clearly seen that the Factorization Method yields the least error.)

Table 6.1: 'Error Parameter' Values for the Three Methods of Inverting [Q]

	Error Parameter	
	for n = 13	for n = 20
DINV	10^{-3}	(solution not found)
MA2IAD	10^{-4}	10^{+10}
FACTORIZATION METHOD	10^{-8}	0.06

DINV is a double precision I.B.M. subroutine that inverts the matrix [Q] by elementary transformations ('pivots' are selected so that rounding errors are minimized). MA2IAD is a Harwell subroutine that 'factorizes' matrices in order to reduce the effects of ill-conditioning.

The 'error parameter' is obtained as follows: the matrix [Q] is multiplied by the computed inverse. The product is a matrix with diagonal terms of unity. The non-diagonal terms should theoretically be zero, but due to rounding errors are usually non-zero. The largest non-diagonal term is termed the 'error parameter' and is a rough guide to the errors generated by the inversion routine.

An alternate representation of the meridian is obtained using a cubic spline interpolation technique [92, page 156]. A spline can be briefly described as follows:-

A spline of degree m through a set of points (z_i, R_i) for $i = 1, 2 \ldots n$ is a function which is a polynomial of degree m in each interval $[z_j, z_{j+1}]$ for $(1 \leq j \leq n-1)$ and of continuous $(m-1)^{th}$ derivative throughout the whole interval $[z_i, z_n]$ and which takes the values R_i at z_i, $i = 1, 2 \ldots n$. It has (m-1) degrees of freedom and in general (m-1) pieces of information define it completely. If P and Q are two splines passing through (z_i, R_i), $i = 1, 2 \ldots n$, then $\lambda P + (1 - \lambda)Q$ is another spline passing through (z_i, R_i), $i = 1, 2 \ldots n$.

A cubic spline (m = 3) has two degrees of freedom and therefore two pieces of information are required to define it completely. In VACTIL the spline-subroutine uses the supplied data (i.e. n pairs of R and Z values) to estimate $\frac{\partial^2 R}{\partial z^2}$ at $z = z_1$ and $z = z_2$. There are other methods of obtaining the two pieces of information that are required. For example, the user could specify the information or alternatively the routine can be made to chose the spline by minimizing the sum of the wrighted squares of

the jumps in the third derivative at the data points. However, whilst these other methods may be more suitable for specific problems, in general the option chosen for use in VACTIL appears to give very satisfactory results.

The above methods have been discussed with respect to the 'R and Z' values defining the meridia of a general curve. However, the techniques discussed above are also used in the program to interpolate other geometrical information, such as thickness variation along the shell.

Of the two methods discussed, the author has found that in general the cubic spline interpolation technique is preferable for defining cooling tower meridia.

6.2 Transformation from Cylindrical to Curvilinear Displacements

As will be seen later, the leg-supports of cooling towers are modelled by beam-elements [70] in the program VACTIL. The coordinate system of the beam element is cylindrical whilst the local coordinate system of the shell element is orthogonal-curvilinear as discussed in Section 4.2. Therefore, a common or global coordinate system must be used. This is chosen to be the cylindrical coordinate system. This section details the theoretical and computational aspects of the co-ordinate transformation.

From the geometry of Fig. 6.1 we obtain:

$$\begin{bmatrix} u_s \\ v_s \\ w_s \end{bmatrix} = \begin{bmatrix} \sin\phi & 0 & \cos\phi \\ 0 & 1 & 0 \\ -\cos\phi & 0 & \sin\phi \end{bmatrix} \begin{bmatrix} u_b \\ v_b \\ w_b \end{bmatrix}$$

SHELL

U_S = DISPLACEMENT TANGENTIAL TO SHELL SURFACE

W_S = DISPLACEMENT NORMAL AT SHELL SURFACE

V_S = DISPLACEMENT ORTHOGONAL TO U_S AND W_S CONSISTENT WITH A 'RIGHT-HAND' SET OF AXES

BEAM

U_b, V_b, W_b ARE THE DISPLACEMENTS ALONG THE CYLINDRICAL COORDINATE AXES (I.E. GLOBAL DISPLACEMENTS – SEE TEXT)

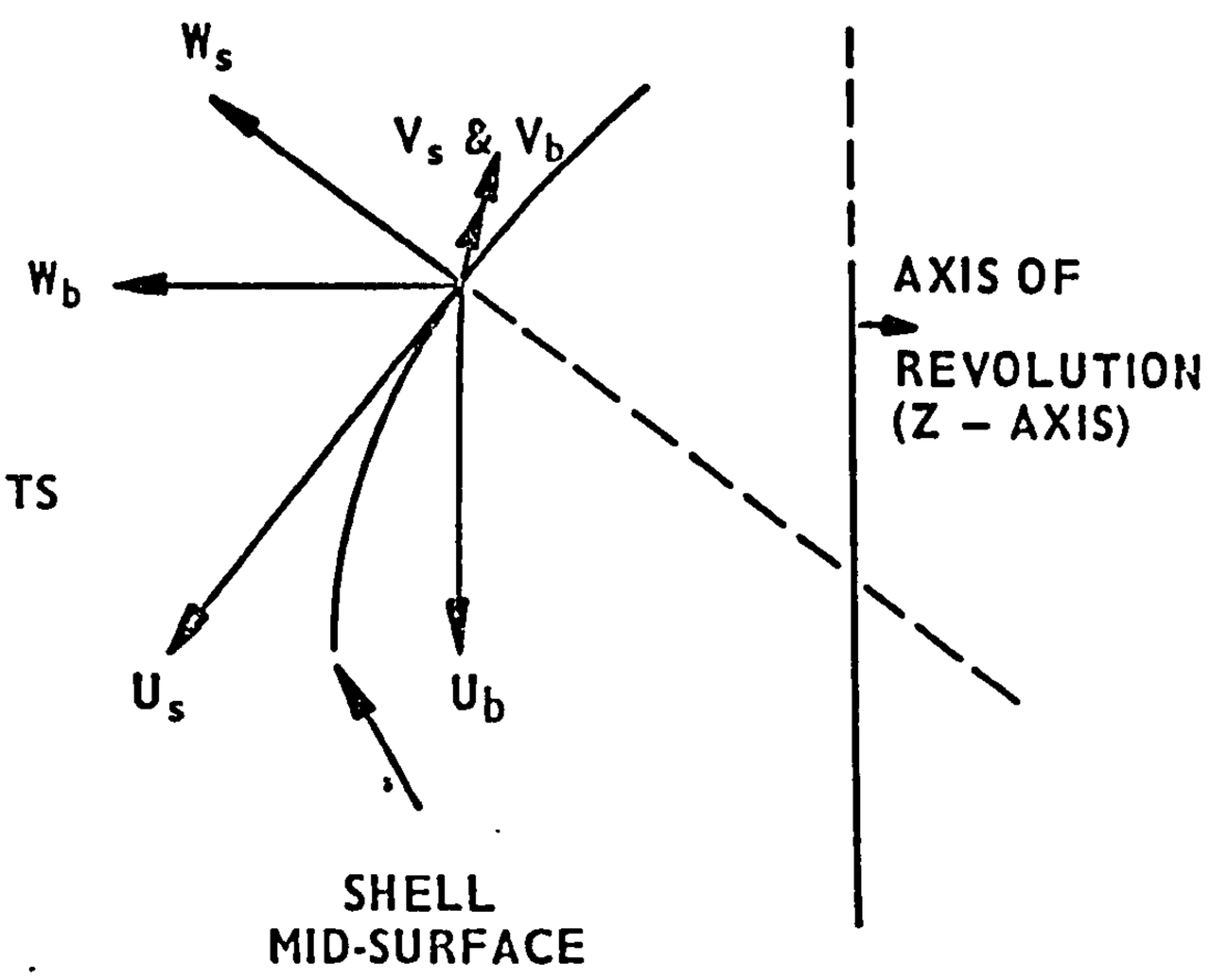

FIG. 6.1 DISPLACEMENTS IN THE LOCAL AND GLOBAL COORDINATE SYSTEMS

As shown in Chapter 4 $\frac{\partial Z}{\partial s} = \sin \phi$. The derivatives of u_b, v_b and w_b can easily be obtained:-

$$\left[u_s \frac{\partial u_s}{\partial s} \quad \frac{\partial u_s}{\partial \theta_o} \frac{\partial u_s}{\partial s \partial \theta_o} v_s \ldots\ldots \frac{\partial w_s}{\partial s \partial \theta_o} \right]^T$$

$$= \left[T_c \right] \left[u_b \frac{\partial u_b}{\partial Z} \ldots\ldots\ldots \frac{\partial w_b}{\partial Z \partial \theta_o} \right]^T$$

The coordinate transformation matrix $\left[T_c \right]$ is given by

$$\begin{bmatrix}
A & 0 & 0 & 0 & 0 & 0 & 0 & 0 & B & 0 & 0 & 0 \\
A' & (A^2Q) & 0 & 0 & 0 & 0 & 0 & 0 & B' & (ABQ) & 0 & 0 \\
0 & 0 & A & 0 & 0 & 0 & 0 & 0 & 0 & 0 & B & 0 \\
0 & 0 & A' & (A^2Q) & 0 & 0 & 0 & 0 & 0 & 0 & B' & ABQ \\
0 & 0 & 0 & 0 & 1 & 0 & 0 & 0 & 0 & 0 & 0 & 0 \\
0 & 0 & 0 & 0 & 0 & (QA) & 0 & 0 & 0 & 0 & 0 & 0 \\
0 & 0 & 0 & 0 & 0 & 0 & 1 & 0 & 0 & 0 & 0 & 0 \\
0 & 0 & 0 & 0 & 0 & 0 & 0 & (QA) & 0 & 0 & 0 & 0 \\
-B & 0 & 0 & 0 & 0 & 0 & 0 & 0 & A & 0 & 0 & 0 \\
-B' & -ABQ & 0 & 0 & 0 & 0 & 0 & 0 & A' & (A^2Q) & 0 & 0 \\
0 & 0 & -B & 0 & 0 & 0 & 0 & 0 & 0 & 0 & A & 0 \\
0 & 0 & -B' & -ABQ & 0 & 0 & 0 & 0 & 0 & 0 & A' & A^2Q
\end{bmatrix}$$

where $A = \sin \phi$, $B = \cos \phi$, $Q = 1.0$, $A' = \frac{\partial \sin \phi}{\partial s}$ and $B' = \frac{\partial \cos \phi}{\partial s}$

(Note that if it is desired to transform between normalised displacements, i.e.

$$\left[u_s \frac{\partial u_s}{\partial \bar{s}} \quad \frac{\partial u_s}{\partial \bar{\theta}} \ldots\ldots \right] \text{ to } \left[u_b \frac{\partial u_b}{\partial \bar{z}} \frac{\partial u_s}{\partial \bar{\theta}} \ldots\ldots \right],$$

then $Q = L/H$ where L and H are the meridional and axial lengths

of an element, respectively, and $A' = \frac{\partial \sin \phi}{\partial \bar{s}}$ and $B' = \frac{\partial \cos \phi}{\partial \bar{s}}$.)

The coordinate transformation matrix T_c is used to transform the stiffness (and mass) matrices of the shell elements. If K_e is the stiffness matrix before the transformation and K'_e after transformation, then

$$[K'_e] = [T_c]^T [K_e][T_c] \quad \text{(see Reference 4, page 10)} \qquad \ldots(6.5)$$

The matrix K_e is large; (48 × 48) for the twelve nodal d.o.f. shell element. Thus, evaluation of the above equation would normally require a correspondingly large computer core allocation. However, the following treatment would allow a considerable saving in core requirements:-

We re-write equation (6.5) in terms of sub-matrices:-

$$[K_e'] = \begin{bmatrix} T_{a1} & 0 & 0 & 0 \\ 0 & T_{a2} & 0 & 0 \\ 0 & 0 & T_{a3} & 0 \\ 0 & 0 & 0 & T_{a4} \end{bmatrix} \begin{bmatrix} k_{11} & \text{symmetrical} & & \\ k_{21} & k_{22} & & \\ k_{31} & k_{32} & k_{33} & \\ k_{41} & k_{42} & k43 & k_{44} \end{bmatrix} \times \begin{bmatrix} T_1 & 0 & 0 & 0 \\ 0 & T_2 & 0 & 0 \\ 0 & 0 & T_3 & 0 \\ 0 & 0 & 0 & T_4 \end{bmatrix} \qquad \ldots(6.6)$$

Here $[T_{a1}]^T = T_1$, $[T_{a2}]^T = T_2$..... and so on.

0 is a zero matrix of order (12 × 12). For the four-noded twelve-d.o.f. shell element the submatrices are of order (12 × 12).

Equation (6.6) reduces to

$$[k'_e] = \begin{bmatrix} (T_{a1} & k_{11} & T_1) & & & & & & & & & \\ (T_{a2} & k_{21} & T_1) & (T_{a2} & k_{22} & T_2) & & & & & & \\ (T_{a3} & k_{31} & T_1) & (T_{a3} & k_{32} & T_2) & (T_{a3} & k_{33} & T_3) & & & \\ (T_{a4} & k_{41} & T_1) & (T_{a4} & k_{42} & T_2) & (T_{a4} & k_{43} & T_3) & (T_{a4} & k_{44} & T_4) \end{bmatrix}$$

(Symmetrical)

Consider the sub-matrix term $T_{a1} k_1 T_1$. A routine can conveniently evaluate this term. As the term is of order (12 × 12) the computer core required for the operations are small. The same routine can be used to evaluate the other sub-matrix terms.

6.3 Generation of Pseudo-Nodes

Consider a rectangular beam element. It is necessary to describe its orientation in space, with respect to its principal moments of area. One method of doing so is to define 'pseudo-nodes'; this technique is discussed fully by Thomas and Wilson [70]. Pseudo-nodes, as the name implies, are hypothetical nodes that define the position of the actual nodes; the line joining a pair of pseudo-nodes is taken to be parallel to the axis about which Moment 1 of the beam is taken. (The Moment 1 and Moment 2 of the beam are given by $\frac{a^3 b}{12}$ and $\frac{b^3 a}{12}$, respectively, where a and b are the cross-sectional dimensions with b measured in parallel to the first principal axis.)

In the program VACTIL the pseudo-nodes of a beam element can be entered by the user. If the beam elements are used to model the 'V-pair' of leg-supports for a cooling tower, as for the tower at Didcot (see Fig. 7.1) the pseudo-nodes can be calculated by the method given below. (If requested by the user the calculation is performed within the program VACTIL.)

The orientation of the beam representing a leg-support is given in Fig. 6.2. In the figure, P_1 and P_2 are the 'real' nodes of the beam and P_1'', P_1', P_2'' and P_2' are the pseudo-nodes. The calculation proceeds as follows:-

With reference to Fig. 6.2a and 6.2b:

P_2P_1 is the representative leg-support of length L.

P_2 is the node at the top of the leg-support (i.e. the node is at the bottom of the shell of the tower).

P_1 is the node at the bottom of the leg-support.

β is half the angle subtended by the bottom nodes of the 'V-pair' of leg-supports at the centre of the bottom circle in Fig. 6.2a.

m is the length shown in Fig. 6.2a.

Let the cylindrical coordinates of P_1 and P_2 be (R_1, θ_1, Z_1) and (R_2, θ_2, Z_2) respectively.

α is the acute angle the tangent to the shell surface at node P_2 makes with the horizontal. (Note that the value of α can be given to an accuracy of $\pm 5^{\circ}$ without affecting the accuracy significantly.)

Thus,

$$\tan \alpha = (Z_1 - Z_2)/(R_1 - R_2) \qquad \ldots(6.7)$$

From the geometry of Fig. 6.2 equations (6.8) and (6.9) are:-

$$m^2 = L^2 - (A_1 - Z_2)^2 \qquad \ldots(6.8)$$

$$R_1^2 + R_2^2 - m^2 = 2R_1 R_2 \cos \beta \qquad \ldots(6.9)$$

Solving equations (6.7), (6.8) and (6.9) a quadratic

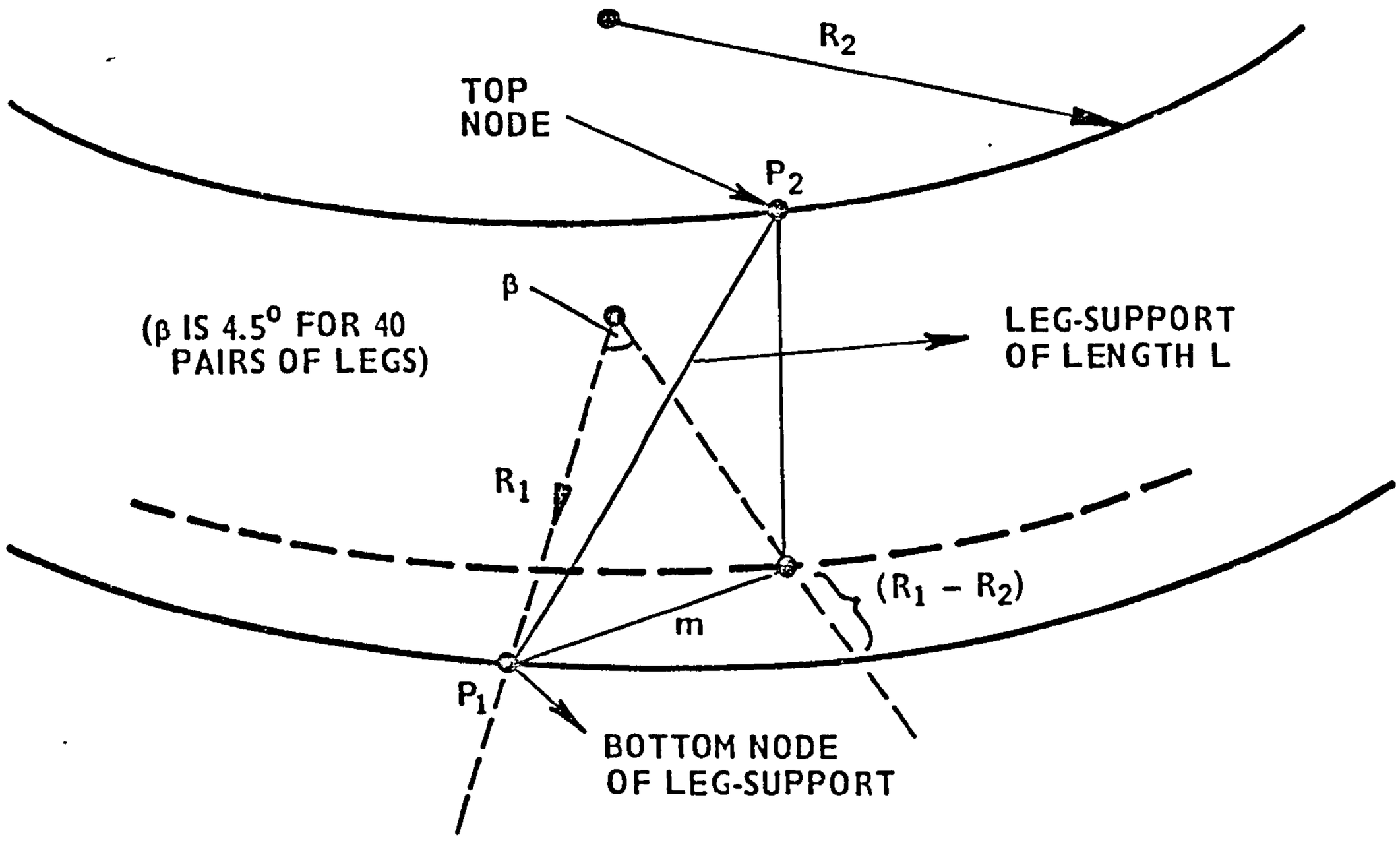

FIG. 6.2a GEOMETRY OF A LEG-SUPPORT OF A 'V-PAIR' OF COOLING TOWER LEGS

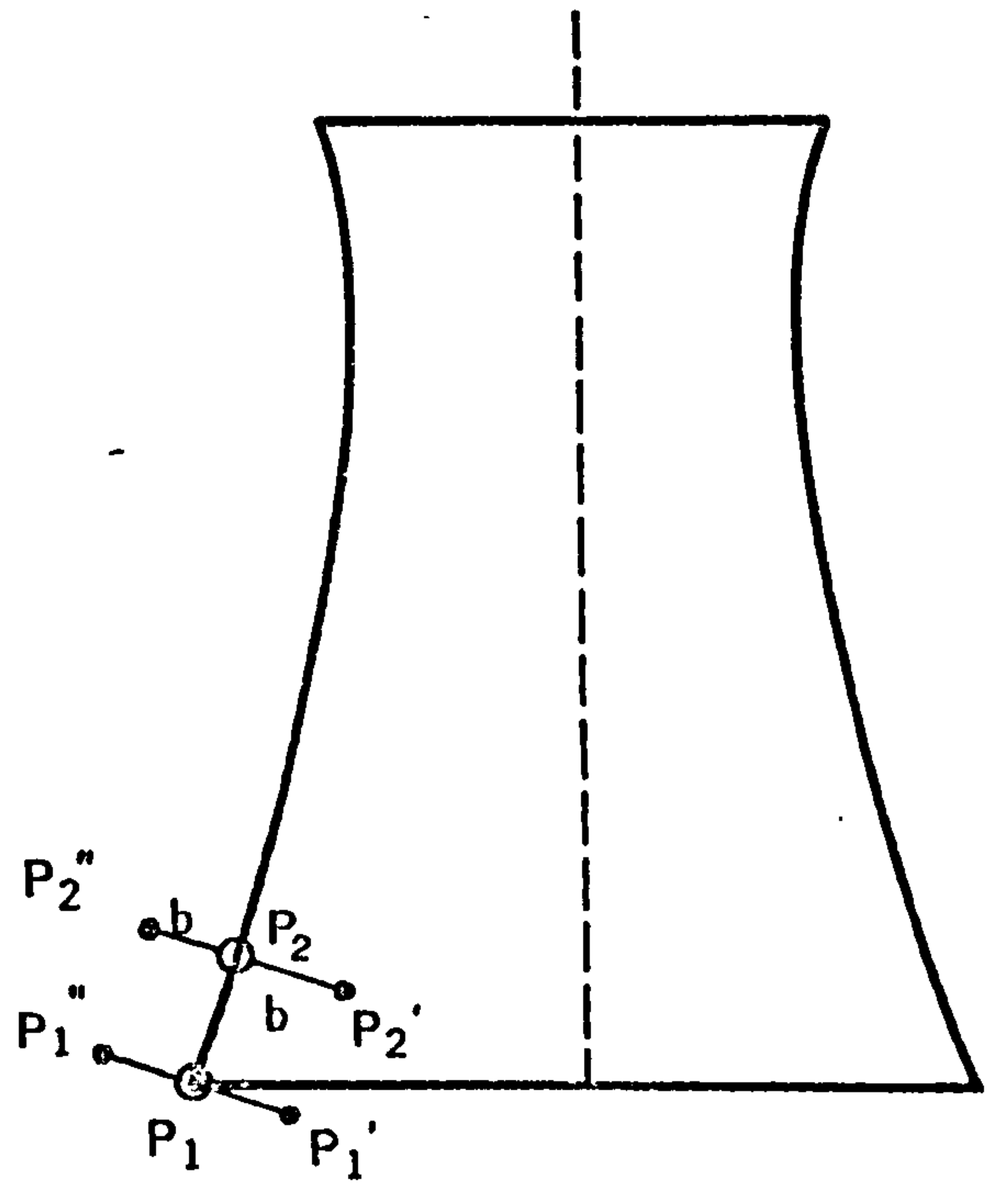

FIG. 6.2b REAL AND PSEUDO-NODES OF A LEG-SUPPORT

is obtained:

$$R_1^2 (1 + \tan^2 \alpha) + R_1 \left[-2R_2(\cos \beta + \tan^2 \alpha) \right]$$

$$+ (R_2^2 \tan^2\alpha - L^2 + R_2^2) = 0 \qquad \ldots(6.10)$$

Thus if α, R_2 and L are given then R_1 is calculated.

With reference to Fig. 6.2a and 6.2b, P_2'' and P_2' are the pseudo-nodes of P_2.

$$P_2'' = \left[(R_2 + b \sin \alpha), \theta_2, (Z_2 - b \cos \alpha) \right]$$

and

$$P_2' = \left[(R_2 + b \sin \alpha), \theta_2, (Z_2 + b \cos \alpha) \right]$$

The pesudo-nodes of P_1 can now be determined if the unit position vectors of P_1, P_2' and P_2'' are known. Hence, the Cartesian coordinates of P_1' and P_1'' are given by the equations

$$P_1'' = P_1 + \tfrac{1}{2}P_2'' - \tfrac{1}{2}P_2'$$

and

$$P_1' = P_1 - \tfrac{1}{2}P_2'' + \tfrac{1}{2}P_2' \quad .$$

(As the global coordinate system is cylindrical, the Cartesian coordinates are re-converted back to the cylindrical system.)

CHAPTER SEVEN

PROGRAM DESCRIPTION

7. PROGRAM DESCRIPTION

This chapter presents an overall description of the finite element program VACTIL ('Vibration Analysis of Cooling Towers Including Legs'). The program has been developed primarily to analyse the free vibration of cooling towers whilst explicitly including the effects of the leg-supports and/or foundation elasticity. An analysis of the cooling tower at Didcot (Fig. 7.1) is presented as an illustration in the use of the program - see Appendix 7.1. VACTIL can also be used to analyse the free vibration of complete or partial shells of revolution with (or without) meridional curvature; the shells of revolution may include cut-outs or openings. When rotationally periodic structures are analysed, a considerable saving in computer storage and computer time may be achieved by using the 'complex constraints' option. Moreover, complete, cylindrically symmetric shells (which are a special case of rotationally periodic shells) can conveniently be analysed by specifying a representative section of the whole structure and then invoking boundary conditions pertaining to their symmetry.

The description given in this chapter is brief as the important programming details have been discussed earlier. Also, note that only the program VACTIL is described; however, the description is broadly applicable to the other two programs referred to in this thesis. VACTILo2 [73], which is also called SACTIL, is an extension of VACTIL and incorporates the stress matrices derived in Chapter 4. SACTIL can calculate resonant stresses, forced response stress (both static and dynamic) as well as resonant frequencies and mode shapes. The program RESAP [72] incorporates

POSITION ON AXIS OF REVOLUTION	RADIUS (m)	WALL THICKNESS (m)
0.0	26.7596	0.3818
3.422	26.2638	0.1778
10.0	25.5680	0.1778
21.660	25.1315	0.1778
30.0	25.4070	0.1778
40.0	26.3314	0.1778
50.0	27.8434	0.1778
60.0	29.8730	0.1778
70.0	32.3431	0.1778
85.0	36.6882	0.1778
100.847	41.8026	0.1778
106.680	43.7421	0.5842

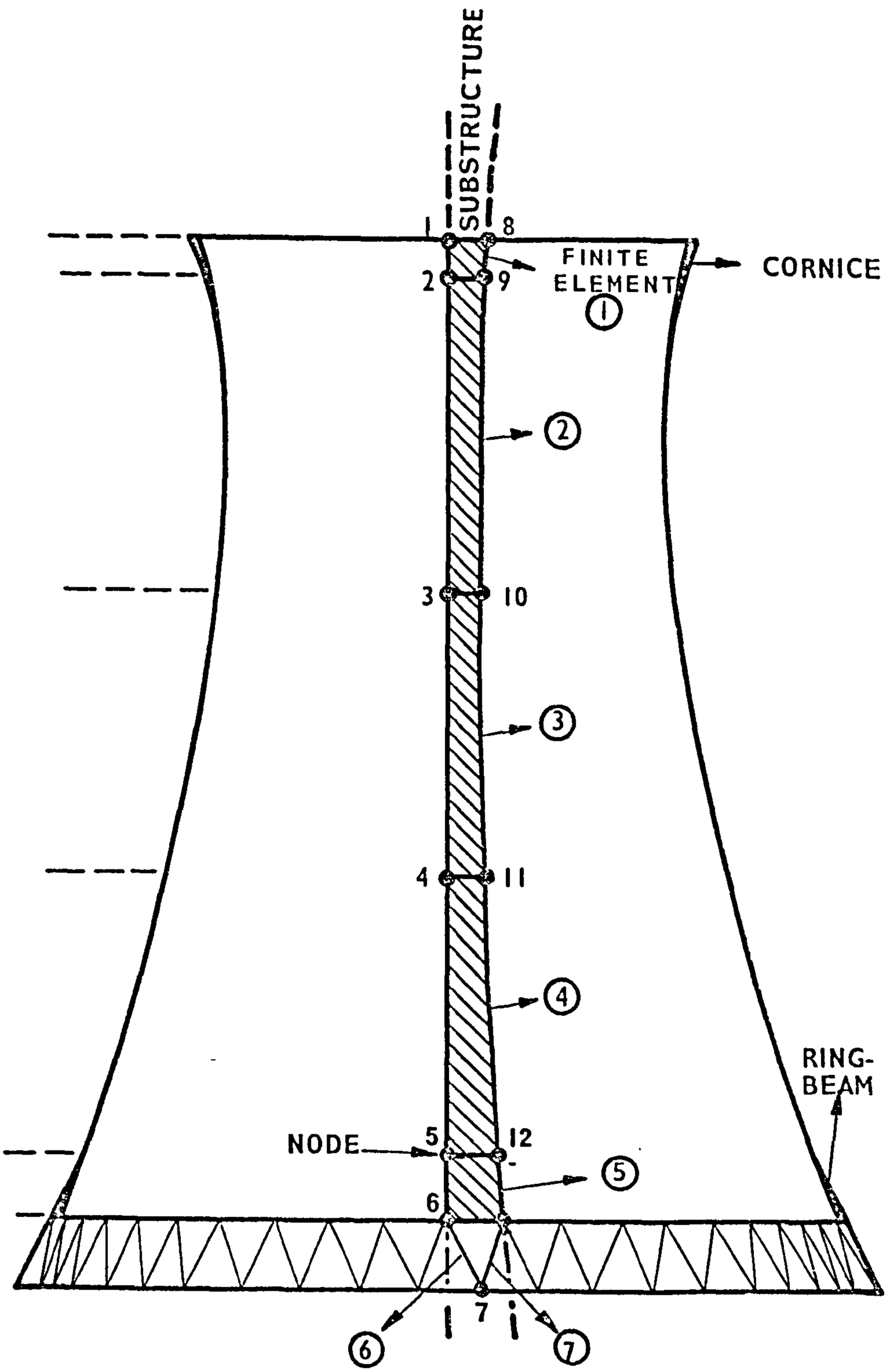

FIG. 7.1 TYPICAL FINITE ELEMENT REPRESENTATION OF A COOLING TOWER WITH LEG-SUPPORTS (ANGLE SUBTENDED AT AXIS-OF-REVOLUTION BY SUBSTRUCTURE IS 9^0)

the ring finite element discussed in Section 4.6.3, and calculates resonant stress, frequencies and mode shapes of axisymmetric structures. All three programs are large multi-segment programs employing about sixty to eighty subroutines.

All three programs are written in FORTRAN and are designed to be executed on the I.B.M. 370 computing system. Computer core requirements for each of the programs are dependent on the type of problem solved (though as indicated in Chapter 3 the degrees of freedom, d.o.f., of the structure are the primary factor). A special 'dynamic storage' facility is incorporated in each of the programs to allow array sizes to be dimensioned at the time of execution. Consequently, storage allocations range from 150 kilo-bytes to 750 K-bytes. The problem described in Appendix 7.1 required about 350 K-bytes of computer core and about 30 seconds of computer (c.p.u.) time. References 5, 73, 72 give complete descriptions and instructions for running the programs.

7.1 General Description

A flow diagram of the program VACTIL is given in Fig. 7.2. The execution of VACTIL is common to most dynamic finite element programs using the displacement method. That is,

(i) Input data is read, checked and printed.

(ii) Element stiffness and mass matrices are formed.

(iii) Element stiffness and mass matrices are assembled to create the stiffness and mass matrices, respectively, of the substructure (if complex constraints are applied) or of the whole structure.

(iv) 'Usual' constraints and/or complex constraints are applied (if required).

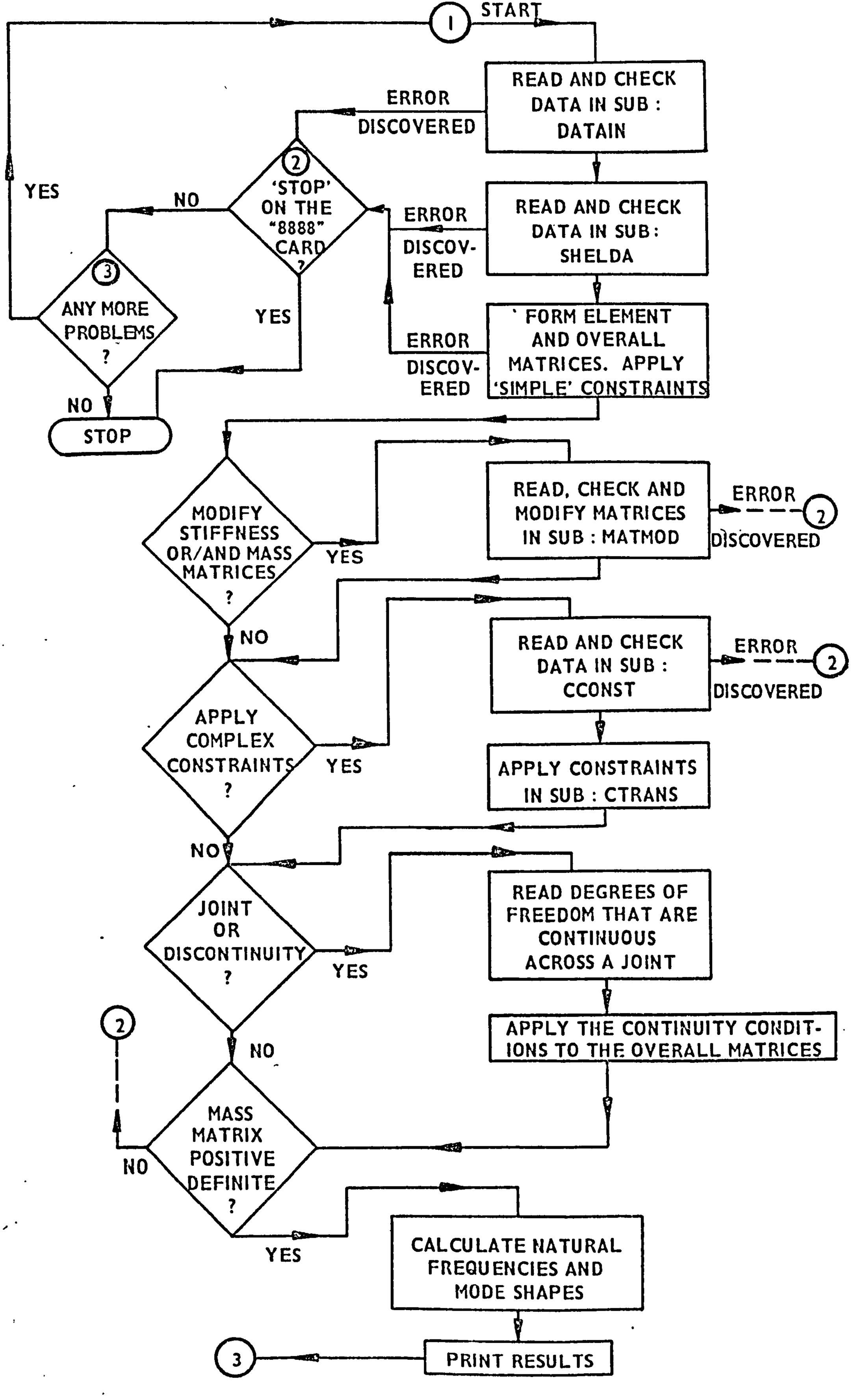

FIG. 7.2 FLOW CHART FOR VACT I L

(v) The equations given in Section 7.3 are solved.

(vi) Results are printed.

With reference to the above, item (ii) has been discussed in Chapter 3; item (iii) is a straightforward finite element technique (see [4, Section 1.6] and [2, Chapter 10]).

When an axisymmetric structure is analysed its symmetry can be invoked to simplify the analysis of the structure. Alternatively, as an axisymmetric structure is a rotationally periodic structure (where the periodicity tends to infinity) complex constraints can be employed (as discussed in Chapter 3). When a rotationally periodic structure is analysed either the whole structure can be defined (indifferent answers will usually result, as a coarse mesh would usually have to be employed) or complex constraints can be applied. For the analysis of cooling towers with leg-supports it is necessary to use complex constraints. An illustrative example with a reproduction of the actual computer printout is given in Appendix 7.1.

VACTIL uses two types of finite elements; a doubly curved shell finite element with four nodes (see Chapter 4) and a straight beam finite element (see Section 6.3). For cooling towers, the shell elements are used to model the shell, whilst the beam elements are used to represent the leg-supports. Each node, for both elements, is allowed twelve degrees of freedom (d.o.f.). These are:

$$u\ ,\ \frac{\partial u}{\partial s}\ ,\ \frac{\partial u}{\partial \theta}\ ,\ \frac{\partial^2 u}{\partial s \partial \theta_o}\ ,\ v,\ \frac{\partial v}{\partial s}\ ,\ \frac{\partial v}{\partial \theta_o}$$

$$\frac{\partial^2 v}{\partial s \partial \theta_o}\ ,\ w,\ \frac{\partial w}{\partial s}\ ,\ \frac{\partial w}{\partial \theta_o},\ \frac{\partial^2 w}{\partial s \partial \theta_o}$$

Six of the twelve d.o.f. are not required by the beam element. These 'dummy' d.o.f. must therefore be constrained at nodes not coincident with those of the shell elements. These dummy d.o.f. are the second, third, fourth, seventh, eighth and twelfth d.o.f. listed above. The orthogonal curvilinear coordinate system in which the shell element is derived, results in u, v and w being the displacements in the meridional, circumferential and normal directions, respectively, with reference to the shell middle surface. On the other hand, the local coordinate system of the beam element is cylindrical. The displacements u and w are then parallel and normal to the axis-of-revolution, respectively; v is the orthogonal displacement consistent with a 'right-hand' set of axes. In Fig. 6.1 the displacements for the shell and beam elements are illustrated where the suffices s and b pertain to the shell and beam respectively.

When both types of finite elements are used a common or 'global' coordinate system is required. The local coordinate system of the beam element is chosen as the global system.' This has been discussed in detail in Chapter 6.

When a node is common to both types of elements it is essential to specify identical coordinates for the common node for both element-definitions. Otherwise, errors will probably be introduced by the discontinuity of both displacement functions (which are different for the beam and shell elements) at the common node.

The 'pseudo-nodes' of the beam element can be explicitly or implicitly defined - see Chapter 6.

The convergence [2, page 201] of the shell element is reasonably good for calculating frequencies and for obtaining an estimate of the displacements. (We shall see later that for the calculation of stress the convergence of the element could be profitably improved.) Hence, only a few elements are usually required to analyse a structure

when the frequency of vibration is the primary consideration. For example, four shell elements were required for the analysis of the cooling tower considered in Appendix 7.1, when constant wall thickness was assumed. The answers were seen to be very similar, especially for the lower eigenvalues, to that obtained when six shell elements were used. Moreover, the shell element has been observed by the author to give satisfactory results for 'aspect ratios' not exceeding 3:10 or 10:3.

Foundation elasticity is represented in the program by a 'spring'. Due to the simplicity of this 'element', it is not explicitly incorporated in the program. The user enters the value of foundation elasticity and specifies the node at which it acts. The program then adds this term directly into the stiffness matrix. (That is, 'direct stiffness terms' are modified to represent foundation elasticity [2, page 15].)

Other shell structures, such as the spherical cap analysed in Chapter 11, can also be investigated. The figures 7.3a to 7.6 are from the user's guide to the program VACTIL [5] and are reproduced here to give an indication of the other types of structures (in addition to complete shells of revolution) that the program is capable of solving.

7.2 Major Assumptions and Limitations

For the shell elements the ratio of the material thickness to the principal radius of curvature must be less than 1:10.

Euler's Theory is assumed for the beam elements.

The materials of both shell and beam elements must be linear, elastic, homogeneous and isotropic. Thin Shell Theory is used.

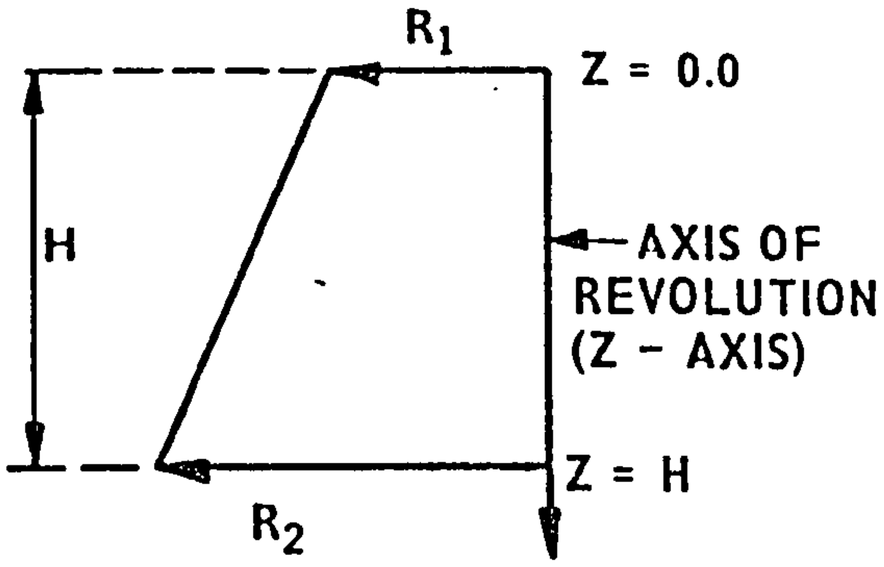

FIG. 7.3a REPRESENTATION OF A FRUSTUM IN CARD TYPE $1H_3$

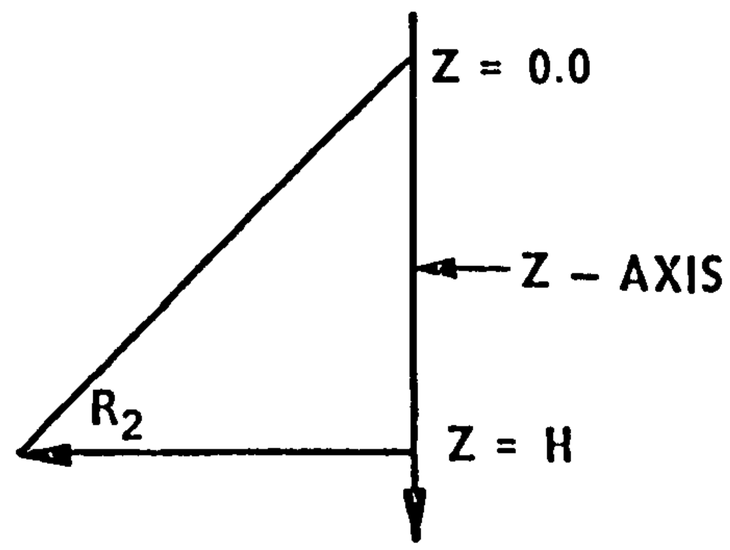

FIG. 7.3b REPRESENTATION OF A CONE IN CARD TYPE $1H_3$

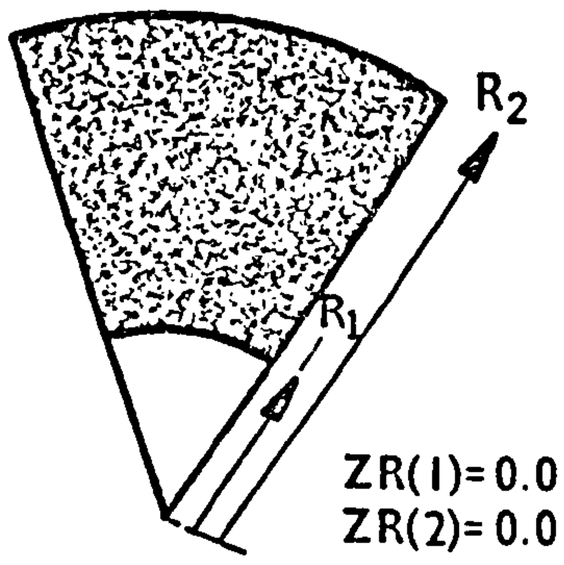

FIG7.3c REPRESENTATION OF AN ANNULAR ELEMENT. CARD TYPE $1H_3$

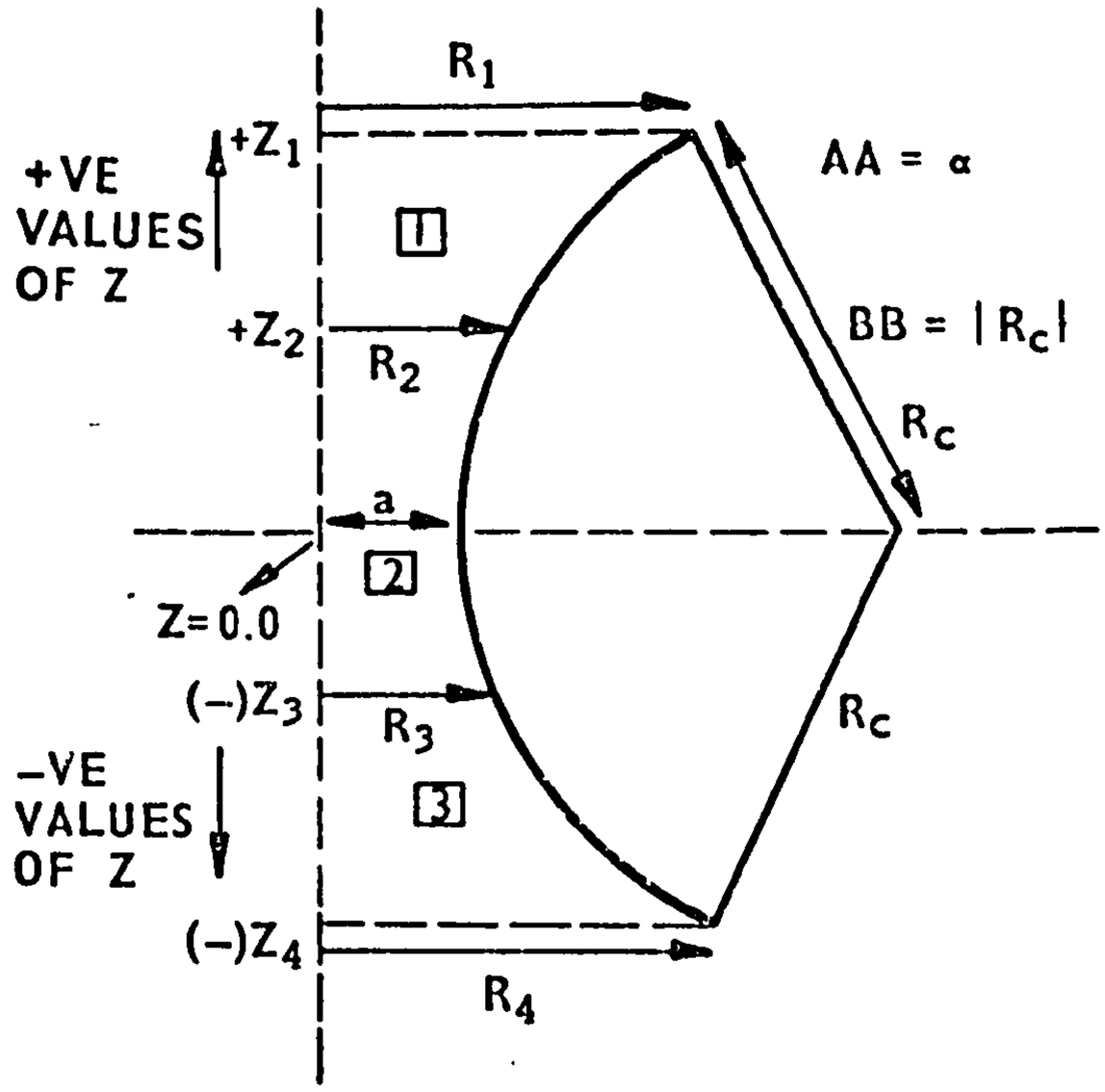

FIG. 7.4 REPRESENTATION OF A TOROIDAL MERIDIAN (BY WAY OF ILLUSTRATION THREE SECTIONS ARE USED).

BB = $|R_c|$. AA = a.

EQUATION : $R = (R_c+a) - \sqrt{R_c^2 - Z^2}$

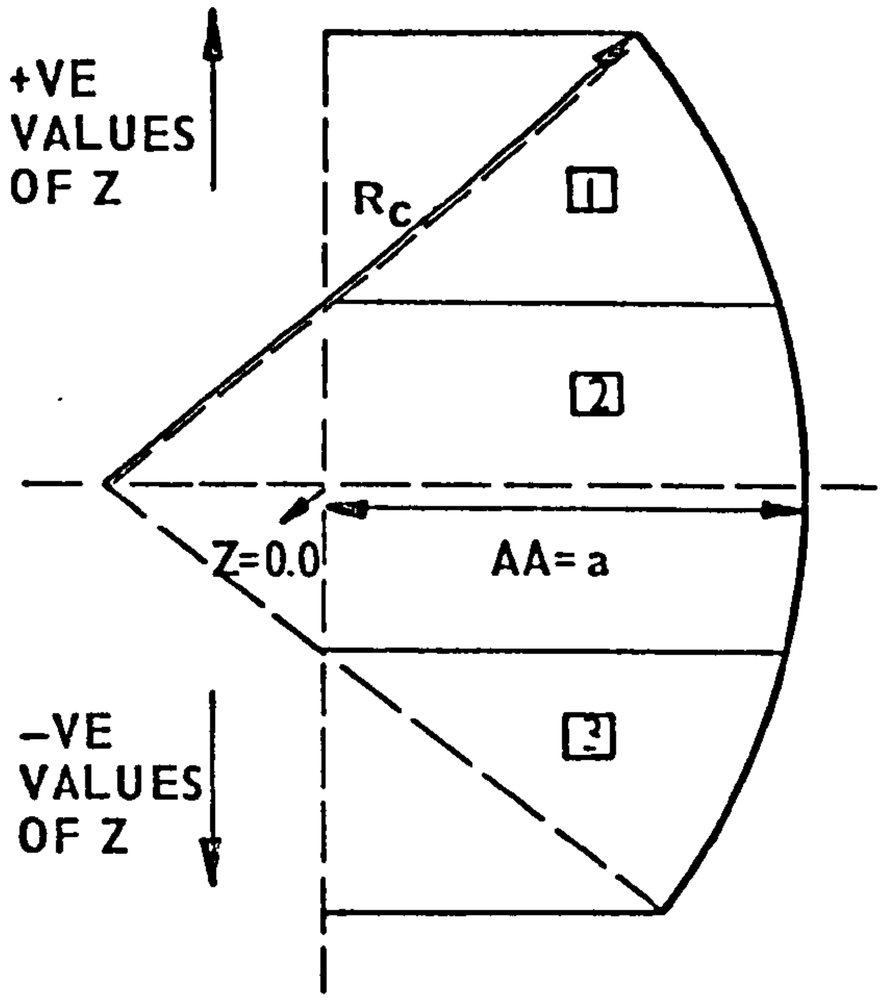

FIG7.5 REPRESENTATION OF MERIDIAN WITH CONSTANT CURVATURE.
THREE SECTIONS ARE ILLUSTRATED. AA IS SHOWN IN THE FIGURE
BB = $-|R_c|$. (CARD TYPE 1H6)
EQUATION : $R = (a - R_c) - \sqrt{R_c^2 - Z^2}$.
FOR SPHERICAL SHELL $a = |R_c|$

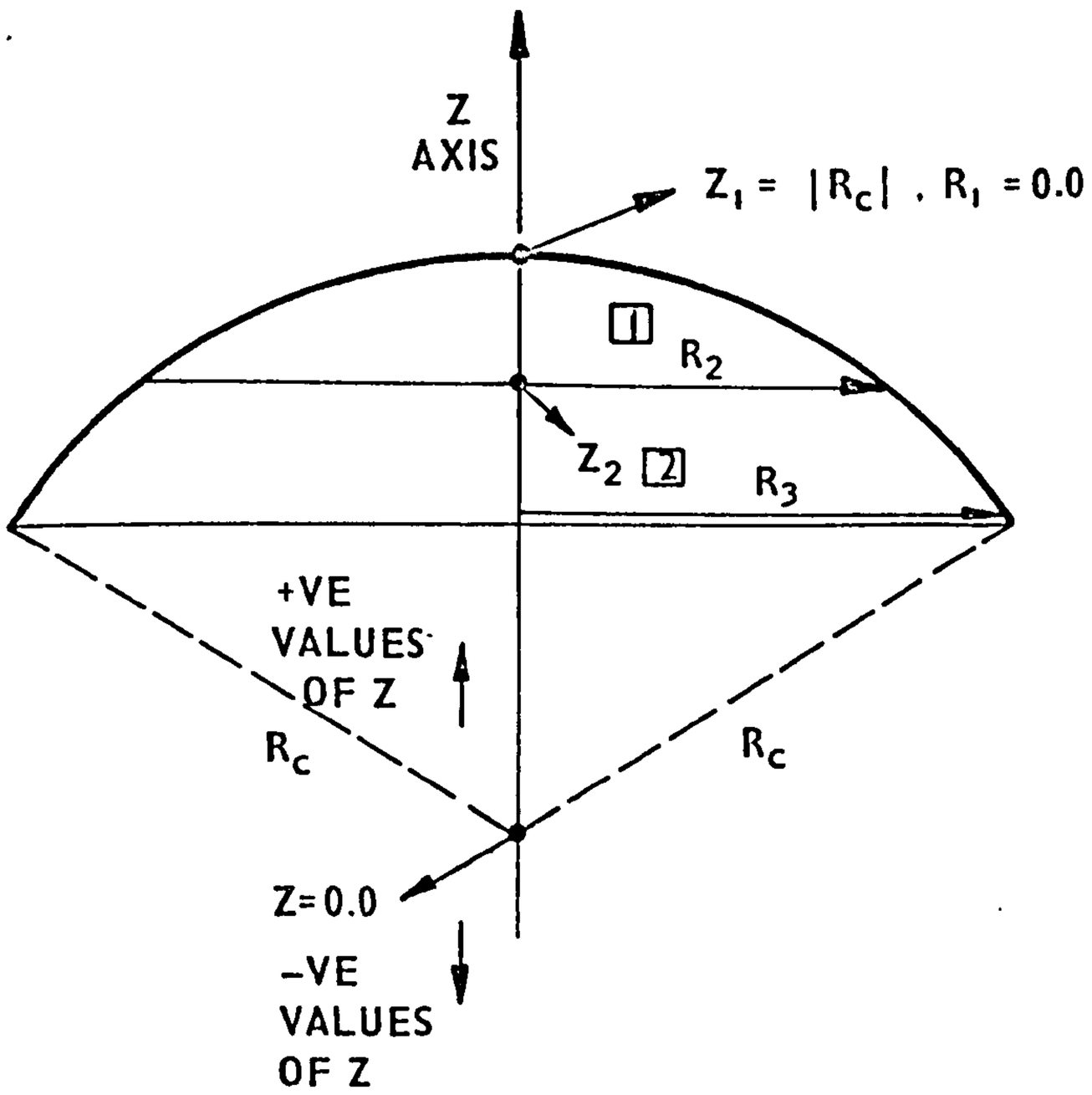

FIG.7.6 CIRCULAR MERIDIAN FORMING A SPHERICAL CAP DIVIDED,
BY WAY OF ILLUSTRATION, INTO TWO SECTIONS
EQUATION : $R = (a - R_c) - \sqrt{R_c^2 - Z^2}$ WHERE $a = |R_c|$

(Basic assumptions used in the analysis have been discussed in greater detail in Chapter 4.)

7.3 Equations Solved

The natural frequencies and mode shapes of the structure are obtained by solving the matrix equation

$$(\underline{K} - \omega^2 \underline{M})\ \underline{x} = 0 \qquad \ldots(7.1)$$

which can be written as $(\underline{A} - \lambda\underline{B})\underline{x} = 0$.

This is a standard eigenvalue problem which can be readily solved by a number of different methods [75]. The C.E.G.B. library subroutines that solve this problem are based on a series of published algorithms [76, 77, 78, 79]. Note that when complex constraints are used the eigenvectors are complex.

In the program SACTIL the 'forced response' facility can be requested. The applied force (or forces) may be specified as positive, negative or zero. For time varying loads the variation is assumed to be sinusoidal and the frequency must be specified. (When the load is static then the frequency is defined as zero.)

For the applied force response the derivation of the equations used for the calculation are as follows:-

When sinusoidal forces are applied to the structure, we get

$$\underline{M}\ \ddot{\underline{x}} + \underline{C}\ \dot{\underline{x}} + \underline{K}\ \underline{x} = \underline{P}\ e^{i\omega t} \qquad \ldots(7.2)$$

where the matrix $\underline{C}$ represents the damping of the structure and $\underline{P}$

represents the applied forces in magnitude and phase. Assuming that

$$\underline{x} = \underline{x}_o \, e^{i\omega t}, \qquad \ldots(7.3)$$

we have

$$(-\omega^2 \underline{M} + i\,\omega\,\underline{C} + \underline{K})\,\underline{x}_o = \underline{P} \qquad \ldots(7.4)$$

If it is assumed that the damping is viscous then the damping term $\omega\underline{C}$ is given by

$$\omega\underline{C} = \omega d_1 \underline{K} \qquad \ldots(7.5)$$

and for hysteretic damping, we have

$$\omega\,\underline{C} = d_2\,\underline{K} \qquad \ldots(7.6)$$

In SACTIL either viscous or hysteretic damping can be specified. The damping is given in a rather more general form as

$$\omega\,\underline{C} = \omega(d_1\,\underline{K} + d_3\,\underline{M}) \qquad \ldots(7.7)$$

or

$$\omega\,\underline{C} = d_2\,\underline{K} + d_4\,\underline{M}\,, \qquad \ldots(7.8)$$

with the constants d_i specified by the user. Thus the following sets of equations are obtained

$$\{-\omega^2 \underline{M} + i(\omega\, d_1 \underline{K} + \omega\, d_3 \underline{M}) + \underline{K}\}\,\underline{x}_o = \underline{P} \qquad \ldots(7.9)$$

or

$$\{-\omega^2 \underline{M} + i(d_2 \underline{K} + d_4 \underline{M}) + \underline{K}\}\,\underline{x}_o = \underline{P} \qquad \ldots(7.10)$$

These equations are solved using complex Gaussian elimination to give the steady state response $\underline{x}_o$ in amplitude and phase.

CHAPTER EIGHT

VIBRATION TESTS ON A 1/250TH SCALE

COOLING TOWER MODEL

8. VIBRATION TESTS ON A 1/250TH SCALE COOLING TOWER MODEL

8.1 Introduction

Experimental investigations reported in the literature usually describe work conducted on idealized cooling tower models and not on exact scaled replicas of full-scale towers. Even so, these investigations have not been very successful (e.g. see References 22, 23, 33, 39) because of the relatively complex nature of the free vibration behaviour of these structures. Whilst simple structures such as cantilevers can be successfully excited in a pure mode by a single point force, this is not possible for cooling towers. Much work has served to identify the general pattern of possible mode shapes of cooling towers. In Fig. 8.1 several of these modes shapes are presented. In practice, the excitation of one of these modes shapes to the exclusion of the others is very difficult, especially if two or more modes have natural frequencies that are very close to each other. However, the excitation of a particular mode can be made easier by a judicious choice of the excitation forces with respect to their (a) number (b) frequency (c) phase and (d) position on the structure. For example, assume that in Fig. 8.1 the Modes I and II relate to a two degree-of-freedom system and that the modes have natural frequencies very close to each other. Then two forces diametrically opposed (see Fig. 8.1) but in-phase would excite Mode II, whilst in anti-phase would excite Mode I. The choice of the number of exciting forces is usually a compromise. To isolate a pure mode with n unconstrained d.o.f. would ideally require n numbers of exciters - see the paper by Traill-Nash [81]. In practice, this number is usually too large and so a smaller number is employed. (In the experimental investigation reported in this chapter six exciters

THE VIBRATION SHAPE ASSOCIATED WITH EACH MODE IS SUMMARISED USING 2 INTEGERS "n" AND "m". "n" IS THE NUMBER OF NODAL DIAMETERS AND "m" IS THE NUMBER OF MERIDIONAL NODES INCLUDING THE BASE NODE.

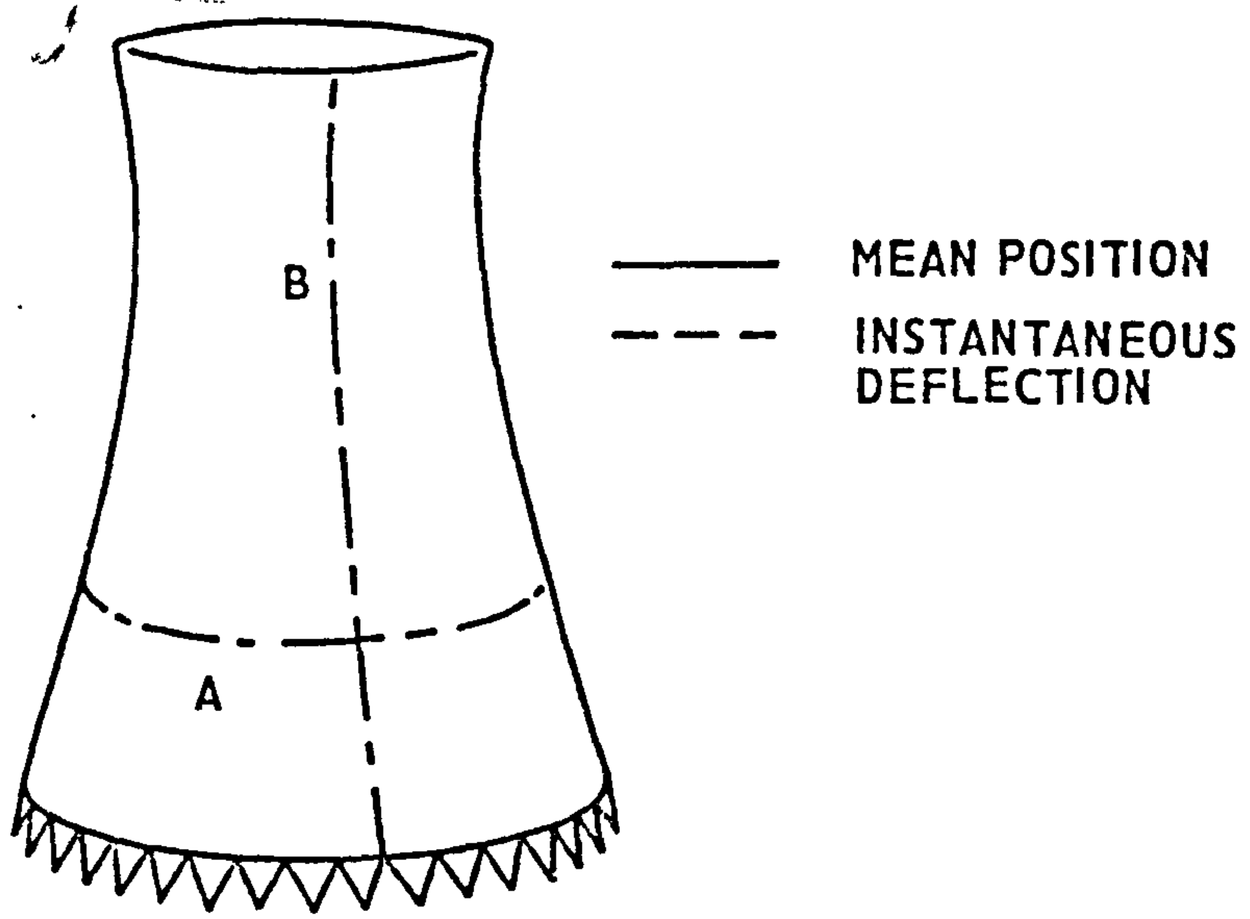

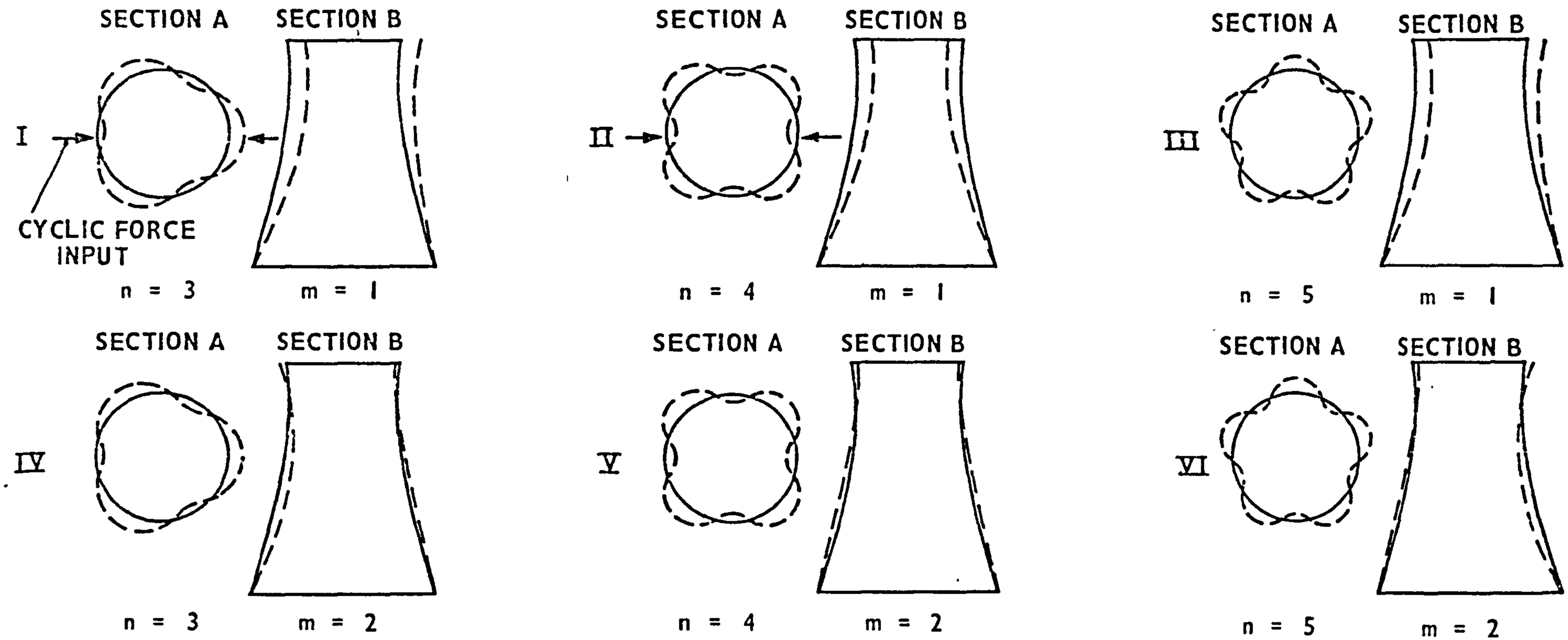

FIG. 8.1 MODE CHARACTERIZATION

were used, though even with this number it was observed that some modes were difficult to excite in isolation.)

As stated earlier, many previous investigations of model cooling towers have tended to idealize the structure by assuming a shell of constant thickness with no leg-supports. However, one of the primary reasons for the investigation reported here, was to validate the theoretical results obtained from the program VACTIL. Hence, great care was exercised in obtaining an exact scaled replica of a full-scale tower. The model had to comply with important scaling criteria - see Armitt [25]. (The author is grateful for the expertise gained at the Central Electricity Research Laboratories, C.E.R.L., Leatherhead, which enabled these requirements to be satisfied.) Thus the thickening of the wall of the tower shell at the base (ring-beam) and at the top (cornice) were accurately modelled. Also the leg-supports were included to scale - see Fig. 8.2.

8.2 Experimental Apparatus and Measurement Technique

The principles of resonance testing have been well documented - see References 80 to 85. The semi-automatic excitation system used in the investigation is based on that originally used by Taylor, Gaukroger and Skingle [85]. (However, several improvements have been made that enabled speedier and more accurate results to be obtained.) The process of setting up a pure mode using the system is as follows:-

The cooling tower is first vibrated using one exciter. The frequency is adjusted till the correct resonance phase condition exists between the exciter and the response transducer that is placed close to the exciter. (At resonance the velocity response will be

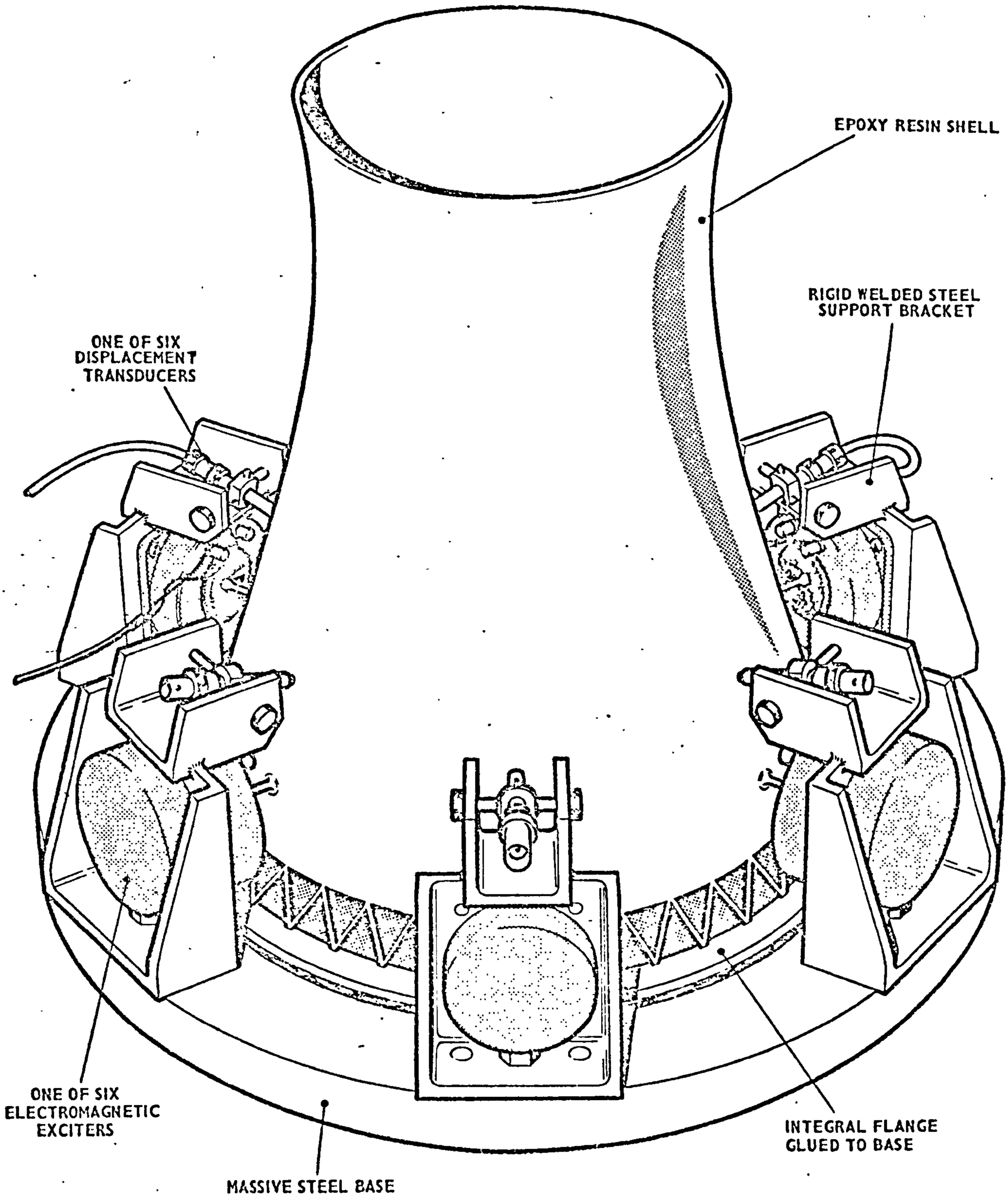

FIG.8.2 MODEL OF DIDCOT COOLING TOWER 3S WITH EXCITERS AND TRANSDUCERS

in-phase with the force input, the displacement response will lead by 90° and the acceleration will lag by 90°.) The Servo-Control Unit is then switched on so that it maintains the required phase condiiton. This is important as when the second exciter is switched-on the relative phase of the first exciter will tend to change. The force output of the second exciter is adjusted until it is in phase (or anti-phase) with the first. The other four exciters are switched-on and adjusted, one at a time, until the whole structure is vibrating in the desired mode.

A 1/250th scale model of the full-scale cooling tower at Didcot was chosen for the investigation. This was because the experimental results for the corresponding full-scale tower [42] were also available. The model tower was made from an epoxy resin with added steel powder called 'Devcon B'. (The manufacturer also calls it 'Plastic Steel B".) The model was approximately 457 mm in height. The outer surface was painted with a reflective paint, 'Codit'. The model was fixed to a large (diameter = 535 mm), thick (25 mm), steel base-plate by an adhesive. The steel base plate fixed to a turn-table which in turn was placed on a metal table. It was assumed, therefore, that the base of the tower was perfectly rigid.

Six electromagnetic vibrators were spaced equally about the periphery of the tower about 30 mm above the base plate. The arm of each exciter was fixed to the wall of the tower using a little epoxy resin (Devcon). During the preliminary stages of the investigation the exciters shown in Fig. 8.2 were used. However, in order to reduce the effective mass of the armatures and the stiffness of the armature suspension, smaller more compact exciters were employed. An added advantage of this change was that less of the tower surface

was obscured by the exciters thus enabling more displacement measurements near to and around the exciters to be made. A displacement measuring capacitance-transducer was mounted immediately above each exciter - see Fig. 8.2. The transducers did not come into contact with the tower. (A capacitance-transducer forms one plate of a capacitor whilst the tower structure coated with an electrically conducting paint forms the other plate. The capacitor is nominally a parallel plate capacitor and is included in the negative feedback circuit of an amplifier. The varying voltage produced by the amplifier is thus proportional to the normal displacement of the tower.)

A block diagram of the multipoint excitation system is given in Fig. 8.3. The description of the system is as follows:-

A sinusoidal signal generator with two outputs in quadrature with each other is employed. The frequency of the generator is controlled by means of a d.c. input voltage. It is thus referred to as a voltage-tuned oscillator, (V.T.O.). The '0^{o}' output of the V.T.O. is amplified and fed to the six exciters. The design of the amplifiers used for this purpose is such as to minimize the phase shift of the amplified signal. The '90^{o}' output of the V.T.O. is fed to six cathode ray oscilloscopes (C.R.O.). The output of each displacement (capacitance) transdicer is also fed to a C.R.O. Hence, the C.R.O. displays, (i.e. "Lissajous Figures") compare the relative phases of the respective displacement transducer outputs with the '90^{o}' output signal of the V.T.O.

The output from any one of the six displacement transducers is fed to the Servo-Control Unit. The '90^{o}' output of the V.T.O. is also fed to the Unit. The Servo-Control Unit 'limits'* both the

---

*amplifies the signal till clipping takes place. Thus, a sinusoidal signal is converted to a square wave-form.

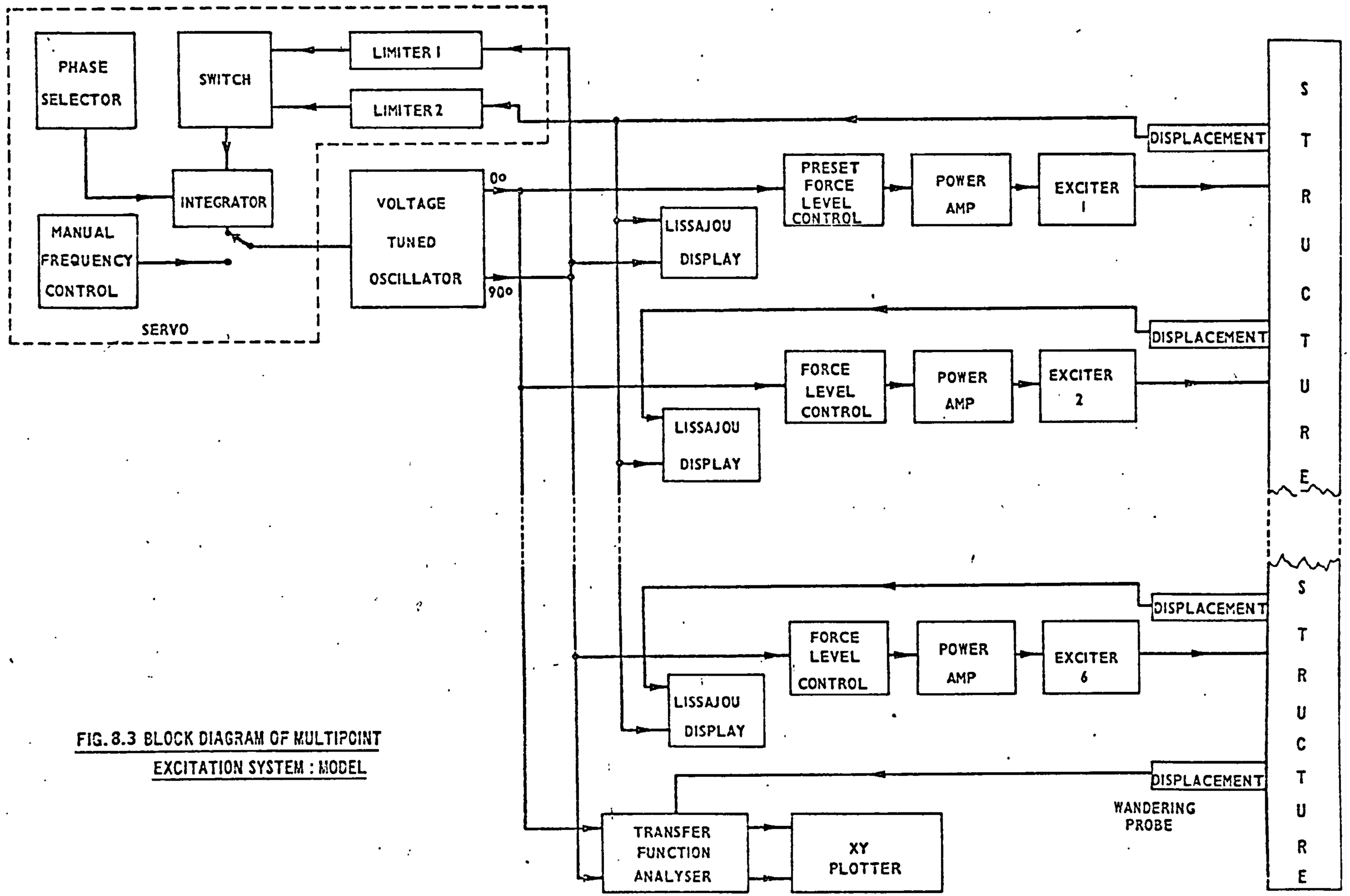

FIG. 8.3 BLOCK DIAGRAM OF MULTIPOINT EXCITATION SYSTEM : MODEL

'90°' and displacement transducer outputs. The phase difference, say θ^{o}, between the limited signals is measured. If θ^{o} is that value set by the user (180^{o} or 0^{o} for resonance), the d.c. input to the V.T.O. from the Servo-Control Unit is unaltered. Hence, the frequency of the V.T.O. remains almost constant. However, if θ^{o} is not equal to the required value, the d.c. voltage input to the V.T.O. is altered; an increase in the d.c. voltage causes an increase in the frequency of the V.T.O. and vice-versa.

A record of the Lissajous display was found to be very useful. At resonance, the six displays are straight lines inclined acutely or obtusely to the horizontal (i.e. the outputs of the displacement transducers are in anti-phase or in-phase with the '90^{o}' output of the V.T.O. respectively). A polaroid photograph of all six Lissajous displays was taken for each mode. For the modes of vibration reported in this thesis the patterns of displays were unique. Hence, when it was desired to return to a particular mode, the record of the particular mode could be referred to, so that the setting-up procedure could be expedited. This was particularly useful in exciting Mode 5 (see Section 8.3).

A feature of the experimental investigation was the innovatory use of a laser as a displacement transducer. This unique remote measuring transducer is made by Decca Radar Ltd., Walton-on-Thames 'DECCOM FAST TRACKER', RL/LG/96801. A 5 mW helium-neon laser and an interferometer (similar to a Michelson's interferometer) are central to the functioning of the instrument. The unit works on the Doppler Shift Principle. That is, laser light reflected from the surface of the vibrating structure undergoes a change in frequency in comparison to

the primary or reference laser beam. The greater the velocity of vibration of the structure the greater the phase difference between the reference and reflected beams. This difference in phase is converted by an interferometer into a series of moving interference fringes. These fringes are translated into an output voltage by means of electronic instrumentation ('tracker-box'). The magnitude of the output voltage is proportional to the velocity of the vibrating structure. Note that both the magnitude and direction of the vibration are detected by the DECCOM laser unit.

The maximum velocity of a point on a homogeneous resonating body is proportional to its maximum displacement, for small vibrations. The maximum output voltage of the tracker-box is therefore proportional to the maximum displacement, along the line of the laser beam, of the wall of the cooling tower, with respect to the particular point the laser beam is aimed at.

The DECCOM was phase-adjusted by aiming the laser beam at a very tightly clamped non-resonating body. The phase of the output voltage of the trancer-box was then adjusted (by means of a 'Brookdeal' Model 421 phase shifter) so that it was in-phase with the '90^{o}' output of the V.T.O. It must be noted that it was found necessary to re-adjust the DECCOM when the excitation frequency was changed.

Initially, in order to establish the reliability of the exciter used for the phase-adjustment of the laser, several different types of tightly clamped non-resonating exciters were used. It was confirmed that the phase of the output voltage of the tracker-box was similar for any of the exciters employed, for a given frequency.

Ideally, when the laser is aimed at a resonating structure,

the voltage will be wholly in-phase with the '0^{o}' output of the V.T.O. If the resonance is not perfect, however, a component of voltage in-quadrature with the '0^{o}' output will be detected. This voltage component will be referred to as the 'impure component'. Therefore, in order to obtain a measure of the purity of the mode, the relative magnitudes of both the component in-phase with the '0^{o}' output (i.e. 'pure component') and the impure component must be determined. Hence, the output voltage of the tracker-box is fed to a 'Transfer Function Analyser' (T.F.A.), which is also fed with the '0^{o}' and '90^{o}' outputs of the V.T.O. The T.F.A. has two d.c. output voltages which are proportional to the impure and pure components, respectively. These voltages are displayed separately on digital multimeters during experimentation. At resonance, as expected, the multimeter displaying the magnitude of the pure component tended to a maximum reading.

The DECCOM was found to be most safisfactory as a 'wandering' displacement measuring device. It was possible to speedily and accurately measure the displacements over the tower surface. With a little practice it was possible to move the laser beam over the tower surface and then obtain an approximate idea of the 'purity' and other characteristics of the mode. Two important aspects affecting the use of the DECCOM should be noted. The signal-to-noise ratio of the voltage output would sometimes be degraded. This would usually be due to poor reflection off the structure. This was corrected by changing the point of incidence of the beam slightly, and by ensuring that the beam was incident normal to the tower surface. Re-painting of a particularly bad area was also found to be beneficial. Thus, continuous monitoring of the output of the tracker-box of the

DECCOM (by means of a C.R.O.) is advocated.

A second though uncommon reason for a poor signal-to-noise ratio arises from the coherent nature of the laser beam. At multiples of the laser tube length, the coherency is weakest. Therefore, if the total distance travelled by the beam is an integer multiple of the tube length, the DECCOM may not operate as expected.

8.3 Results and Discussion

In order to establish that the equipment was performing satisfactorily the mode with the lowest frequency, Mode 1, was excited. At a vertical distance (height) of approximately 375 mm from the base plate the pure and impure components of displacement were noted as functions of angular position. The results are displayed in Fig. 8.4. It is noted that there are four circumferential wave-lengths (i.e. n = 4).

If 'perfect' excitation of a mode could be obtained, the ratio of the pure to the impure components of displacement would be infinite. In a practical case, however, the ratio is finite and is a measure of the purity of the mode. In Fig. 8.4 the ratio is observed to be approximately 3¼. The purity of the mode is also described by plotting the impure component against the pure component. The 'average' line drawn through the points gives the phase angle, since the impure component is in quadrature with the pure component; see Fig. 8.5. (A phase angle of less than 30^{o} is found to be acceptable in practice.)

Fig. 8.6 is a representation of the variation of displacements perpendicular to the central axis, with the vertical distance above the base plate. It is observed that the curve is asymmetric and that there are two meridional nodes, m = 2. (For several other modes the asymmetry was observed to be more pronounced.) The curve can be represented by a polynomial of order between 5 and 7.

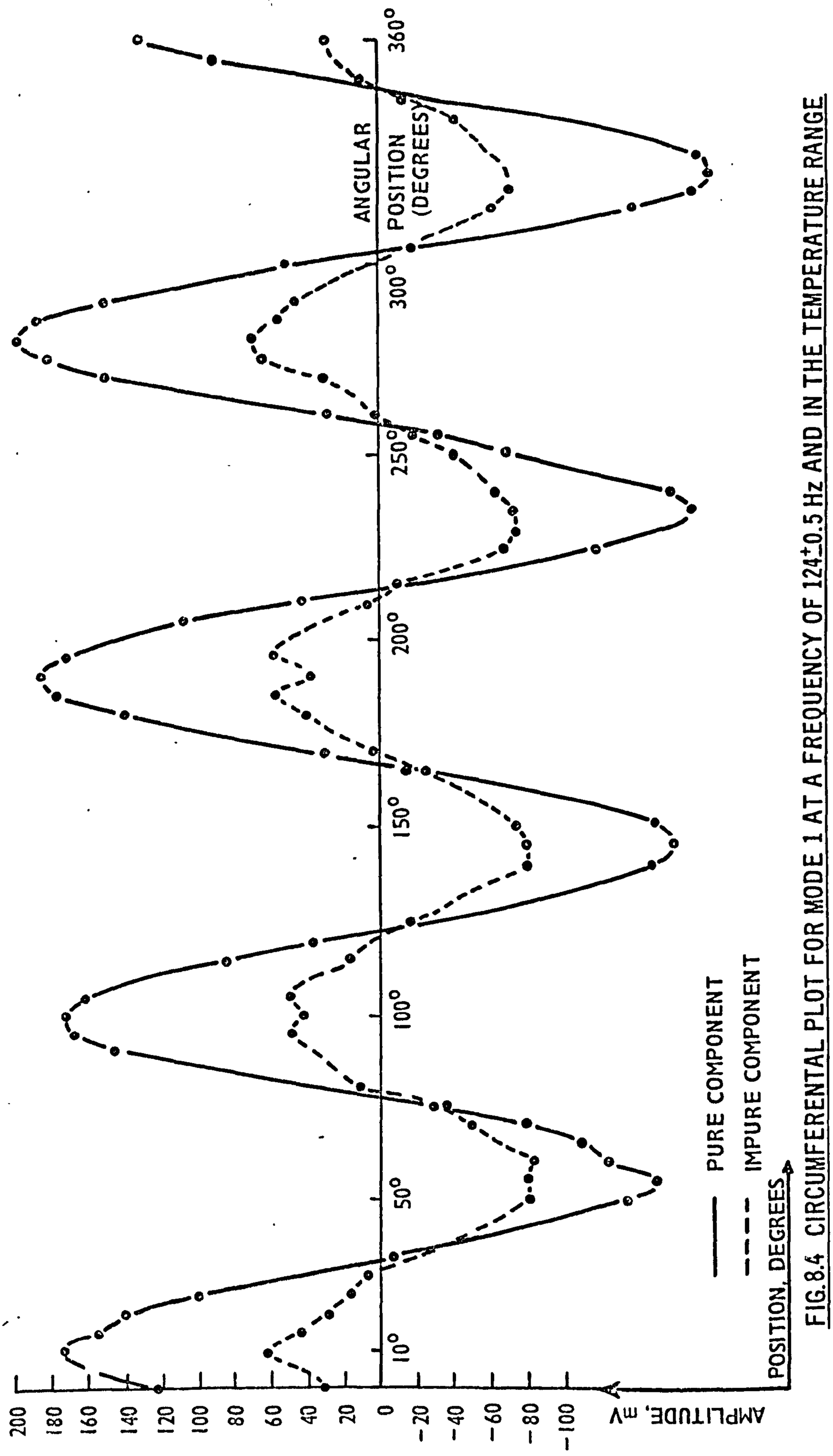

FIG.8.4 CIRCUMFERENTIAL PLOT FOR MODE 1 AT A FREQUENCY OF 124±0.5 Hz AND IN THE TEMPERATURE RANGE 20.4 TO 23.5°C (n = 4, m = 2) AT A HEIGHT OF 375 mm

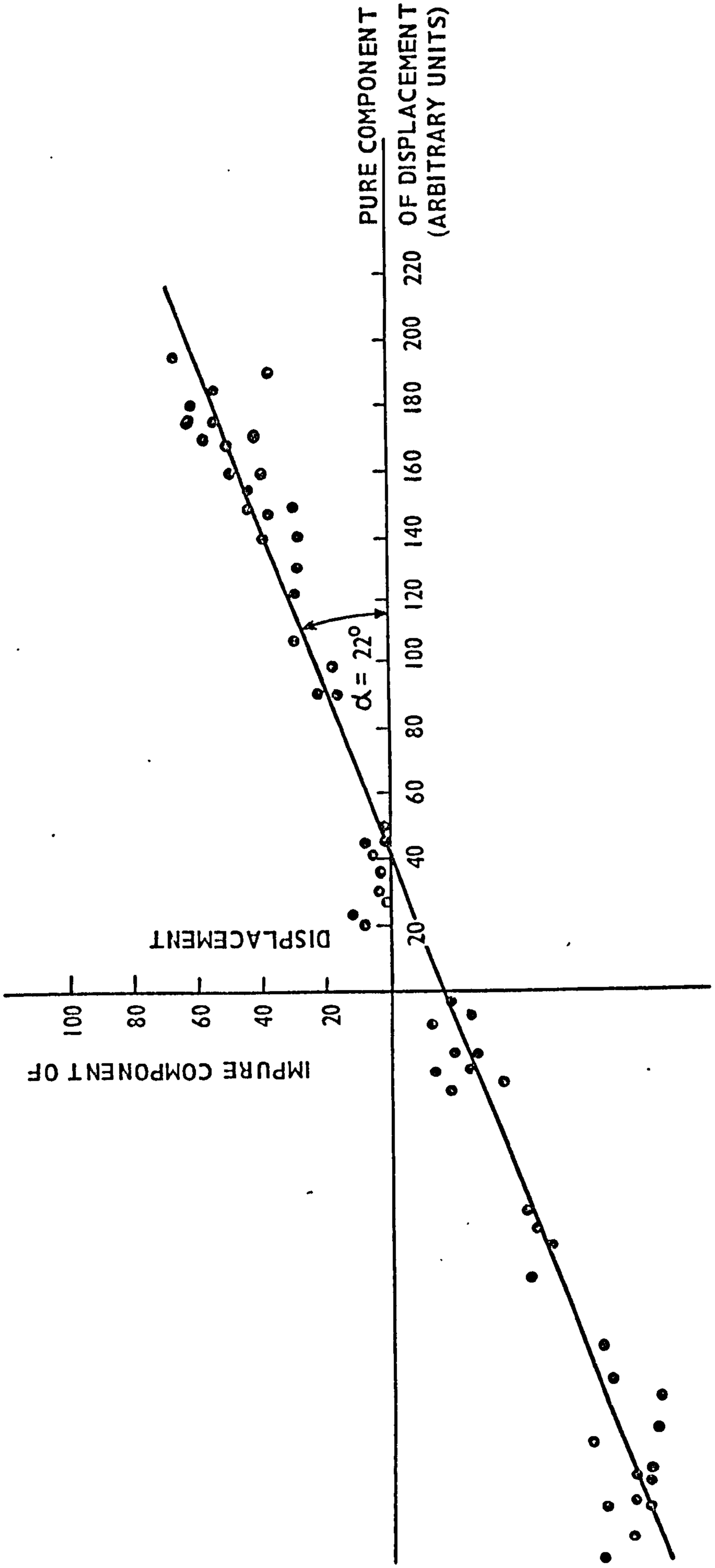

FIG. 8.5 PHASE PLOT OF CIRCUMFERENTIAL DISPLACEMENT (ALSO SEE FIG. 1)

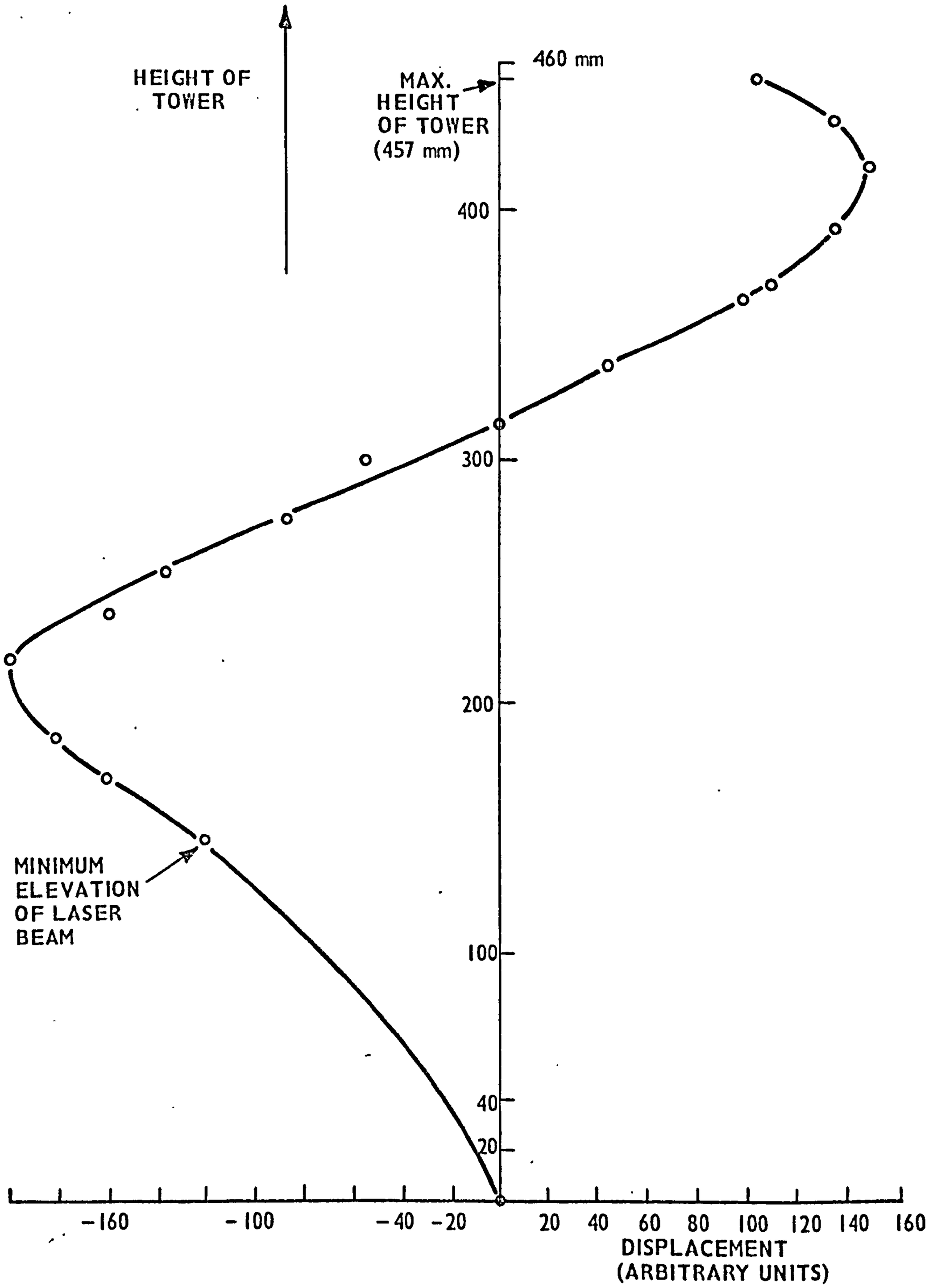

FIG. 8.6 MERIDIONAL PLOT FOR MODE 1 AT FREQUENCY OF 124±0.5 Hz AND TEMPERATURE 22°C±1.5°C (n = 4, m = 2)

Fig. 8.7 displays the variation of the impure and pure components of displacement at and near resonance. The values are seen to tend to form a circle. Again, this is coercive evidence that the mode is reasonably pure. The damping ratio is calculated by the Kennedy and Pancu [80] method to be approximately 0.01.

The preliminary results indicated that the apparatus was functioning as expected. Hence, as for Fig. 8.4, fifteen sets of measurements at various distances from the base plate were obtained for Mode 1; this necessitated about 500 displacement measurements. The results were used to obtain a contour map of the displacements, (i.e. the surface of the tower is projected onto a plane rectangle and points of equal displacement are joined together). It must be noted that intermediate points are interpolated using a cubic spline function, Greville [69]. The C.E.G.B. program 'CONTCT' (C.E.G.B. '370 Subroutine Package') was used to obtain the contour map. The information obtained from the map correlated with information already presented in Fig. 8.4 and 8.6. (Note that this contour map is given together with the contour maps for all the other modes in Fig. 8.9a and 8.9b.)

Fig. 8.8a is a contour map for Mode 2. The map shows that there are three meridional nodes; one node is very near the top of the tower. From cursory measurements of the displacements made near the top of the tower it was not evident that the latter node was present. Moreover, Winney [42] has reported two and not three meridional nodes for the second mode of vibration of the full-scale tower. Hence, some doubt was cast as to the validity of the extrapolations made by the contour mapping program CONTCT. However, the finite element computer program 'VACTIL' [5] predicted three

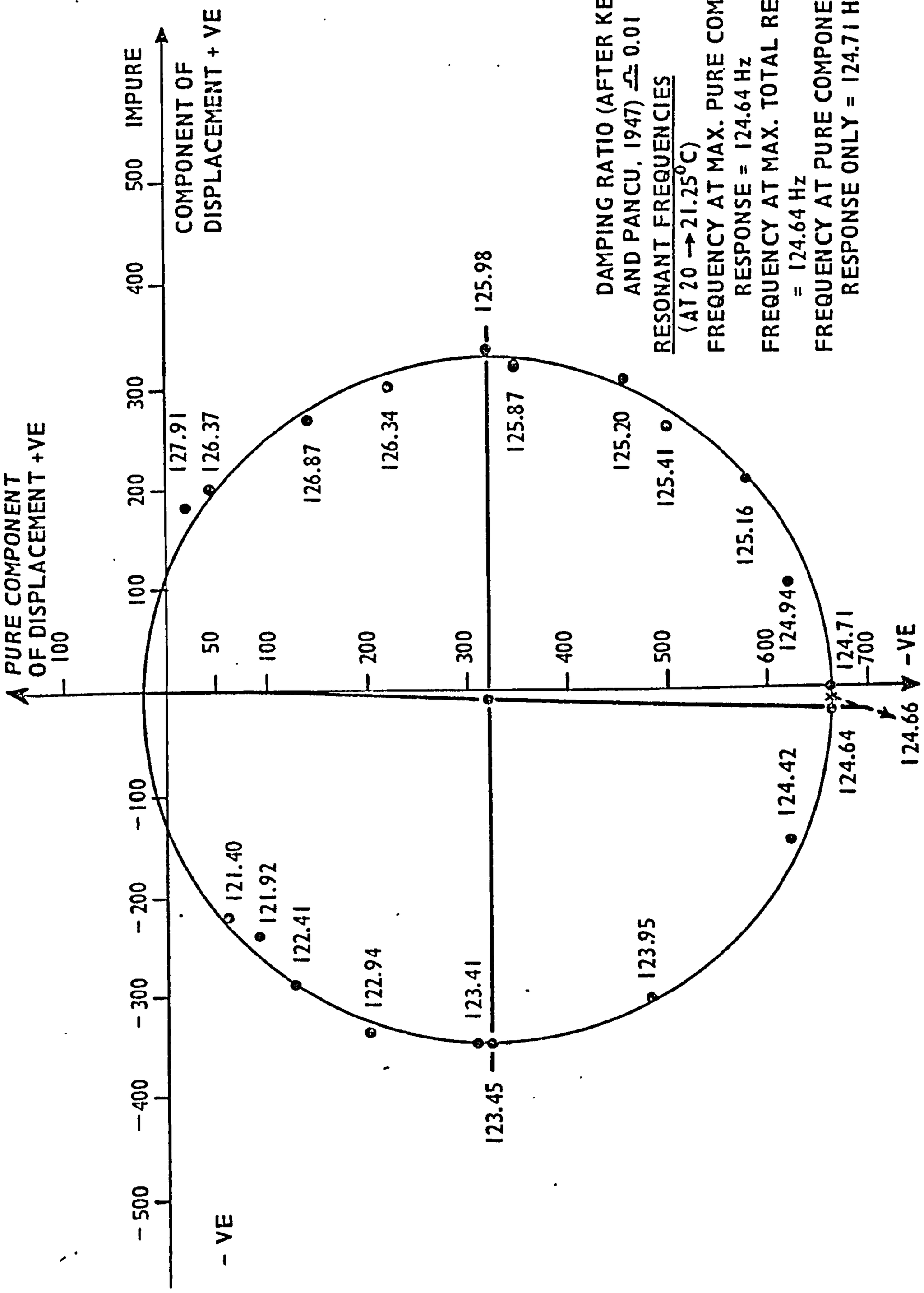

DAMPING RATIO (AFTER KENNEDY AND PANCU, 1947) $\leq$ 0.01

RESONANT FREQUENCIES (AT 20 → 21.25°C)

FREQUENCY AT MAX. PURE COMPONENT RESPONSE = 124.64 Hz

FREQUENCY AT MAX. TOTAL RESPONSE = 124.64 Hz

FREQUENCY AT PURE COMPONENT RESPONSE ONLY = 124.71 Hz

FIG. 8.7 VECTOR DIAGRAM SHOWING BEHAVIOUR OF PURE AND IMPURE COMPONENTS OF DISPLACEMENT AT AND NEAR RESONANT FREQUENCY FOR MODE 1 (n = 4, m = 2)

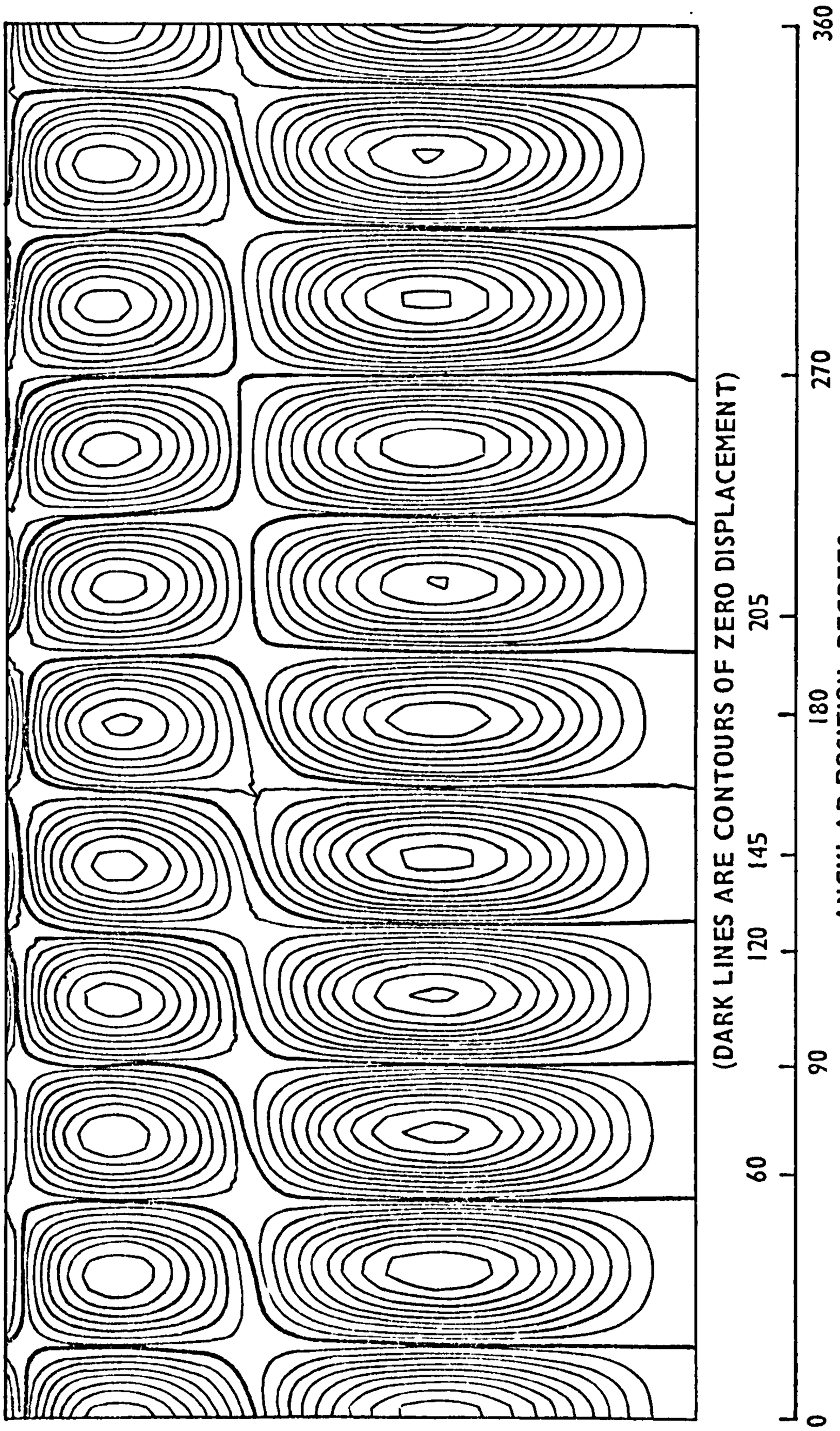

FIG. 8.8a COMPLETE CONTOUR MAP OF MODE 2
(FREQUENCY = 136.6 Hz AT TEMPERATURE 20°C)

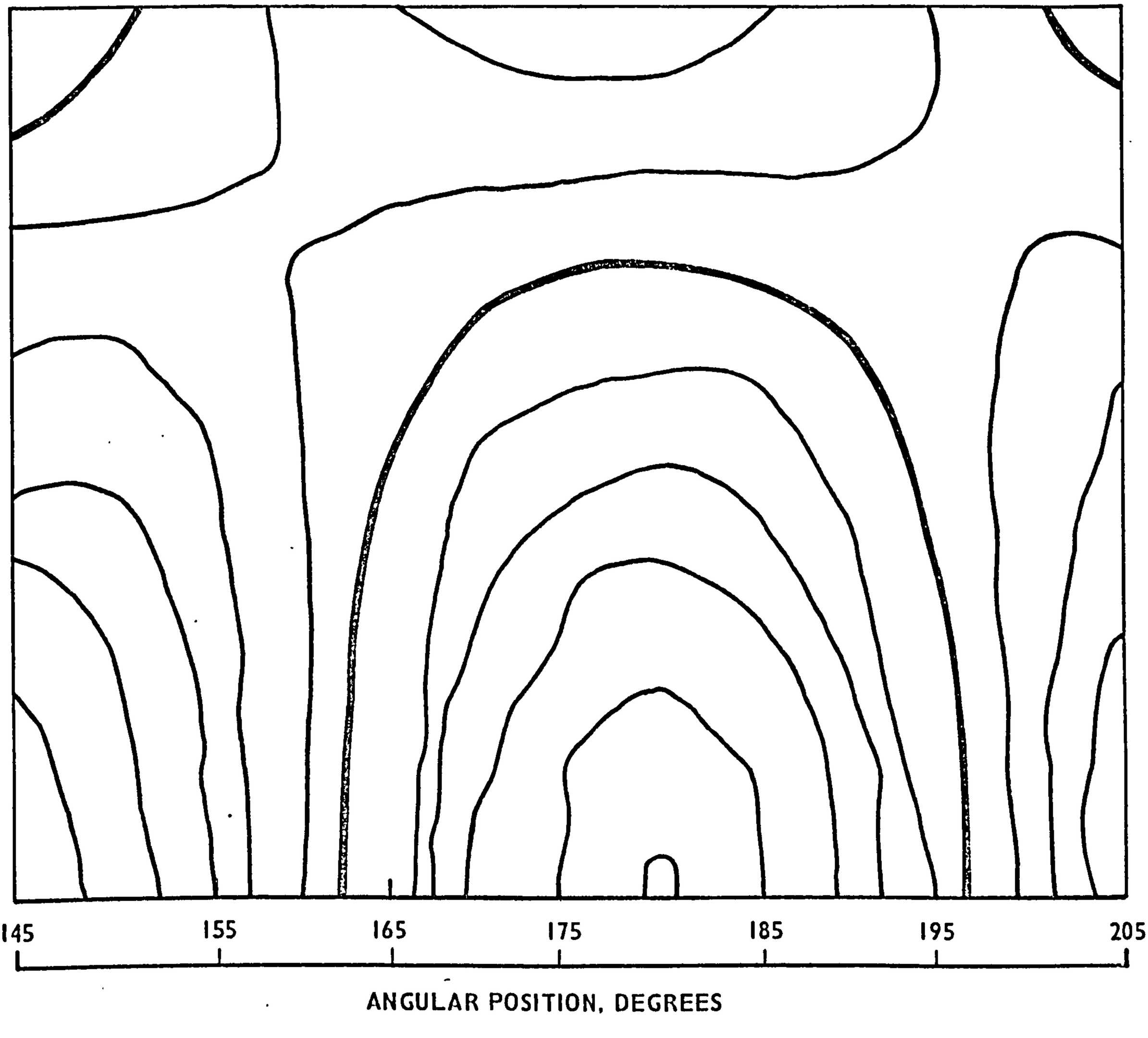

(DARK LINES ARE CONTOURS OF ZERO DISPLACEMENT)

FIG. 8.8b DETAILED CONTOUR MAP OF A SECTION OF THE TOWER FOR MODE 2 (WITH REFERENCE TO FIG. 5(a))

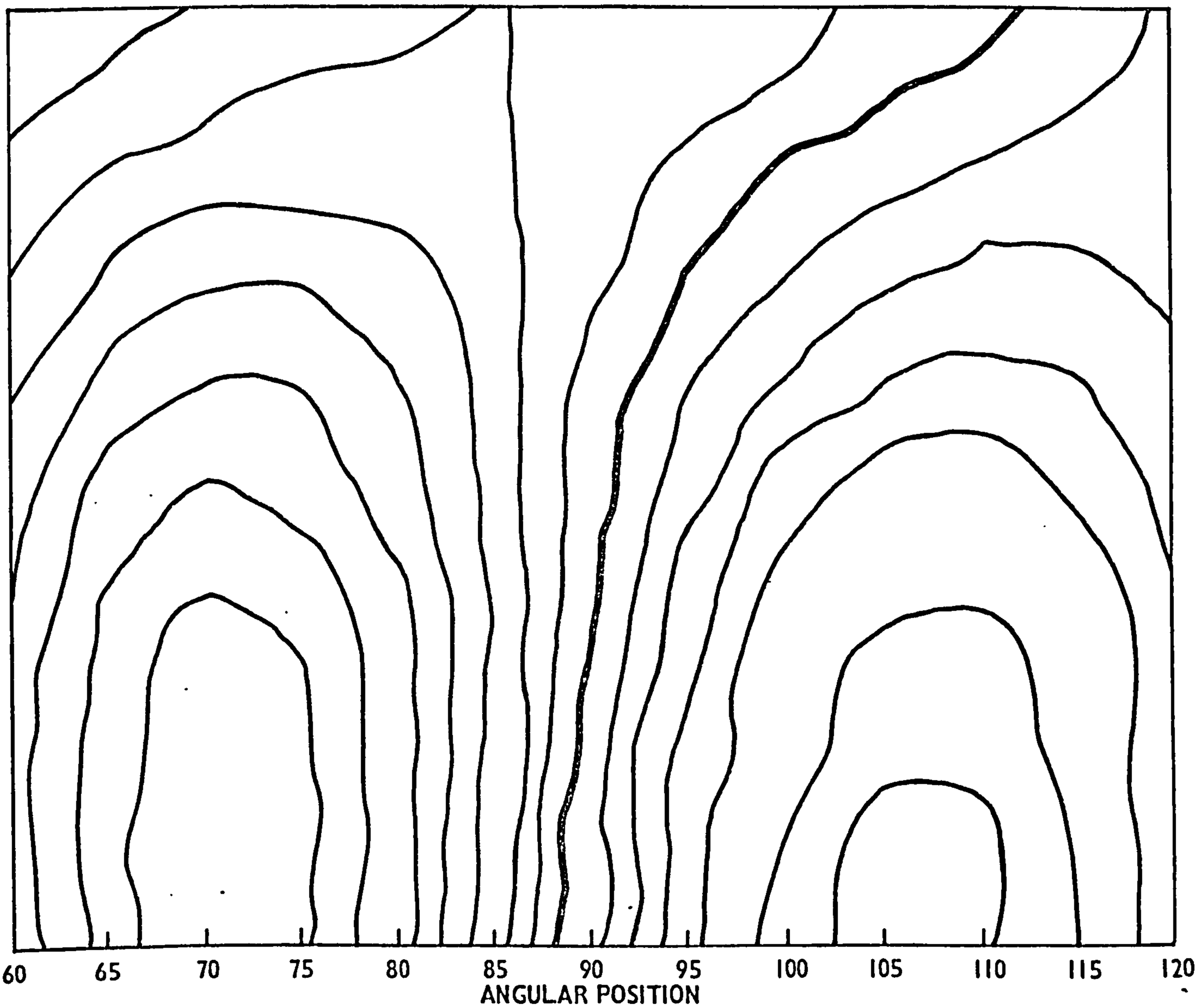

(DARK LINES ARE CONTOURS OF ZERO DISPLACEMENT)

FIG. 8.8c DETAILED CONTOUR MAP OF A SECTION OF TOWER FOR MODE 2 (WITH REFERENCE TO FIG. 5(c)

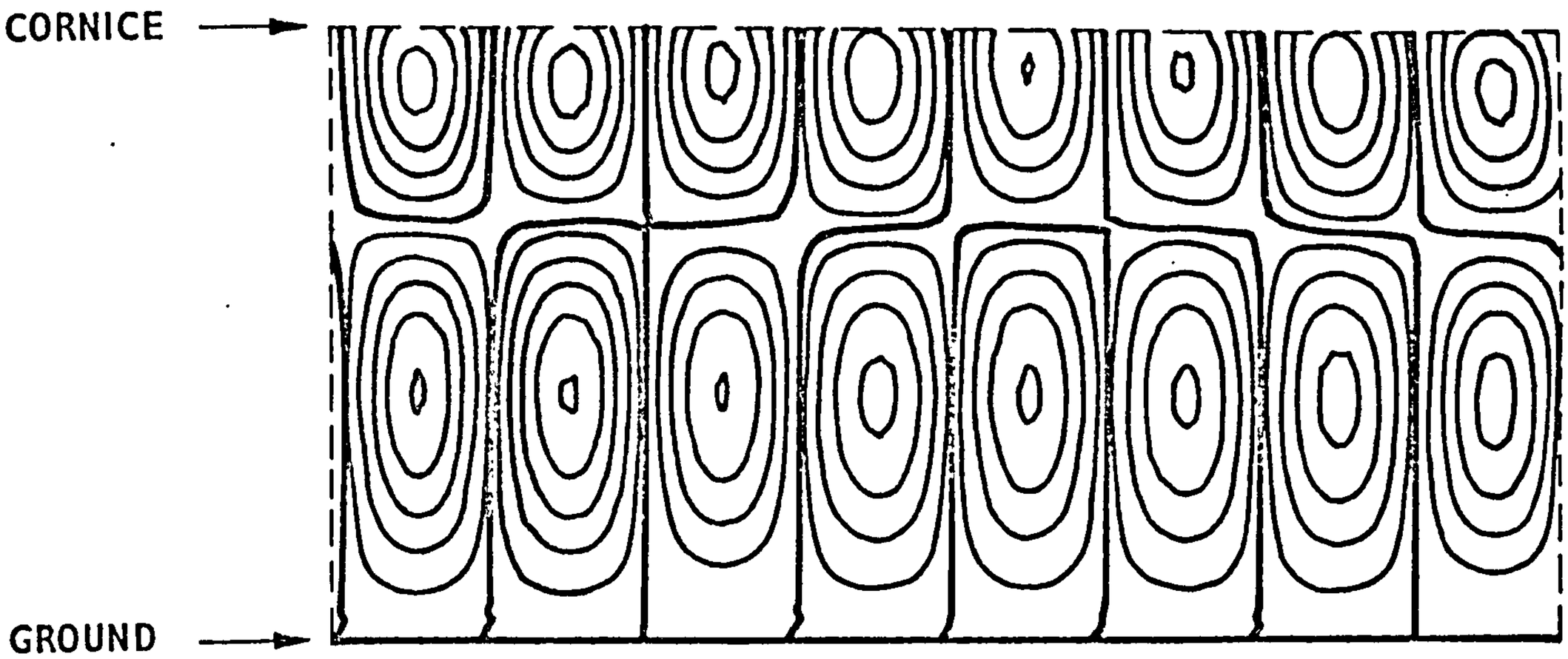

MODE ONE

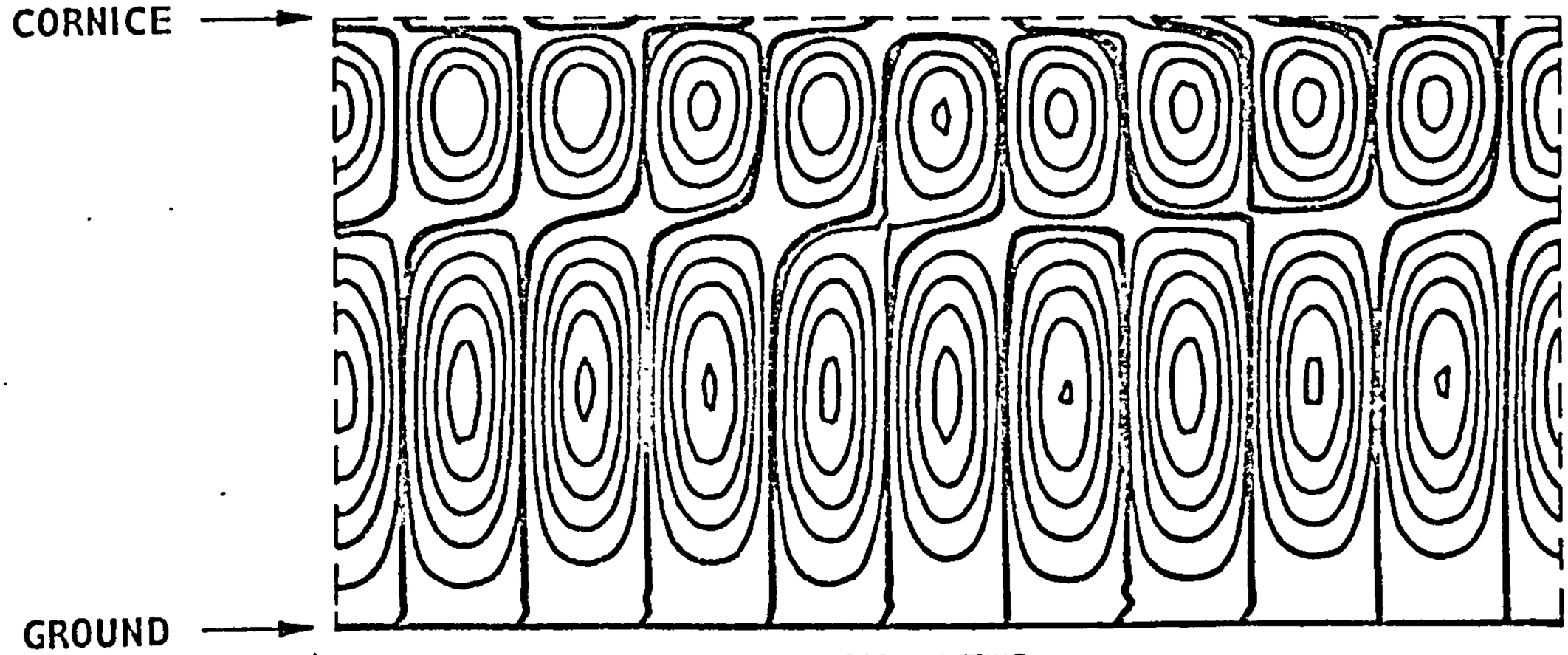

MODE TWO

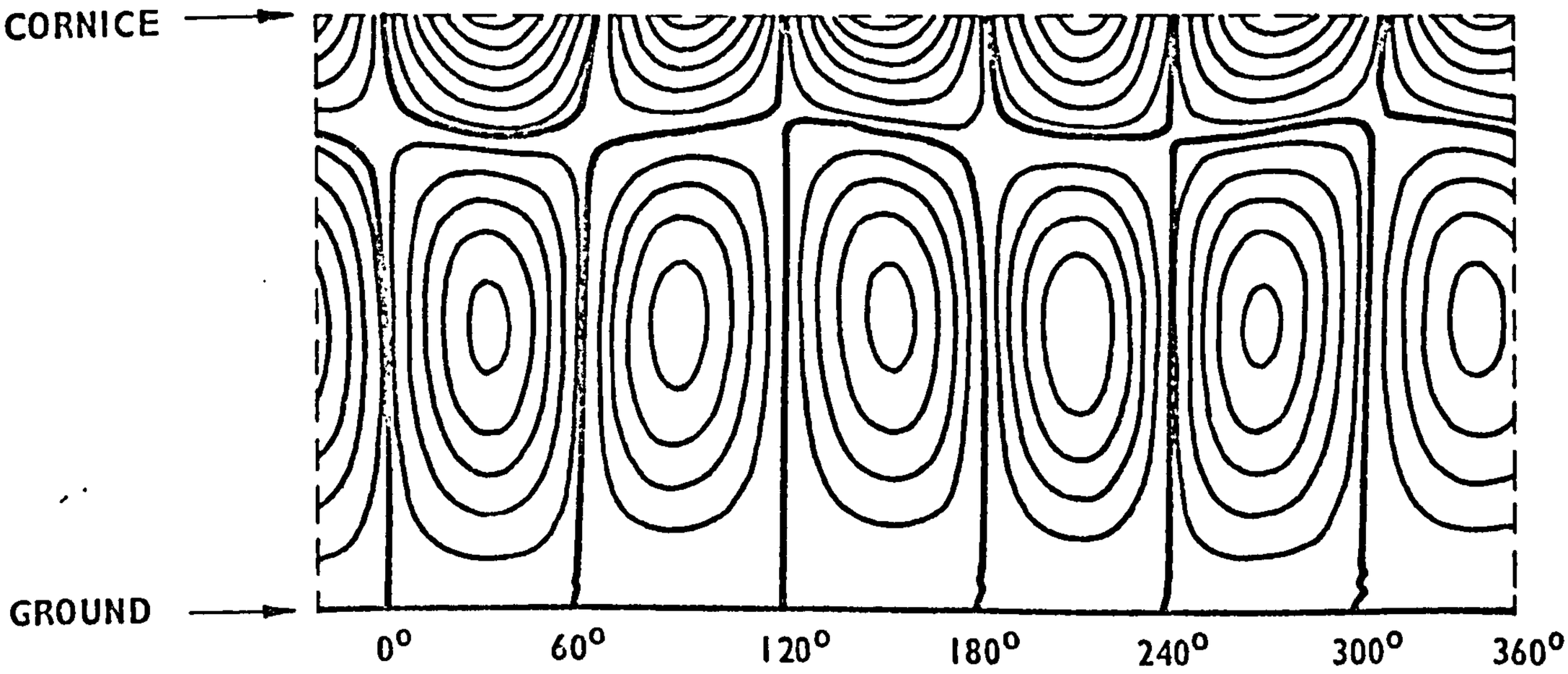

MODE THREE

FIG. 8.9a MODEL TOWER MODE SHAPES (1 TO 3)

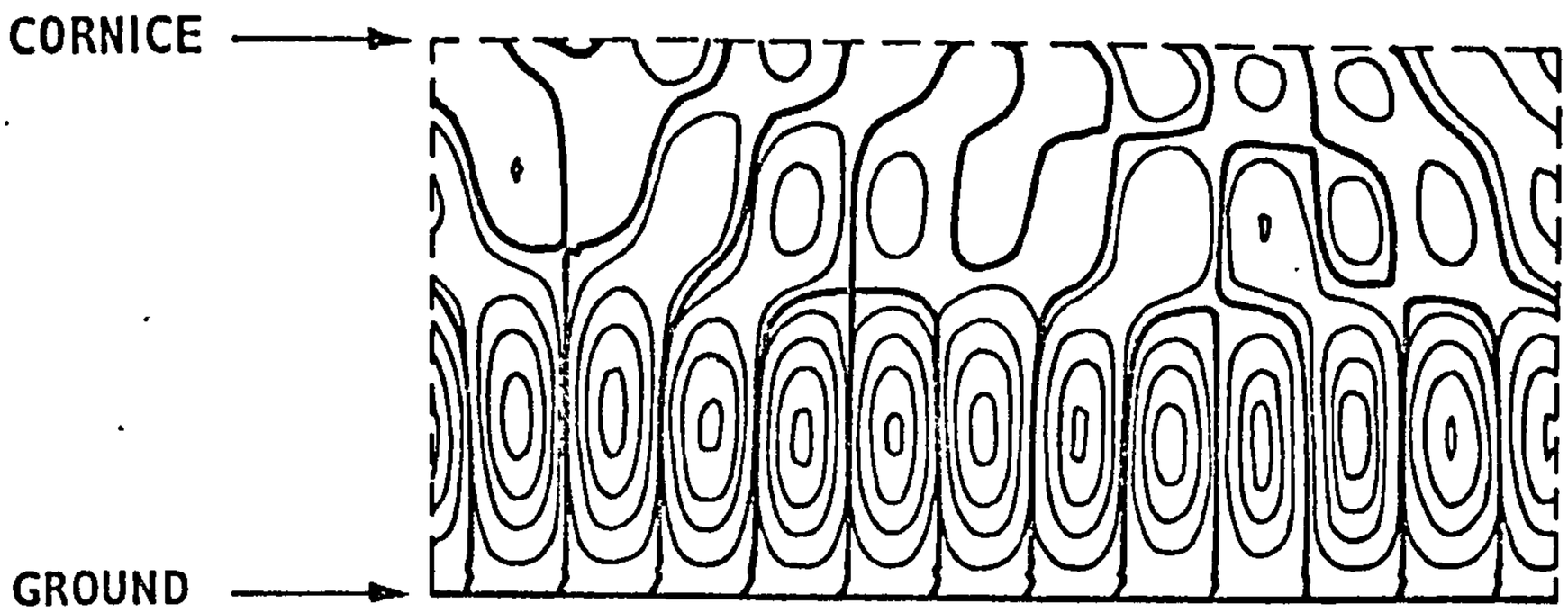

MODE FOUR

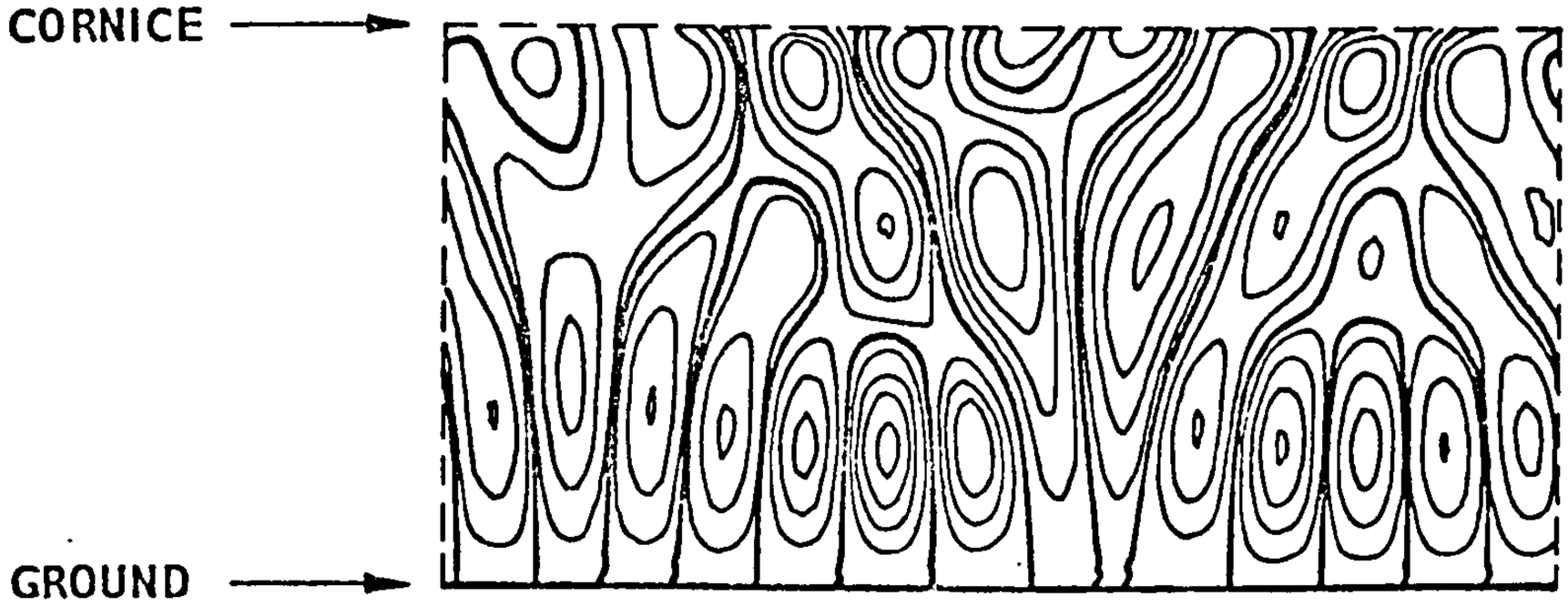

MODE FIVE 'a'

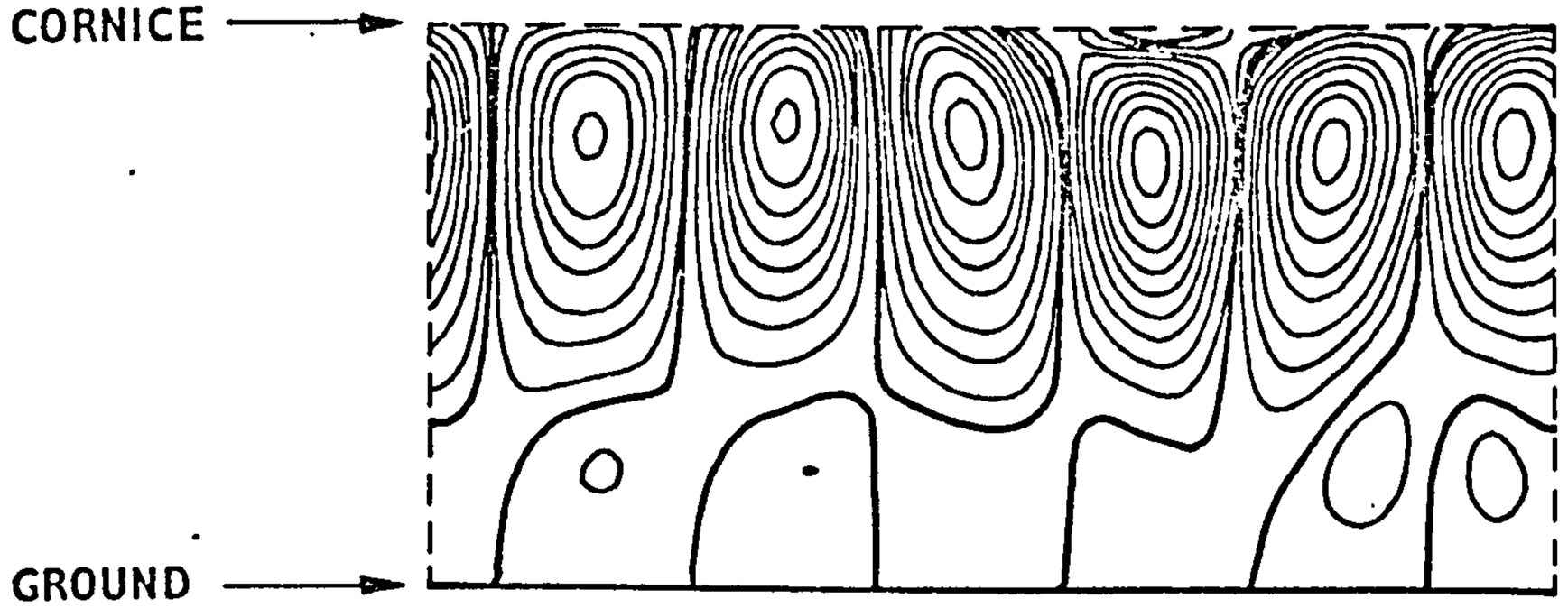

MODE FIVE 'b'

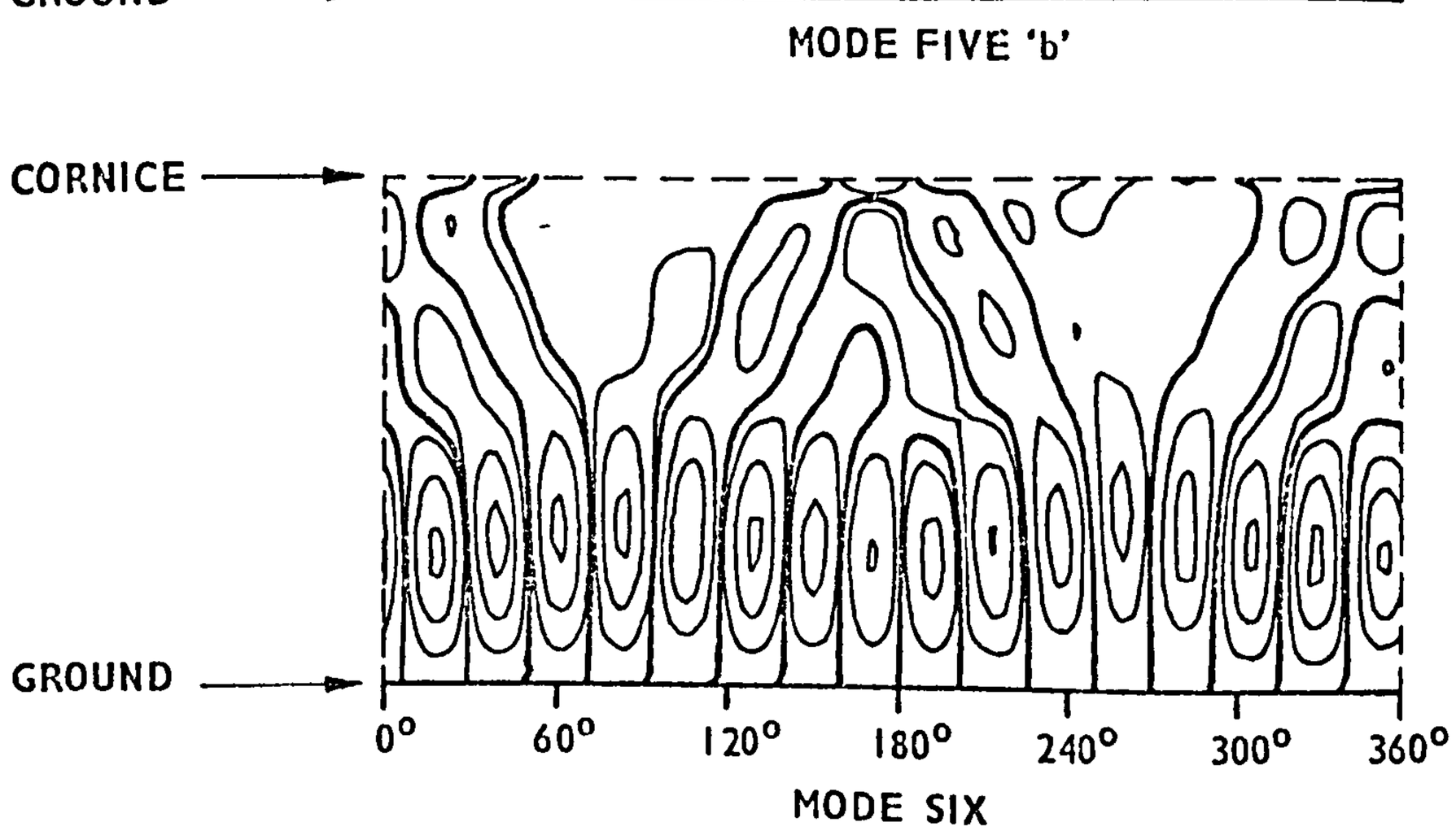

MODE SIX

FIG.8.9b MODEL TOWER MODE SHAPES (4 TO 6)

meridional nodes with one node near the top of the tower*. Thus, it was thought that a closer examination of Mode 2 was advisable.

With reference to Fig. 8.8a the displacements between the angular positions 145^{o} and 205^{o}, and, from the top of the tower to a depth of 70 mm were measured at very close intervals; about 200 readings were obtained. The results were plotted by hand and are displayed in Fig. 8.8b. The pattern of contour lines, especially the top of the contour of zero displacement in the middle of the figure, is very similar to the unique pattern obtained by CONTCT in Fig. 8.8a. between the angular positions 145^{o} and 205^{o}. Hence, it can be concluded that the contour map produced by the program CONTCT is a reasonably accurate representation of the practical situation.

Fig. 8.8c was obtained by the method described previously for Fig. 8.8b, and is the detailed measurement of displacements between angular positions 60^{o} and 120^{o} in Fig. 8.8a. This figure explains why it is not immediately obvious that a third meridional node is present near the top of the tower. For this node to be readily detected, the vertical line of zero displacement should be deviated at right-angles when it is near the top of the tower, to form the third meridional node. Examination of Fig. 8.8c shows that in the practical case the vertical contour of zero displacement is deviated by an angle less than the 90^{o} that is expected. In Fig. 8.8a, however, the extrapolations made by CONTCT enable the meridional node to be clearly observed. It is concluded, therefore, that Mode 2 has three meriodinal nodes, and that cursory measurements of displacements

*In order to keep the logical flow of the discussion in this chapter it is necessary to refer to information that will be presented in the next chapter.

at the top of the tower can be misleading.

Although Modes 3 and 4 were excited with comparative ease, excitation of Mode 4 was relatively difficult because of harmonic interference from other modes. The unwanted harmonics can probably be attenuated by the use of six more exciters; see Section 8.4. (It is interesting to note that the contour map obtained for Mode 3 was very similar to a hologram of displacements presented by Leim, Hazell and Blasko [86, Plate 1] for a vibrating cylinder.)

It was found difficult to correctly excite the mode with the fifth lowest frequency. This is because there are, in fact, several modes within a very narrow band of frequencies. For convenience, and to be concordant with past practice, these modes will be referred to as "Mode 5". The lowest frequency measured (at a temperature of 20°C) for Mode 5 was 174 Hz with m and n values of 3 and 7, respectively. Also, two more modes between the former frequency and approximately 180 Hz were obtained; the m, n values were 3, 5 and 2, 3. VACTIL predicts mode shapes (m, n) of (3, 7) and (3, 5) within this frequency range; the mode shape (2, 3) is not, however, predicted. The measurements made by Winney [42] show that the full-scale tower has a mode shape of (3, 7). It is possible therefore that the mode shape (2, 3) was measured due to interaction between the other two modes (see Section 8.4.)

Mode 6 was investigated as VACTIL predicted a mode of vibration at a frequency of approximately 206 Hz. The measured value was 209.5 Hz (as seen in Table 1) and the mode shape was (3, 8). Winney [42] obtained the same values of m and n for the full-scale structure at a frequency close to the 'normalised' frequency (see below and Table 8.1). Hence, in both the model and full-scale work a meridional node was observed very close to the

top of the tower. VACTIL, however, predicts two meridional nodes with a third node very close to, but just above, the top of the tower.

Table 1 presents the resonant frequencies and mode shapes obtained for the model cooling tower. The corresponding results for the full-scale structure, reported by Winney [42], are also given for comparison. It must be noted that all the model frequencies were measured at $20^{o}C$.

'Normalisation' (extrapolation to the corresponding full-scale values) of the resonant frequencies obtained for the model tower is a convenient method of comparing the frequencies obtained for the model and corresponding full-scale structure. The normalised frequency, $\bar{F}$, is given by the equation:-

$$\bar{F} \simeq \frac{F_s}{250}\left(\frac{M_s}{E_s} \times \frac{E_f}{M_f}\right)^{\frac{1}{2}} \qquad \ldots(8.1)$$

where F, M and E are frequency, mass density and Young's Modulus, respectively. (It is assumed that the values of Poisson's ratio are sufficiently similar to be ignored; see Armitt [25], page 5.) The subscripts s and f pertain to the model and full scale structures, respectively. (The denominator 250 is the scale factor.) Burrough [87] reports that

$$E_f = 29.5 \times 10^{9}\ N\ m^{-2} \quad \text{and} \quad M_f = 2323\ kg\ m^{-3}$$

The values of E_s and M_s must now be considered.

The Young's Modulus of 'Devcon B', E_s, was measured by Blow [88] to be $(5.24 \times 10^{9} \pm 0.1\%)\ N\ m^{-2}$ at a temperature of $20^{o}C$. He also measured the mass density, M_s, to have a value of

$(2.31 \times 10^3 \pm 0.1\%)$ kg m^{-3}. It must be noted that the samples used by Blow were a few months old. Also, that various different values for E_s and M_s have been reported by other workers (see below). Blow states that the variation in values quoted for M_s is probably due to differences in the concentrations of air bubbles formed in the epoxy during the mixing process.

Assuming values for E_s and M_s reported by Blow [88], the normalised frequency of Mode 1, using equation (8.1) is:-

(1.187 ±0.0086) Hz .

Table 8.1: Comparison of Resonant Frequencies and Mode Shapes of Model and Full-Scale Structures (Didcot Cooling Tower) (Temperature 20°C for Model)

Mode No.	Model				Full-Scale Tower	m,n
	Measured Frequency Hz	Normalised* Frequency 1, Hz	Normalised* Frequency 2, Hz	m,n	Measured Frequency Hz	
1	124.5	1.16 (7.4)†	1.14 (5.6)	2,4	1.08	2,4
2	136.6	1.27 (8.1)	1.25 (6.4)	3,5	1.175	2,5
3	147.0	1.37 (5.3)	1.34 (3.1)	2,3	1.30	2,3
4	156.0	1.45 (2.8)	1.43 (2.8)	3,6	1.41	3,6
5a	174.0	1.62 (-1.8)	1.59 (-3.6)	3,7	1.65	3,7
5b	180.0	1.67 (1.2)	1.64 (-.6)	3,5 and 2,3		
6	209.5	1.95 (-1.5)	1.91 (-3.5)	3,8	1.98	3,8

*See text; †Presentage difference, with full-scale values as reference

However, if the values quoted by other sources are used, different frequencies are calculated; e.g. using the manufacturer's specifications,

$$E_s = 5.86 \times 10^9 \text{ N m}^{-2} \quad \text{and} \quad M_s = 2.5 \times 10^3 \text{ kg m}^{-3},$$

a value of 1.159 Hz is obtained. Alternatively, Deb Nath's [89] values which are

$$E_s = 5.516 \times 10^9 \text{ N m}^{-2} \quad \text{and} \quad M_s = 2243 \text{ kg m}^{-3}$$

yield a frequency of 1.13 Hz. Finally, if Armitt's [90] values of

$$E_s = 5.96 \times 10^9 \text{ N m}^{-2} \quad \text{and} \quad M_s = 2400 \text{ kg m}^{-3}$$

are taken the frequency is 1.153 Hz. The average of all four values is 1.155 Hz. (It is pertinent to note that VACTIL predicts a resonant frequency of 1.154 Hz.)

Hence, it is not immediately apparent which value of E_s and M_s are to be used in the present work. The careful measurements made by Blow are particularly noteworthy. However, ageing tends to produce a small change in the properties of Devcon (Blow, personal communication and Devcon Ltd.); remember that the samples tests by Blow were only a few months old. The resonant frequencies measured by Blow in May 1973 (unpublished data) are consistently higher than those measured in 1972 (by J. Hannah, unpublished data) when the model tower was new, by a factor of about 1.036 (≈4%). This would indicate that the ratio of E and M has increased by a factor of 1.036^2 (= 1.0737). Hence,

multiplying Blow's [88] value of E_s/M_s (i.e. 2.268×10^6 N m kg^{-1} for 'new' Devcon), by this factor yields a value of 2.435×10^6 N m kg^{-1}. This is less than the E/M value obtained from Deb Nath's data (2.456×10^6 N m kg^{-1}) and is greater than that quoted by Armitt (2.371×10^6 N m kg^{-1}) and the manufacturer (2.344×10^6 N m kg^{-1}).

Blow's E/M value of 2.268×10^6 N m kg^{-1} appears therefore to be a lower-bound to the value of this ratio. Any increase in the value of E/M above Blow's value is probably due to ageing. Deb Nath's value of 2.45957×10^6 N m kg^{-1} is probably an upper bound to the value of E/M. It is pertinent to note that Armitt's and the manufacturer's values are close to the mean of the upper and lower bound of values which is 2.364×10^6 N m kg^{-1}. Thus, the four values of E/M appear to span the possible range of E/M values. The average value of the four readings is 2.3607×10^6 N m kg^{-1}. This value is very close to the mean of the upper and lower bound of values and also the manufacturer's value. The manufacturer's value is based on very many measurements on a large number of samples of Devcon and thus appears to be a valid base for the normalization of the model frequencies. Therefore this value together with equation (8.1) is used to obtain the values in the column headed 'Normalised Frequency 1' in Table 8.1. Blow's value of E/M adjusted for ageing (i.e. 2.435 MN m kg^{-1}; see above) is as tenable, and is used to obtain 'Normalised Frequency 2' in column 4 of the Table. The number in parentheses in columns 3 and 4 refer to the percentage difference between the normalised and full-scale frequencies. It is important to note the similarity in both sets of normalised frequencies whilst remembering that the material properties of Devcon used in the two normalisation procedures depend on the measurements made by two different sources. In the absence

of firm arguments to the contrary, and in the knowledge that any error so obtained would be small, we shall adopt the manufacturer's values for the material properties of Devcon in the normalisation of the model cooling tower frequencies (see Chapter 9).

Table 8.1 shows that the maximum discrepancy between the normalised frequencies 1 and 2 of the model and full-scale structure is 8.1%. However, it is observed that the maximum discrepancy between the higher three modes is less (maximum difference is 3.6%). The discrepancies between the lower modes is almost certainly due to differences in the foundation elasticity* - see Chapter 9. The model foundations are assumed to be rigid, see Section 8.2, whereas the full-scale structure has a vertical foundation elasticity of approximately 1.6×10^{9} N m^{-1}, [91]. This will be discussed in Chapter 9 in detail. It therefore appears likely that if the foundation elasticity of a model tower is simulated to be equivalent to that of the full-scale structure good correlation (better than 5%) between the measured values for the full-scale and model structures can be achieved.

8.4 Suggested Improvements to the Measurement Techniques

Whilst the apparatus and technique used for this work is satisfactory it is thought that the higher modes can be more conveniently determined by several changes.

During the present experimental programme it was found possible to resonate the tower such that while the vibration of the bottom half of the tower was clearly defined (i.e. the contour map of this area was clearly defined, as for example, in the whole of

*A crude though interesting experiment illustrated this point. During excitation of the higher modes, touching the base of the legs of the vibrating cooling tower had very little effect. However, for the lower modes the effect was very pronounced.

Fig. 8.8a) the vibration of the top half of the tower was not (i.e. the contour map of the top half was composed of 'distorted ellipses' - see Fig. 8.9b). This is very probably not due to a non-classical mode of vibration as proposed by Williams [33] but is very probably caused by harmonic interference from neighbouring modes. This interference can be greatly attenuated by the use of more exciters. For example, 'Mode 5', which is not one but two or more modes could be probably investigated by employing six exciters at the bottom of the tower and six exciters at the top of the tower. (It must be appreciated that theoretically, a system with N unconstrained independent degrees of freedom requires N exciters to excite a pure mode; Traill-Nash [81].)

Phase shifters should be used to correct a small phase inaccuracy as described below:-

The excitation forces are supplied by the '0^{o}' output of the oscillator. Resonance is defined as a θ^{o} phase relationship between response and excitation forces. θ^{o} is '0^{o}' or '$\pm 90^{o}$' depending on whether a velocity or displacement/acceleration response is being considered. The Lissajous displays are used to compare in-phase signals. Hence, the excitation force is represented by the '0^{o}' or '90^{o}' outputs of the oscillator, for an 'in-line' display, depending on whether θ^{o} is '0^{o}' or '90^{o}', respectively.

In practice, however, the '0^{o}' output of the oscillator undergoes a small phase change, α^{o}, before it supplies the excitation force. Thus, when the Lissajous display is 'in-line' the relationship between the response and excitation force is not θ^{o} as required but $(\theta \pm \alpha)$ degrees. This small phase error can easily be negated by

by the use of phase shifters* acting on the '0^{o}' and '90^{o}' outputs of the V.T.O.

8.5 Conclusions

1. The free vibration of a 1/250th scale model of the Didcot tower has been described by measuring its resonant frequencies and mode shapes. Six modes of vibration have been observed. These modes agree, to a large extent, with those observed for the full-scale structure. The 'fifth mode' appears really to consist of two or more modes at similar resonant frequencies. Adopting the improvements advocated in Section 8.4 would enable a more accurate description of these modes.

2. The use of a laser as a displacement measuring device for the model structure has been shown to be highly satisfactory, provided a few simple precautions are observed. Such measurements are more speedily and accurately obtained, when compared with the use of other devices such as capacitance transducers.

3. The resonant behaviour of the model tower is similar to that reported for the full-scale structure for the first six modes investigated. The mode shapes are the same (except for Mode 2; the reason for the discrepancy is explained below), whilst the values of resonant frequency agree to within 8.1%. The agreement is better (less than 5%) for higher modes. The poorer agreement between the resonant frequencies for the lower modes is very probably due to differences in foundation elasticity between the model and full-scale structures. Foundation elasticity thus appears to be an important

---

* Two 'Brookdeal' Model 421 phase shifters were purchased for this purpose during the latter stages of the project. While time did not allow for the inclusion of these in the present work, preliminary results were seen to be envouraging. Also, the T.F.A. has been modified to incorporate the phase shifters.

property which must be considered in all future model work.

4. The mode with the second lowest frequency, Mode 2, has three and not two meridional nodes as appears from a cursory examination (and as hitherto believed). This observation agrees with that predicted by the finite element program VACTIL.

CHAPTER NINE

FINITE ELEMENT ANALYSIS OF MODEL AND FULL-SCALE COOLING TOWERS

9. FINITE ELEMENT ANALYSIS OF MODEL AND FULL-SCALE COOLING TOWERS

This chapter describes the finite element free vibration analysis of the model and corresponding full-scale tower at Didcot. The effects of leg-supports, foundation elasticity and variation in thickness of the wall of the tower shell will be explicitly included in the analysis. It will be shown that good agreement is obtained between the results of the finite element analysis and the experimental results for the model and corresponding full-scale structures. Having validated the finite element method, several parameters that affect the resonant behaviour of cooling towers will be investigated. (The parameters concerned, for example foundation elasticity, could not have been investigated with any degree of confidence in the past.) The discrepancies that exist between model and full-scale experimental data will then be explained. Proposals will be made, including the corrections required, to accurately normalize model frequencies for meaningful comparison with full-scale values.

9.1.1 Summary of Previous Attempts

In Chapter 2 a review of the work by previous authors was presented. In order to make this chapter more readable and self-contained we shall summarize and add a little to the findings of that review:

The resonant frequencies of a cooling tower are very dependent on its geometry. (It will be seen that even small changes in geometry affect the resonant frequencies.) Thus, to a considerable degree, the free vibrational behaviour of a tower is dictated at the design stage. It would be of great value, therefore, to predict the values of the resonant frequencies for a given design and, also, to explore the effect of small alternations to the design. This would

lead, very probably, to economies in construction of the tower. (As a cooling tower costs, very roughly, about three-quarter of a million pounds, a small fractional saving is appreciable in real terms.)

Previous methods used to predict the dynamic behaviour of cooling towers have used several techniques, for example:

(i) Solving the equations of motion of an idealized tower.

(ii) Conducting experimental investigations on scaled models.

(iii) Finite element solutions.

These methods have not proved to be entirely satisfactory. For example method (i) is limited to particular geometries and extrapolation of the results to practical structures have not produced very satisfactory information. The model investigation requires a considerable experimental effort. The information has then to be extrapolated in order to predict the behaviour of the full-scale structure; the extrapolation contributes to the degree of uncertainty. Discrepancies are also observed between the experimental results obtained for the model and corresponding full-scale structure. In Chapter 8 it was observed that the values of the resultant frequencies measured for the model, after normalisation, were relatively higher for the lower modes than the corresponding values for the full-scale structure [42], whereas the agreement between the higher modes was very much better.

The finite element solutions are probably the most convenient. Whilst the method is capable of yielding a considerable degree of accuracy the finite element representation of cooling towers has not been particularly accurate. For example, the leg-supports of the

towers have not been correctly included in the analyses, and foundation elasticity has not (in general) been considered. Consequently, the better finite element solutions (e.g. Deb Nath [40] usually predict resonant frequencies that are within only 10 to 20% of the values obtained experimentally. Moreover, there is usually some discrepancy between the mode shapes. It is of interest to note that finite element methods tend to yield results that are in poorer agreement with the results obtained for full-scale structures than with results for the corresponding models.

The above shows that several questions must be answered in a successful investigation of the free vibrational behaviour of cooling towers. It is hoped to answer many of these questions in the following sections. Initially, it is instructive to summarize briefly some relevant information (gleaned from the literature) regarding the free vibration of cooling towers:

(a) Self-load stresses (i.e. due to dead weight) appear to have a marginal effect on the natural frequencies of cooling towers.

(b) Rotationally symmetric shells of revolution, without singularities, appear to have no modes of vibration which are 'non-classical' (i.e. the circumferential wave-number, n, does not vary with the meridional position on the structure.).

(c) The lower range of natural frequencies, i.e. $3 \leq n \leq 8$, is increased by an increase in the thickness of the cornice (thickening at the top of the cooling tower); however, for the predominantly extensional type modes the resonant frequencies are decreased. For values of n greater than 7, the effect of increasing the thickness of the cornice is negligible.

(d) The greatest resonant response of a tower to wind excitation occurs in the mode having the lowest natural frequency (which is usually found to have a value greater than 0.5 Hz).

(e) As a general rule, the resonant frequency of a tower decreases by up to 5% for wind speeds increasing from zero to the design wind speed.

(f) Wind-induced maximum resonant stress varies inversely as the square of the resonant frequency and directly as the fourth power of the wind speed.

9.1.2 Review of the Finite Element Method for Cooling Towers

The shell of the cooling tower is represented by doubly curved shell finite elements (Chapter 4). The leg-supports of the tower are modelled by beam elements (Section 6.3). The cylindrical coordinate system is chosen as the global system for both elements. Therefore it is necessary to transform the shell element matrices to be compatible with this system (Section 6.2). A representative substructure is choosen. In the case of cooling towers with 'V-pairs' of leg-supports the substructure includes one pair of legs. A typical finite element mesh and substructure is illustrated in Fig. 7.1. Complex constraints are applied to the substructure and the eigenvalue equation solved as detailed in Chapter 3. The number of circumferential wave lengths, n, is fixed by the appropriate choice of the phase angle $\psi = \frac{2\pi}{N} \times n$ (see Chapter 3 and Appendix 7.1) where N is the number of identical substructures forming the structure. Thus, if the angle subtended by the substructure (CQ) is 9^{o} (see Fig. 7.1) then for $\psi = 36^{o}$ a mode with n = 4 would be obtained.

9.2 Circumferential Wave Number (n)

At this point it is pertinent to explain the author's interpretation of the value to be ascribed to n, when axisymmetric or rotationally periodic structures are analysed. For an axisymmetric structure n is identical to the number of sinusiodal (or cosinusoidal) wave lengths around any circumferential line of the structure and is equal to half the number of nodes around the circumference. For rotationally periodic structures n is as defined in Section 9.1.2. That is, if the displacements at substructure boundaries are alone noted, these displacements can be placed on a sinusoidal wave of wave length which is $(\frac{1}{n})$th the circumference. Note, however, that no assumption is made regarding the pattern of displacements between substructure boundaries. Thus for a non-axisymmetric structure that is rotationally periodic the circumferential displacement patterns may be different at different meridional positions; however, the sinusoidal relationships of the displacements at substructure boundaries alone, over any given circumferential line, will remain. Hence, if n is calculated by counting the number of 'zero crossings' of a displacement-circumferential-wave, the resulting value may be different from that obtained by using the definition given above. Thus while the method of calculating n used in this thesis will result in a constant value (of n) at any meridional position on a cooling tower with leg-supports, the 'zero-crossings method' may give different values of n at different meridional positions. This may explain why Deb Nath [40], who attempted to model cooling tower leg-supports by having 'cut-outs' at the base of the shell, states that 'non-classical' modes are present in the free vibration of cooling towers.

9.3 Preliminary Tests

Initially, in order to verify that the program (VACTIL) could accurately analyse comparatively simple shells of revolution, preliminary tests were performed.

VACTIL was used to analyse a cylinder 'simply supported' (see Section 11.2.1) at both ends. Complex constraints were applied for the mode with n = 4. A resonant frequency of 91.13 Hz was obtained with m = 2. This compares reasonably with an analytical solution [94, page 194] which predicts a frequency of 91.09 Hz.

It must be noted that, in the above example, VACTIL was used with CQ (see Section 9.12) equal to 9^{o}. If CQ was made smaller, e.g. 4^{o}, marginally higher accuracy would have resulted as this is equivalent to using a finer mesh of elements. In the analysis of the cooling towers (described in Sections 9.4 and 9.5) it was necessary to initialize CQ to 9^{o}. Hence, this value was used for the preliminary tests.

The accuracy of the coordinate transformation described in Chapter 6 was verified by comparing the resonant frequencies obtained for a hyperboloid, with no constraints, with and without a coordinate transformation. The resonant frequencies were observed to be exact (to the eight significant figures given in the print-out) for the 'non-rigid body frequencies'. (The 'rigid body frequencies' were very small - theoretically they should be zero - and equal to five significant figures.) Moreover, when the eigenvectors in the cylindrical coordinate system were transformed back to a curvilinear system, the displacements were sensibly the same (rounding errors cause very small differences) as the eigenvectors

obtained when no transformation was invoked.

The exact resonant frequencies for a hyperboloid (with approximately the dimensions of the cooling tower at Didcot) can be obtained by solving the differential equations given by Carter, Robinson and Schnobrich [1]. These values are given in Table 9.1 column 1. Also, the results obtained using VACTIL to analyse the hyperboloid are given in column 2. The agreement is seen to be satisfactory.

In the construction drawings of a cooling tower shell the meridional shape is defined by a series of points. The interpolation curve passing through these points may not represent a true hyperbolic curve. It is more accurate, in this case, to define the meridian in terms of a polynomial or cubic spline. This type of meridia is referred to as a 'general curve' (see Chapter 6). This facility was initially tested by generating R and Z values from the equation for a hyperbola and thereby representing the meridian of the hyperboloid as a general curve. The result of this analysis is given in column 3 of Table 9.1. The agreement is observed to be good.

Table 9.1: Resonant Frequencies Obtained for the Carter et al. [1] Hyperboloid for the First Three Modes with Four Circumferential Waves (n = 4)

Method of Analysis			Meridional Nodes, m
Solutions of Differential Equations (Carter et al., [1])	VACTIL		
	(i) Representation as a Hyperboloid	(ii) Representation as a General Curve	
1.1808	1.1921	1.1880	2
1.4474	1.4655	1.5203	2
2.7772	2.8390	2.8198	3

Further tests were conducted on structures that were not perfectly hyperboloidal. These results (which are not reported here) showed that the program was giving consistent and accurate answers.

The accurary of the beam element routines was investigated by comparing the answers obtained for a simple rectangular structure using VACTIL, with those obtained by a well-proved program 'VOSTAFo2' [93]. The answers in both cases were observed to be identical.

Thus, the preliminary tests described indicated that VACTIL was giving satisfactory solutions.

9.4 Model and Program Results

Whilst preliminary investigation showed that the accuracy of the shell or beam element used separately in the program (VACTIL) was satisfactory, it was necessary to establish that the results obtained when both elements were employed together were accurate.

It was not possible to devise a simple and straightforward test (as for example in Section 9.3) to achieve this. Controlled experimentation on model structures, under laboratory conditions, is capable of yielding accurate information (Chapter 8). Therefore it was decided to use VACTIL to analyse a cooling tower with legs and compare the results with experimental data obtained for a model. A 1:250 scale model of a cooling tower at Didcot was chosen for this purpose as the resonant behaviour of the corresponding full-scale structure has been measured by Winney [42]. A detailed account of this work has been given in Chapter 8. Table 9.2, columns 2, 3 and 4, summarize the findings.

Normalization (extrapolation to the corresponding full-scale values) of the model tower is a convenient method of comparing the

frequencies obtained for the model and corresponding full-scale structures (see Section 6.2). To a first approximation the normalized frequency, $\bar{F}$, is given by the equation:

$$\bar{F} \simeq \frac{F_s}{(\text{scale factor} = 250)} \times \left(\frac{M_s}{E_s} \times \frac{E_f}{M_f} \right)^{\frac{1}{2}} \times \left[f(\rho_s, \rho_f) = \text{terms in } \rho_s \text{ and } \rho_f \right] \quad \ldots(9.1)$$

where F, M, E and ρ are the resonant frequency, mass density, Young's Modulus and Poisson's Ratio, respectively. The subscripts s and f pertain to the model and full-scale structures, respectively.

Burrough [87] reports that $E_f = 29.5 \times 10^9$ N m^{-2} and $M_f = 2323$ kg m^{-3} for the concrete used for the full-scale cooling tower at Didcot. The model tower was made from 'Devcon B' epoxy resin. The manufacturer specifies $E_s = 5.86 \times 10^9$ N m^{-2} and $M_s = 2500$ kg m^{-3}.

Poisson's Ratio for the full-scale tower (0.19; Burrough [87]) is different from that for the model (0.24; Armitt [37]). In order to obtain a value for $f(\rho_s, \rho_f)$ it is often assumed that the mode of vibration of a tower is due to coupled bending/extensional vibration and that the relation

$$f(\rho_s, \rho_f) \simeq \left(\frac{1 - \rho_s^2}{1 - \rho_f^2} \right)^{\frac{1}{2}} \quad \ldots(9.2)$$

holds. In the present case where $\rho_s = 0.24$ and $\rho_f = 0.19$, $f(\rho_s, \rho_f)$ is almost unity. Moreover, as will be shown in Section 9.6.2, the effect is even smaller than predicted from the simple expression given above. (Also, the effect of Poisson's Ratio on Mode 3 is different; See Section 9.6.1.) Therefore, the values given in column 3 of

Table 9.2 were obtained by assuming that $f(\rho_s,\rho_f)$ in equation (9.2) was unity.

The results form VACTIL are given in columns 5 and 6 in Table 9.2. For comparison, results from a previous finite element technique [40, Table 2], where the column supports were regarded as extensions of the tower surface, are presented in columns 7 and 8 of Table 9.2. (Note that the frequencies given in Reference 40 were corrected for the more accurate values of M_f and E_f due to Burrough [87].)

The immediate observation made from Table 9.2 is that the finite element program accurately predicts the free vibrational behaviour of the tower. The values of resonant frequency agree to within ±4%. Moreover, except for Mode 6, the number of meridional nodes (m) and circumferential wave lengths (n) are in exact agreement. During the experimentation described in Chapter 8 a meridional node was observed to be very close to, but below, the top of the tower. The computed results predict a node very close to, but above, the top of the tower. Hence, this difference cannot be regarded as an important discrepancy.

The comparison of Modes 3 and 4 is interesting; while the discrepancy between the computed and experimental results is not large, the relative magnitude of the frequencies in each case is different. This is probably due to the 'sensitivity' of Mode 3 to slight imperfections in the geometry of the model, or to similar unquantifiable parameters; the basis for this premise is expanded in Section 9.6.1.

The good correlation obtained between the computed and measured values for Mode 1 is of particular note. The mode with the

lowest frequency is of primary importance in predicting the probable dynamic behaviour of a cooling tower under adverse conditions. The previous theoretical predictions for this mode in particular have been unsatisfactory. (The predicted frequencies for the lower modes, in general, have been much higher than the measured values.) For example, the finite element techniques of Webster [29] and Deb Nath [40] (using ring finite elements) predict a frequency of approximately 1.3 to 1.4 Hz for Mode 1; i.e. a difference of more than +12%. The reason for the higher frequencies predicted by previous methods is that the effects of leg-supports were not accurately included in the analyses. (In retrospect, contrary to suggestions by previous workers, errors due to assigning incorrect values to the material properties are of secondary importance.) Comparison of columns 3, 5 and 7 in Table 9.2 clearly illustrate these points; the first three modes, in particular, are markedly affected (note the m and n values associated with the second lowest frequency, predicted by the method of Deb Nath [40]). The inclusion of the effects of column supports appears to make a less rigid structure.

It is interesting to note that VACTIL predicts that Modes 3 and 4 have very similar resonant frequencies; in practice, this would make the modes difficult to measure. However, Mode 3 appears to be sensitive to small changes in the properties of the tower which do not appreciably affect the other modes (see Section 9.6.1). Hence, for a practical situation, it is unlikely that Modes 3 and 4 will have very similar resonant frequencies.

Table 9.2: Comparison of Resonant Frequencies and Mode Shapes Obtained Experimentally and Theoretically For the Model Cooling Tower at Didcot

Column Number							
1	2	3	4	5	6	7	8
Mode No.	$\frac{1}{250}$th Scale Model Cooling Tower			Finite Element Method		A Previous Finite Element Method [40]. Column Supports Not Explicitly Defined	
	Measured Frequency (Hz)	Normalised Frequency (Hz)	m,n	Frequency (Hz)	m,n	Frequency (Hz)	m,n
1	124.5	1.159	2,4	1.155 (-0.4)*	2,4	1.375 (+18.6)	2,4
2	136.6	1.272	3,5	1.241 (-2.4)	3,5	1.451 (+14.0)	2,5
3	147.0	1.369	2,3	1.399 (+2.2)	2,3	1.730 (+26.4)	2,3
4	156.0	1.452	3,6	1.394 (-4.0)	3,6	1.660 (+14.3)	3,6
5a	174.0	1.620	3,7	1.630 (+2.0)	3,7	1.836 (+13.3)	3,7
5b	180.0	1.676	3,5	1.696 (+1.2)	3,5	1.872 (+11.7)	3,5
6	209.5	1.950	3,8	1.924 (-1.3)	2,8	2.040 (+4.6)	2,8

*The numbers in parentheses refer to the percentage difference from the values given in Column 3

9.5 Full-Scale and Program Results

It has been shown in Section 9.4 that the finite element method (VACTIL) can be used to analyse accurately the free vibration of model cooling towers with legs. It is now opportune to study the theoretical analysis of the full-scale cooling tower at Didcot and compare the findings with the full-scale experimental data obtained by Winney [43].

The values of Young's Modulus, Poisson's Ratio and Mass Density used for the finite element analysis are as given in Section 9.4, for E_f, ρ_f and M_f. An approximate value for the foundation elasticity in the vertical direction is given by Haydon and Winney [91] as 1.6×10^9 N m^{-1}, although they state that it is likely that the elasticity varies, somewhat, around the base of the tower. The foundation elasticity must be considered in the finite element analysis as discussed in Section 7.1 - this is the crucial difference between the model and full-scale structures. Fig. 7.1 gives the dimensions of the full-scale cooling tower. The results of the analysis are given in columns 5 and 6 of Table 9.3. The experimental data are summarized in columns 2 to 4 of the Table. The modal frequencies were found to exist as 'orthogonal pairs' [43] and are given in column 2. Apparently, the orthogonal pairs are due to the small deviation of the tower shell from the geometry of a perfect shell of revolution. (Probably other 'parameters' like the variation in foundation elasticity around the base of the tower also contribute to this phenomenon.) A consequence of this hypothesis is that the orthogonal pair of frequencies should converge to a single value as the cross-section of the tower

shell becomes more symmetrical about the axis of revolution. This single value would be approximately equal to the mean of the orthogonal pair. The mean values of the orthogonal pairs are therefore given in column 3 and are used for comparison with the theoretical values.

The agreement between the experimental and theoretical resonant frequencies is good. The maximum discrepancy obtained between the computed and measured values is less than 5%. Except for Modes 2 and 6, the mode shapes are in agreement. The disagreement for Mode 6 is not important as explained in Section 9.4.

As observed in Chapter 8 for the model, the third meridional node is sometimes difficult to detect experimentally. Experimentation on a full-scale tower is an order of magnitude more difficult than for a model structure. Hence, similarly it is possible that the third meridional node for Mode 2 was not observed.

The overall observation is, therefore, that the program accurately predicts the behaviour of full-scale cooling towers that are geometrically perfect. It would be advantageous, however, if the program could be developed to include the effects of geometrical imperfections. The theoretical framework employed in VACTIL can, with a few modifications, be used to analyse structures which are almost, but not perfectly, periodic (e.g. towers with small azimuthal variations in the wall thickness, small eccentricities in the tower shell cross-section, etc).

Table 9.3: Comparison of Resonant Frequencies and Mode Shapes Obtained by Experimental and Finite Element Analysis of Full-scale Cooling Tower (at Didcot Power Station)

Column Number					
1	2	3	4	5	6
Mode No.	Full-scale Experimental Results			Finite Element Program (VACTIL)	
	Measured Frequency (Hz)	Average Value (Hz)	m,n	Computed Frequency (Hz)	m,n
1	1.06 1.1	1.08	2,4	1.064 (-1.5*)	2,4
2	1.16 1.19	1.175	2,5	1.180 (+0.42)	3,5
3	1.29 1.31	1.30	2,3	1.253 (-3.6)	2,3
4	1.40 1.42	1.41	3,6	1.351 (-4.1)	3,6
5	1.62 1.68	1.65	3,7	1.589 (-3.7)	3,7
6	1.98 -	1.98	3,8	1.897 (-4.1)	2,8

*The numbers in parentheses refer to the precentage difference between values given in column 5 and column 3

Cracks in the wall of the tower that are almost periodic, as sometimes happens [38], can be analysed by making a few modifications to the program. It must be noted that the present version of the program utilizes about 300 to 400 K bytes for a typical problem - see Appendix 7.1. However, larger finite element idealizations can be used (a region size of 750 K bytes is possible), subject to other limitations (e.g. maximum number of degrees of freedom). Therefore, larger and more complex substructures can be defined, compared with that given in Fig. 7.1.

9.6 Effect of Poisson's Ratio and Foundation Elasticity

The effects of varying Poisson's Ratio and the foundation elasticity on the modes of free vibration of cooling towers have not previously been successfully studied. Experimental investigations are arduous whereas theoretical methods have not been sufficiently reliable. Hence, it is of immediate interest to study these effects.

Table 9.4 presents the variation of modal frequencies (the foundations are assumed to be perfectly rigid) with change in Poisson's Ratio. It is observed that, except for Mode 3, the modal frequencies increase with Poisson's Ratio, as predicted by simple theoretical considerations - see Section 9.4, equation (9.2). Equation (9.2) predicts a frequency variation of 0.13% for a change in Poisson's Ratio from 0.19 to 0.24. The program shows, however, that the variation depends on the mode considered and varies from approxiamtely 0.1% to 0.7%. (This information is used in Section 9.6.2.) The small variation of model frequencies with Poisson's Ratio is instructive because it vindicates the use of a material in model work that does not have the same value of Poisson's Ratio as the full-scale structure. However, the difference in the behaviour of Mode 3

compared with the other modes must be considered when the relative behaviour of Modes 3 and 4 are being examined.

The effect of varying the foundation elasticity, in the vertical direction, S, on the first four modes of free vibration is illustrated in Fig. 9.1. It is observed that when S is much less than 10^{10} N m^{-1} there is a significant decrease in the resonant frequencies of these modes; for higher values of S the frequencies are unaffected. Further investigation showed that the corresponding effects of varying S on the higher modes was less. This is seen in Table 9.5. (This can also be deduced from Fig. 9.1, when it is realised that Mode 3 is an exception; see Section 9.6.1) For example, for Mode 6, when $S \to \infty$ the resonant frequency was 1.91 Hz and when $S \to 0$ the value was 1.884 Hz. Therefore, with the exception of Mode 3, the difference between the resonant frequencies obtained when S is large ($> 10^{11}$ N m^{-1}, say) and when S is small ($< 2 \times 10^{7}$ N m^{-1}, say) is approximately an inverse function of the number of the mode.

The effect of foundation elasticity of the free vibration of the Didcot Cooling Tower has obvious implications for other towers. The foundations at Didcot are relatively inelastic ($S \simeq 1.6 \times 10^{9}$ N M^{-1}) when compared with other cooling tower sites. Hence, it appears likely that foundation elasticity would be a significant factor affecting the resonant behaviour of other cooling towers. Foundation elasticity is thus an important factor to be considered at the design stage. Very inelastic foundations are prohibitively expensive. In practice, the foundation rigidity that can be achieved without undue engineering effect will depend on the nature of the site chosen. Increasing the value of S further would progressively incur a proportionally greater economic

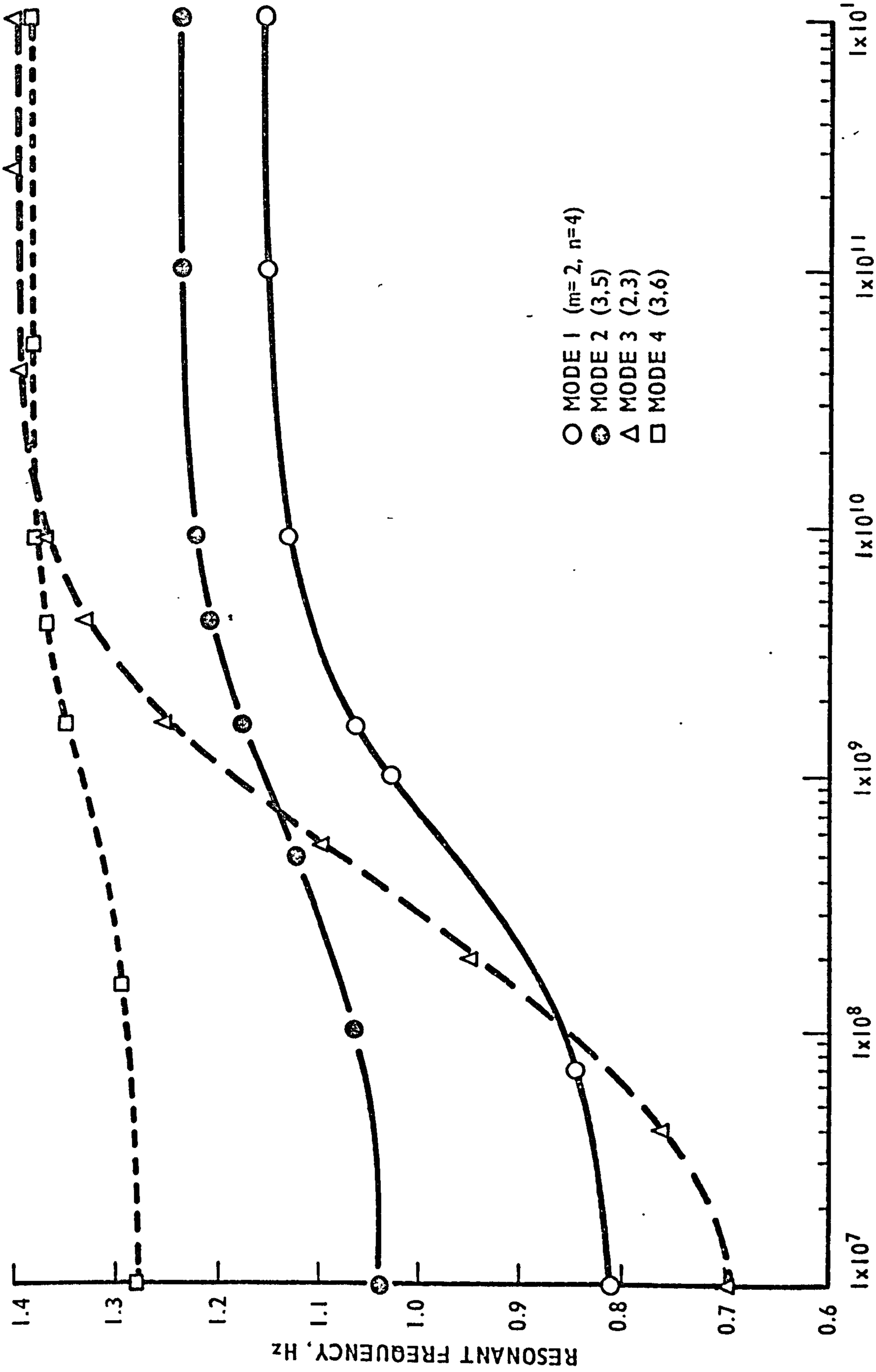

FIG.9.1 EFFECT OF FOUNDATION ELASTICITY ON RESONANT FREQUENCIES OF MODES 1, 2, 3 AND 4 OF THE DIDCOT COOLING TOWER (Full Scale)

Table 9.4: The Effect of Varying Poisson's Ratio on the Modes of Vibration of the Didcot Cooling Tower (With Rigid Foundations)

Mode 1 (2,4)*	Mode 2 (3,5)	Mode 3 (2,3)	Mode 4 (3,6)	Mode 5 (3,7)	Mode 6 (2,8)	Poisson's Ratio
1.1536	1.2392	1.4031	1.3875	1.6203	1.9112	0.19
1.1546	1.2403	1.4004	1.3912	1.6255	1.9180	0.22
1.1553	1.2413	1.3986	1.3941	1.6295	1.9235	0.24
1.1563	1.2427	1.3971	1.3974	1.6341	1.9296	0.26

* The numbers in parentheses refer to the modal shape (m,n)

penalty in relation to the increase in resonant frequencies achieved. Hence, an optimum value of S exists for a given site. This value will also depend on other design parameters (see Section 9.7) and must be determined after a detailed study.

The previous discussion has been concerned with foundation elasticity in the vertical direction (S) only. Intuitively, foundation elasticity in a rotational direction about the vertical axis can be argued to have a negligible effect. This was proved by assuming an elasticity of 10^6 N rad^{-1} (much smaller than in a practical case) in a rotational direction about the vertical axis and computing the frequencies (with S = 1.6×10^9 N m^{-1}). The change in frequency was found to be negligible. Similarly, it is expected that foundation elasticities in other d.o.f.s are of secondary importance, and also, that the magnitude of the elasticity in these d.o.f. is sufficiently large to ensure that the effect on the resonant frequency is neglibible.

9.6.1 Mode 3

Mode 3 exhibits different characteristics in comparison to the other modes considered in this chapter. It is very sensitive to changes in S (see Fig. 9.1), whereas usually the sensitivity of the modal frequency to change in S is approximately an inverse function of the number of the mode. Moreover, as seen from Table 9.4, the variation of the resonant frequency of Mode 3 with change in Poisson's Ratio is contrary to the behaviour of the other modal frequencies.

Further tests (using VACTIL) have shown that Mode 3 is very sensitive (in comparison to the behaviour of the other modes) to geometrical changes. When the 'throat' dimension (minimum distance from the central axis to the mid-surface of the tower wall) was altered slightly, the change in the frequency of Mode 3 was much

more that for Modes 2 and 4. Also, when the meridional section was corrugated (i.e. the radii of curvature of the wall of the tower was allowed to oscillate) the effect on the frequency of Mode 3 was significant and was much larger than the effect on the frequency of Mode 1.

It must be emphasized that during the present investigation only a comparitively few modes have been studied (because the modes concerned are in the frequency range of engineering interest and also in order to optimize the investigative effort required.) Mode 3 has the lowest value of n among this limited number. Thus it is possible that other modes with $n < 3$ also exhibit similar characteristics.

It is of interest to study the experimental observations made by Armitt [37] when he was determining the resonances of a model cooling tower under fluctuating wind pressure. He observed that the mode with the lowest frequency had a m-value of 3. Subsequently, he learnt that the foundation of the model tower was not rigid as the metal plate used to support the structure was not of sufficient thickness.

It would be of interest to ascertain experimentally whether the behaviour of Mode 3 relative to the other modes can be used as a sensitive indicator of imperfections in geometry and unexpected variations in other parameters.

9.6.2 Normalization of Model Frequencies

Tables 9.4 and 9.5 show the effect of Poisson's Ratio, ρ, and vertical foundation elasticity, S, on the resonant frequencies of the modes of vibration. It would be interesting, therefore, to assume the theoretical relationships between the model frequencies and S and ρ, respectively, exhibited in Table 9.4 and 9.5, and then

to normalize the model frequencies.

That is:

$$\text{(measured model frequency)} \times \frac{1}{250} \times \left(\frac{M_s}{E_s} \times \frac{E_f}{M_f} \right)^{\frac{1}{2}} = F_1$$

$$\xrightarrow[\text{differences in } \rho]{\text{corrected for}} F_2 \xrightarrow[\text{differences in } S]{\text{corrected for}} F_3.$$

Table 9.6 summarizes the normalisation procedure. (Note that at first sight this discussion may appear to be a 'circular argument'.)

Table 9.6: Normalization of Resonent Frequencies of Modal Tower After Corrections for Effects of Different Values of Poisson's Ratio and Vertical Foundation Elasticity

Mode No.	Model Results					Full-scale Results	
	Measured Frequency (Hz)	F_1 (Hz)	F_2 (Hz)	F_3 (Hz)	m,n	Averaged Measured Frequency, m,n (Hz)	
1	124.5	1.1591	1.1574	1.0672 (-1.2)*	2,4	1.08	2,4
2	136.6	1.2718	1.2696	1.2091 (+2.9)	3,5	1.175	2,5
3	147.0	1.3686	1.3730	1.2262 (-5.7)	2,3	1.30	2,3
4	156.0	1.4524	1.4455	1.4074 (-0.9)	3,6	1.42	3,6
5	174.0	1.620	1.6108	1.5910 (-3.0)	3,7	1.64	3,7
6	209.5	1.9505	1.9379	1.9237 (-2.8)	3,8	1.98	3,8

*The numbers in parentheses refer to the percentage difference between the values in columns 5 and 7.

It is noted that the correlation between the values given in column 5 (i.e. F_3) and column 7 is good (except for Mode 3) - better than 3.5%. The poor agreement† obtained for Mode 3 is probably due to the sensitivity of Mode 3 to small geometrical and other unquantifiable differences in both model and full-scale structures. Also, the dependence of Mode 3 on S is marked; see Fig. 9.1. For example, if S is taken to be 4.0×10^9 N m^{-1} (as compared with $S = 1.6 \times 10^9$ N m^{-1} as was assumed for the normalization procedure described above), the value of F_3 for Mode 3 is 1.3054 Hz and the difference becomes -0.421%. (Note that the other resonant frequencies are not significantly affected.) Thus, the overall conclusion is that the results obtained for the model and full-scale are in good agreement, if corrections are made for the difference in foundation elasticity during the normalization procedure.

9.7 Cornice and Ring-beam Effects

An important application of a predictive method is in the design procedure. It is interesting to study, as a preliminary step, the effects of varying the dimensions of the ring-beam and cornice on the resonant behaviour of the Didcot Tower (full-scale). The material properties assumed for the tower are as given in Section 9.5. Mode 1, which is probably the most important mode, is considered in this preliminary study.

The thicknesses of the cornice and ring-beam are assumed to increase linearly with axial length, as is true for the Didcot Cooling Tower, while the thickness of the shell is maintained at

---

†Note that earlier workers in the field would have considered this to be in excellent agreement - see Chapter 2 and Table 2.2

0.17780 metres. The results of this study are summarized in Table 9.7. It is observed that a significant increase in the resonant frequency (of Mode 1) can be obtained by increasing the thicknesses of the cornice and ring-beam. On the other hand, the effect of changing their lengths is small. However, when both the lengths and maximum thicknesses are increased the increase in frequency is higher than for an increase in only the maximum thicknesses (Case numbers 8 and 9). (It may be noted that the above observations may not necessarily apply for other modes of vibration; see item (c) in Section 9.1.1.)

The dimensions of the cornice and ring-beams and the degree of foundation elasticity must be decided after consideration of economic and other factors. For example, note that Case 7 in Table 9.7 has an equivalent effect to increasing the vertical foundation elasticity of the tower to 3.5×10^9 N m^{-1}; see Fig. 9.1 and Section 9.6.) The effect of changing these dimensions on the other modal frequencies should be investigated in the future. Also, it would be interesting to verify item (c) in Section 9.1.1.

9.8 Conclusions

1. The finite element method that has been derived yields the most accurate theoretical prediction to date, as far as the author is aware, of the free vibrational behaviour of cooling towers. The agreement between theoretical and experimental values of resonant frequency is better than 5%. The theoretically predicted and experimentally observed mode shapes are almost identical.

2. Foundation elasticity in the vertical direction has an important effect on the free vibrational behaviour of cooling towers.

Table 9.7: Effect of Ring-beam and Cornice Dimensions on the Resonant Frequency of Mode 1 (m = 2, n = 4) of the Didcot Tower (Full-scale)

Case Number	Ring-beam		Cornice		F_r	χ	Comments
	M.T* (m)	Length (m)	M.T. (m)	Length (m)			
1	0.5842	5.833	0.3818	3.422	1.064	0.0	Actual dimensions of the Didcot Tower
2	0.17780	-	0.17780	-	1.012	(-)4.9	i.e. the tower shell is of constant thickness
3	0.70104	5.833	0.3818	3.422	1.071	0.7	20% increase in maximum thickness of ring-beam, c.f. Case 1
4	0.84709	5.833	0.3818	3.422	1.081	1.5	45% increase in maximum thickness of ring-beam c.f. Case 1
5	0.99314	5.833	0.3818	3.422	1.090	2.5	70% increase in maximum thickness of ring-beam
6	0.5842	2.833	0.5727	3.422	1.098	3.2	45% increase in maximum thickness of cornice, c.f. Case 1
7	0.5842	5.833	0.649	3.422	1.115	4.8	70% increase in maximum thickness of cornice
8	0.99314	5.833	0.649	3.422	1.141	7.2	(i) 70% increase in maximum thickness of ring-beam (ii) 70% increase in maximum thickness of cornice
9	0.99314	8.166	0.649	6.842	1.185	11.4	(i) 100% increase in length of cornice (ii) 70% increase in maximum thickness of cornice and ring-beam (iii) 40% increase in length of ring-beam
10	0.5842	11.666	0.3818	3.422	Less than 1% change in frequency in comparison with Case No. 1		100% increase in length of ring-beam
11	0.5842	5.833	0.3818	6.844			100% increase in length of cornice
12	0.5842	8.166	0.3818	6.844			(i) 40% increase in length of ring-beam (ii) 100% increase in length of cornice

* Key M.T. - Maximum thickness

F_r - Resonant frequency in Hertz

χ - % change in resonant frequency with respect to Case 1

The effect of varying this parameter on the first four modes of the Didcot cooling tower has been graphically illustrated. The resonant frequencies of the lower modes are significantly reduced. However, the corresponding decrease in the frequencies of the higher modes is very much smaller. Foundation elasticity, other than in the vertical direction, does not appear to have a significant effect on the vibration of the tower. Judging from the effects of the relatively inelastic foundations of the Didcot tower, it appears probable that foundation elasticity is a significant factor affecting the behaviour of other cooling towers.

3. The effect of Poisson's Ratio on the modes of vibration of a cooling tower is small, and is less than predicted by simple theoretical approximations. Except for Mode 3 (see below), there is a small increase in frequency with increase in Poisson's Ratio.

4. When foundation elasticity is considered in the normalisation of model frequencies, the correlation between the normalised frequencies and corresponding full-scale values is good for all modes except Mode 3.

5. The change in frequency of Mode 3 with change in foundation elasticity in the vertical direction is marked. The resonant frequency of this mode decreases with increase in Poisson's Ratio. Mode 3 exhibits different characteristics from those of the limited number of other modes investigated, and it also may be relatively more sensitive to small unquantifiable differences in the properties of the model and full-scale structures.

6. The magnitude of the dimensions of the ring-beam and cornice affects the values of resonant frequency. Increasing the maximum thicknesses of the ring-beam and cornice has a greater effect on the

resonant frequency of Mode 1 than increasing their extents. (This may not be necessarily true for the other modes.)

7. The finite element method that has been developed is ideally suited for evaluating cooling tower designs (from a dynamic response viewpoint) during the initial design stages.

9.9 Recommendations for Future Work

In view of the success of the method, the finite element program VACTIL should be developed further. Whilst the resonant frequencies of cooling towers with perfect geometry can be accurately predicted, the behaviour of structures with imperfections (cracks, thickness irregularities etc.) should be considered in future work.

Preliminary investigations have shown that it is possible to include the analysis of structures under transient force conditions (e.g. seismic disturbances) in the program. This facility should be incorporated.

The program should be used to optimize the design of cooling towers with reference to their structural integrity.

CHAPTER TEN

DIFFICULTIES ENCOUNTERED

10. DIFFICULTIES ENCOUNTERED

This is a short chapter that recounts some of the difficulties encountered during the research investigation reported in this thesis, and may be of assistance to other workers who may engage in similar work.

10.1 Oscillatory Polynomial Function

As discussed in Chapter 6 the R and Z values can be related by a polynomial function which passes through each point. The order of the polynomial is equal to (n - 1) where n is the number of pairs of R and Z values entered as data. Note that the use of a least-squares method alone to generate a low order polynomial within the program is unacceptable because the coordinates of the common node will not then be known a priori (see Chapter 6).

As n is typically about 12 a high order polynomial function is obtained. The function passes through each and every data point. If one point (say) is outside the fit of a smooth curve the polynomial function will still pass through this point; however, this will cause the function to oscillate in the vicinity of the point. Moreover, the oscillation will not be localised and will be propagated along the function (unlike in the case of a cubic spline where the perturbation remains localised).

The problem referred to above occurred during the development of the programs VACTIL and RESAP. The wall of a structure analysed was then in effect corrugated (due to the oscillatory behaviour of the meridional function) and the finite element analysis was for a stiffer body than was intended. (The doubly curved finite elements discussed in this thesis are sensitive to even small perturbations in the geometrical parameters.) This error was discovered during the

preparation of Table 9.7. A small variation in the value of one R-value resulted in a large, disproportionate, change in the resonant frequency. (All the tables were re-calculated once the solution to the difficulty was found.) The solution was to (a) ensure that all data points were generated from a smooth curve, or (b) employ a cubic-spline interpolation technique. It was determined that the cubic spline function could deal accurately with localised perturbations in one or more R-values. The programs (VACTIL, SACTIL and RESAP) were also modified to incorporate a check so that the user would be informed if oscillations of the function used to represent the meridian took place.

10.2 Complex Displacements and Stresses

When complex constraints are applied (for a free vibration problem) the eigenvectors are complex. The displacements that have been constrained on the right-hand boundary (say) of the structure are printed as zero by the eignevalue solution routine - purely due to computational convenience - whilst the right-hand displacements are printed. The displacements on the left-hand boundary are re-generated by the use of equation (3.1). Note, however, that the sign of the exponential operator in equation (3.1) (given as + ve in the text) is dependent on the direction of travel of the displacement wave (which in turn is dependent on the sign of ψ; see Chapter 3). This fact was overlooked during the development of the program and the wrong sign used. The error was discovered by observing that the circumferential variation of the displacements (and displacement-derivatives) for a cylinder were very different from the approximate sinusoidal/cosinusoidal variations expected. When the sign of the exponential operator was reversed the circumferential variation of the displacements were observed to be almost sinusoidal or cosinusoidal (and were very

similar to those given in Fig. 10.1).

The circumferential variation of the displacements for a hyperboloid is given in Fig. 10.1. Complex constraints were not used. Instead, the hyperboloid was analysed by applying boundary conditions that invoke the symmetry of a section of the structure bounded by parallel meridia (symmetry boundary conditions). The displacements (and derivatives) are observed to be either approximately sinusoidal or cosinusoidal except for the displacement-derivative $\frac{\partial^2 w}{\partial \bar{\theta}^2}$ which is a linear function of $\bar{\theta}$. This is because a third order polynomial is used to interpolate the displacements (see Chapter 4). Hence, double differentiation with respect to $\bar{\theta}$ produces a straight line. However, the linear function appears to be an acceptable approximation to a sinusoidal function.

Another difficulty was encountered when it was observed that complex stresses generated by the program were not accurate. The circumferential displacements for a hyperboloid analysed using complex constraints were obtained and are displayed in Fig. 10.2. These were compared to the results obtained for the same hyperboloid (see Fig. 10.1) analysed using symmetry-boundary-conditions. It is observed that whilst the displacements (eigenvectors) at a node (i.e. $\bar{\theta} = 0$) are similar in both figures the displacements calculated using the displacement functions do not agree. When comparing Fig. 10.1 and 10.2 the following should be noted. The angle subtended by the parallel meridional edges of the symmetrical section (Fig. 10.1) was 45^{o} whilst the angle subtended by the substructure (Fig. 10.2) was 9^{o}. Thus whilst displacements at $\bar{\theta} = 0$ can be compared, those for $\bar{\theta} > 0$ cannot be directly compared. Also note that different scales have been used in Fig. 10.1 and 10.2. It is important to note that the resonant

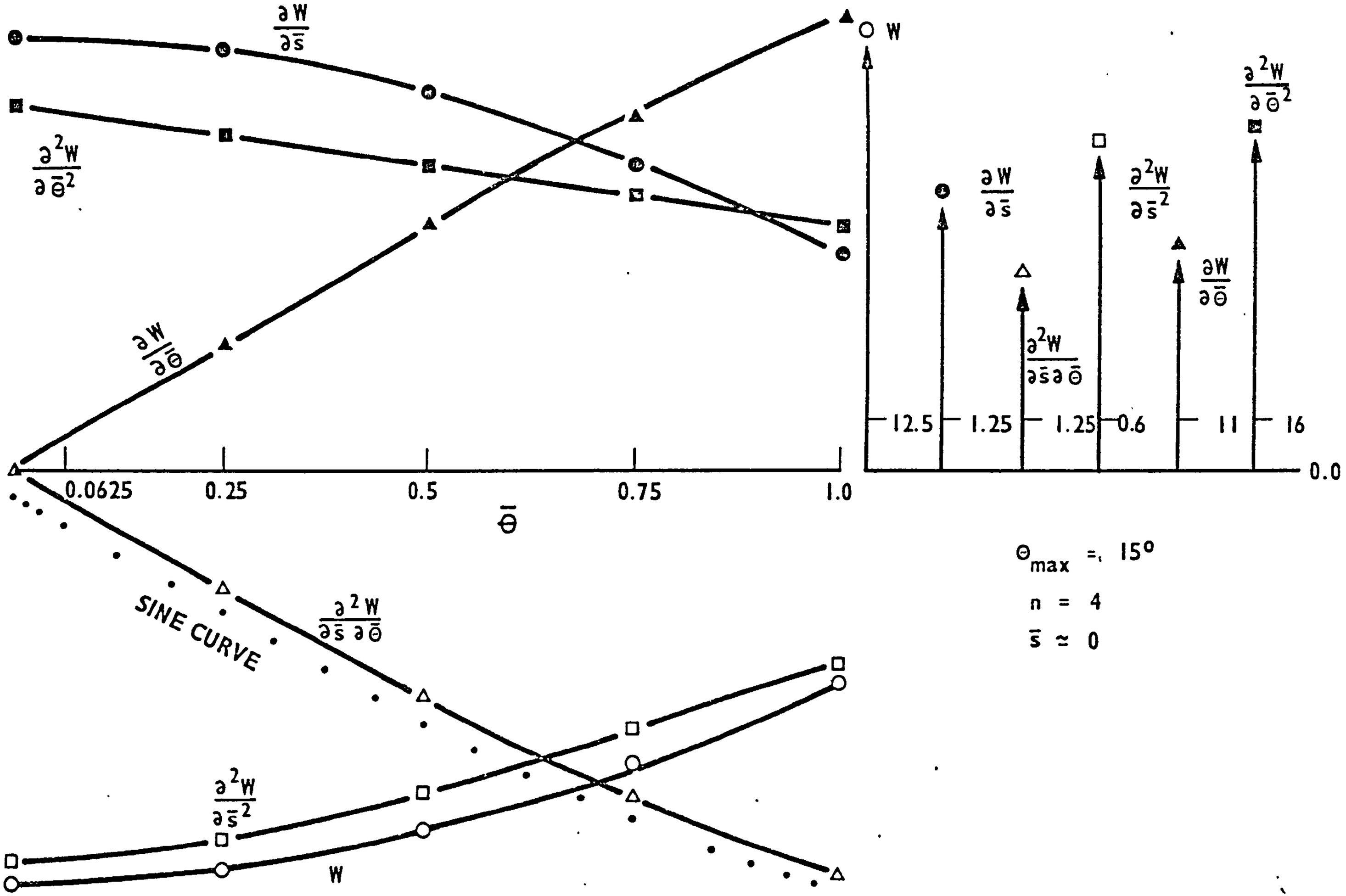

FIG. 10.1 W AND ITS DISPLACEMENT-DERIVATIVES AS A FUNCTION OF $\bar{\theta}$ FOR A HYPERBOLOID

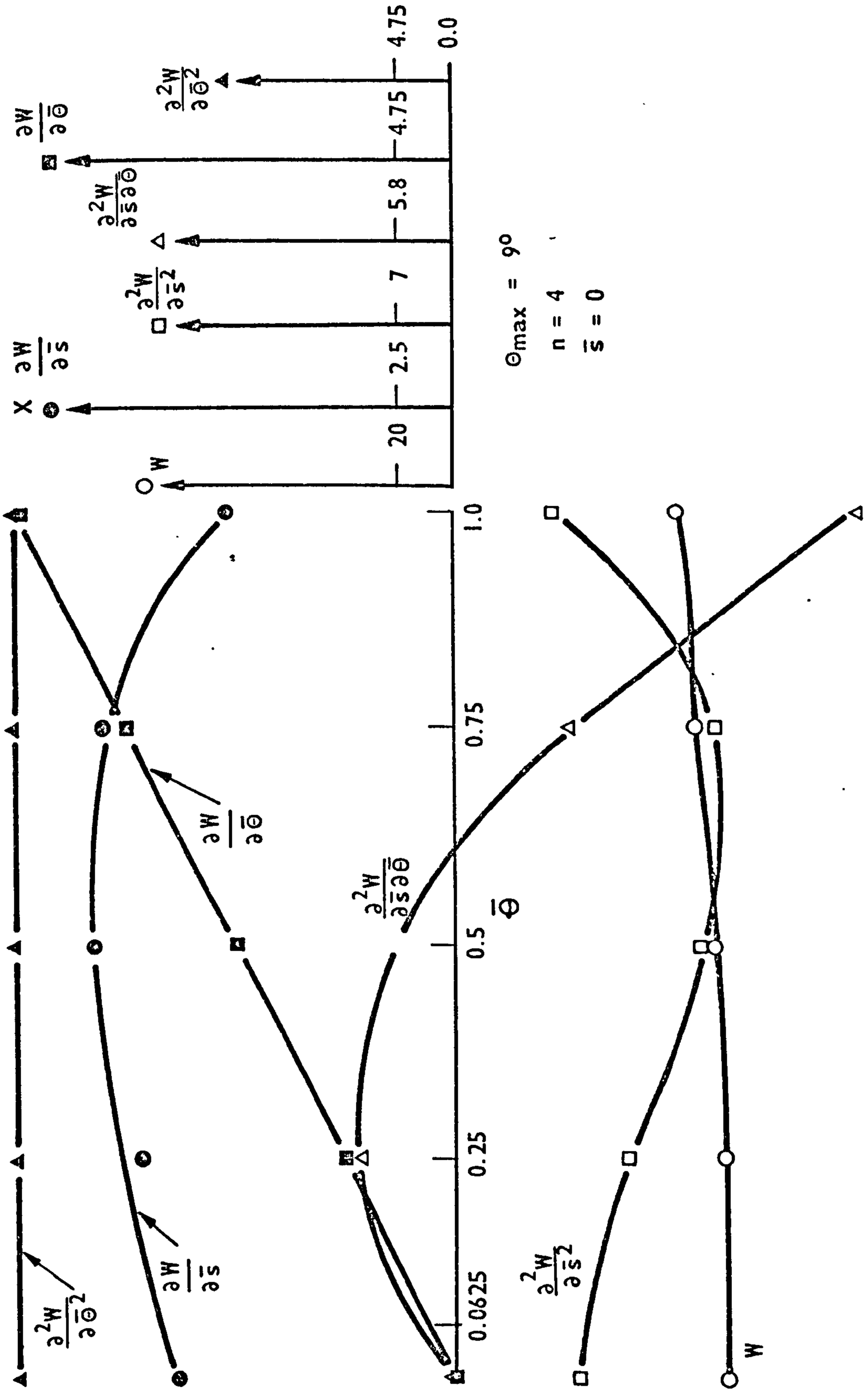

FIG. 10.2 W AND ITS DISPLACEMENT-DERIVATIVES USING THE 'COMPLEX EIGENVALUE ROUTINE'

frequencies predicted by both methods were identical to eight significant figures. Also, that the orthogonal displacements u, v and w were almost identical - i.e. resonant frequencies and values of m and n predicted by using complex constraints were identical to that obtained using symmetry-boundary-conditions. The reasons for the errors in Fig. 10.2 were found to be due to a FORTRAN coding anomaly in the library routine that calculated the complex eigenvectors. Small errors were thus obtained in the eigenvectors. Thus, when the displacement function was used to calculate the displacements at points on the middle-surfaces of the elements the very small errors in the eigenvectors, especially in the nodal displacement-derivatives, gave rise to the exaggerated errors in the circumferential variations shown in Fig. 10.2. The reasons for the inaccurate stresses when complex constraints were applied were only established after a great deal of time had been expended in conclusively establishing the accuracy of the very many other subroutines used in VACTIL. (Unfortunately, the accuracy of the library routine was not questioned by the author for much of this period.) The error in the eigenvalue routine was rectified and all values given in this thesis checked for accuracy. However, as the fault in the eigenvalue routine was rectified only towards the end of the work reported in this thesis, time did not allow for the calculation of stresses in rotationally periodic structures (such as cooling towers.) Hence, in Chapter 11 the investigation of stresses in axisymmetric and shell structures is confined to analysing the structure without the application of complex constraints. However, the stress subroutines are dependent only on the nodal displacements. (The eigenvectors are copied on backing-up disc

for later use by the stress subroutines.) The method by which the displacements are obtained has no direct bearing on the functioning of the stress solution routines. Hence, the results obtained in Chapter 11 serve as a secure base for validating the accuracy of the stress routines. Thus, the stress subroutines can be used with confidence to calculate stresses in rotationally periodic structures.

CHAPTER ELEVEN

CALCULATION OF STRESSES, MODE SHAPES AND FREQUENCIES USING DOUBLY CURVED FINITE ELEMENTS

11. CALCULATION OF STRESSES, MODE SHAPES AND FREQUENCIES USING DOUBLY CURVED FINITE ELEMENTS

11.1 INTRODUCTION

Finite element computer programs are powerful tools in the analysis of vibrating structures. Programs are now available that can accurately predict the resonant frequencies and mode shapes of particularly complicated structures such as hyperboloids with 'cut-outs' and cooling towers with leg-supports. Finite element programs can also be used to calculate stress distrubutions in structures. However, in common with other theoretical methods, it is easier to obtain fairly accurate resonant frequencies for the structure being analysed than it is to obtain accurate displacements - calculation of stresses are even more difficult. Thus, if a program is unable to predict the vibration frequencies of a structure to the desired accuracy, the stresses calculated by the program will be subject to even greater error.

Computer programs that enable the calculation of resonant stresses and/or stresses induced by dynamic and static forces of axisymmetric structures are not widely available. (SHEL [35], is a program with this capability. Unfortunately the version of this program at C.E.R.L. did not execute satisfactorily.) Programs that analyse the dynamic and static stresses of non-axisymmetric structures are even less widely available. Now, however, two new finite element programs are available that enable the calculation of the frequency of vibration, displacements (and thus mode shapes) and stresses in shell and axisymmetric structures. The program RESAP [72] employs a doubly curved ring (axisymmetric) finite element and is able to calculate the resonant frequencies, mode shapes and resonant stresses of axisymmetric shell structures. The accuracy, convergence and efficiency (i.e. the accuracy obtainable for a given number of degrees

-of-freedom) of the ring element is excellent. The program VACTILo2 [73], also called SACTIL, employs a doubly curved shell finite element. The program is designed primarily to calculate the resonant stresses in cooling towers with leg-supports*. However, it is expected to be invaluable in calculating stresses in other non-axisymmetric structures. The program can calculate the vibration frequency, displacement (and therefore mode shapes), and stresses (both resonant and forced) in shell structures.

11.1.1 Differences in theoretical formulations

When comparisons are made between the results obtained for a shell or axisymmetric shell structure using different theoretical methods the following must be noted: various authorities give somewhat different expressions for the relationships between the strain and the displacements. For example, the expressions given by Flügge [95], Vlasov [9], Kraus [62] and Novizhilov [8] differ.

In finite element analysis the strains at any point on the middle surface of an element are related to the displacements at the point. The stress resultants which are functions of strains, would therefore be expected to differ if the expressions used for strain and displacements are different. (Usually, however, these differences are small.) Also, most authors assume a linear variation of strain through the thickness of the wall of the structure.

The derivation of the ring and shell element are, however, based on the same elasticity equations of Vlasov [9], and a quadratic variation of strain through the thickness are assumed for

---

*Stress results for cooling towers were not available at the time of writing this thesis for the reasons given in Chapter 10.

both elements. It is therefore informative to compare the stresses obtained from the programs RESAP and SACTIL. The comparison of results should be made in the light of the similarities and differences between the two elements which are:-

1. The strain-displacement expressions are the same.

2. The ring element can be regarded as a special case of the doubly curved shell finite element. The ring element has the same number of degrees-of-freedom (d.o.f.) per node (twelve) as the shell element; however, the stresses across elemental boundaries are more continuous as all the second derivatives of w with respect to s are included as nodal variables. This is not so for the shell element (see Section 7.1). (The nodal variables of the ring element are u, $\frac{\partial u}{\partial s}$, $\frac{\partial u}{\partial s^2}$, $\frac{\partial u}{\partial s^3}$, v, $\frac{\partial v}{\partial s}$, $\frac{\partial v}{\partial s^2}$, $\frac{\partial v}{\partial s^3}$, w, $\frac{\partial w}{\partial s}$, $\frac{\partial w}{\partial s^2}$ and $\frac{\partial w^3}{\partial s^3}$.)

3. For the ring element displacements on the circumference are assumed to vary sinusoidally/cosinusoidally. That is the orthogonal curvilinear displacements are assumed to be given by the expressions

$$u = u_o \cos n\theta$$

$$u = v_o \sin n\theta$$

$$w = w_o \cos n\theta$$

The suffix 'o' denotes maximum amplitude and n is the circumferential wave number. The six stress resultants, N_α, N_β, $N_{\alpha\beta}$, M_α, M_β, $M_{\alpha\beta}$, thus vary as cos nθ, cos nθ, sin nθ, cos nθ, cos nθ and sin nθ, respectively. This simplifies the displacement function (see [40, Section 3.1]) and increases the accuracy of the element. On the other hand, no assumptions are made a priori regarding the displacements along the circumference of the shell element. Hence, the displacemen function is correspondingly more complex (see Chapter 4, Section 4.5.2) and the

shell element does not appear to converge as quickly as the ring element (as will be deduced from the results obtained using both elements and reported later in this chapter).

11.2 Boundary Conditions

Before using the programs RESAP (with ring elements) and SACTIL (with shell elements) to analyse shell structures it is important to establish equivalent boundary conditions. Displacement boundary conditions and hybrid* boundary conditions for the ring element can be readily specified as all the relevant displacement-derivatives such as $\frac{\partial^2 w}{\partial s^2}$ and $\frac{\partial^2 w}{\partial \theta_o^2}$ are available as nodal degrees-of-freedom (d.o.f.). However, these d.o.f. are not available as nodal variables in the shell element. Hence approximations to the required boundary conditions† may be obtained. These approximate boundary conditions are of a debatable nature. For example Thomas [15] is in disagreement with some of the approximate constraint conditions recommended by Deb Nath [97].

11.2.1 Simply supported

For the ring element we define a 'simply supported' edge when the bending moments and direct forces are zero together with the displacements v and w. (The supporting surface is taken to be normal to the axis-of-revolution.) This is the same as that defined be Herrmann and Shaw [96] and Webster [29]. The support conditions can thus be expressed as:-

$$v = w = \frac{\partial u}{\partial s} = \frac{\partial^2 w}{\partial s^2} = 0$$

---

*Hybrid boundary conditions describes the attempt to equate forces or moments as well as displacements to zero. See for example Herrman and Shaw [96, equation (5)], or Webster [29, page 565].

†Note that 'boundary conditions per se', refer to any type of boundary constraint.

For the shell element it has been recommended [97] that the following constants are applied:-

$$u = w = v = \frac{\partial u}{\partial \theta_o} = \frac{\partial v}{\partial \theta_o} = \frac{\partial w}{\partial \theta_o} = 0 \qquad \ldots(11.1)$$

However, it can he argued that a better approximation is

$$w = v = \frac{\partial v}{\partial \theta_o} = \frac{\partial w}{\partial \theta_o} = 0 \qquad \ldots(11.2)$$

Therefore, in order to resolve this uncertainty the free vibration of a cylinder for the n = 4 mode was analysed using SACTIL with the clamping conditions given by equations (11.1) and (11.2), respectively and compared with the results obtained by RESAP and an analytical method. The analytical solution for a cylinder simply supported at both ends is documented in the well known paper by Arnold and Warburton [109]. The properties of the cylinder are given in Table 11.1.

Table 11.1: Properties of Cylinder

Length	0.3048 m (12 in)
Thickness	0.254×10^{-3} m (.01 in)
Radius	0.0762 m (3 in)
Mass Density	7839.8 kg m^{-3} (0.733×10^{-3} lb s^2/in^4)
Young's Modulus	204.085 MN m^{-2} (29.6×10^6 lb/in^2)
Poisson's Ratio	0.29

The cylinder given in Table 11.1 has been analysed in detail by Smith and Haft [99] and Vronay and Smith [32]. (The latter present a particularly interesting discussion on the effects of different clamping conditions on the cylinder.) The axis-of-revolution of the cylinder was assumed to be vertical and both ends were simply supported. The results of the analyses are given in Table 11.2.

Table 11.2: Frequencies for Simply Supported Cylinder

Method	Resonant Frequencies (Hz)	
	First Eignevalue (m=2)	Second Eigenvalue (m=3)
Analytical solution [109]	415.94	1388.47
RESAP (ring element)	415.98	1388.50
SACTIL (Shell element) with boundary conditions given by equation (11.1)	762.00	1750.20
SACTIL with boundary conditions given by equation (11.2)	417.90	1389.71

Four elements were used in both programs. In the case of SACTIL complex constraints were used.

From a comparison of the results it is clear that the constraints prescribed by equation (11.2) are a better approximate to those boundary conditions described as simply supported than the constraints defined by equation (11.2).

11.2.2 Clamped

For the ring element a 'clamped' edge is here defined as

$$u = v = w = \frac{\partial w}{\partial s} = 0 \qquad \ldots(11.3)$$

(This is identical to the constraints recommended in Reference 98, for a similar axisymmetric element.) The approximate boundary conditions recommended in Reference 97 for the shell element about an edge parallel to the circumference are:-

$$u = v = w = \frac{\partial u}{\partial \theta_o} = \frac{\partial v}{\partial \theta_o} = \frac{\partial w}{\partial \theta_o} = \frac{\partial w}{\partial s} = \frac{\partial^2 w}{\partial s \partial \theta_o} = 0 \qquad \ldots(11.4)$$

Again, in order to confirm that similar if not identical boundary conditions are imposed on both types of element meshes, the cylinder described in Section 11.2.1 was analysed for the n = 4 mode using both programs. Both ends of the cylinder are clamped. The results from both programs were compared to that obtained by Smith and Haft [99]. The results of this investigation are given in Table 11.3.

Table 11.3: Frequencies for Clamped Cylinder

Method	Resonant Frequencies (Hz)	
	First Eigenvalue (m=2)	Second Eigenvalue (m=3)
Solution by Smith and Haft [99]	769.73	1770.2
RESAP (ring element)	763.54	1754.89
SACTIL (shell element)	782.57	1826.0

The clamping conditions for the shell element appear to be reasonably satisfactory though it is noted that the approximations in the constraints for the shell element, probably tend to give a structure somewhat less rigid that that analysed.

11.3. Dynamic Analysis of Cylinders

11.3.1 Cylinder with both ends clamped

A cylinder identical to that analysed by Adelman et al. [98] was first considered. The properties of the cylinder are given in Table 11.4.

Table 11.4: Properties of "Adelman's Cylinder"

Length	12 inches $(3.048 \times 10^{-4}$ m)
Thickness	0.01 ins $(0.254 \times 10^{-6}$ m)
Radius	3 inches $(76.2 \times 10^{-6}$ m)
Mass density	7.33×10^{-4} lb s^2 in^{-4} 7839.924 kg m^{-3}
Young's Modulus	3×10^7 lb in^2 (206.8428 MN m^{-2})
Poisson's Ratio	0.3

The cylinder was clamped at each end. The mode chosen by Adelman et al. [98] for investigation, i.e. the n = 3 mode, exhibited almost discontinuous changes in stress near to the constrained edges. This mode was also chosen for the present investigation as steep changes in stress constitute a severe test of a finite element.

It should be noted that though the stress distribution in this mode is quite complicated near the edges, no attempt was made in the present investigation to use more elements in these regions. The elements were ordered so that they were of almost equal meridional length. This enabled a more realistic appraisal of the elements. However, when the elements are used to analyse a structure it is recommended that more elements are used in the region of the stress concentrations.

The exact solutions for the cylinder, obtained by Adelman et al. [98], were based on ideas originally advanced by Flügge [95] and then developed further by Forsberg [100]. However, Adelman et al. used Novozhilov's [8] shell theory in preference to that of Flügge's. The clamping conditions used by Adelman et al. are those defined by equation (11.3).

The exact solutions together with the solutions obtained by the programs RESAP and SACTIL are presented in Fig. 11.2 to 11.6. For comparison the finite element solutions also obtained by Adelman et al. are given in Fig. 11.2 and 11.6. Note that different criteria are used for the normalisation of displacements and hence stresses for each method. Therefore the value of the stresses at the middle of the meridian of the cylinder ($L_o = 0.5$) was used as a reference. That is, the stresses from each method were multiplied by a scale factor so that the values at $L_o = 0.5$ were coincident.

The values of direct stress, N_α, along the meridian of the cylinder predicted by the exact solution are given in Fig. 11.1. The stress distribution is smooth and does not exhibit steep or sudden variations. The values of N_α predicted by RESAP using four ring elements were found to be indistinguishable from the values

predicted by the exact solution and are therefore not displayed. A mesh of eighteen shell elements was used in the analysis using SACTIL - six elements along the meridian of the cylinder and three elements along the circumference. The angle subtended by the meridional edges of the element mesh was 45^{o}. Boundary conditions involving the symmetry of the cylinder were employed. The angular (or circumferential) dimensions of all the elements were equal. (For typographical convenience we will refer to the mesh as having (6 × 3) elements. A (6 × 3) mesh is illustrated in Fig. 11.29.)

The results for the circumferential stress resultant, N_{β}, are given in Fig. 11.2. The exact solution is depicted as a continuous line. It will be noted that there is a steep change of stress near the clamped edges (i.e. a stress boundary is present). The stresses predicted by SACTIL are observed to oscillate about the exact values. This is somewhat similar to the oscillation exhibited by the stresses obtained by the finite element method of Adelman et al. - see Fig. 11.2. However the stresses due to Adelman et al. exhibit discontinuities at the element boundaries. The values predicted by RESAP also oscillate about the exact values. In Fig. 11.2, the Point D, is the maximum negative stress given by the exact solution, B that predicted by RESAP, A the value given by SACTIL and C the maximum negative value predicted by the finite element method of Adelman et al. (This nomenclature is also used in the Fig. 11.3 to 11.6.) It is observed that the maximum negative stress resultant predicted by the three finite elements (i.e. Points A, B and C) are reasonably accurate when compared with the exact solution (point D). The oscillatory behaviour of the stresses predicted by all three finite element

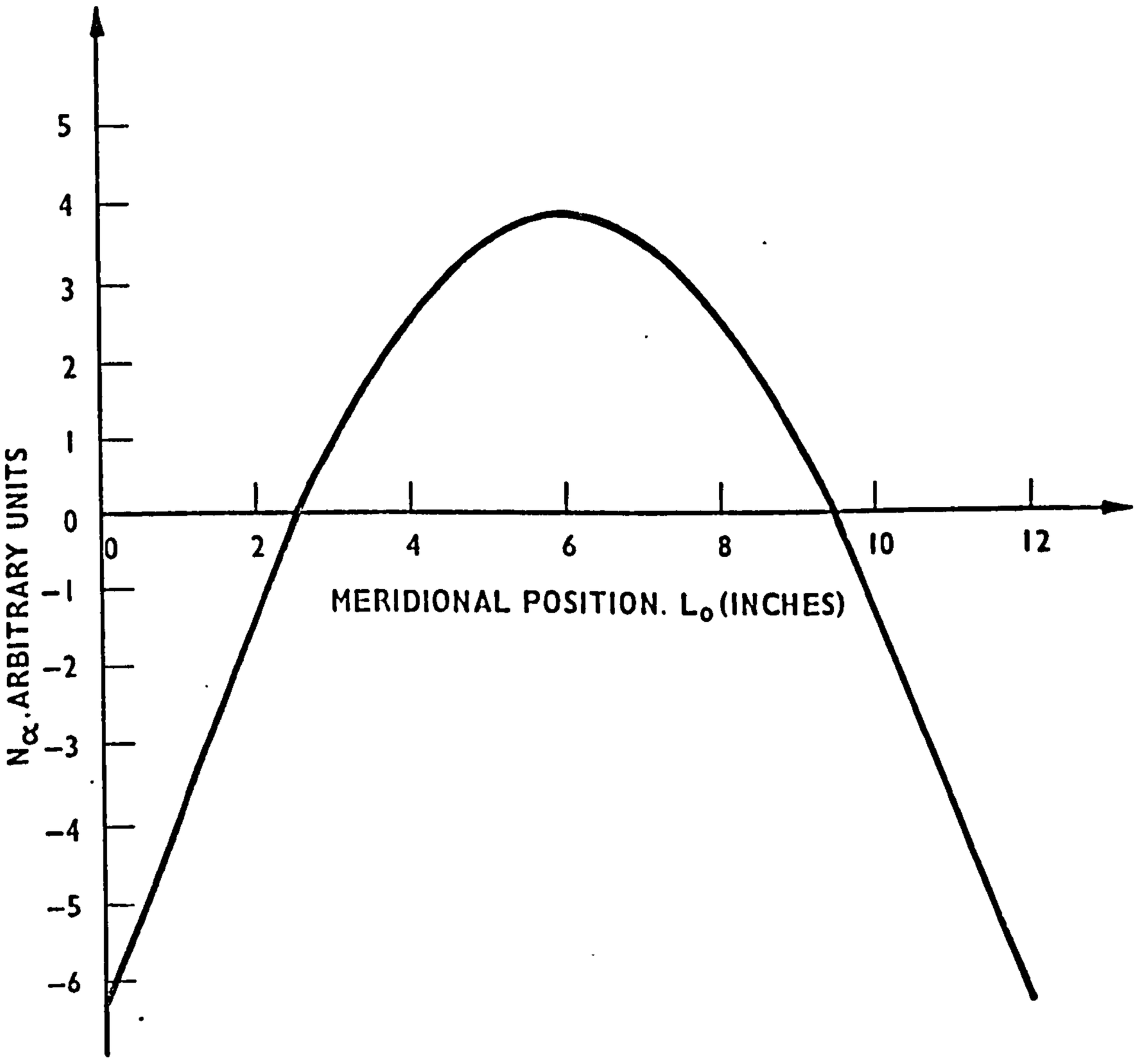

FIG. 11.1 MERIDIONAL (AXIAL) STRESS RESULTANT, N_α
(ADELMAN'S CYLINDER)

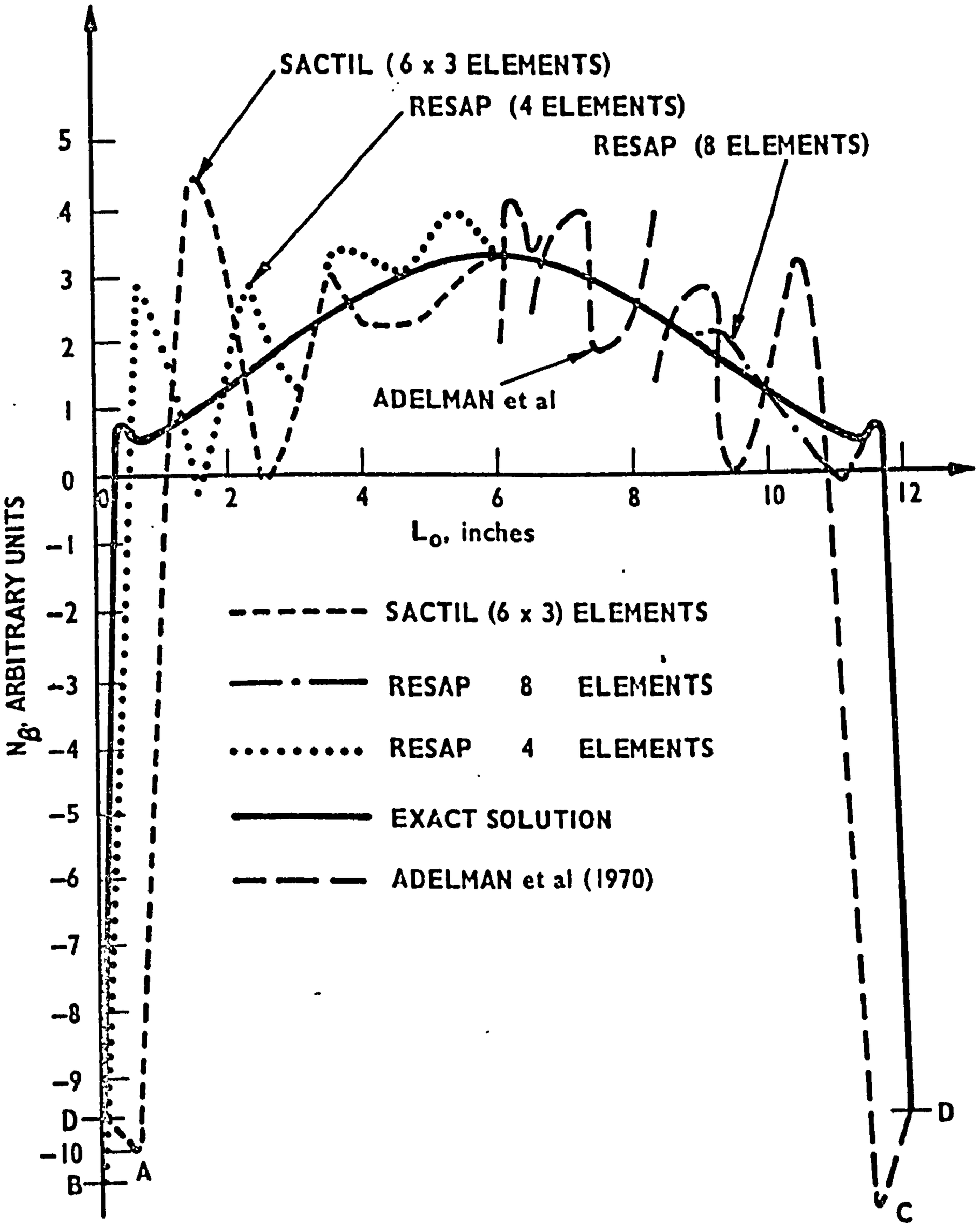

FIG.11.2 CIRCUMFERENTIAL STRESS RESULTANT, N_β

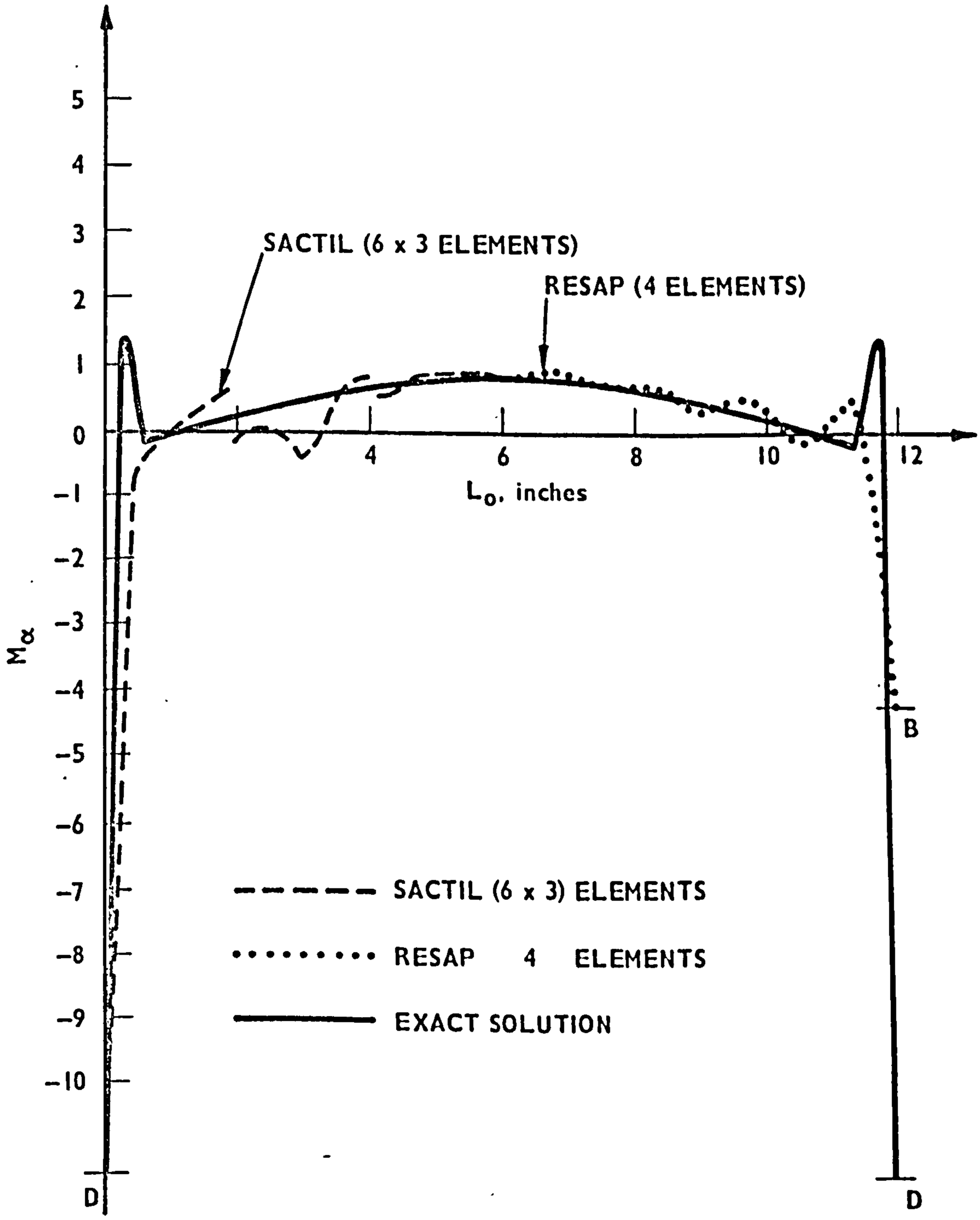

FIG. 11.3 RESULTANT MOMENT ABOUT MERIDIONAL (AXIAL) DIRECTION, M_α

Text cut off in original

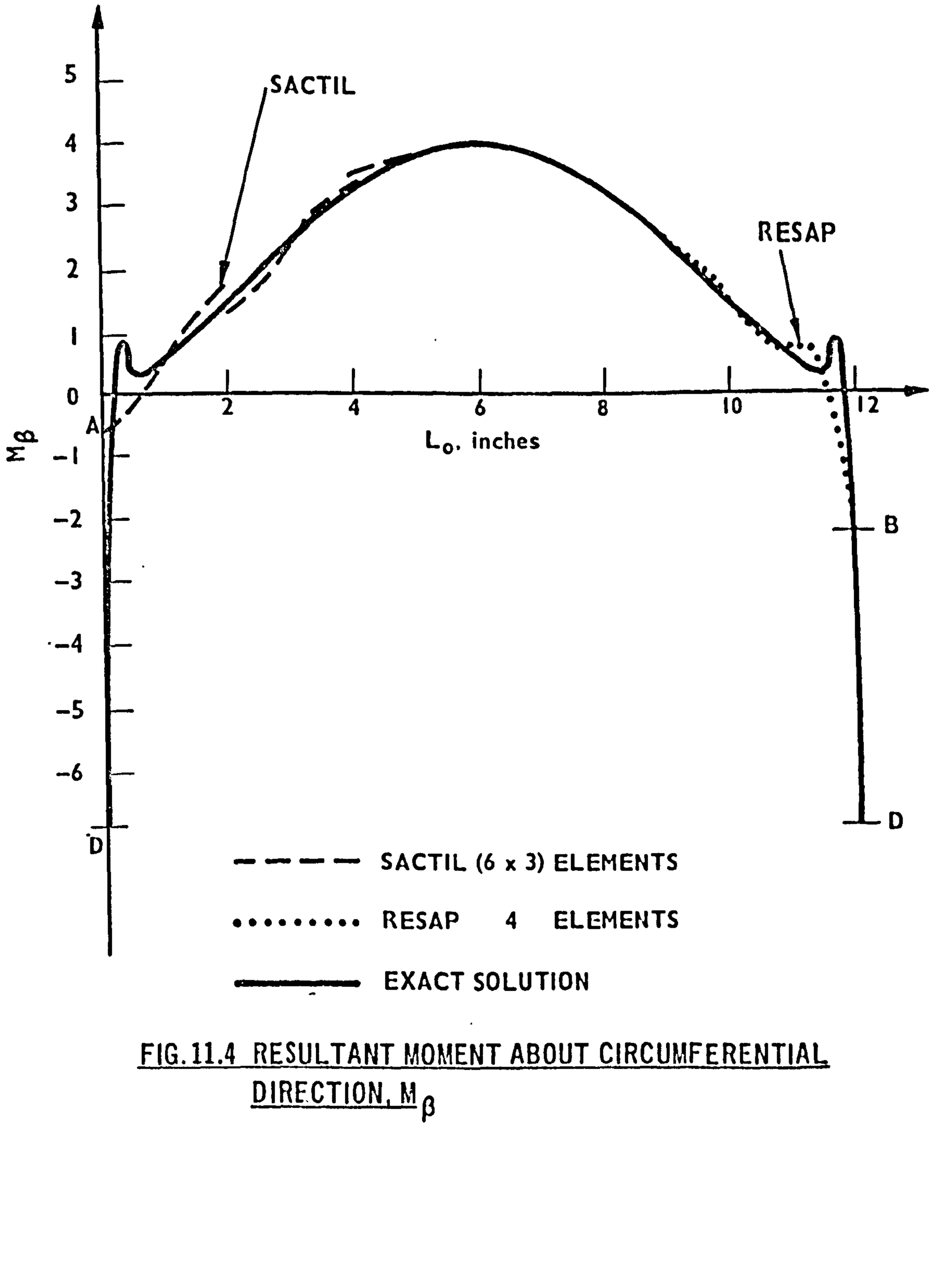

FIG. 11.4 RESULTANT MOMENT ABOUT CIRCUMFERENTIAL DIRECTION, M_β

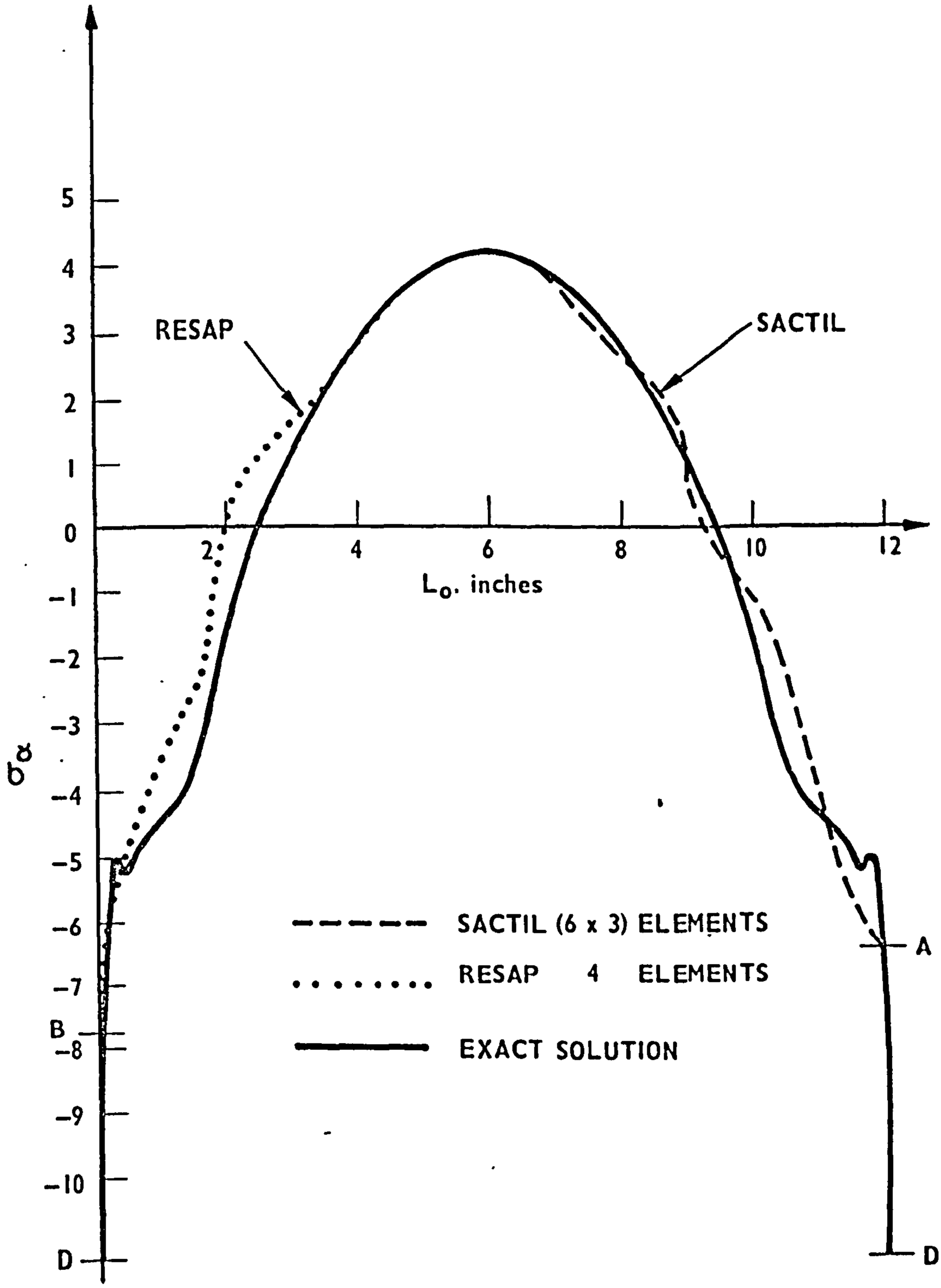

FIG. 11.5 OUTER FIBRE MERIDIONAL STRESS COMPONENT, σ_α

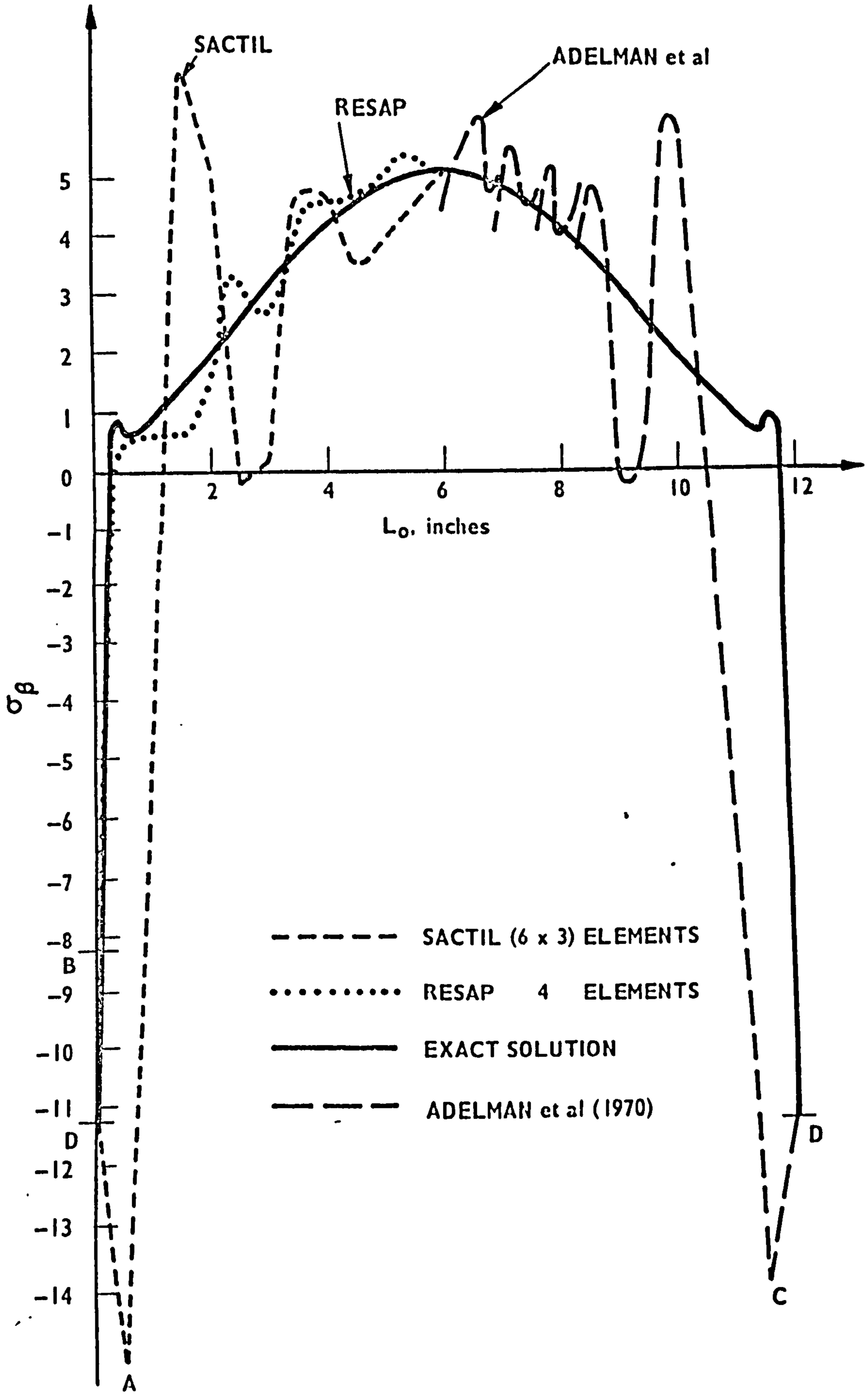

FIG.11.6 OUTER FIBRE CIRCUMFERENTIAL STRESS COMPONENT, σ_β

methods is due to employing too few elements in the analyses, especially near the stress boundary. When eight ring elements were used the stresses predicted by RESAP were observed to lie very close to the exact values (see Fig. 11.2) - over most of the meridian the predicted stresses are indistinguishable from the exact solution. When twenty* ring elements were used the predicted stresses and exact values were seen to be coincident over the whole meridian. A similar test was not conducted with the shell element as the computer storage required for the (6 × 3) mesh was nearing the limits imposed by the computing system. (Complex constraints will enable the same problem to be analysed with an appreciable reduction in core storage and c.p.u. time.) Note that more accurate stress values could have been obtained with the (6 × 3) element mesh by a judicious choice of the meridional lengths of the elements. Adelman et al. obtained values of N_β that were identical to the exact values by (a) increasing the number of elements used, (b) by carefully selecting the meridional length of each element and (c) by increasing the order of the interpolation polynomials used in the displacement function of their element. In Chapter 12 a detailed method of increasing the order of the polynomials used in the shell element is given. This would probably result in an increase in efficiency in predicting stresses (using the shell element) in a similar manner to that observed by Adelman et al. when implementing (c) above.

The variation in values of M_α (resultant moment about the meridional direction) along the meridian of the cylinder is given

---

*Note that twenty ring elements were chosen so as to be reasonable sure that convergence had occurred. The convergence of the ring element is discussed in detail later in the text.

in Fig. 11.3. Again, the exact solution shows that a stress boundary layer is present. The stress moment, M_α, predicted by SACTIL is now seen to be discontinuous at element boundaries. It will be noticed in Fig. 11.1 to 11.6 that only the moments predicted by SACTIL, not the direct stresses, exhibit discontinuities. The explanation for this is given in the next chapter. Adelman et al. also obtained stress discontinuities (not shown in Fig. 11.3) when employing third order polynomials in the displacement function of the finite element - they reported that when the order of the polynomial was increased to order five, the discontinuities were no longer obtained: however, a limited degree of oscillation near the ends of the cylinder was noticed. (These observations directly support the proposals made in Chapter 12.) The values of M_α predicted by RESAP do not exhibit discontinuities unlike the values obtained from SACTIL. This is because the ring element is more accurate than the shell element for a given number of d.o.f. - see Section 11.1.1. The maximum negative value of M_α predicted by RESAP (Point B) is grossly in error when compared to the value given by the exact solution (Point D). (Note that the maximum stress predicted by SACTIL is almost coincident with the value for Point D. However, this is considered to be a chance result and of no real consequence - see Fig. 11.4, Point A.) The oscillating behaviour of M_α predicted by RESAP was observed to die-out and the maximum negative stress approach D as the number of ring elements were increased. When fourteen ring elements were used, the predicted values of M_α and the exact values were indistinguishable.

The variation of M_β along the meridian of the cylinder

is depicted in Fig. 11.4. The comments made for M_α also apply to this figure. In addition, however, it is seen that the maximum negative value predicted by SACTIL (Point A) is in gross error.

In Fig. 11.5 the variation of the meridional stress components σ_α (see Chapter 4, Section 4.6.1 for the definition of stress components) at the surface of the cylinder along the meridian is given. The variation of σ_α is somewhat similar to N_α. However, near each end there is a rapid change in stress; also there is a 'ledge'. Consequently, the correlation between the exact stresses and values predicted by both programs is not perfect. However, a reasonable approximation to the exact curve is observable, expecially in the middle region of the cylinder. The maximum negative values of stress at the ends of the cylinder are predicted incorrectly by both programs. (As expected it was noted that as the number of ring elements were increased the predicted maximum negative stress approached the exact value.)

The variation of the outer fibre circumferential stress component (σ_β) along the meridian is shown in Fig. 11.6. Because of the very steep stress gradients near the ends of the cylinder, the stresses predicted by RESAP and SACTIL oscillate about the exact value. This oscillatory behaviour is somewhat similar to the stresses predicted by the finite element method of Adelman et al. (values from which are also given in Fig. 11.6). The values obtained by Adelman, however, exhibited discontinuous behaviour at element boundaries.

The maximum negative stresses predicted by Adelman et al. (Point C), SACTIL (Point A) and RESAP (Point B) are in error when compared with the exact value (Point D).

It is now opportune to discuss the convergence of the ring element. (The detailed examination of the convergence of the shell element must be deferred for a future investigation.) With reference to Fig. 11.7 the resonant frequencies predicted by RESAP, using several different element meshes show that the convergence is monotonic and rapid. Note that the resonant frequency predicted with 172 and 240 d.o.f. respectively were identical to the accuracy of the print-out (six significant places). This implies that complete convergence has, or very nearly has occurred. The exact solution is 1159.1026 Hz for the first engenvalue*. There is a difference of 0.002% between the value predicted by RESAP and the exact value. This very small difference is not of singificant importance; it could be due to the small differences in the theoretical assumptions of both techniques (as discussed in Section 11.1.1). Hence, the resonant frequency obtained with twenty elements (244 d.o.f.) is very probably the value for complete convergence. In Fig. 11.7 the percentage difference is therefore with respect to the resonant frequency obtained with twenty elements. It is observed that for both the first and second eigenvalues the convergence of the resonant frequency is rapid. (This is satisfactory especially as the mode selected is a particularly difficult one.) When the d.o.f. exceed 100 the frequency has almost converged (i.e. error << 0.026%).

In order to obtain an estimate of the probable convergence characteristics of the stresses predicted by RESAP a test was devised. The outer fibre stress component σ_β was chosen for the test,

*For archival purposes it should be noted that SACTIL predicted a frequency of 1181.09 Hz, i.e. a difference of 1.9%.

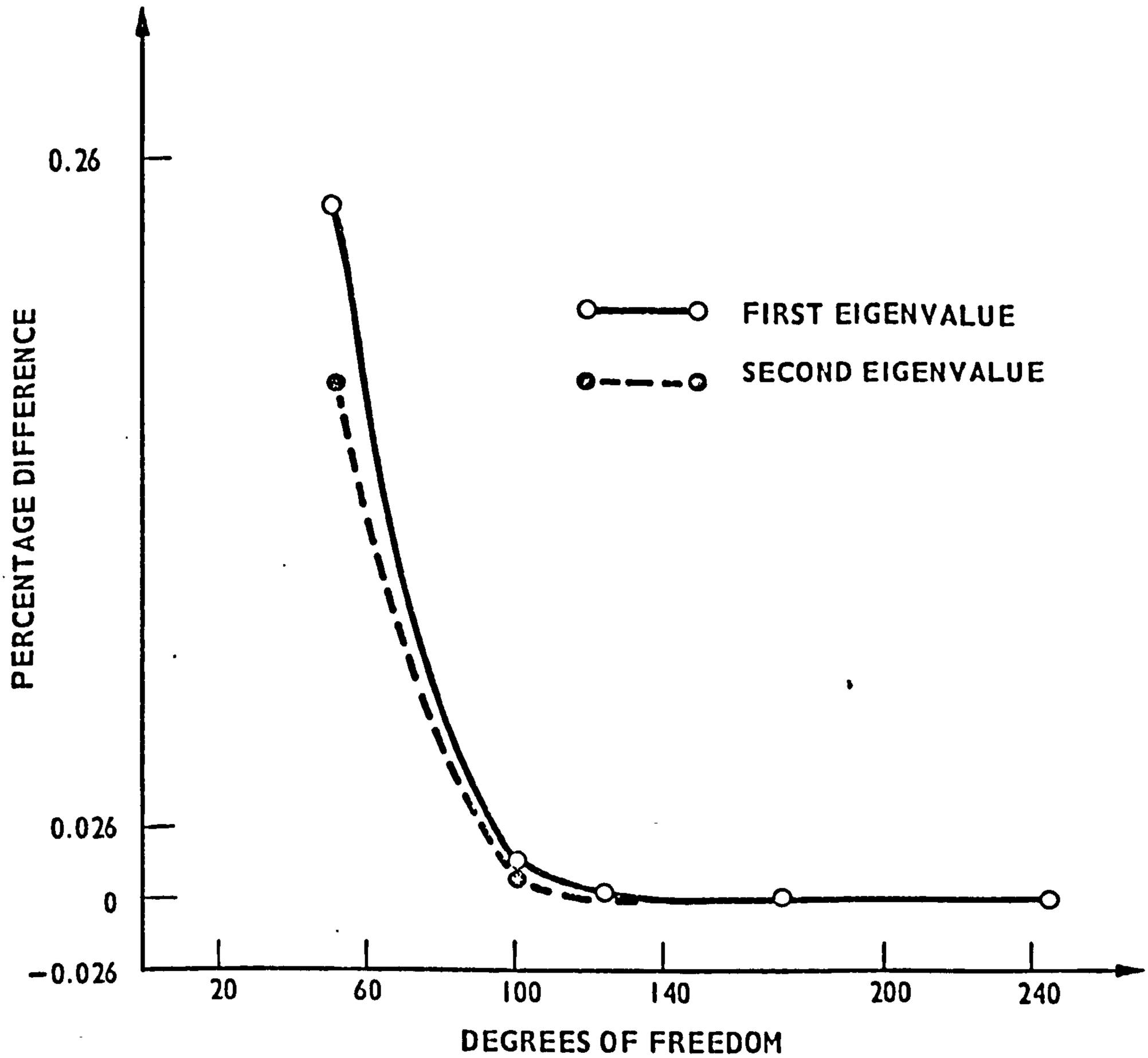

FIG.11.7 CONVERGENCE OF RESONANT FREQUENCY VALUES FOR THE PROGRAM RESAP

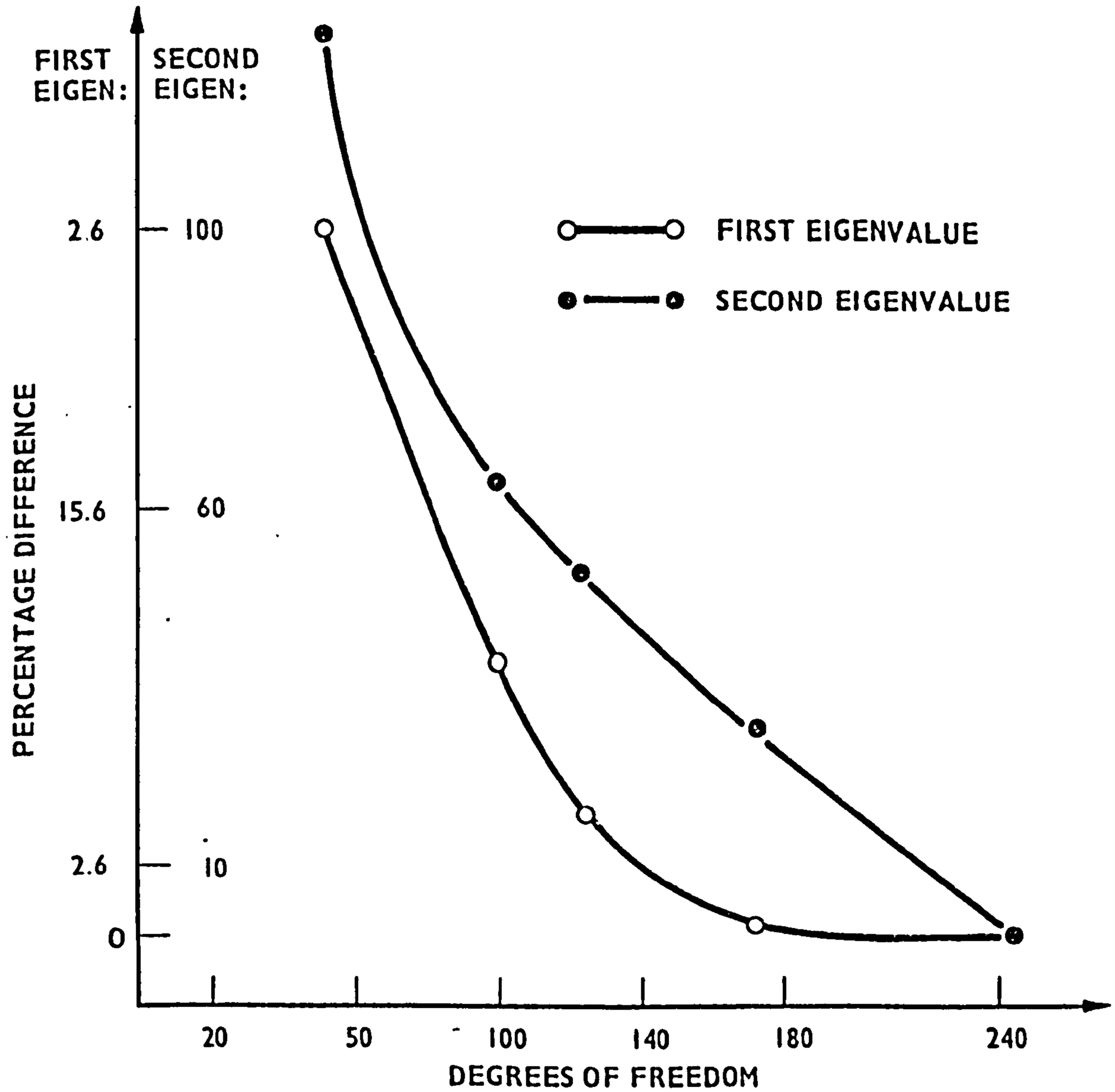

FIG. 11.8 CONVERGENCE TEST FOR σ_β (SEE TEXT) FOR PROGRAM RESAP

albeit a severe one. As seen in Fig. 11.6, the maximum negative stress predicted by RESAP is in error by about 26%. It was assumed that the rate at which the predicted value (i.e. the maximum negative stress) approached the exact value would be an indication of the convergence characteristics. The σ_β values, for the first eigenvalue is seen to converge monotonically; for d.o.f. > 180 this error is probably acceptably small. The σ_β values obtained for the second eigenvalue is seen to converge monotonically, but even with twenty elements the convergence gradient is steep. However, as a particularly difficult example has been considered this is probably reasonable.

To complete the study of the cylinder clamped at both ends the variation of the orthogonal displacement u, v and w along the meridian are given in Fig. 11.9. These displacements were obtained using RESAP with twenty elements. Note that the scales used for each displacement component are different.

11.3.2 Cylinder clamped at one end .

It is of interest to observe the stresses present in a resonating cylinder clamped at one end for a n = 4 mode. This is a less severe case than that described in Section 11.3.1. The cylinder chosen for the test is that described in Section 11.2.1; it was deemed to be clamped at one end. A mesh of (4 × 3) elements was chosen for SACTIL and four ring elements were used with RESAP.

In Section 11.3.1 it was seen that a large number of ring elements yield a solution indistinguishable to the exact solution, even for the severe case examined. Therefore, for the less severe case examined here it was considered unnecessary to obtain an exact solution. Instead, results were obtained using twenty ring elements and these results were considered to be the 'correct solution'.

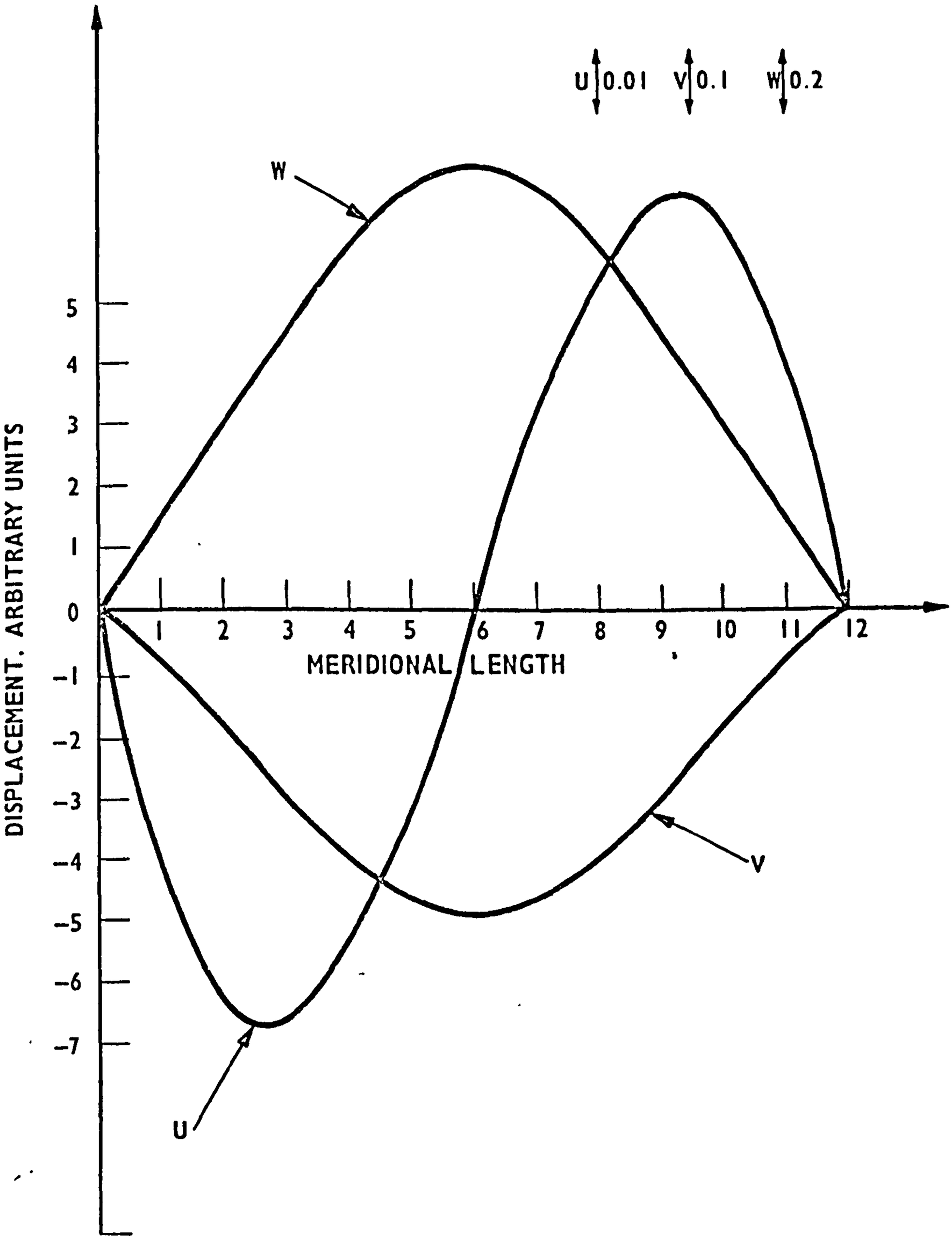

FIG. 11.9 ORTHOGONAL DISPLACEMENTS U, V AND W ALONG MERIDIAN

The resonant frequency (for the first eigenvalue) given by the correct solution was 209.872 Hz. The frequency predicted by RESAP (with 4 elements) was 210.05 Hz (i.e. 0.085% error). SACTIL predicted a frequency of 211.12 Hz; i.e. an error or 0.59%. (Previously, in Section 11.3.1, a larger number of shell elements were used and the error was greater - 1.9%.)

Fig. 11.10 gives the variation of N_α along the meridian. At a free edge elementary theoretical considerations predict that the values of N_α, M_α and $N_{\alpha\beta}$ are zero. (The correct solution gives $N_\alpha \doteqdot 0$ at the free end.) The value of N_α predicted by RESAP at the free end is almost zero. The value predicted by SACTIL is reasonably close given the greater approximations involved in the formulation of the shell element. The overall conclusion is that the N_α values predicted by both programs are reasonably close to the correct solution.

The outer fibre circumferential stress σ_β is depicted in Fig. 11.11. Reasonable agreement is obtained.

The outer fibre circumferential shear stress $\sigma_{\alpha\beta}$ is depicted in Fig. 11.12. The correct solution shows sharp changes in stress near the ends of the cylinder. The values predicted by RESAP are not very close to the correct values, especially near the stress boundary and more ring elements could probably be employed. The values predicted by SACTIL clearly show that the element mesh used, i.e. a (4 × 3), should be refined if reasonable agreement is to be achieved.

The resultant moments were seen to be very small for the cylinder and are not presented.

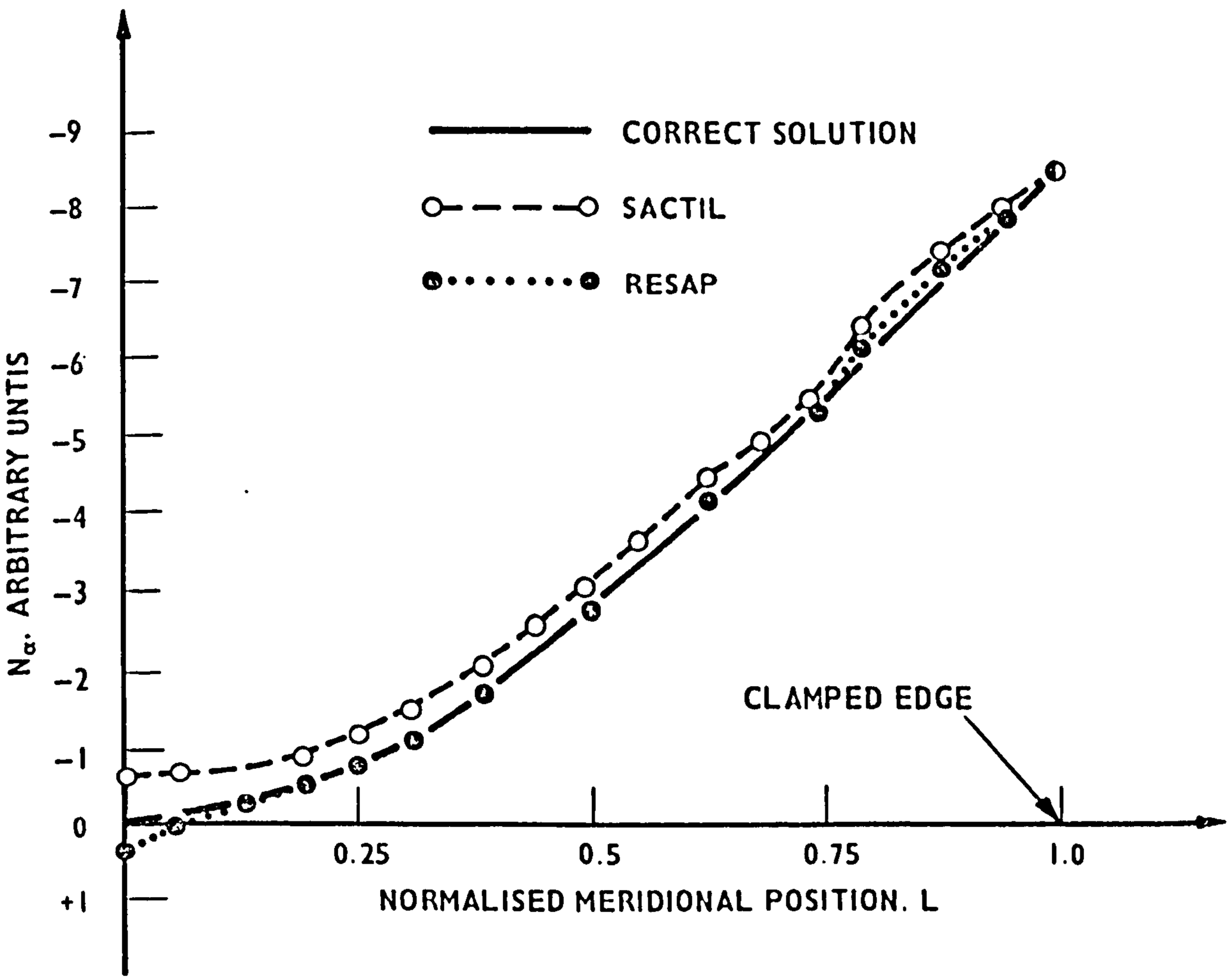

FIG.11.10 MERIDIONAL STRESS RESULTANT, N_α (CLAMPED CYLINDER)

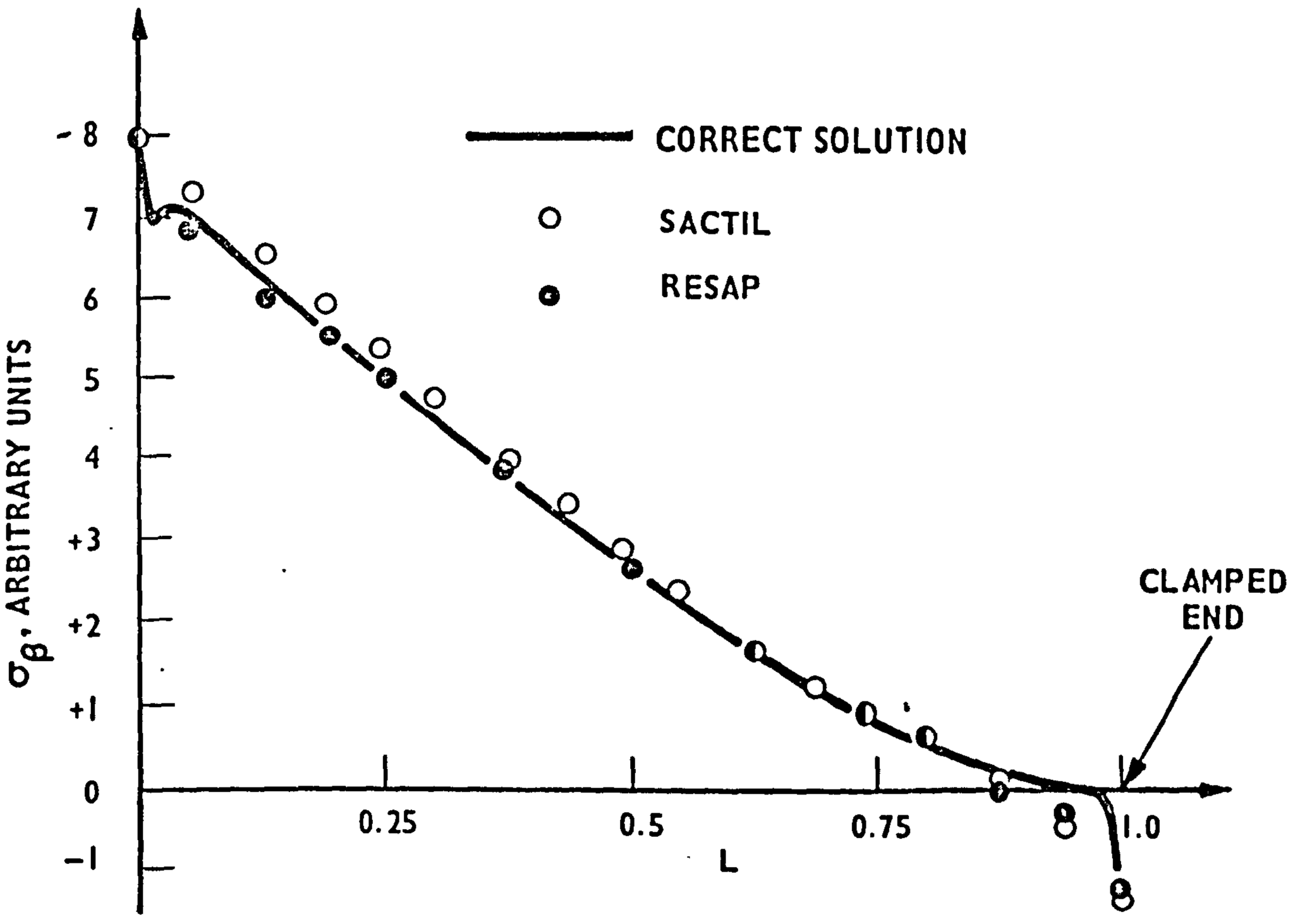

FIG. 11.11 OUTER FIBRE CIRCUMFERENTIAL STRESS, σ_β

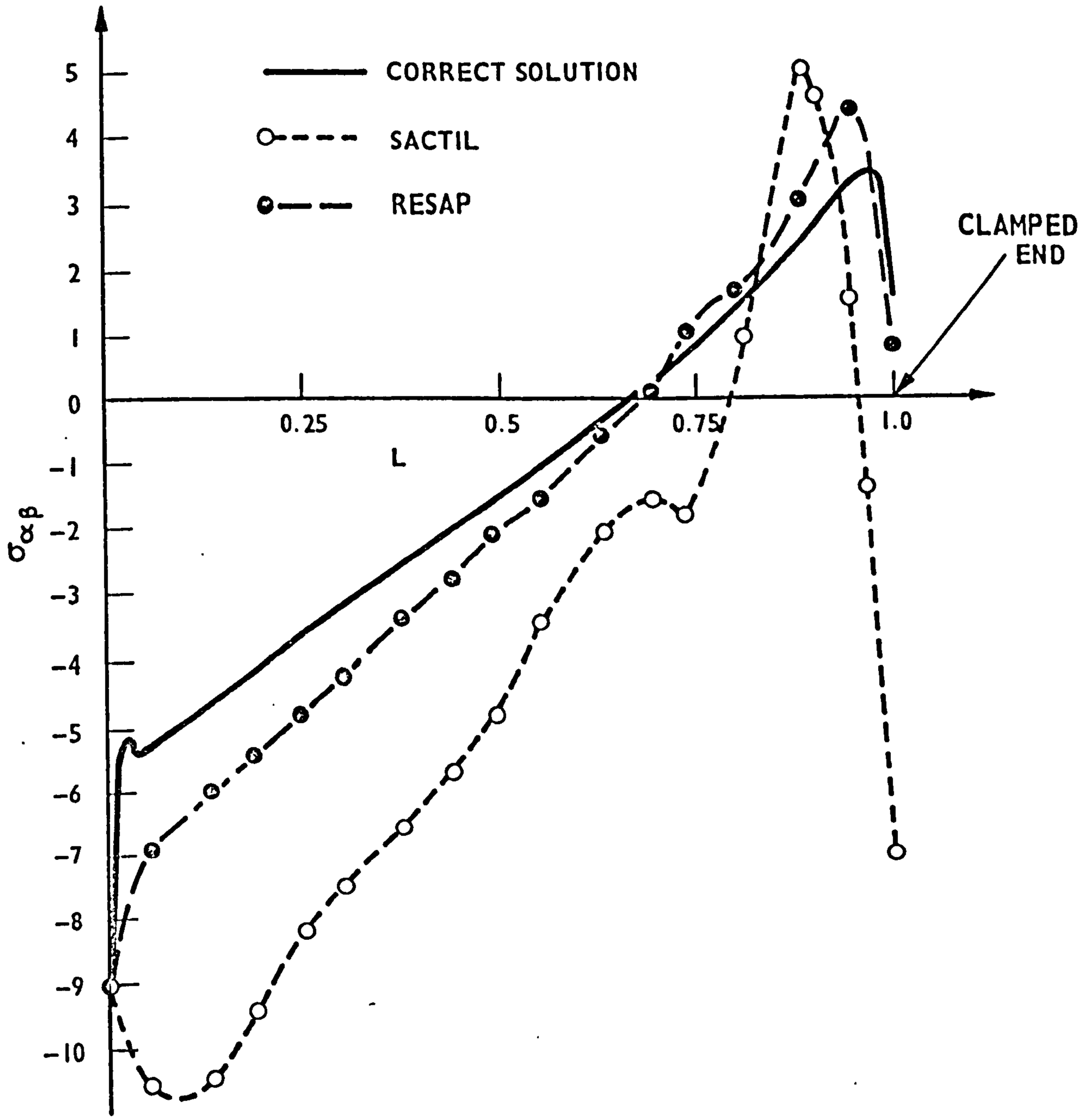

FIG.11.12 OUTER FIBRE SHEAR STRESS, $\sigma_{\alpha\beta}$

The orthogonal displacements along the meridian of the cylinder are given in Fig. 11.13. (This was obtained using RESAP with twenty elements.)

11.3.3 Closure for Section 11.3

The programs RESAP and SACTIL predict reasonably accurate stresses for a stress distribution that exhibits gradual variations. When steep stress gradients are encountered and the mesh is sparse, the element displacement function cannot adequately represent the true solution in that region and hence the stress values predicted by the finite element mesh tend to oscillate about the true values. Tests using the program RESAP show that the convergence of the ring element is excellent - when a large number of ring elements were used the predicted values were indistinguishable from the exact solution.

11.4 Static Force Response

The purpose of this section is to (a) show that the 'applied force response' subroutines in SACTIL function correctly and (d) to determine whether the stress subroutines execute correctly for structures with meridional curvature. (The stress subroutines are dependent only on the nodal displacements. These nodal displacements can be obtained by any method and can even be entered by the user. The method by which the displacements are obtained, therefore, have no direct bearing on the functioning of the stress solution routines.)

A translational thin shell with two constant radii of curvature (spherical cap) under a central load was investigated. The dimensions and material properties of the spherical cap are given in Fig. 11.14. This particular problem is well documented. It was initially solved by Gallagher [101]. Yang [66] then investigated the shell by using two methods which were the series solution method due to

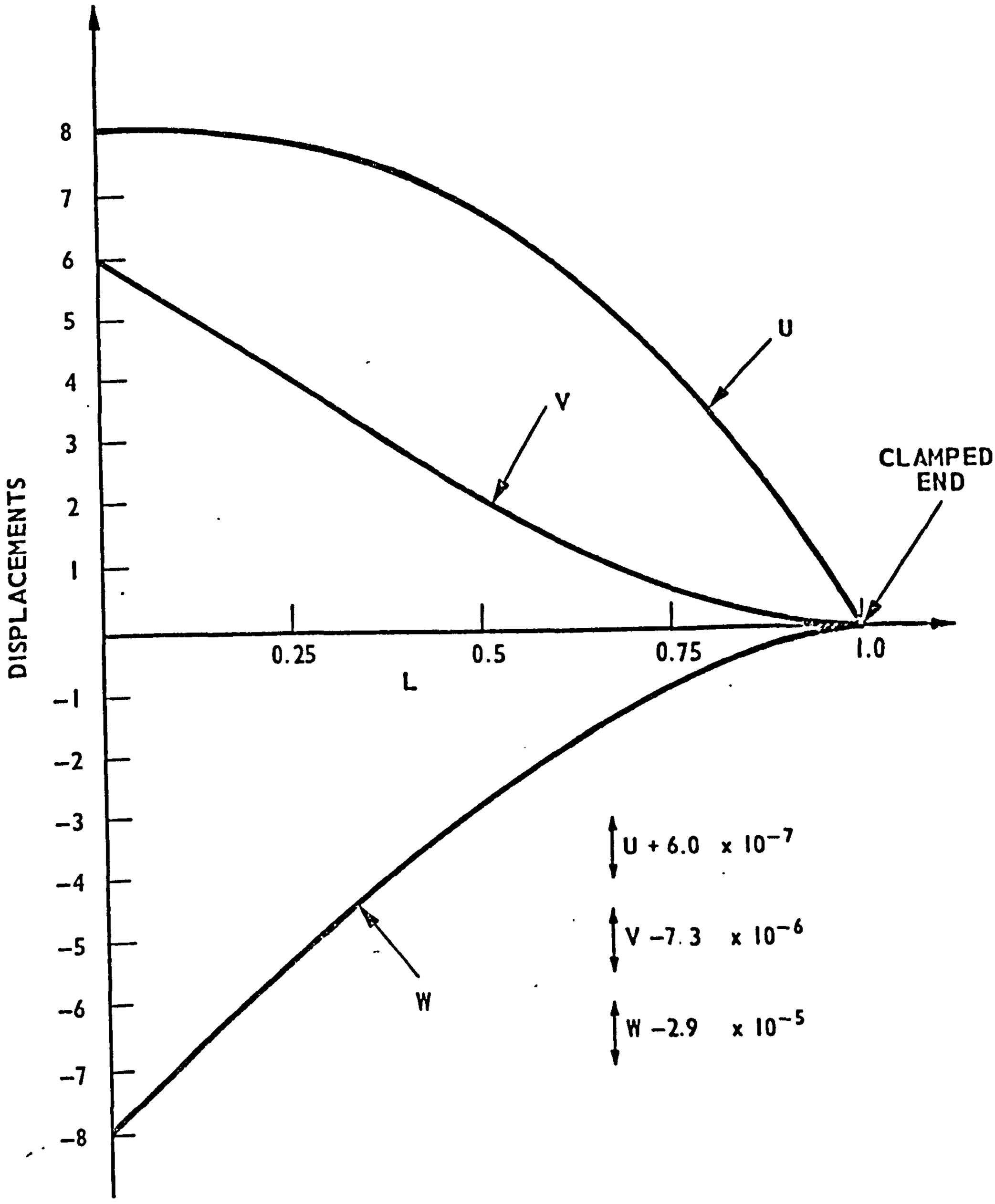

FIG.11.13 ORTHOGONAL DISPLACEMENTS U, V AND W ALONG MERIDIAN

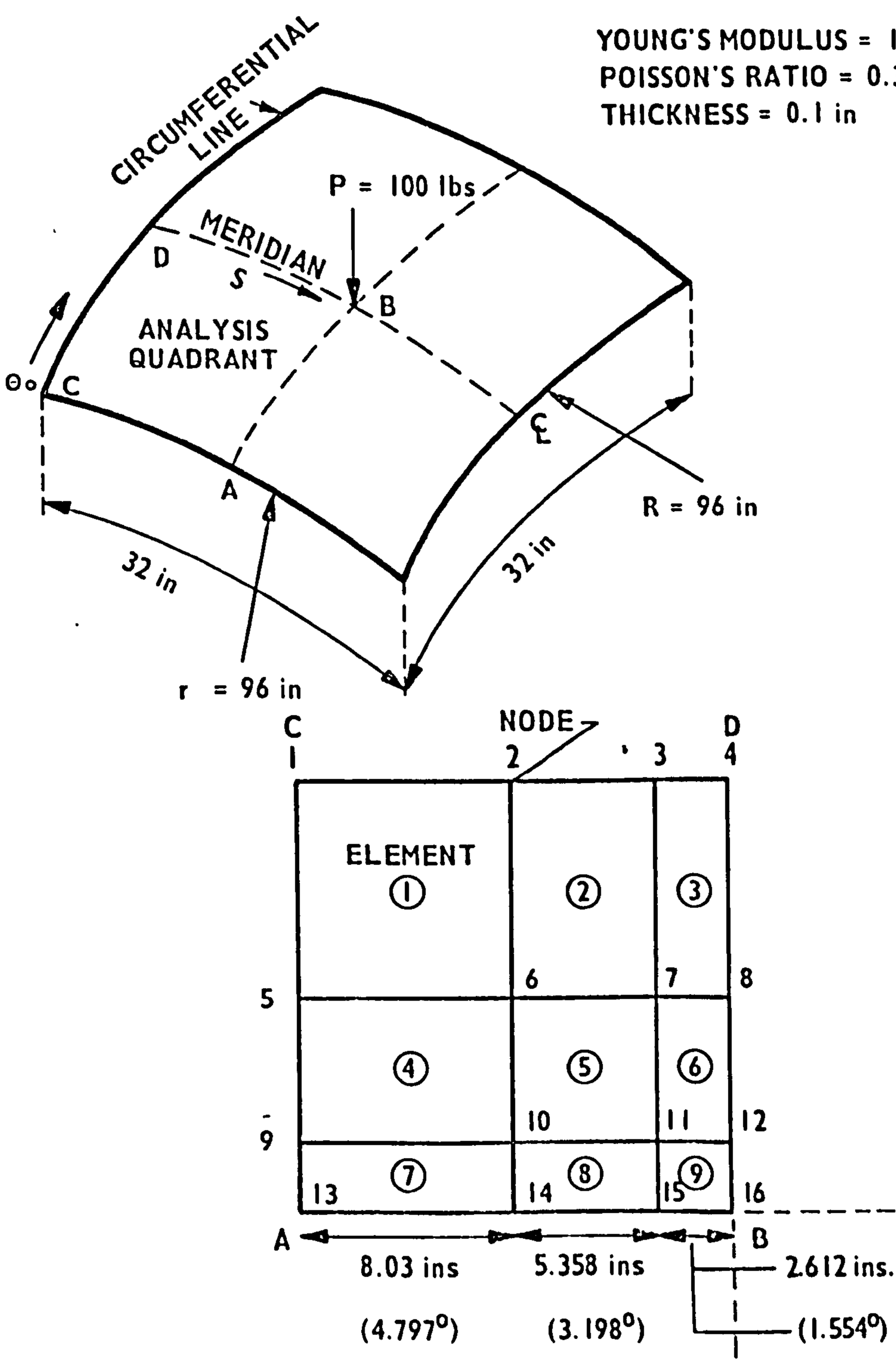

FIG. 11.14 SPHERICAL CAP GEOMETRY AND MESH FOR POINT LOADING FORCE

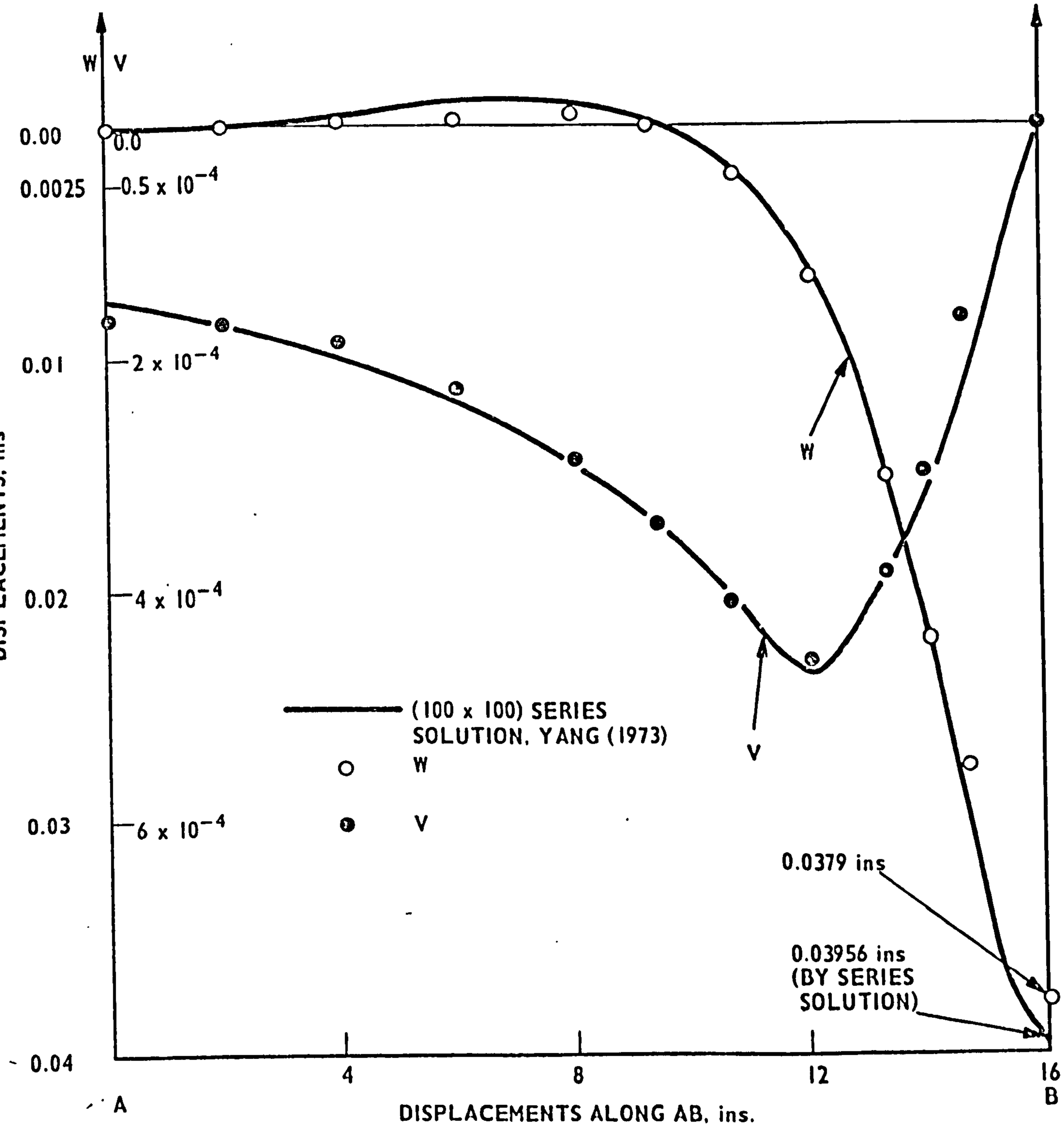

FIG. 11.15 SPHERICAL CAP DISPLACEMENTS ALONG AB

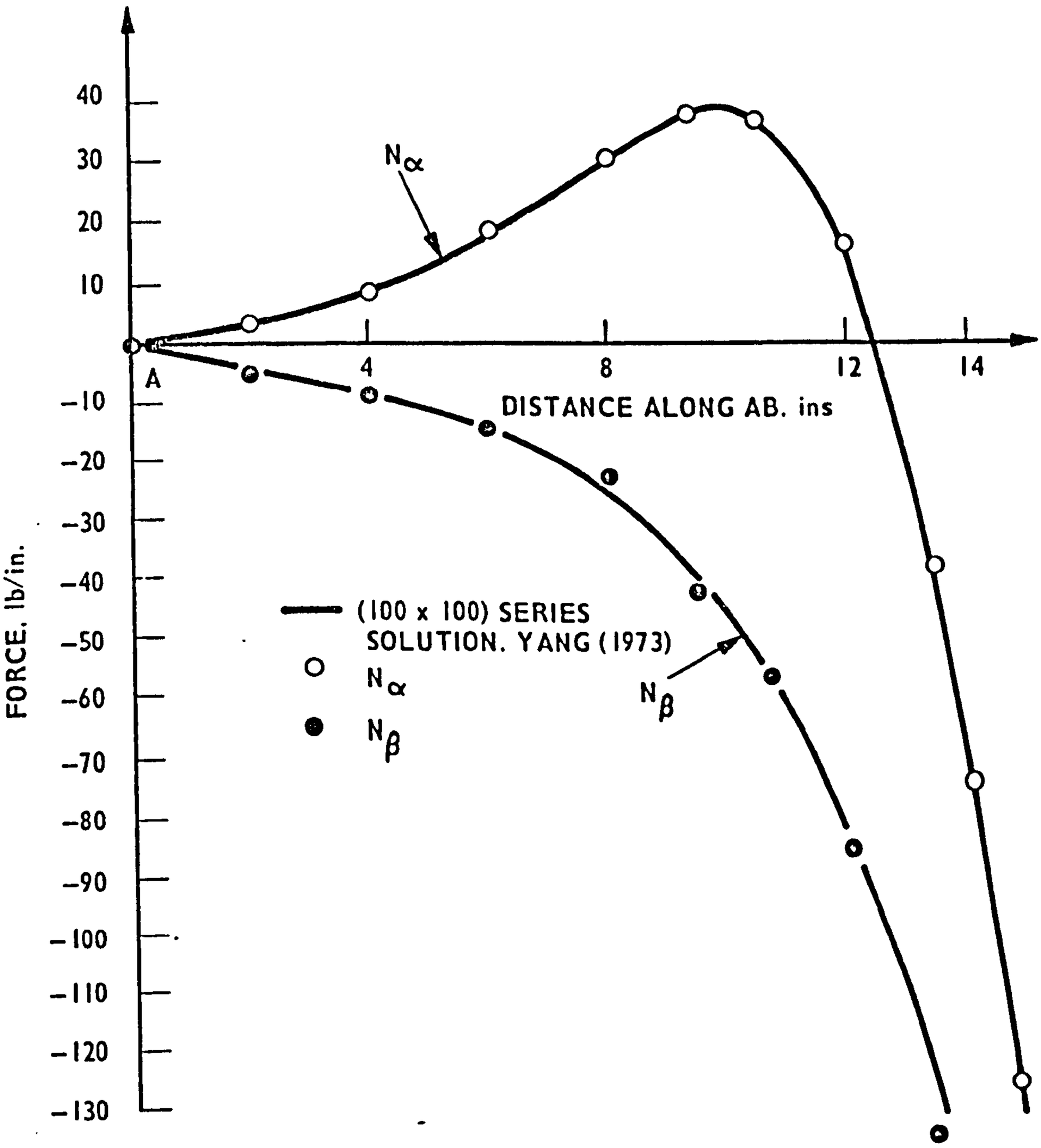

FIG. 11.16 MERIDIONAL AND CIRCUMFERENTIAL STRESS RESULTANTS N_α AND N_β ALONG AB

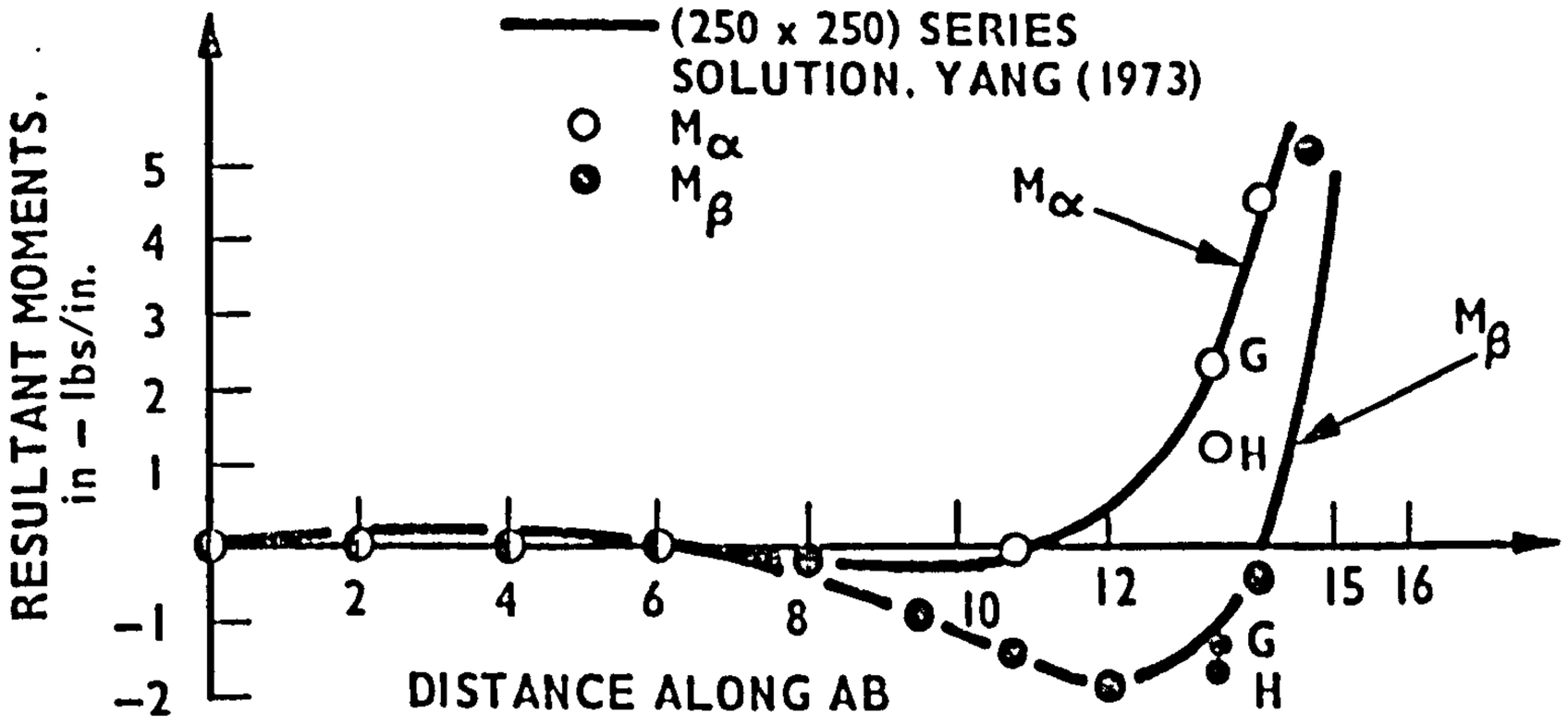

FIG.11.17 RESULTANT MOMENTS ABOUT MERIDIONAL AND CIRCUMFERENTIAL DIRECTIONS, M_α AND M_β

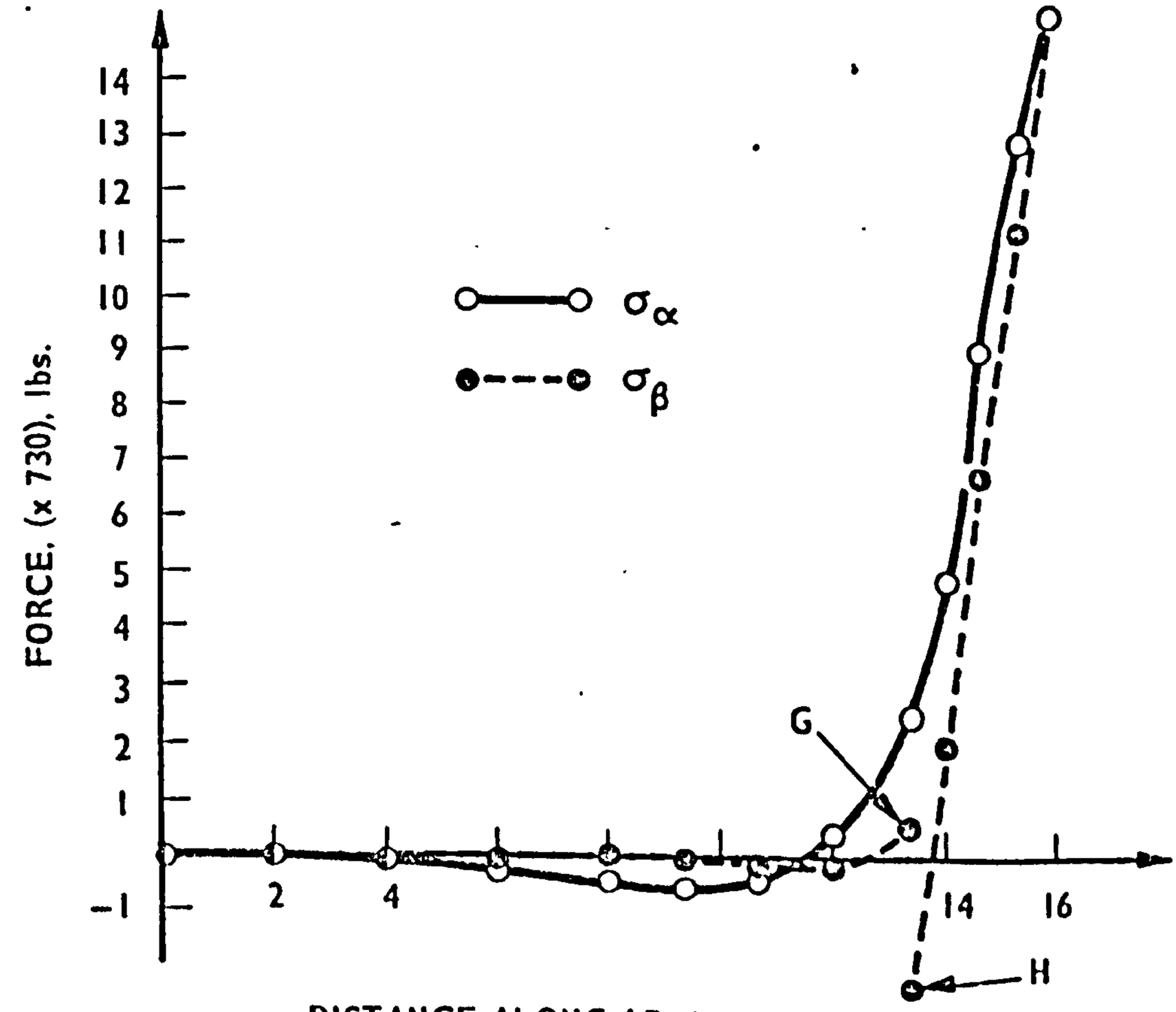

FIG.11.18 OUTER FIBRE STRESSES σ_α AND σ_β

Vlasov [9, page 495-514] and a shell finite element method. (Yang's finite element is similar to the shell finite element described in this thesis.) The problem was then solved by Dawe [102] who incorporated a shell element in the finite element program suite BERSAFE (Phase 1) [103] for the purpose.

The spherical cap, which is illustrated in Fig. 11.14, was deemed to be simply supported (see equation 11.2). As the spherical cap is doubly symmetrical only a quadrant of the shell was analysed. The mesh used for the problem is also given in Fig. 11.14. The centre of the cap was subjected to a point load of 100 lbs. Smaller elements were used near to the point load.

The orthogonal displacements were calculated using SACTIL and compared to those obtained by the series solution of Yang [66] and Dawe [102]. The correlation between the result obtained from SACTIL and that given by the series solution is good as can be seen in Fig. 11.15. The results obtained by Dawe are also very similar and are therefore not reproduced in the figure.

Fig. 11.16 shows the variation of the meridional and circumferential stress resultants N_α and N_β along AB. The correlation between the series solution and the values predicted by SACTIL is good. The stresses predicted by the finite element method of Dawe are very similar and are therefore not reproduced in the figure.

The resultant moments predicted by SACTIL are given in Fig. 11.17. Note that there is a sharp bend or 'elbow' in the values near to the point load. Note also that there is a discontinuity in the stress moments - Point G (in Fig. 11.17) denotes the moment predicted by SACTIL at the end of Element 8 (see Fig. 11.14) whilst Point H denotes the moments at the beginning of Element 9. The reason for this is discussed in the next chapter. Note that the terms of

the series solution was increased to (250 × 250) terms as the (100 × 100) term series solution did not yield a satisfactory result. The finite element solutions of Yang [66] and Dawe [102] gave very similar values to that predicted by SACTIL and are therefore not given in the figure.

The outer fibre stresses σ_α and σ_β are given in Fig. 11.18. These components were not calculated by previous workers and therefore values for comparison are not available. The stress components exhibit a sharp elbow near to the point load. The variation in stress values appear to be reasonable. That is, there is almost no (surface) stress away from the point load; the stress then increases sharply as the point load is approached and then becomes very large (values not plotted) when very near to the point load. Again notice the discontinuity in the value of σ_β at the element boundaries - Points G and H on Fig. 11.18.

11.5 Dynamic Analysis of a Hyperboloid

Accurate resonant stresses for a doubly curved structure (with meridional curvature) are very difficult to obtain analytically. The author was unable to obtain a reference from the literature which gave the values of resonant stress for the free vibration of a doubly curved shell, such as a hyperboloid. It was therefore considered to be of interest to use the program RESAP and SACTIL to analyse a thin hyperboloid of constant thickness clamped at the base (where the base was deemed to be the end-circle of larger diameter). The dimensions of the hyperboloid are very roughly, smiliar to those for the shell of the full-scale cooling tower analysed in Chapter 9. Given the equation of the hyperbola, $\frac{R^2}{a^2} - \frac{Z^2}{b^2} = 1$, then the dimensions of the hyperboloid are defined by the parameters given in Table 11.5.

Table 11.5: Properties of the Hyperboloid

a	25.6032 m
b	63.9064 m
Wall thickness	0.127 m
Axial length of neck of hyperboloid from end-circle of smaller diameter	18.5928 m
Mass density	2404.4 kg m^{-3}
Young's Modulus	20.648 MN m^{-2}
Poisson's Ratio	0.15

The resonant frequency calculated by the analytical solution of Carter, Robinson and Schnobrich [1] was 1.1808 Hz for m = 2 and n = 4.

A convergence test for the hyperboloid using RESAP was conducted. The resonant frequency is seen to converge monotonically in Fig. 11.19. It is observed that when 180 d.o.f. are exceeded the resonant frequency has completely converged. However, even the value predicted using 56 d.o.f. (four elements) differs from the answer obtained with 180 d.o.f. only by the small percentage of - 0.007%, from the value predicted using 236 d.o.f. (i.e. ninteen elements).

The reader will observe that the frequency predicted with 56 d.o.f., i.e. 1.18081 Hz, is nearer to the value of 1.1808 Hz predicted by solving the differential equations of Carter et al. [1], then the value of 1.18072 Hz given by using 236 d.o.f. At first sight this appears

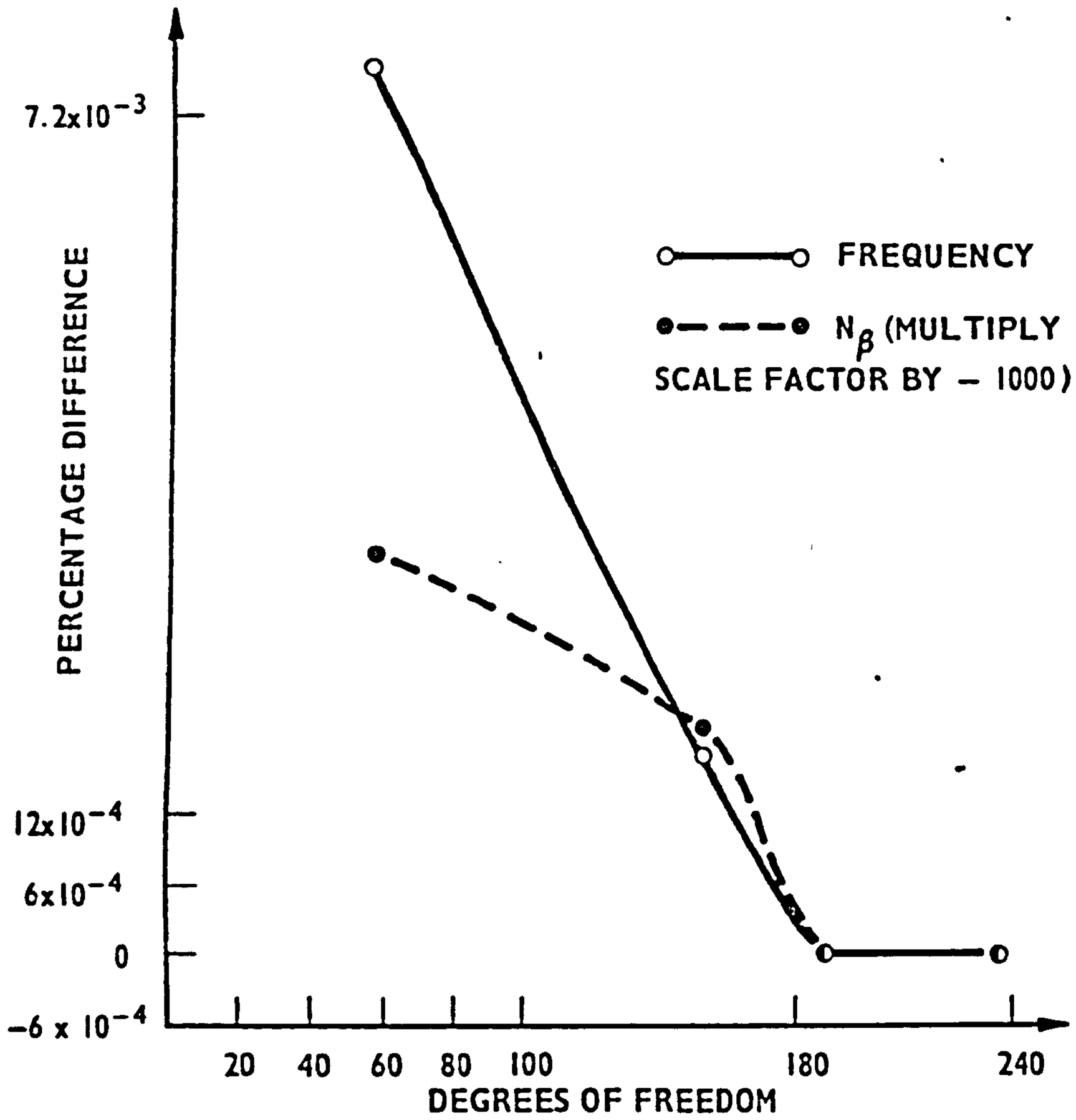

FIG.11.19 CONVERGENCE OF RESONANT FREQUENCY AND CIRCUMFERENTIAL STRESS RESULTANT (N_β) FOR RESAP – HYPERBOLOID

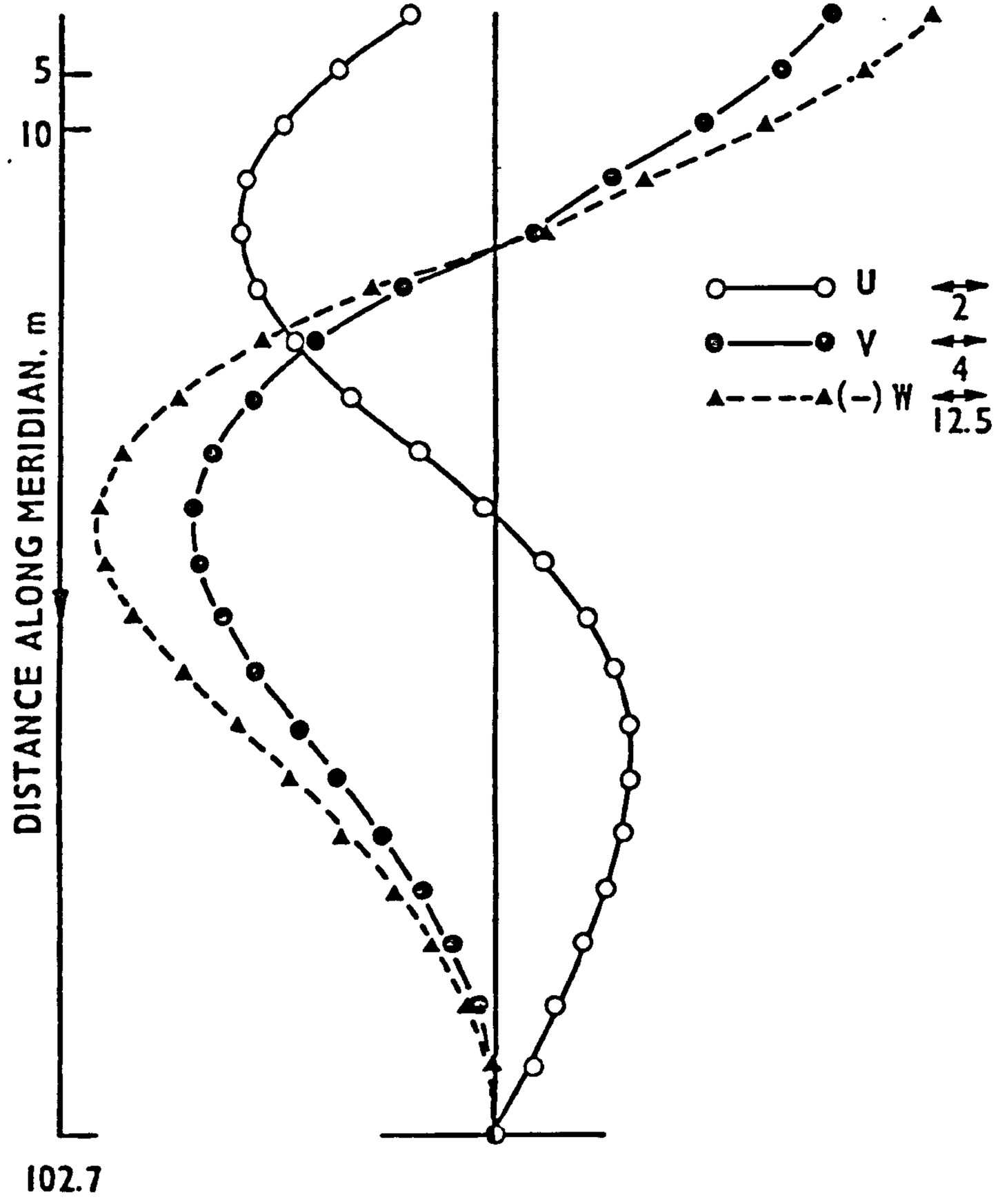

FIG.11.20 ORTHOGONAL DISPLACEMENTS U, V AND W ALONG MERIDIAN OF HYPERBOLOID (RESAP, 19 ELEMENTS)

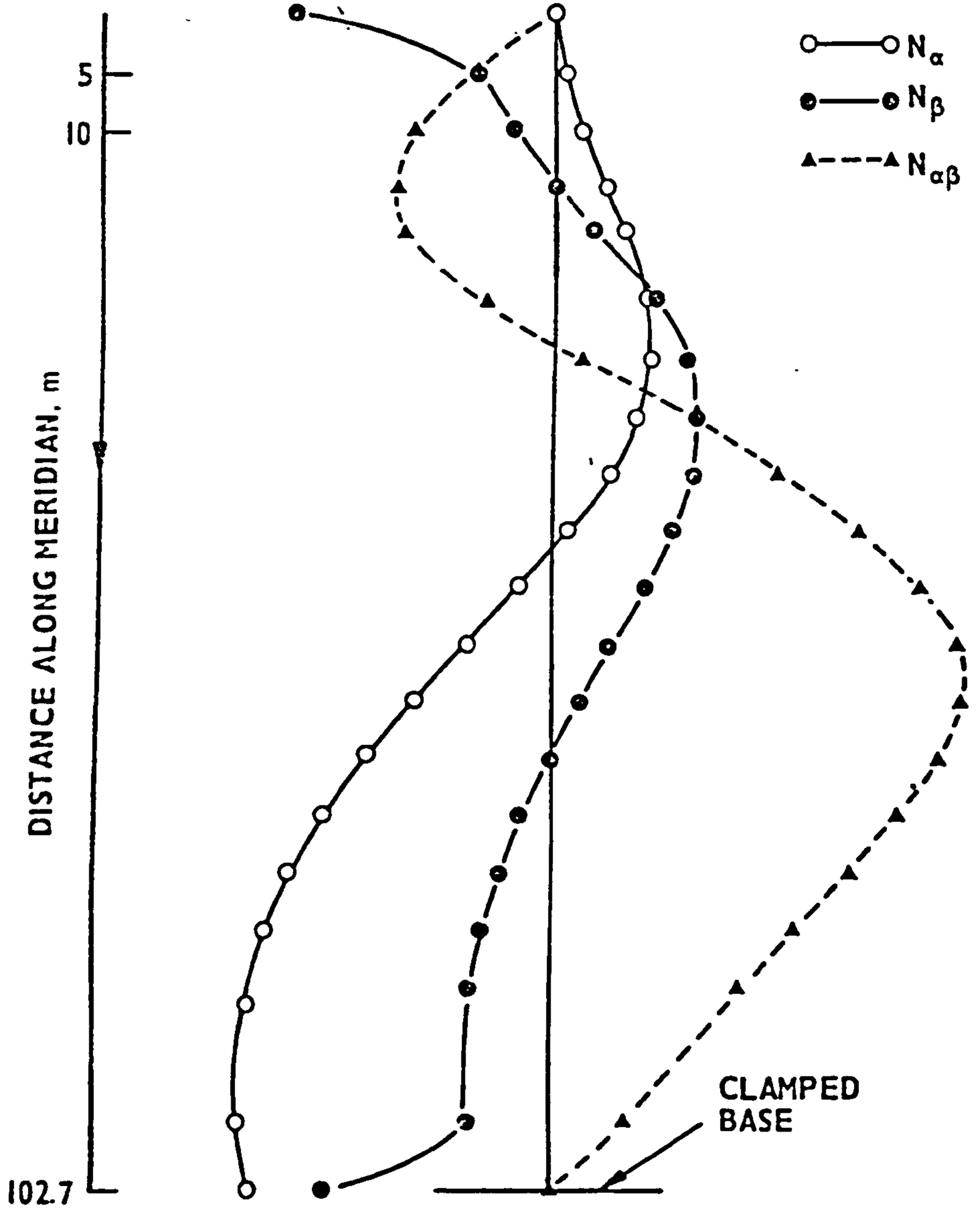

FIG.11.21 STRESS RESULTANTS ALONG MERIDIAN OF HYPERBOLOID (RESAP, 19 ELEMENTS)

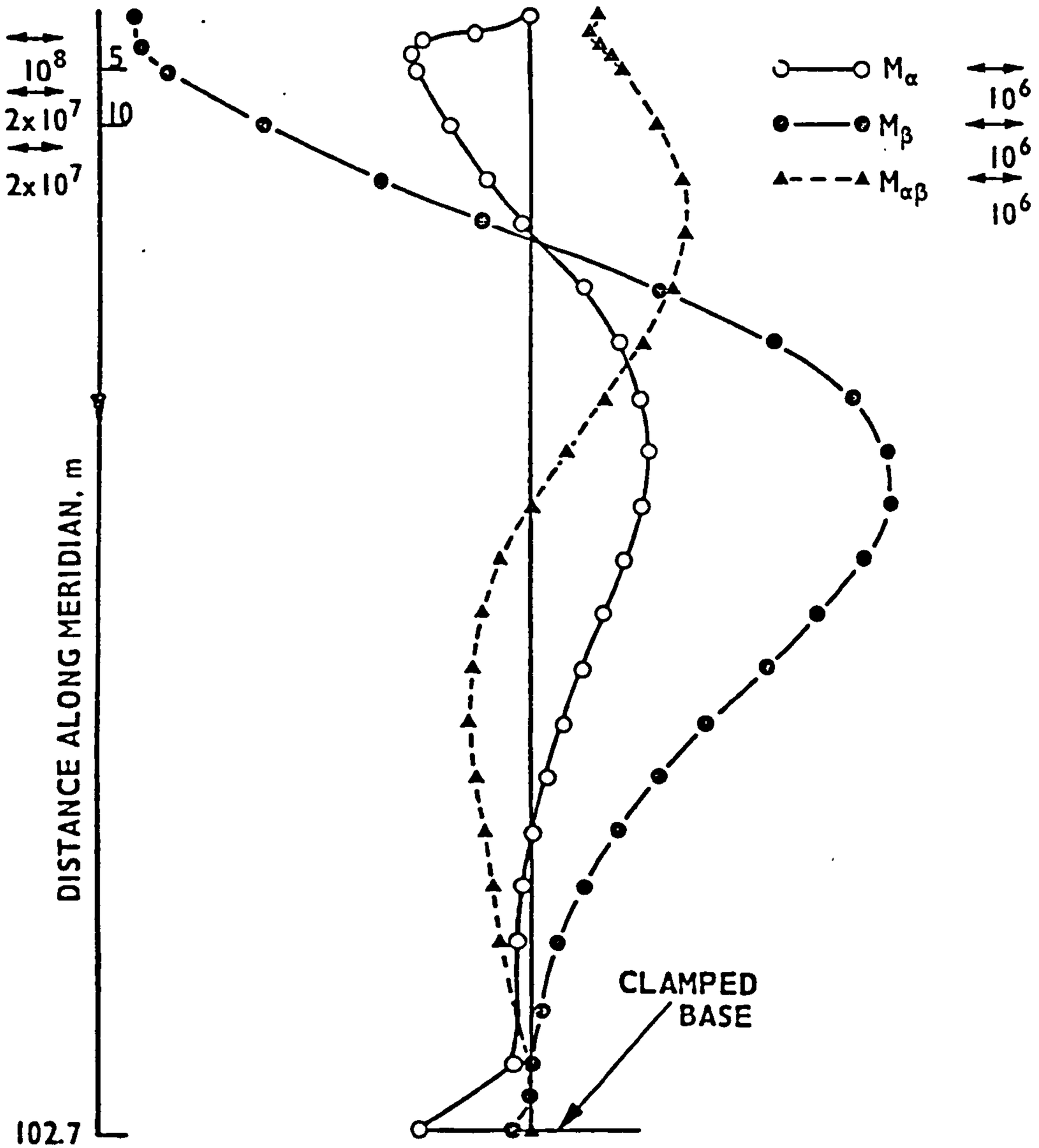

FIG.11.22 RESULTANT MOMENTS ALONG MERIDIAN OF HYPERBOLOID (RESAP, 19 ELEMENTS)

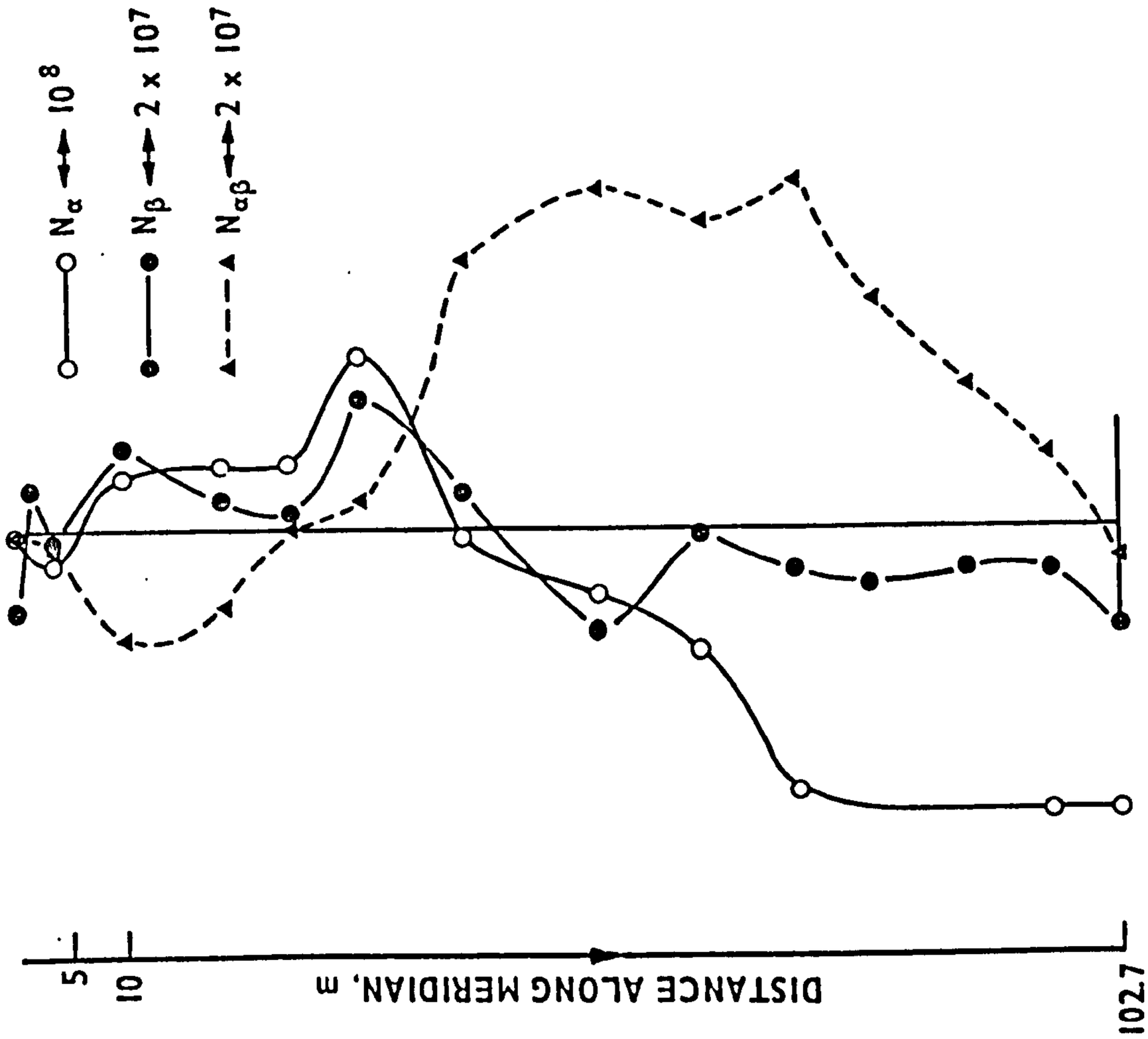

FIG.11.24 STRESS RESULTANTS ALONG MERIDIAN OF HYPERBOLOID SHOWING POOR CONVERGENCE (SACTIL, 4 x 3 ELEMENTS)

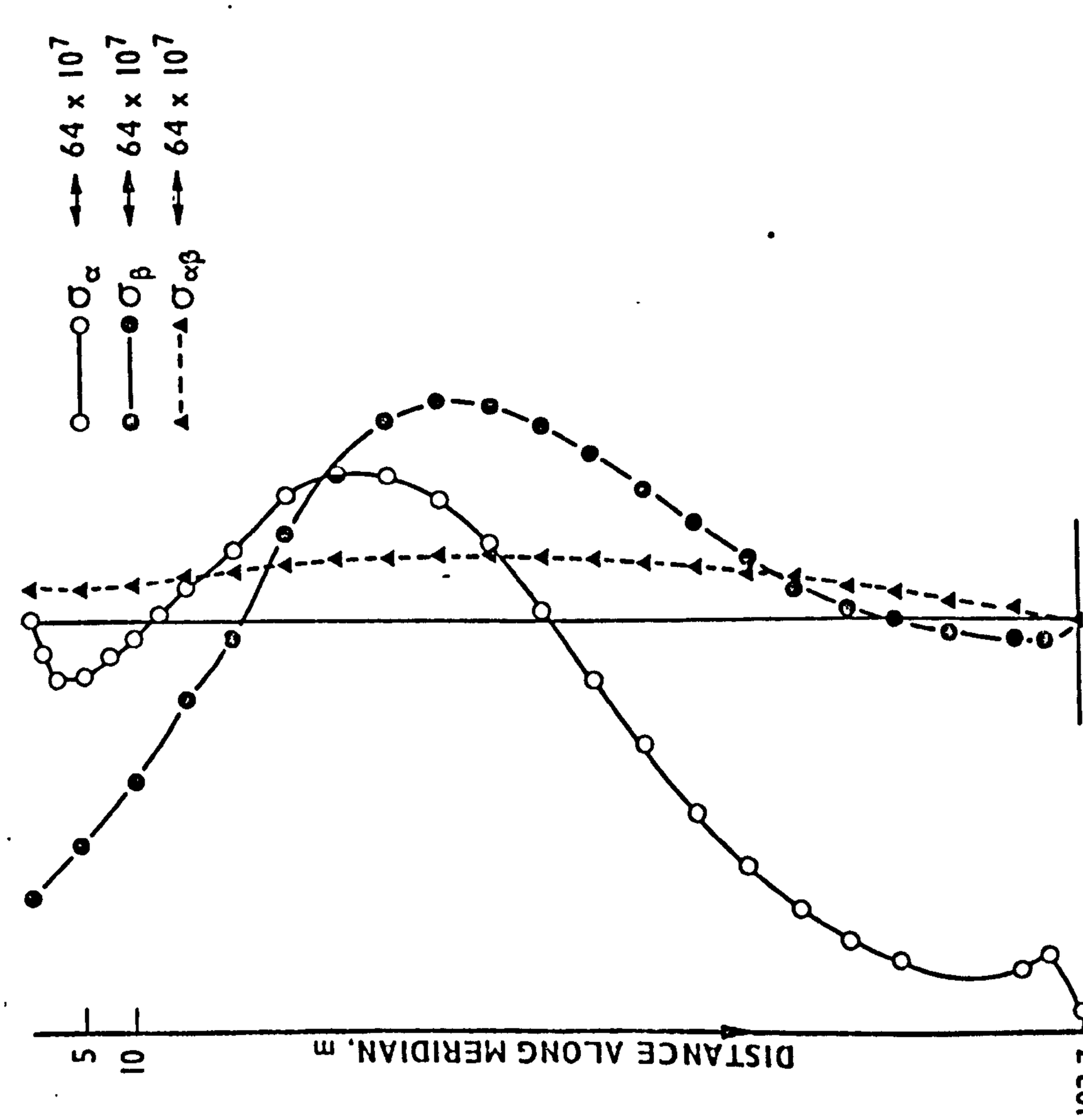

FIG.11.23 OUTER FIBRE STRESS COMPONENTS ALONG MERIDIAN OF HYPERBOLOID (RESAP, 19 ELEMENTS)

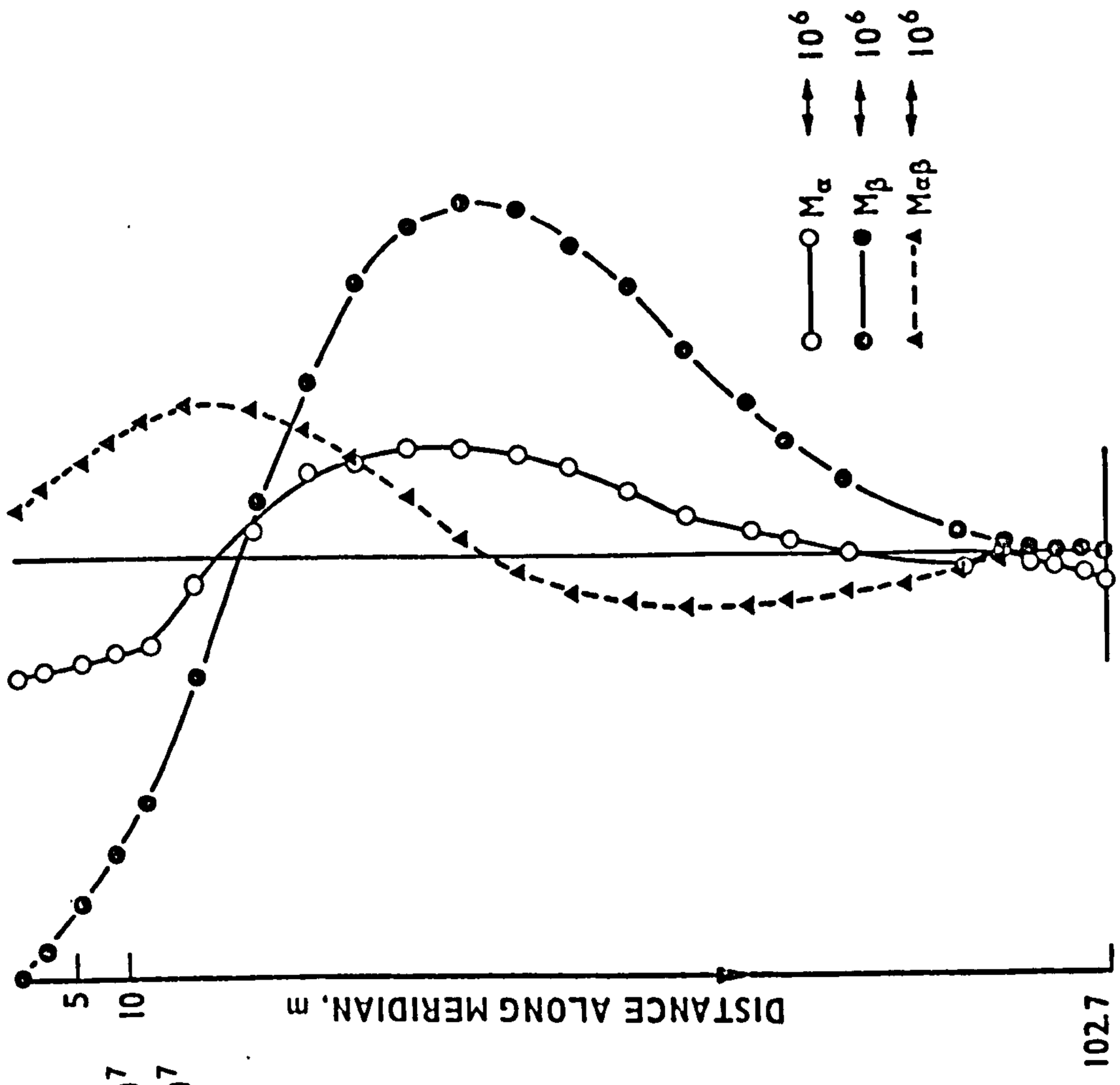

FIG.11.26 STRESS MOMENTS FOR HYPERBOLOID
(SACTIL, 6 x 3 ELEMENTS)

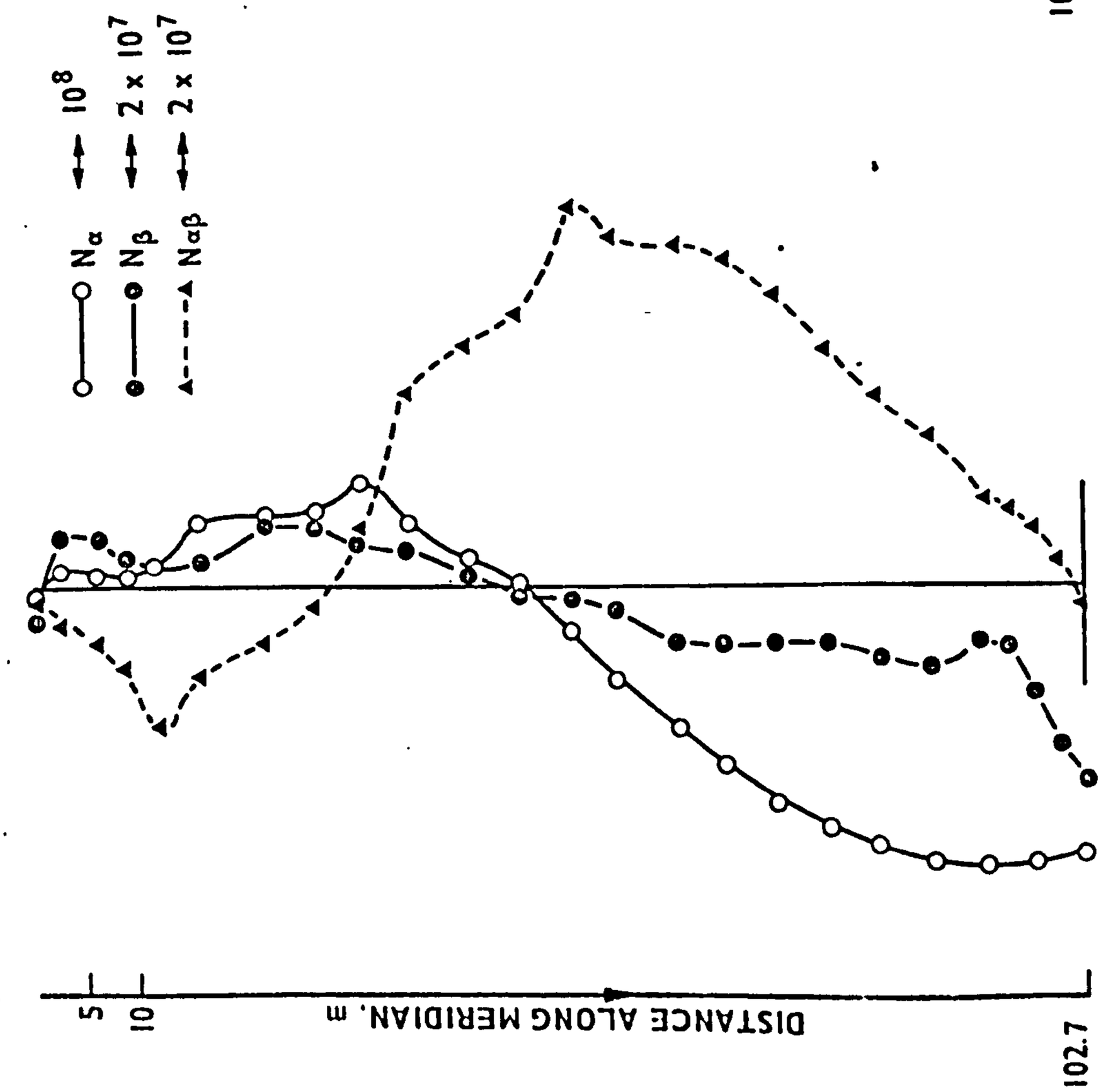

FIG.11.25 STRESS RESULTANTS FOR HYPERBOLOID
(SACTIL, 6 x 3 ELEMENTS)

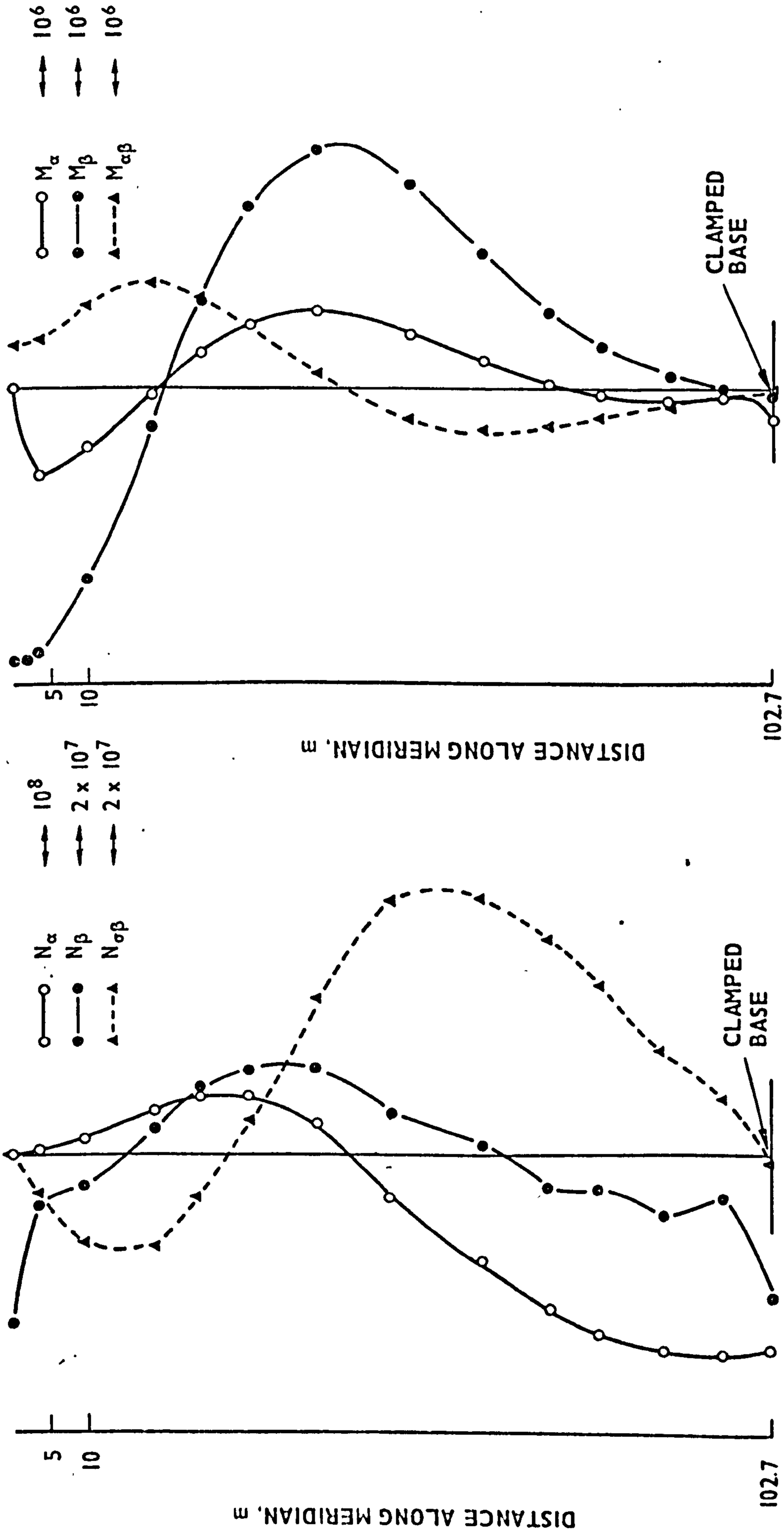

FIG.11.28 RESULTANT MOMENTS ALONG MERIDIAN OF HYPERBOLOID(RESAP, 4 ELEMENTS)

FIG.11.27 STRESS RESULTANTS ALONG MERIDIAN OF HYPERBOLOID (RESAP, 4 ELEMENTS)

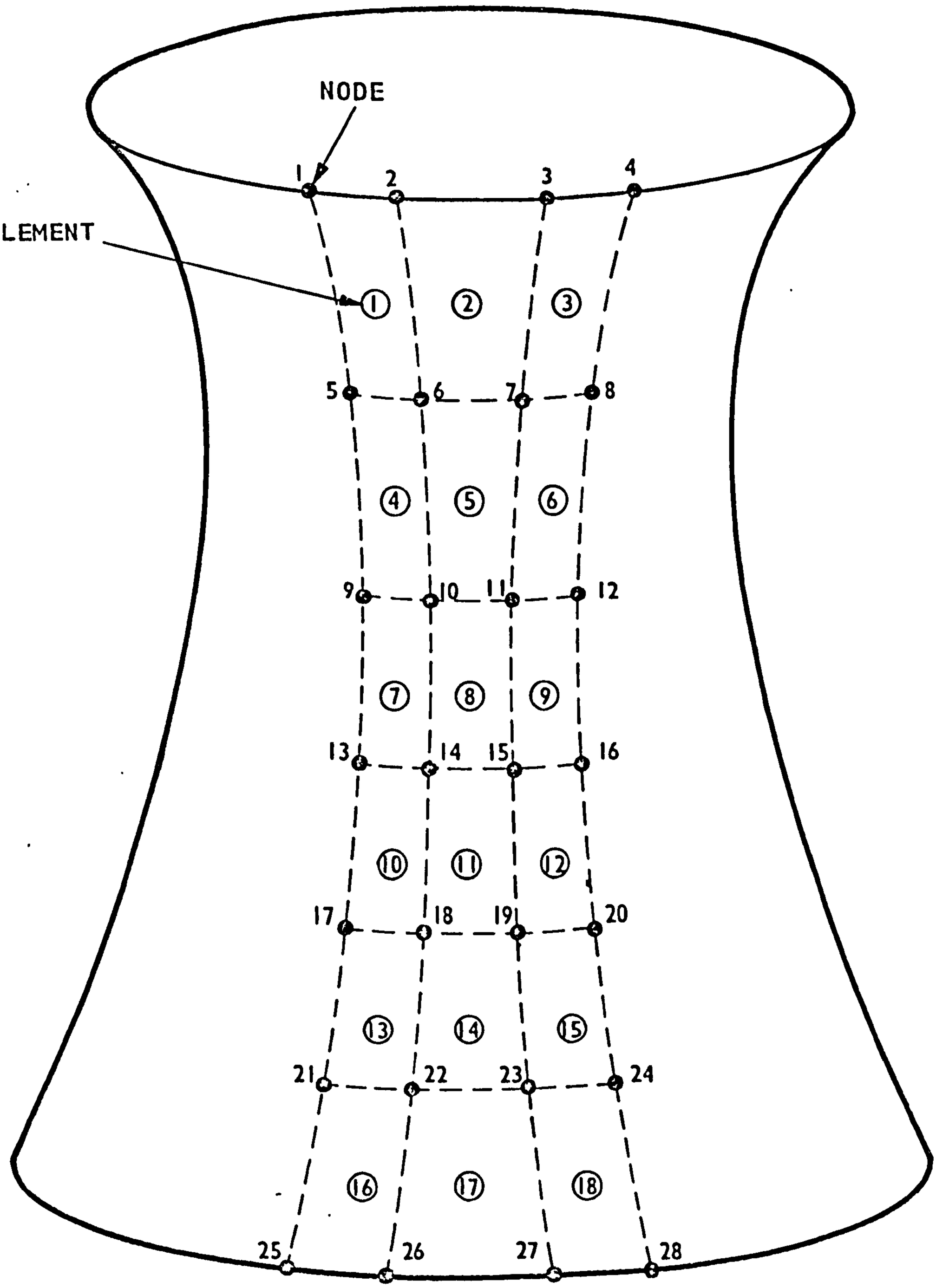

FIG. 11.29 (6x3) SHELL ELEMENT MESH FOR THE ANALYSIS OF A DOUBLY CURVED STRUCTURE WITH SYMMETRY BOUNDARY CONDITIONS (FOR THE SAKE OF CLARITY THE CIRCUMFERENTIAL DIMENSION OF THE MESH HAS BEEN EXAGGERATED)

to imply that the value obtained using 56 d.o.f. is more accurate. However, this is regarded as a coincidence. Small differences due to rounding errors in the solution routines, or in the theoretical formulation of the analytical and numerical methods may be present that give rise to the above result. (In any event the difference is small; - 0.007%.)

The convergence behaviour of the meridional stress resultant, N_α, is also depicted in Fig. 11.19. The convergence appears to be complete for more than 180 d.o.f. The convergence characteristics exhibited by N_α are, however, unusual. The reason for this is not understood.

The variations of the orthogonal displacements u, v and w along the meridian of the hyperboloid are given in Fig. 11.20. Note that for reasons of clarity, different scales have been used for all three displacements.

The stress resultants for the hyperboloid are given in Fig. 11.21. The resultant moments are given in Fig. 11.22. The stress components at the outer surface of the structure are given in Fig. 11.23 where it is seen that the meridional outer fibre stress σ_α is dominant. Note that the above values were obtained using nineteen ring elements (236 d.o.f.) thus ensuring that convergence had occurred. In this section we will regard the above values as representative of the true or exact values.

The hyperboloid was then analysed by SACTIL using a (4 × 3) element mesh. The results for the stress resultants are given in Fig. 11.24. The stresses do not vary uniformly over the meridian and the overall picture bears little resemblance to the stresses given in Fig. 11.21. Note that the agreement in the 'shapes' of

$N_{\alpha\beta}$ given in Fig. 11.24 and Fig. 11.21 is especially poor. The element mesh was refined so that a (6 × 3) element mesh was employed (see Fig. 11.29). The result is given in Fig. 11.25. It is now observed that the correlation between the values given in Fig. 11.21 and the stresses predicted by SACTIL is appreciably better. The interpolation lines shown in Fig. 11.25 show somewhat non-uniform variation. However, if the values predicted by SACTIL, using the (6 × 3) mesh, are superimposed on the stress distribution given in Fig. 11.21, it will be seen that reasonable agreement has been achieved. The unsatisfactory results depicted in Fig. 11.24 are due to the use of an inadequate number of shell elements. The somewhat non-uniform variation exhibited in Fig. 11.25 implies that more elements could be profitably employed in analysing the structure. The overall observation is that the stresses predicted by the shell element are accurate if a sufficient number of elements required for adequate convergence are employed.

The analysis of the hyperboloid using four ring elements is summarised by Fig. 11.27 and 11.28. The stress distribution is almost identical to that produced with nineteen ring elements. Hence, it is concluded that usually four ring elements can be used to accurately analyse the free vibration of doubly curved axisymmetric structures.

11.6 Conclusions

Cylinders with two different support conditions have been analysed using the two finite element programs RESAP and VACTILo2.

It has been shown that the resonant stresses predicted by the ring and shell element are in reasonable agreement with published information.

It has been shown that the ring finite element can be used to obtain

very accurate stresses; when a large number of elements were used, the predicted stresses were virtually identical to that given by an exact solution (even though a difficult case was considered).

The analysis of a spherical cap with a static point load has been analysed by the shell element and shown to be in good agreement with published information. Finally, the resonant stresses obtained for a hyperboloid using the ring and shell elements have been compared and shown to be in good agreement.

CHAPTER TWELVE

PROPOSALS FOR IMPROVED DOUBLY CURVED SHELL FINITE ELEMENTS

12. PROPOSALS FOR IMPROVED DOUBLY CURVED SHELL FINITE ELEMENTS

In this chapter it is argued that a significant increase in the accuracy convergence and efficiency (i.e. the accuracy obtainable for a given number of degrees of freedom) of a doubly curved shell finite element can be achieved by comparatively small changes in its derivation. Several alternate formulations have been presented. The theoretical and computational considerations have been discussed in detail.

12.1 Introduction

Finite elements are widely used in the static and dynamic analysis of structures. In finite element analyses the structure is represented by an assemblage of elements. The accuracy of the solution depends on the number of finite elements employed as well as the sophistication of the element itself. Whilst in principle, it is possible to achieve very high accuracies by using as many finite elements as it necessary for convergence, practically this is not always a viable solution. A large number of elements require a correspondingly large computer region and execution time is increased. (The computer time and region required can be said to vary as a power law of the degrees of freedom (d.o.f.) of the finite element mesh employed.) Generally, elements using a simple displacement function (e.g. low-order interpolation polynomials) and consequently a few nodal degrees of freedom would yield a less accurate solution, when compared to the use of elements employing high-order polynomial displacement functions. For example, McLeod [104] states that a crucial factor affecting the accuracy and rate of convergence in the finite element method is the maximum degree of polynomial used in

the displacement function. (Note that the use of high-order polynomial displacement functions usually, but does not necessarily, implies that the 'effective' d.o.f. of the element are correspondingly increased - see Section 12.3.)

The development of new finite elements is also influenced by the above considerations. The impetus is to develop finite elements that yield accurate results without excessive use of computer facilities. Elements that fall within this category are said to have a high efficiency.

One method of increasing the efficiency of finite elements is to derive elements whose shapes resemble the portion of the structure to be analysed. Conical frustum elements* [19], cylindrical elements [105] and geometrically exact elements [29] are typical examples. Unfortunately, such elements are not versatile - there is a serious loss of efficiency when using, for example, a conical frustum element for the analysis of a hyperboloid - or they are inconvenient to use.

With regard to optimizing computing facilities and the accuracy of the solutions required there is some debate as to whether it is preferable to use a large number of simple elements of a smaller number of more sophisticated elements. Percy, Pian et al. [19] and Klein [106]; suggest that the use of a large number of simple elements is the preferable alternative. On the other hand, Webster [29] showed that for a cylindrical shell a small number of elements with high-order displacement polynomials achieved better accuracy whilst requiring less computing facilities than a larger

---

*This element is used in the finite element computer program BACTo2 [20].

number of simpler elements. Adelman, Catherines and Walton [98] have also investigated cylindrical structures in order to contribute to the debate. Their firm conclusions support the observations made by Webster [29].

The doubly curved shell finite element used in VACTIL and SACTIL have been discussed in Chapter 4 - it has four nodes with twelve degrees of freedom per node. It employs a complicated displacement function (see Section 12.3) and the strain is assumed to vary quadratically through the thickness. Whilst the convergence of this element is not as good as that of its sister element, a doubly curved ring element (see Section 4.6.3.) for reasons that will be discussed in Section 12.2 - it is much more versatile. The shell element can be used to analyse cylinders and hyperboloids as well as non-axisymmetric structures such as cooling towers with legsupports. It is now being employed in calculating stresses in shell structures (Chapter 11). Results show, however, that the convergence of the shell element, whilst being satisfactory for reasonably accurate stress results could profitable be improved as mesh sizes required for reasonable convergence approach the present limit (i.e. 750 kilodytes of storage) on the IBM 370, M.V.T. (Multiprogramming Variable Task) system, for certain problems. Recalling the conclusions of Webster [29] and Adelman, Catherines and Walton [98] it is felt that an increase in the order of the polynomials used in the displacement function of the shell element would improve its convergence. Moreover, by the technique of 'Nodal Condensation' (see Section 12.3) the efficiency of the element can probably be significantly improved. (Arguments to support this hypothesis are presented in Section 12.2.)

12.2 Preliminary Observations

The doubly curved ring finite element can be regarded as a special case of the doubly curved shell finite element (Section 4.6.3). The convergence of the ring element is superior to the shell element. It is therefore instructive to compare relevant characteristics of the two elements.

When a structure is axisymmetric, as for example, a cylinder or hyperboloid, the assumption is usually made that the displacements vary sinsoidally (or cosinusoidally) around a circumferential line. This assumption allows a simpler definition of the displacement function than would otherwise have been possible. (The displacement function relates the displacements at any point on the middle-surface of the element to the displacement at the nodes.) That is, the displacement function is only a function of the meridional coordinate s (see Notation). The degrees of freedom (d.o.f.) of the element are thus not functions of the circumferential coordinate, θ. For example, Wilson [107] employs a third order polynomial in s and the technique of nodal condensation to obtain an axisymmetric finite element (used in the program DVISOR3, [107]) having four d.o.f. per node. Deb Nath [40, Section 3.1] uses a polynomial in s of order seven in the derivation of an axisymmetric or ring finite element with twelve d.o.f. per node. As all the twelve nodal d.o.f. of the ring element are used to describe the variations of the displacements with respect to s, and as a high-order polynomial of order seven is employed in the displacement function, the convergence and efficiency of the ring element is excellent. The disadvantage, however, of not explicitly including d.o.f. that are functions of θ is that

non-axisymmetric structures cannot be analysed. This restriction is removed by defining a displacement function that is not subject to the prior assumption that displacements vary sinusoidally/cosinusoidally about the circumference.

One of the better examples of this type of function has been defined by Bognor, Fox and Schmitt [105] and used by Woodman and Severn [32], Schmit, Bognor and Fox [109] and Deb Nath [40, Section 3.2]. This displacement function represents the displacement patterns in each element in terms of the products of one-dimensional, third order Hermite interpolation polynomials and undetermined nodal displacements. (A similar, though less convenient, displacement function using Legendre polynomials has also been described by Butlin and Leckie [67] and Mason [114].) The displacement function of Bognor et al. [116] is used in the shell element and is much more complicated than that used in the ring element. Note, however, that the order of the polynomials used in the displacement function for the shell element is three, which is less than the order (seven) employed in the function of the ring element. Finite elements using the function of Bogner et al. [105] must designate some d.o.f. to describe the circumferential variation of the displacements. Thus, either the stiffness and mass matrices of the finite element are increased in size, or some d.o.f. which are derivatives with respect to s (and as a consequence, probably some d.o.f. which are also derivatives with respect to θ) must be omitted. The latter alternative has been chosen in the derivation of the shell element. The d.o.f. that have been omitted (in comparison to the d.o.f. of the ring element) are $\frac{\partial^2}{\partial s^2}$ and $\frac{\partial^3}{\partial s^3}$ with respect to u, v and w. Of these six d.o.f.

the displacement derivative $\frac{\partial^2 w}{\partial s^2}$, and consequently $\frac{\partial^2 w}{\partial \theta_o^2}$, are used in the expression that relates the strain at the middle-surface of the element to the corresponding displacements - see equations 4.9(a) and 4.9(b). These displacement-derivatives therefore enter into the expressions for the stress components and resultants (see Chapter 4). The resultant moments about the meridional and circumferential direction, especially, are affected. When the present shell element was used to calculate the stresses in a spherical cap in Chapter 11 the moments were observed to be markedly discontinuous at the element common boundaries. Admittedly, the particular example referred to exhibited steep changes in the moments, but it is felt that a significant contribution to the discontinuity is due to the absence of the second derivatives of the radial displacement (w). An alternate description of the above is to state that the second derivatives of w involve the double differentiation of the cubic interpolation polynomials (see Section 12.3) used in the displacement function which then results in linear functions in s and θ; consequently steep changes in w and related functions cannot be accurately represented. Thus if the d.o.f. of the shell element can be increased to include the two relevant d.o.f., without explicitly* admitting the other four d.o.f., it is expected that the convergence and efficiency of the elements will be significantly improved. The implementation of this scheme is discussed in the following sections.

---

*The four d.o.f. must be at least implicit in the formulation of the element if they have been introduced by virtue of the displacement function. This concept will be made clearer when discussing the technique of 'Node Condensation'. In this context an implicit d.o.f. will be equivalent to a 'slave' d.o.f. and an explicit d.o.f. will be equivalent to a 'master' d.o.f. - see Section 12.3. Alternatively the four d.o.f. can be omitted during derivation of the displacement function.

12.3 Theory

The shell finite element has already been discussed in detail in Chapter 4. We shall develop the theme in this section by initially considering the displacement function used in the shell element.

It is assumed that the three orthogonal displacements, i.e. $u(s,\theta) = u$, say, v and w can be written as the products of one-dimensional, cubic interpolation polynomials and undetermined displacements at the nodes of the element. For w the expression is:

$$w = \sum_{i=1}^{i_m} \left\{ f_a g_b (w_i) + L\, f_{(a+1)}\, g_b \left(\frac{\partial w}{\partial s}\right)_i + R\psi f_a\, g_{(b+1)} \left(\frac{\partial w}{\partial \theta_o}\right)_i \right.$$

$$\left. + LR\psi_{(a+1)}\, g_{(b+1)} \left(\frac{\partial^2 w}{\partial s \partial \theta_o}\right) \right\} \qquad \ldots(12.1)$$

Here, $\theta_o = R \times \theta$. The expressions for u and v are similar. (Note that the variables $(R\psi)$ and L appear in the equation due to the following normalization:-

$$\frac{1}{L} \times \frac{\partial}{\partial \bar{s}} = \frac{\partial}{\partial s} \quad \text{and} \quad \frac{1}{(R\psi)} \times \frac{\partial}{\partial \bar{\theta}} = \frac{\partial}{\partial \theta_o} .$$

In equation (12.1),

a = 1 when i = 1 or 2

= 3 when i = 3 or 4

and b = 1 when i = 1 or 3

= 3 when i = 2 or 4

Also, $f_1(\bar{s}) = f_1$ (say) $= 1 - 3\bar{s}^2 + 2\bar{s}^3$. Similarly $g_1(\theta) = g_1$ (say) $= 1-3\theta^2 + 2\bar{\theta}^3$

$$f_2 = \bar{s} - 2\bar{s}^2 + \bar{s}^3 \qquad g_2 = \bar{\theta} - 2\bar{\theta}^2 + \bar{\theta}^3$$

$$f_3 = 3\bar{s}^2 - 2\bar{s}^3 \qquad g_3 = 3\bar{\theta}^2 - 2\bar{\theta}^3$$

$$f_4 = -\bar{s}^2 + \bar{s}^3 \qquad g_4 = -\bar{\theta}^2 + \bar{\theta}^3 .$$

The interpolation polynomials given here are known as Hermite polynomials. (Hermite interpolation is a special case of Lagrange interpolation and is discussed in detail by Ciarlet and Raviart [108]). The accuracy, and usefulness, of the above displacement function has been verified by several authors [66, 40, 32, 7]. Thus, several important requisites, like for example, the continuity of displacements and slopes between adjacent elements along an entire edge, are satisfied.

We now need to develop the displacement function so that the second differentials of w with respect to s and θ, are introduced as nodal variables. As Hermite interpolation is a convenient and accurate technique which has been used successfully with finite elements we can extend the shell element by adopting higher-order Hermite polynomials. Thus the displacement function w is written as

$$w = \sum_{i=1}^{4} w_i f_a g_b + \left(\frac{\partial w}{\partial s}\right)_i Lf_{(a+1)} g_b + \left(\frac{\partial w}{\partial \theta_o}\right)_i R\psi f_a g_{(b+1)} + L^2 f_c g_b \left(\frac{\partial^2 w}{\partial s^2}\right)_i + (R\psi)^2 f_a g_d \left(\frac{\partial^2 w}{\partial \theta_o^2}\right)_i + R\, Lf_{(a+1)} g_{(b+1)} \left(\frac{\partial^2 w}{\partial s \partial \theta_o}\right)_i \qquad \ldots(12.2)$$

The expressions for u and v are similar.

Hermite's interpolation formulae (or the formulae for oscillating interpolation) [110] are now used to obtain the required Hermite polynomials. (Alternatively, the polynomials of required order can be subject to the desired boundary conditions and the coefficients obtained by solving the ensuing simultaneous equations.) Note that the degree of the polynomials is determined by the maximum value of the derivative of the variable to be interpolated. These are found to be:-

$$f_1 = (1 - 10\,\bar{s}^{-3} + 15\,\bar{s}^{-4} - 6\,\bar{s}^{-5})$$

$$f_2 = (\bar{s} - 6\,\bar{s}^{-3} + 8\,\bar{s}^{-4} - 3\,s^{-5})$$

$$f_3 = (10\,\bar{s}^{-3} - 15\,\bar{s}^{-4} + 6\,\bar{s}^{-5})$$

$$f_4 = (-\,4\,\bar{s}^{-3} + 7\,\bar{s}^{-4} - 3\,s^{-5})$$

$$f_5 = \tfrac{1}{2}(\bar{s}^{-2} - 3\,\bar{s}^{-3} + 3\,\bar{s}^{-4} - \bar{s}^{-5})$$

$$f_6 = \tfrac{1}{2}(\bar{s}^{-3} - 2\,\bar{s}^{-4} + \bar{s}^{-5})$$

The 'g-polynomials' are similar to the above with $\bar{\theta}$ being substituted for $\bar{s}$.

In equation (12.2) a and b vary with i as defined for equation (12.1). However, c and d vary as given below:

c = 5 when i = 1 or 2

and c = 6 when i = 3 or 4

Also, d = 5 when i = 1 or 3

and d = 6 when i = 2 or 4.

An interpolation displacement function should, and usually has, the property that at any node the displacements (and displacement-derivatives) predicted by the function are identical to the nodal displacements. The displacement function used in equation (12.1) is at variance with this particular criterion for certain d.o.f. such as $\frac{\partial^2 w}{\partial s \partial \theta_o}$ - see Appendix 12.1. However, it can be seen (by differentiating the Hermite polynomials and substituting for $\bar{s}$ and $\bar{\theta}$) that the displacement function introduced in equation (12.2) is now in agreement with the above criterion, as displacement-derivatives such as $\frac{\partial^2 w}{\partial s^2}$ are explicitly included in the formulation prescribed in equation (12.2).

The variation in the values of the Hermite interpolation polynomials with $\bar{s}$ are depicted in Fig. 12.1. Note that the polynomials f_1 and f_3 are mirrored about the central meridional point (i.e. where $\bar{s} = 0.5$). Similarly, f_5 and f_6 are mirror-pairs. f_2 and f_4 are mirror-pairs but with sign reversals.

We now have an eighteen degree of freedom per node, four-noded shell finite element which untilizes interpolation polynomials of order five and which includes the important nodal variables such as $\frac{\partial^2 w}{\partial s^2}$ and $\frac{\partial^2 w}{\partial \theta_o^2}$. However, the less important variables such as $\frac{\partial^2 u}{\partial s^2}$, $\frac{\partial^2 u}{\partial \theta_o^2}$, $\frac{\partial^2 v}{\partial s^2}$ and $\frac{\partial^2 v}{\partial \theta_o^2}$ are also included. The inclusion of the latter four d.o.f. would increase the region size and computing time required, for a given number of elements, without contributing appreciably to the convergence.

It is not admissible to merely neglect these terms in

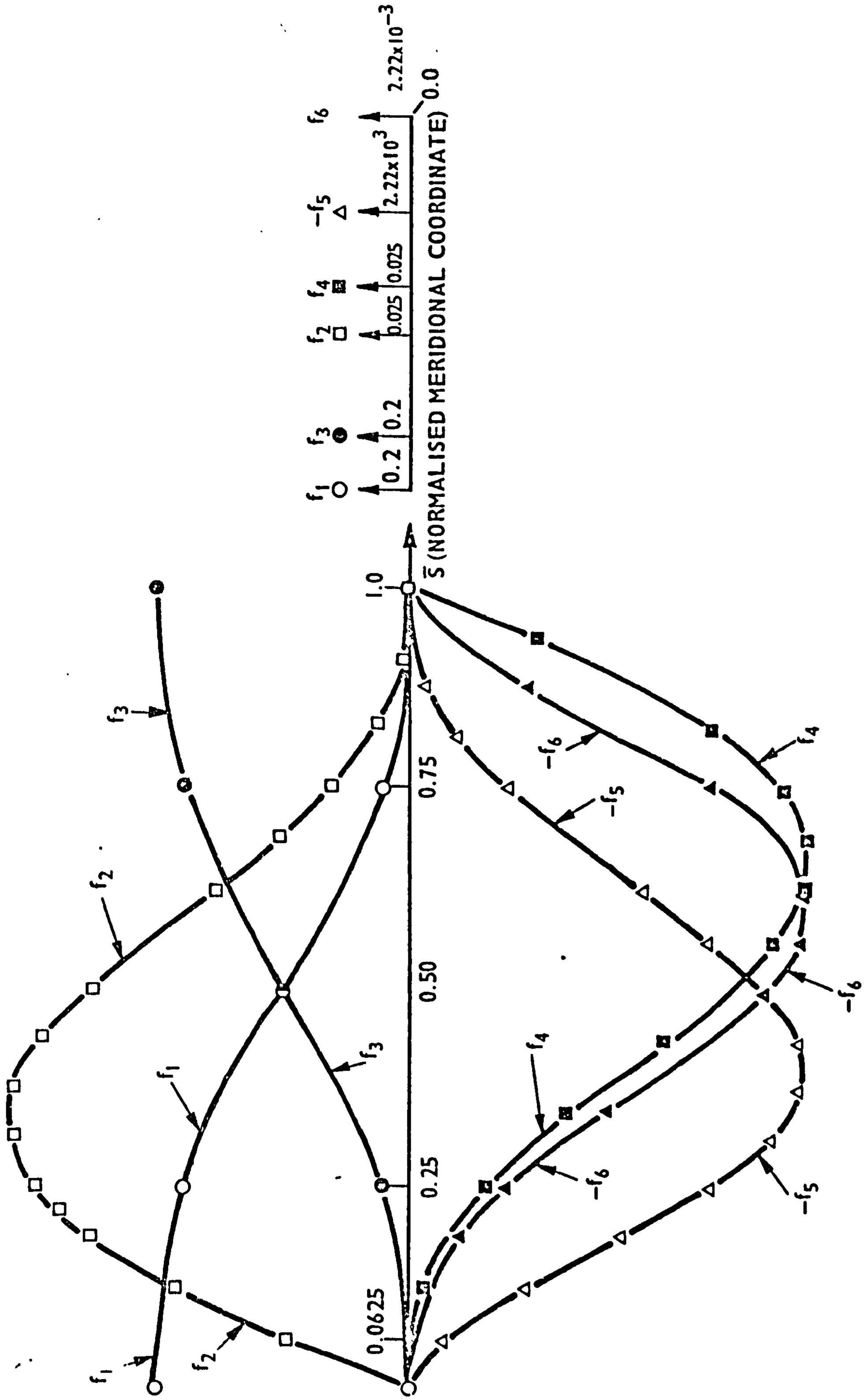

FIG.121 GRAPHICAL REPRESENTATION OF THE HERMITE INTERPOLATION POLYINOMIALS OF ORDER 5

the formation of the stiffness and mass matrices as coefficients of the interpolation polynomials will be mathematically unspecified. On initial considerations it appears feasible to employ the 'Node Condensation' or 'Eigenvalue Economizer' technique. The method has been well documented by Guyan [111] and Irons [112]. This technique will allow the reduction of the nodal d.o.f. from eighteen to fourteen while maintaining mathematical consistency. The d.o.f. 'condensed-out' are referred to as 'slave' d.o.f.; the remaining d.o.f. are known as 'master' d.o.f. (The technique is mathematically accurate for static problems and is a good approximation for dynamic problems for the lower eigenvalues.)

Note, however, that the condensation technique can only be applied in the present case, to the system stiffness and mass matrices - it is not admissable to condense out the four d.o.f. from the element matrices. This is because the continuity of these four displacement-derivatives along the element edges is important to obtain a conforming element. (Condensation of system matrices, however, preserves continuity of displacements and derivatives.) Non-conforming element (e.g. in the first-differentials of the radial displacements) have been developed that yield good results. However, in the present case if the four displacement-derivatives referred to are not made continuous across element common edges, the physical representation of the structure being analysed would include gaps or holes. This would probably result in a significant reduction in the potential accuracy of the proposed element. Thus one criticism that can be levied at the above formulation is that the nodal condensation technique is applied to the system matrices

and the d.o.f. that are to be condensed-out are defined a priori; however, these very d.o.f. may be of importance in the particular structure being investigated. The optimum d.o.f. to be retained as masters and those to be condensed-out should ideally be selected using the technique described by Henshell and Ong [113].

An alternative method is now proposed that does not require the use of the nodal condensation technique. That is, the displacement-derivatives $\frac{\partial^2 u}{\partial \theta_o^2}$, $\frac{\partial^2 u}{\partial s^2}$, $\frac{\partial^2 v}{\partial \theta_o^2}$ and $\frac{\partial^2 v}{\partial s^2}$ are not included even implicitly as nodal variables. In this formulation the displacement function defined by equation (12.2) is used to describe the variation of the w displacement (and its derivatives) only, giving six nodal variables per node. The in-plane displacements u and v are described by the existing displacement function (given by equation (12.1)) resulting in eight nodal variables. This proposal would result in a finite element with fourteen d.o.f. per node which utilizes a 'mixed order polynomial' displacement function. The advantage of this formulation is that the application of the condensation technique to the system stiffness and mass matrices is unnecessary, and the maximum size of the system matrices is smaller than for the previous formulation. The disadvantage, however, is that two types of interpolation functions have to be processed. Thus the numerical scheme required to form the element matrices becomes somewhat more sophisticated with an attendant increase in computing time. Also, the anomaly inherent in the displacement function used for the current shell finite element is now present for the in-plane displacements. (It should be noted, however, that an investigation by the author indicates that the performance of the element is not adversely

affected to any significant degree by the anomaly. Also, for the element proposed above the important radial displacements are not subjected to the anomaly.)

In addition to the advantages outlined above in including $\frac{\partial^2 w}{\partial s^2}$ and $\frac{\partial^2 w}{\partial \theta_o^2}$ as nodal variables there is the advantage that various boundary conditions can usually be specified more accurately. When a structure is 'simply supported' some analysists prefer to stipulate 'hybrid' boundary conditions (see Section 11.2). It would then be required that $\frac{\partial^2 w}{\partial s^2}$ or $\frac{\partial^2 w}{\partial \theta_o^2}$ is zero (together with other lower order displacement-derivatives), depending on the direction of the support. (This is because the relevant direct forces and bending moments and the corresponding displacement-derivatives at the supported edge should be specified as zero.) In the present element it is not possible to constrain these d.o.f. Consequently these boundary conditions involve arguable approximations.

It is now interesting to examine the d.o.f. $\frac{\partial^2 u}{\partial s \partial \theta_o}$ and $\frac{\partial^2 v}{\partial s \partial \theta_o}$. These d.o.f. are used in the present element and are included as nodal variables in the two formulations proposed above. However, these two d.o.f. are not used in the expression that relates the strain at the middle surface to the corresponding displacements. Moreover, it is not important for these two d.o.f. to be continuous across common element boundaries. Thus, condensing these d.o.f. out at the element stage will increase the efficiency of the element. This process can be applied to both formulations referred to above. One disadvantage, albeit small, is that

specification of certain boundary conditions may then involve some approximations.

Table 12.1 presents several different types and forms of doubly curved shell finite elements:-

Table 12.1: Different Types (or Forms) of Doubly Curved Shell Finite Elements

Element Ref. No.	Nodal D.O.F. in final Element	Order of Interpolation Polynomials u	v	w	Condensed D.O.F.	Comments
A	12	3	3	3	-	An anomaly exists in the displacement function. (However, the performance of the element does not appear to be affected, to any noticeable degree, by the anomaly.) Efficiency of the element is moderate. Hybrid boundary conditions cannot always be specified accurately.
B	18	5	5	5	-	Element is theoretically sound. However, too many d.o.f. detract from the efficiency of the element. Maximum size of system matrices is large. Boundary conditions can be accurately specified.
C	16	5	5	5	$(\partial^2 u/\partial s \partial\theta_o)$ $\left(\frac{\partial^2 v}{\partial s \partial\theta_o}\right)$	Efficiency of element may be better than for element B. Maximum size of system matrices smaller than for B. Some uncommon boundary conditions cannot be accurately specified.
D	14	3	3	5	-	Efficiency of element high. Maximum size of system matrices smaller than for B and C. Anomaly is present for displacements in the in-plane directions. Some uncommon boundary conditions cannot be specified accurately.
E	12	3	3	5	$\left(\frac{\partial^2 u}{\partial s \partial\theta_o}\right)$ $\left(\frac{\partial^2 v}{\partial s \partial\theta_o}\right)$	Efficiency of element is probably higher than for element D. (Other comments as for element D.)

Those elements will be discussed further in Section 12.5.

12.4 Programming Considerations

The computing task will be greatly assisted by using the subroutines written to assemble the element stiffness and mass matrices of the present version of the shell finite element - see Chapter 5. Due to the modular, structured nature of the subroutines it will be required, in principle, to modify only a few of the subroutines. The subroutines to be modified are small; they perform simple manipulations on the Hermite interpolation polynomials.

It is recommended that the modular nature of the subroutines is maintained to facilitate any further development of the element. Also that the user shall be allowed to specify the form of the shell element he requires. That is, by specifying '12' the present shell finite element is obtained, by specifying '14' the shell element Type D is obtained; by specifying '18' the shell element Type B is obtained. Also, it is desirable to have an option that enables the user to request twelve d.o.f. per node but where the displacement function utilizes the fifth order interpolation polynomials in the radial direction (i.e. the nodal condensation technique is used to reduce the nodal d.o.f. from fourteen to twelve). It is recommended that the modified subroutine package be incorporated in the finite element program VACTILo2.

12.5 Discussion

In this chapter four shell elements have been proposed. The shell element currently used in the programs VACTIL and SACTIL element Type A in the Table in Section 12.4 - has been reported to have a moderate degree of efficiency. This is probably due to the use of a comparatively low-order polynomial in the important radial direction w.

Also an anomaly is present in its displacement function. Consequently an eighteen nodal d.o.f. element, Type B, has been proposed. Whilst the anomaly in the displacement function is no longer present and the displacement-derivatives $\frac{\partial^2 w}{\partial s^2}$ and $\frac{\partial^2 w}{\partial \theta_o^2}$ are included as nodal variables, the nodal d.o.f. include variables that are not thought to contribute to the efficiency of the element. The efficiency of element B can be improved by internal nodal condensation of two not particularly important d.o.f. to give element C. The element type D is of interest as it employs a fifth order interpolation polynomial for the important radial displacement and the less important in-plane displacements use third order polynomials. Thus the anticipated efficiency of the element is high and the technique of node condensation is not required. The element Type E is an attempt to improve the efficiency of element D even further.

Of the four new elements proposed in this text elements B and D are the basis for the other elements (i.e. the elements, excluding A, are different forms of the basic elements B and D). In an investigation to decide the most useful and efficient element, initial preference should be given to elements D and E. Whilst at this stage it would be premature to select a particular element as the best, the element Type E appears to satisfy most of the theoretical and other requirements necessary for fast convergence with optimum use of computing resources.

Whilst the primary purpose of this chapter is to advocate the increase of the displacement expansion in the radial direction from cubic to quintic polynomials, it would be of theoretical interest to use the node condensation technique to also investigate

the effects of varying explicit (i.e. 'master') and implicit (i.e. 'slave') d.o.f. on the behaviour of the element. For example, it would be instructive to specify quintic polynomials to represent the variation of all three orthogonal displacements and to then condense out all the six newly introduced d.o.f. and observe whether an increase in the accuracy and/or efficiency of the element is obtained. It must be noted that no difference was observed when a similar investigation was conducted with a beam element by Thomas [115]. However, the displacement function of the beam element is simpler than that of the shell element. Moreover, the anomaly referred to in the Appendix 12.1 for the lower-order displacement function of the shell element is removed by the use of the higher-order displacement function.

12.6 Conclusions

It has been argued that the efficiency of a finite element is improved by the use of higher-order interpolation polynomials in the displacement function. The efficiency and convergence of a doubly curved shell finite element has been critically compared to that of a sister element, a doubly curved axisymmetric (ring) finite element. It is therefore postulated that an increase in the efficiency of the shell element can be obtained by increasing the displacement expansion in the radial direction from a cubic to a quintic polynomial. Several alternate elements that embody this requirement have been derived. The comparative advantages of these elements have been discussed. The theoretical and computational aspects have been discussed in detail. Finally it is expected that implementation of the implied recommendations in this chapter will result in a useful insight into the characteristics of the shell finite element

CHAPTER THIRTEEN

CONCLUSIONS

13. CONCLUSIONS

As far as the author is aware the finite element method described in this thesis yields the most accurate prediction, to date, of the resonant frequencies and mode shapes of cooling tower shells supported on columns. It has been shown that for the cooling tower at Didcot Power Station the resonant frequencies predicted by the method are within 5% of the corresponding experimental values for both model and full-scale structures.

With reference to the resonant behaviour of cooling towers, foundation elasticity has been shown to be very important. The effect of Poisson's Ratio, however, has been shown to be small. An important observation is that the small discrepancies that exist between the experimental data obtained for both model and full-scale structures can be explained on a rational basis.

The finite element method described in this thesis is a useful design tool. As a preliminary study and, as an illustrative example the dimensions of the ring-beam and cornice of a cooling tower have been shown to have an affect on the values of resonant frequency of an important mode.

Though not as convenient as the finite element method that has been described, the investigation of model cooling towers has been shown to be a useful adjunct to understanding the behaviour of full-scale structures. An important finding is that a realistic simulation of foundation elasticity of the model structure is necessary if reliable results are to be obtained. The multipoint excitation system, originally developed at Farnborough (R.A.E.), has been shown to be useful in the experimental investigation of

cooling towers. However, it was observed that even six exciters were not sufficient in number to excite, in isolation, some of the cooling tower modes.

'Non-classical' modes of vibration were probably not experimentally observed by the author. Admittedly, some modes were observed to exhibit characteristics associated with non-classical modes. This is thought, however, to be due to harmonic interference between neighbouring modes. On theoretical grounds it is argued that the manner in which n (circumferential wave number) is defined can be a probable reason for stating that non-classical modes exist for cooling towers.

The use of a laser as a displacement measuring device for the model structure has been found to be highly satisfactory, provided a few simple precautions are observed. Such measurements are more speedily and accurately obtained, when compared with the use of other devices such as capacitance transducers.

The finite element method described in this thesis has been developed primarily for the analysis of cooling towers. However, the method has applications in the analysis of similar structures. (For example chimneys with appendages.)

Stress-displacement matrices were derived for the doubly curved finite elements used in the project. The analyses of several structures have established that accurate stresses are predicted. Following from a detailed study of the elements, proposals were made for the improvement of their accuracy and convergence. An algorithm has been developed that should enable the reliable coding of the new elements. The algorithm is at present being successfully

employed in evaluating the stiffness and mass matrices of the finite elements used in this thesis.

The mechanics of wave propagation in periodic and symmetric structures have been shown to be well established in the literature. Wave propagation methods have been used in recent years for studying vibration of structures such as aircraft wings. It has been shown that these techniques can be successfully applied to the analysis of cooling towers by regarding such structures as rotationally periodic. (Thus the approximations involved in assuming the tower to be an idealized axisymmetric structure are not necessary.) In this thesis the finite element method has been applied to rotationally periodic structures. However, it is deemed possible to analyse structures that are almost but not quite rotationally periodic by regarding the structure as periodic, but with small perturbations (involving the parameter concerned).

CHAPTER FOURTEEN

SUGGESTIONS FOR FUTURE RESEARCH

14. SUGGESTIONS FOR FUTURE RESEARCH

In view of the success of the finite element method described in this thesis the method should be developed further. One important limitation of the present method is that only 'perfect' cooling towers can be accurately analysed. Kemp and Croll [117] claim that even moderate imperfections in the meridian of a tower induce hoop stresses in the vicinity of the imperfection that are of the same order of magnitude as the meridional stresses that would occur in the corresponding area of the perfect shell. Soare [118] supports this claim; he states that meridional imperfections contribute little to the meridional and shear forces, but that the hoop forces are strongly influenced. Tentative proposals have been made in this thesis to develop the finite element method to enable imperfect cooling towers to be analysed.

Another important aspect that is gaining relative importance at the present time is the behaviour of cooling towers under transient force conditions (e.g. seismic disturbances). The Beta-Newmark method [119] has been used in VACTIL and preliminary results are promising.

The optimum shape of cooling towers is another topic that is of interest [120]. The shape of a tower is dictated not only by its structural integrity but by its cooling performance. The program VACTIL would be a useful aid in studying the structural aspects.

The doubly curved shell element used in the project has been shown to give good results. However, as discussed in Chapter 12 the element can probably be improved further. It was suggested

for example that the use of mixed-order interpolation polynomials in the displacement function together with the nodal condensation technique could probably improve the efficiency of the shell element and is therefore worthy of investigation.

With respect to the experimental work on cooling towers described in this thesis it is recommended that twelve exciters are employed in the multi-point excitation system to enable more satisfactory excitation of some of the more complex modes, as this will reduce unwanted harmonic interference from neighbouring modes. Also, that phase shifters are employed to correct the small phase difference that exists between the output of the voltage-tuned oscillator and excitation force.

APPENDIX 5.1

EXPRESSION FOR DUO-OPERATORS

In Fig. 5.1 the term C_{11} is associated with the mono-operator $\frac{\partial}{\partial \bar{s}}$. However, the term C_{35} is associated with three differential operators; namely 'no differentiation', $\frac{\partial}{\partial \bar{s}}$ and $\frac{\partial}{\partial \bar{\theta}^2}$.

It can be shown that dealing with such operators introduces only a little more computing sophistication. As an example the derivation of the expression for duo-operators is given below:

Consider equation (5.7).

Assume that duo-operators are present. We can then write equation (5.7) as:

$$k_{m\ell}^{ij} = \int_{\bar{s}=0}^{1} \int_{\bar{\theta}=0}^{1} \sum_{\bar{k}=1}^{6} \sum_{\bar{h}=1}^{6} \left({}^{1}H_{m\bar{k}}\ {}^{1}A_{m\bar{k}}\ t^{i} + {}^{2}H_{m\bar{k}}\ {}^{2}A_{m\bar{k}}\ t^{i} \right) \left(k_{\bar{k}\bar{h}} \right)$$

$$\left({}^{1}H_{\bar{h}\ell}\ {}^{1}A_{\bar{h}\ell}\ t^{i} + {}^{2}H_{\bar{h}\ell}\ {}^{2}A_{\bar{h}\ell}\ t^{j} \right) d\bar{s}.d\bar{\theta} \qquad \ldots(A5.1)$$

where the pre-suffix is used to distinguish between different operators of the same term in the matrix C.

Equation (A5.1) can be expanded as

$$k_{m\ell}^{ij} = \iint \sum \sum \left\{ \left({}^{1}H_{m\bar{k}}\ {}^{1}A_{m\bar{k}}\ t^{i}\ z_{\bar{k}\bar{h}}\ {}^{1}H_{\bar{h}\ell}\ {}^{1}A_{\bar{h}\ell}\ t^{j} \right) + \left({}^{1}H_{m\bar{k}}\ {}^{1}A_{m\bar{k}}\ t^{i}\ z_{\bar{k}\bar{h}}\ {}^{2}H_{\bar{h}\ell}\ {}^{2}A_{\bar{h}\ell}\ t^{j} \right) + \left({}^{2}H_{m\bar{k}}\ {}^{2}A_{m\bar{k}}\ t^{i}\ z_{\bar{k}\bar{h}}\ {}^{1}H_{\bar{h}\ell}\ {}^{1}A_{\bar{h}\ell}\ t^{j} \right) + \left({}^{2}H_{m\bar{k}}\ {}^{2}A_{m\bar{k}}\ t^{i}\ z_{\bar{h}\bar{k}}\ {}^{2}H_{\bar{h}\ell}\ {}^{2}A_{\bar{h}\ell}\ t^{j} \right) \right\} d\bar{s}.d\bar{\theta} \qquad \ldots(A5.2)$$

Note that each of the four terms given in Equation (A5.2) is in a form similar to that given by equation (5.7) for mono-operators. Each term is thus evaluated as for a mono-operator. The numerical values for each of the terms are then summed. Thus the procedure is very similar to that for mono-operators.

APPENDIX 7.1

SAMPLE DATA AND OUTPUT

This example is an analysis of the full-scale cooling tower at Didcot. The meridian of the tower is treated as a 'general curve'. Complex constraints are applied. The matrix modification option has been used to include a term in the overall stiffness matrix to represent foundation elasticity in the vertical direction.

The finite element mesh used for the analysis is as depicted in Fig. 7.1. Note that five shell elements have been used; if the tower had been of uniform thickness, four such elements would have been satisfactory. (Two elements are required to represent the cornice and ring-beam, respectively. Three shell elements are then used to ensure that the 'middle' of the tower is adequately represented.)

The following material properties have been used. (Acknowledgements are due to Mr H.L. Burrough for these values which were obtained from measurements made on a sample from the Didcot Tower.)

Young's Modulus	=	29.5×10^9	$N\ m^{-2}$
Mass Density	=	2323	$kg\ m^{-3}$
Poisson's Ratio	=	0.19	

Other data:-

Number of pairs of leg-supports = 40

Angle subtended by a pair of 'V-legs' at the axis of the symmetry	=	$\frac{360^o}{40} = 9^o$
Angle the tangent makes with the horizontal at point where leg-support meets tower	≃	71^o
Maximum thickness of cornice	=	0.3818 m
Maximum thickness of ring-beam	=	0.5842 m
Thickness of 'middle' of tower	=	0.1778 m
Foundation elasticity in vertical direction (i.e. d.o.f. 1)	=	1.6×10^9 N m^{-1}

The Z and R data are as given in the sample output.

Interpretation of Results

The complex angle is 36^o. Hence the number of circumferential wavelengths, n is $\frac{36}{9} = 4$. From the value of w at nodes 1, 2, 3, 4, 5 and 6 the number of meridional nodes is seen to be 2. The resonant frequency of this mode for the first eigenvalue is 1.064 Hz.

It will be noticed that the displacements printed by the program for the right-hand nodes of the substructure are zero. This is only because of programming convenience. The actual displacements at these nodes can easily be calculated. For example the 'w-displacement' (due to one of the orthogonal modes) at node 8

$$= \text{Real part of } \{(24.6 - i \times 0.43 \times 10^{-5})(\cos 36^o + i \sin 36^o)\}$$

$$\simeq 19.9$$

(The displacement due to the other mode is given by the imaginary part and is 14.46.)

Note that the program-calculated length of a leg-support is 8.813 m.

The pseudo-nodes printed by the program were calculated within the program. The real nodes were specified by the user.

DIDCOT TOW.SEC ANG=9.COM ANG=9*4(N=4).FOUND ELAST=9D9 A

NUMBER OF ELEMENTS	=	7
NUMBER OF NODAL POINTS	=	13
NUMBER OF MATERIALS	=	1
NUMBER OF GROUPS OF ELMS	=	7
NUMBER OF DEGREES OF FREEDOM AFTER APPLYING CONSTRAINTS	=	(NOT GIVEN)
NUMBER OF DEGREES OF FREEDOM PER NODE	=	12

COMPLEX CONSTRAINTS OPTION CHOSEN

OPTION TO MODIFY OVERALL STIFFNESS/MASS MATRICES REQUESTED.

NATURAL FREQUENCIES: THOSE BETWEEN NUMBER 3 AND NUMBER 1 ARE REQUIRED

SAMPLE RUN USING 'COMPLEX CONSTRAINTS'.MATRIX MOD. OPTION REQUESTED.AUTO-I/P OF REZ DATA AFTER FIRST SET.REZ VALUES OBTAINED FROM CEGB DR. NO. 378/7/1/20 TO 23

MATERIAL PROPERTIES FROM M.L.BURROUGH WHO MEASURED AN ACTUAL SAMPLE FROM TOWER.

DIDCOT TOW.SEC ANG=9.COM ANG=9*4(N=4).FOUND ELAST=9D9 A

MATERIAL PROPERTIES

MATERIAL NUMBER	POISSONS RATIO	MASS DENSITY	YOUNGS MODULUS	SHEAR MODULUS
1	0.190	2323.0	0.29500D 11	0.0

DIDCOT TOW.SEC ANG=9.COM ANG=9*4(N=4).FOUND ELAST=9D9 A

ELEMENT PROPERTIES

ELEMENT NUMBER	ELEMENT TYPE	MATERIAL NUMBER	1ST NODE	2ND NODE	3RD NODE	4TH NODE	GROUP NO	ANGLE CI	LENGTH	C.S.AREA	1 ST MOM:	2 ND MOM:	TORSION
1	1	1	1	8	2	9	1.0000	0.15708					
2	1	1	2	9	3	10	2.0000	0.15708					
3	1	1	3	10	4	11	3.0000	0.15708					
4	1	1	4	11	5	12	4.0000	0.15708					
5	1	1	5	12	6	13	5.0000	0.15708					
6	2	1	6	7	-	-	6.0000	-	8.808	0.209	3.6412D-03	3.6412D-03	6.47D-03
7	2	1	7	13	-	-	7.0000	-	8.808	0.209	3.6412D-03	3.6412D-03	6.47D-03

PROGRAM-CALCULATED NUMBER OF DEGREES OF FREEDOM= 145

NOTE THAT FOR THE TYPE 2 BEAM ELEMENT THE FOLLOWING DEGREES OF FREEDOM MUST BE CONSTRAINED,
AT ANY NODE WHICH IS NOT CONNECTED TO ANOTHER ELEMENT TYPE REQUIRING THESE D.O.F. :-

2 3 4 7 8 12

BOUNDARY CONDITIONS

1 FOR CONSTRAINT 0 FOR NO CONSTRAINT

NODE	U	DU/DX	DU/DY	D2U/DXDY	V	DV/DX	DV/DY	D2V/DXDY	W	DW/DX	DW/DY	D2W/DXDY
1	0	0	0	0	0	0	0	0	0	0	0	0
2	0	0	0	0	0	0	0	0	0	0	0	0
3	0	0	0	0	0	0	0	0	0	0	0	0
4	0	0	0	0	0	0	0	0	0	0	0	0
5	0	0	0	0	0	0	0	0	0	0	0	0
6	0	0	0	0	0	0	0	0	0	0	0	0
7	0	1	1	1	1	1	1	1	1	1	1	1
8	0	0	0	0	0	0	0	0	0	0	0	0
9	0	0	0	0	0	0	0	0	0	0	0	0
10	0	0	0	0	0	0	0	0	0	0	0	0
11	0	0	0	0	0	0	0	0	0	0	0	0
12	0	0	0	0	0	0	0	0	0	0	0	0
13	0	0	0	0	0	0	0	0	0	0	0	0

THE MERIDIAN FOR THIS SET OF ELEMENTS IS R=F(Z)

NPR=12 NPH= 2 IG=24 IBEG= 1 IEND= 2 IS= 2 ALP= 0.0 RADS

POINT	Z	R
1	0.0	26.7595800
2	3.42200000	26.2637746
3	10.0000000	25.5679867
4	21.6600000	25.1315211
5	30.0000000	25.4070114
6	40.0000000	26.3313953
7	50.0000000	27.8434682
8	60.0000000	29.8730090
9	70.0000000	32.3429550
10	85.0000000	35.6882242
11	100.847000	41.8025736
12	106.680000	43.7421369

GROUP= 1 ELEMENT NO= 1
OPTION=0

POINT	IT	TH
1	1	0.381800000
2	2	0.177800000

END OF INPUT IN SHELDA FOR THIS SET OF ELEMENTS

THE ELEMENT MATRICES ARE TRANSFORMED TO GLOBAL (Z,THETA) SYSTEM,ALP NOT USED

THE MERIDIAN FOR THIS SET OF ELEMENTS IS R=F(Z)

NPR=12 NPH= 1 IG=24 IBEG= 2 IEND= 6 IS= 2 ALP= 0.0 RADS

****
VALUES OF Z AND R AS ABOVE
****
GROUP= 2 ELEMENT NO= 2
OPTION=1

```
POINT                    IT        TH
    1                    2    0.177800000

                                                END OF INPUT IN SHELDA FOR THIS SET OF ELEMENTS

   THE ELEMENT MATRICES ARE TRANSFORMED TO GLOBAL (Z,THETA) SYSTEM,ALP NOT USED

                                                THE MERIDIAN FOR THIS SET OF ELEMENTS IS R=F(Z)

NPR=12   NPH= 1   IG=24   IBEG= 6   IEND= 9   IS= 2   ALP= 0.0          RADS


 ***************************
  VALUES OF Z AND R AS ABOVE
 ***************************
  GROUP= 3 ELEMENT NO= 3
  OPTION=1

POINT                    IT        TH
    1                    5    0.177800000

                                                END OF INPUT IN SHELDA FOR THIS SET OF ELEMENTS

   THE ELEMENT MATRICES ARE TRANSFORMED TO GLOBAL (Z,THETA) SYSTEM,ALP NOT USED

                                                THE MERIDIAN FOR THIS SET OF ELEMENTS IS R=F(Z)

NPR=12   NPH= 1   IG=24   IBEG= 9   IEND=11   IS= 2   ALP= 0.0          RADS


 ***************************
  VALUES OF Z AND R AS ABOVE
 ***************************
  GROUP= 4 ELEMENT NO= 4
  OPTION=1
```

POINT	IT	TH
1	9	0.177800000

END OF INPUT IN SHELDA FOR THIS SET OF ELEMENTS

THE ELEMENT MATRICES ARE TRANSFORMED TO GLOBAL (Z,THETA) SYSTEM,ALP NOT USED

THE MERIDIAN FOR THIS SET OF ELEMENTS IS R=F(Z)

NPR=12 NPH= 2 IG=24 IBEG=11 IEND=12 IS= 2 ALP= 0.0 RADS

****
VALUES OF Z AND R AS ABOVE
****
GROUP= 5 ELEMENT NO= 5
OPTION=1

POINT	IT	TH
1	11	0.177800000
2	12	0.584200000

END OF INPUT IN SHELDA FOR THIS SET OF ELEMENTS

THE ELEMENT MATRICES ARE TRANSFORMED TO GLOBAL (Z,THETA) SYSTEM,ALP NOT USED

****
AUTOMATIC GENERATION OF PSEUDO-NODES FOR COOLING TOWER LEGS
****

MERIDIONAL TANGENTIAL ANGLE= 71.00 DEGREES

NODAL INPUT DATA FOR BEAM TYPE2

NODE	R1	TH1	Z1	R2	TH2	Z2
6	43.526	0.0	106.754	43.958	0.0	106.606
7	45.904	4.52	114.374	46.337	4.48	114.226

CALCULATED LENGTH OF COOLING TOWER LEG= 8.813 METRES

THE XYZ COORDINATES ARE LISTED BELOW

NODE	X1	Y1	Z1	X2	Y2	Z2
6	43.5260	0.0	106.754	43.958	0.0	106.606
7	45.7607	3.62	114.374	46.196	3.6188	114.226

ALL NODAL INPUT & DISPLACEMENT OUTPUT IS IN CYLINDRICAL COORDINATES

END OF INPUT IN SUB: "TYPE2" FOR ELEMENTS IN GROUP 6

AUTOMATIC GENERATION OF PSEUDO-NODES FOR COOLING TOWER LEGS

MERIDIONAL TANGENTIAL ANGLE= 71.00 DEGREES

NODAL INPUT DATA FOR BEAM TYPE2

NODE	R1	TH1	Z1	R2	TH2	Z2
13	43.526	9.00	106.754	43.958	9.00	106.606
7	45.909	4.48	114.374	46.332	4.52	114.226

THE XYZ COORDINATES ARE LISTED BELOW

NODE	X1	Y1	Z1	X2	Y2	Z2
7	45.7686	3.59	114.374	46.188	3.6520	114.226
13	42.9901	6.81	106.754	43.417	6.8766	106.606

```
                ALL NODAL INPUT & DISPLACEMENT OUTPUT IS IN CYLINDRICAL COORDINATES

            END OF INPUT IN SUB: "TYPE2" FOR ELEMENTS IN GROUP  7

IFICATION TO OVERALL STIFFNESS AND/OR MASS MATRICES

 NODE   FREEDOM     2ND NODE   FREEDOM            MASS              STIFFNESS
   7        1             0         0              0.0                0.160000D 10


 DCOT TOW.SEC ANG=9.COM ANG=9*4(N=4).FOUND ELAST=9D9  A

MPLEX CONSTRAINTS ARE USED

E DEGREES OF FREEDOM BELOW HAVE BEEN COUPLED TOGETHER

IDE NODE    1       2       3       4       5       6       7       8       9      10      11      12      COMPLEX ANGLE(DEGREES)
-------------------------------------------------------------------------------------------------------------------------------
 2    9     1       2       3       4       5       6       7       8       9      10      11      12          36.0000
 5   12     1       2       3       4       5       6       7       8       9      10      11      12          36.0000
 1    8     1       2       3       4       5       6       7       8       9      10      11      12          36.0000
 4   11     1       2       3       4       5       6       7       8       9      10      11      12          36.0000
 6   13     1       2       3       4       5       6       7       8       9      10      11      12          36.0000
 3   10     1       2       3       4       5       6       7       8       9      10      11      12          36.0000

          NUMBER OF DEGREES OF FREEDOM NOW=  73

IDCOT TOW.SEC ANG=9.COM ANG=9*4(N=4).FOUND ELAST=9D9  A

IGENVALUE NUMBER   1        1.064      HERTZ
ORRESPONDING EIGENVECTOR:
NODE      U          DU/DX      DU/DY     D2U/DXDY      V          DV/DX      DV/DY     D2V/DXDY      W          DW/DX      DW/DY     D2W/DXDY
 1R    2.20         -31.      6.320-05-6.180-03  2.390D-05-1.740-03 -1.0        16.        24.6        2.0       3.900-05 3.740-03
 11  0.5480-04-0.610-02  -1.1        100.       -5.99       -3.6     -0.140-04 0.160-02 -0.4260-05 0.610-02  -4.1         70.
 2R    2.53         -21.      1.320-04-1.270-04  4.7060-05-4.640-05 -1.2        0.28       26.2        3.7     -4.270-05 2.780-04
 21  0.1300-03-0.100-03  -2.3        6.5        -6.58       -0.42    -0.340-04 0.440-04 -0.7810-04 0.290-03  -5.2       -0.32
 3R    4.10         7.8     -2.360-04-2.990-04 -6.2550-05-6.840-05 0.63       0.58       -12.3       -3.3     6.280-05-2.150-05
 31  -0.2640-03-0.370-03  -0.70       -0.16        3.07        1.4      0.550-04 0.590-04 0.1550-03-0.100-04  2.8         2.8
 4R    8.30         11.     -5.930-04-1.040-03 -1.91E0-04-2.590-04 0.90       0.16       -32.7       3.6      1.230-04 6.070-05
 41  -0.7770-03-0.130-02                          8.17       -0.22      0.130-03 0.220-03 0.2500-03 0.220-03  3.6         0.39
 5R    2.10        -0.21                        0170-03-1.490-03 0.32     -9.480-03 -12.0        3         1.560-03 7.230-04
 51  -0.5640-02-0.7                               -0.59       0.150-02 0.110-02 0.3290-02                    2       -0.510-01
 6R    1.65                                      93-2.490-02 0.21       -0.21      -10.3                          -02-9.780-02
 61  -0.7570-0                                    -1.3      -0.330-02 0.200-01 -0.8430-                            -1.6
 7R  -0.626                                                   0.0        0.0        0.0                              0
 71   0.20                                                   0.0        0.0        0.0
 8R   0
 81

                DIDCOT TOW.SEC ANG=9.COM ANG=9*4(N=4).FOUND ELAST=9D9  A

                    EIGENVALUE NO.        HERTZ          RAD/SEC          REV/MIN

                                 1         1.0541           6.6861           63.847

                                 2         1.7745           11.150           106.47

                                 3         2.3707           14.896           142.24


                THE CPU TIME FOR PROBLEM  1 WAS  38750 MILLI-SECS

                PROBLEM NUMBER(VACTIL)  2


                NO MORE DATA - EXECUTION TERMINATED
```

{Removed To Save Space}

APPENDIX 12.1

ANOMALY OF THE DISPLACEMENT FUNCTION

The displacement function has been referred to in Section 12.3. To simplify this discussion we consider only one of the orthogonal displacements, say w. Let the displacement w be written as

$$w = [T][\delta_w^e] \qquad \ldots(A12.1)$$

where $[\delta_w^e]$ is the nodal displacements in w only; that is, it is a column vector of order 16 of the form:

$$\left[w_1 \left(\frac{\partial w}{\partial s}\right)_1 \left(\frac{\partial w}{\partial \theta_o}\right)_1 \left(\frac{\partial^2 w}{\partial s \partial \theta_o}\right)_1 \ldots\ldots \left(\frac{\partial^2 w}{\partial s \partial \theta_o}\right)_4 \right]^T$$

An interpolation displacement function usually has the property that at any node the displacements predicted by the function are identical to the nodal displacements. For example, for the first node of the shell element, when s = 0 and θ_o = 0, equation (A12.1) reduces to:

$$w = [1\ 0.\ldots\ldots\ldots 0][\delta_w^e].$$

Similarly this is seen to be true for all the d.o.f. predicted by the displacement function except for the cross-derivative $\frac{\partial^2 w}{\partial s \partial \theta_o}$. Differentiating equation (A12.1) with respect to $\bar{s}$ and $\bar{\theta}$ (the bar sign signifies normalisation) gives

$$\frac{\partial^2 w}{\partial \bar{s} \partial \bar{\theta}} = \frac{\partial [T]}{\partial \bar{s} \partial \bar{\theta}} \cdot [\delta_w^e] \qquad \ldots(A12.2)$$

At Node one $\bar{s} = 0$ and $\bar{\theta} = 0$ and equation (A12.2) gives

$$\frac{\partial^2 w}{\partial \bar{s} \partial \bar{\theta}} = \left[0 \quad 0 \quad R\psi \times \frac{L \cos \psi}{R} \quad L\psi R \; 0 \ldots\ldots 0\right] \left[\delta_w{}^e\right] \qquad \ldots(A12.3)$$

It would be expected that the third term that is $\psi R \times \left(\frac{L \cos \psi}{R}\right)$, would reduce to zero so that the expression on the right-hand side of equation (A12.3) reduces to $L\psi R \times \left(\frac{\partial^2 w}{\partial s \partial \theta_o}\right)$, which is then equal to $\frac{\partial^2 w}{\partial \bar{s} \partial \bar{\theta}}$. That is, the predicted displacement-derivative would be identical to the nodal displacement-derivative (normalised). However, the third term (referred to in equation (A12.3) does in fact <u>not</u> appear. This appears to be an anomaly of the displacement function when interpolation polynomials of order three are employed.

REFERENCES

1. Carter, R.L., Robinson, A.R. and Schnobrich, M., 1969, Free vibrations of hyperboloidal shells of revolution, J. Eng. Mechanics Division (Proc. Amer. Soc., Civil Eng.) 1033-1052

2. Rockey, K.C., Evans, H.R., Griffiths, D.W. and Nethercot, D.A., 1976, 'The Finite Element Method: A Basic Introduction', Crosby Lockwood Staples, London

3. Desai, C.S. and Abel, J.F., 1972, 'Introduction to the Finite Element Method: A Numerical Method for Engineering Analysis'. Van Nostrand Reinhold Co.

4. Zienkiewicz, O.C., 1971, 'The Finite Element Method in Engineering Science', McGraw-Hill (London)

5. Nelson, R.Ll., 1976, VACTIL - a program to calculate the natural frequencies and mode shapes of cooling towers whilst explicitly including the effects of leg-supports and foundation elasticity, C.E.G.B. Publication No. RD/L/P 10/76

6. Woodman, N.J. and Severn, R.T., 1970, A double-curvature shell finite-element and its use in the dynamic analysis of cooling towers and other shell structures, Symposium on Structural Dynamics, 23-25, March, Paper A5, Loughborough University of Technology

7. Schmit, L.A., Bogner, F.K. and Fox, R.L., 1968, Finite deflection structural analysis using plate and shell discrete elements, AIAA Journal, 6, (5), pp. 781-791, May

8. Novozhilov, V.V., 1964, 'Thin Shell Theory', (2nd Ed.), P. Noordhoff Ltd., (Netherlands).

9. Vlasov, V.Z., 1964, General theory of shells and its applications in engineering', (N64 - 19883), NASA, Washington, D.C., April

10. Martin, D.W. and Scriven, W.E., 1961, The calculation of membrane stresses in hyperbolic cooling towers, Proc. Institution of Civil Engineering, London, 19, Discussion 23

11. Martin, D.W., Maddock, J.S. and Scriven, W.E., 1964, Membrane displacements in hyperbolic cooling towers due to wind and dead loading, Proc. Inst. Civil Engrs., 28 (paper No. 6732), pp. 327-337

12. Kalnins, A., 1964, Analysis of shells or revolution subjected to symmetrical and non-symmetrical loads, J. Appl. Mech., September

13. Albasiny, E.L. and Martin, D.W., 1967, Bending and membrane equilibrium of cooling towers, Proc. ASCE, EM3, June

14. Tottenham, H., 1967, Stresses in hyperbolic cooling towers due to wind loading, Bull. IASS, N. 32, December

15 Gould, P.L. and Lee Seng-Lip, 1969, Hyperbolics of revolution supported on columns, Proc. ASCE, EM5, October

16. Abu-Sitta, S.H., 1970, Cooling towers supported on columns, Proc. ASCE, ST. 12, December

17. Kalnins, A., 1964, Free vibrations of rotationally symmetric shells, J. of the Acoustical Society of America, 36, No. 7, July

18. Grafton, P.E. and Strome, D.R., 1963, Analysis of axisymmetrical shells by the direct stiffness method, A.I.A.A. J., 1, No. 10, Octobe

19. Percy, J.H., Pain, T.H.H., Klein, S. and Navaratna, D., 1965, Application of matrix displacement method to linear elastic analysis of shells of revolution, A.I.A.A. J., 3, No. 11 pp. 2138-2145

20. Merrylees, S.H., 1969, Bending Analysis of Cooling Towers - BACTo2, C.E.G.B. Publication No. RD/L/N 364

21. Pope, R.A., 1977, Private communication

22. Bailey, R.W. and Fidler, R., 1965, Model tests on the buckling of hyperbolic shells, C.E.G.B. Publication No. RD/L/N 113/65

23. Der, T.J. and Fidler, R., 1968, A model study of the buckling behaviour of hyperbolic shells, Inst. of Civil Engrs. Proc. 41, pp. 105-118

24. C.E.G.B., 1966, Report of the Committee of Inquiry into the Collapse of Cooling Towers at Ferrybridge, Monday 1 November, 1965

25. Armitt, J., 1973, Vibration of Cooling Towers, Paper No. 311 Int. Symp. on Vib. Problems in Industry, Keswick, April (UKAE/NLP

26. Reissner, E., 1941, A new derivation of the equations for the deformation of elastic shells, Am. J. Math., 63, pp. 177-184

27. Myklestad, N.O., 1944, A new method of calculating natural modes of uncoupled bending vibration of air-plane wings and other types of beams, J. Aero. Sci., 11, (2), April, pp. 153-162

28. Prohl, M.A., 1945, A general method for calculating critical speeds of flexible rotors, J. Appl. Mech., 67, September, pp. 142-148

29. Webster, J.J., 1967, Free vibrations of shells of revolution using ring finite elements, Int. J. Mech. Sci., 9 (9), pp. 559-570

30. Hashish, M.G., 1970, Free vibrations of hyperbolic cooling towers, M.Sc., Thesis, The University of Western Ontario, London, Canada, August

31. Neal, B.G., 1967, Natural frequencies of cooling tower shells, J. of Strain Analysis, 2, No. 2

32. Vronay, D.F. and Smith, B.L., 1970, Free vibration of circular cylindrical shells of finite length, AIAA J., 8 (3), pp. 601-603

33. Williams, J.J., 1967, Natural Draught Cooling Towers Conference on Ferrybridge and After, (Proc. of the Conf. held at the Inst. of Civil Engineers), Paper No. 5, pp. 37-43

34. Williams, J.J., Vibration of cooling tower shells, C.E.G.B. Publication No. RD/L/R 1478

35 Ford, R. and Williams, J.J., 1969, KALS - Static load shell program, SHEL - free vibration shell program, C.E.G.B. Pub. No. RD/L/N 357

36. Payne, D.I. and Webster, J.J., 1968, Users guild to program for calculating free vibrations of shells of revolution using ring finite elements - NOTTo2, C.E.G.B. Pub. No. RD/L/N 161

37. Armitt, J., C.E.R.L. Private communication

38. Winney, P., Personal communication

39. Burrough, H.L., Jeary, A.P. and Winney, P.E., 1970, West Burton cooling tower; dynamic response to wind, C.E.G.B. Pub. No. RD/L/N 144/70

40. Deb Nath, J.M., Free vibration stability and 'non-classical modes' of cooling tower shells, J. Sound and Vibration., 33, (1) pp. 79-101

41. Yang, T.Y., Sun, C.T., Lo, H., Kayser, K.W. and Bogdanoff, J.L., 1976, Paper No. 76-JPGC-PWE-11 presented at the IEEE-ASME Joint Power Generation Conference, Buffalo, New York, September 19-22 1976

42. Winney, P.E., 1978,, The modal properties of model and full scale cooling towers, to be published in J. Sound and Vib.

43. Winney, P.E., 1976, The free vibration properties of Model and full-scale cooling towers, C.E.G.B. Pub. No. RD/L/R 1944

44. Przemieniecki, J.S., 1968, 'Theory of Matrix Structural Analysis', McGraw-Hill Book Co., Inc. (N.Y.), pp. 231-263

45. Hurty, W.C., 1964, Dynamic analysis of structural systems by component mode synthesis, Technical Report No. 32-530, Jet Propulsion Lab., Pasadena, California, January

46. Hou, S., 1969, Review of modal synthesis techniques and new approach, Shock and Vibration Bulletin, Naval Research Labs., (U.S.A.), No. 40, pp. 25-39, December

47. Hurty, W.C., 1971, Introduction of modal synthesis techniques, Synthesis of Vib. Systems (American Soc. of Mech. Engrs.), pp. 1-13, November

48. Holze, G.H. and Boresi, A.P., 1975, Free vibration analysis using sub-structuring, Proc. Amer. Soc. Civil Engrs. (J. of Struc. Div.), 101, (ST12), pp. 2627-2639

49. Orris, R.M. and Petyt, M., 1974, A finite element study of harmonic wave propagation in periodic structures, J. Sound and Vib., 33 (2), pp. 223-236

50. Brillouin, L., 1946, 'Wave Propagation in Periodic Structures', New York, Dover Pub. Inc.

51. Mead, D.J. and Sen Gupta, G., 1970, Wave group theory applied to the analysis of the forced vibrations of rib-skin structures, Proc. of the Symp. on Struct. Dyn., Loughborough University of Tech., Paper No. D-3

52. Mead, D.J., 1975, Wave propagation and natural modes in periodic systems: II: Multi-coupled systems, with and without damping, J. Sound and Vib., 40, (1), pp. 19-39

53. Mead, D.J., 1975, Wave propagation and natural modes in periodic systems: I: Mono-coupled systems, J. Sound and Vib., 40 (1), pp. 1-18

54. Heckl, M.A., 1964, Investigations on the vibrations of grillages and other simple beam structures, J. of the Acoustical Soc. of Am., 36, pp. 1335-1343

55. Cremer, L. and Leilich, H.O., 1953, Archiv der Elektrischen Ubertrangung, Zur Theorie der Biegekettenleiter, 7, pp. 261-270

56. Mead, D.J., 1973, A general theory of harmonic wave propagation in linear periodic systems with multiple coupling, J. Sound and Vib., 27, pp. 235-260

57. Abrahamson, A.L., 1973, Flexural wave mechanics - an analytical approach to the vibration of periodic structures forced by convected pressure fields, J. Sound and Vib., 28, pp. 247-258

58. Weyl, H., 1956, 'Symmetry', Lecture given at the Inst. for Advanced Study, reprinted in the World of Mathematics, Simon and Schuster, New York, 1, pp. 671-724

59. MacNeal, R.H., Harder, R.L. and Mason, J.B., 1973, 'NASTRAN Cyclic Symmetry Capability', Nastran Users Experiences, 3rd Colloquium, Langley Research Centre Hampton, Virginia, U.S.A., 11-12 September, pp. 395-421 (NASA Tech. Memo. NASA TMX-2893)

60. Thomas, D.L., 1974, Standing waves in rotationally periodic structures, J. Sound and Vib., 37 (2), pp. 288-290

61. Thomas, D.L., Dynamics of rotationally periodic structures, to be published in Int. J. Numerical Methods in Engineering

62. Kraus, H., 1967, 'Thin Elastic Shell', John Wiley Inc. (U.S.A.)

63. Novozhilov, V.V. and Finkel'Shtein, R.M., 1943, Regarding the errors connected with Kirchhoff's hypotheses in the theory of shells, Prikladnaya Matematika Kikhanika, VII

64. Hearmon, R.F.S., 1961, 'Indroduction to Applied Elasticity', Oxford University Press

65. Turner, C.E., 1965, 'Plate and Shell Theory', Longmans Green and Co. Ltd.

66. Yang, T.Y., 1973, High order rectangular shallow shell finite element, J. of the Eng. Mech. Div. (Proc. Amer. Soc. Civil Engrs.), EMI, pp. 157-181, February

67. Bogner, F.K., Fox, R.L. and Schmit, L.A., 1965, The generation of inter-element-compatible stiffness and mass matrices by the use of interplation formulas, Proc. Conf. Matrix Method in Str. Mech., AFFDL-TR-66-80, pp. 397-444

68. Timoshenko, S., 1969, 'Strength of Materials: Part I'. Van Nostrand Reinhold and Co. (3rd Edition)

69. Kronrod, A.S., 'Nodes and Weights of Quadrature Formulae', Consultants Bureau Enterprises Inc. New York, 1965

70. Thomas, D.L. and Wilson, R.R., 1973, The use of straight beam finite elements for analysis of vibrations of curved beams, J. Sound and Vib., 26 (1), pp. 155-158

71 Wilson, R.R. and Brebbia, 1971, Dynamic behaviour of steel foundations for turbo-alternators, J. Sound and Vib., 18 pp, 405-416

72 Nelson, R.Ll., 1977, RESAP: a program to calculate the resonant stresses, frequencies and mode shapes of axisymmetric structures, C.E.G.B. Pub. No. RD/L/P 9/77

73. Nelson, R.Ll., 1977, VACTILo2: a program to calculate frequencies mode shapes and stresses in shell structures. C.E.G.B. pub. No. RD/L/P /77

74. Wang, Ping-Chun, 1966, 'Numerical and Matrix Methods in Structural Mechanics', Chapter 5, John Wiley Inc.

75. Wilkinson, J.H., 1965, 'The Algebraic Eignevalue Problem', Clarendon Press, Oxford

76. Boothroyd, J., 1967, Algorithm No. 297, J. A.C.M., 10 (3)

77. Wilkinson, J.H., 1962, Householder's method for symmetric matrices, Num. Math. 4, pp. 354-361

78. Wilkinson, J.H., 1962, Calculation of the eigenvectors of a symmetric tridiagonal matrix by inverse interation, Num. Math., 4, pp. 368-376

79. Barth, W., Martin, R.S. and Wilkinson, J.H., 1967, Num. Math., 9, pp. 386-393

80. Kennedy, C.C. and Pancu, C.D.P., 1947, Use of vectors in vibration measurement and analysis, J. Aero. Sci., 14 (11)

81. Traill-Nash, R.W., 1958, On the excitation of pure modes in aircraft resonance testing, J. Aero Sci., 25, pp. 775-778

82. Bishop, R.E.D. and Gladwell, 1963, An investigation into the theory of resonance tesitng. Phil. Trans, 255, (1055), pp. 241-280

83. Bishop, R.E.D. and Johnson, D.C., 1960, 'The Mechanics of Vibration', Cambridge University Press

84. Pendered, J.W. and Bishop, R.E.D., 1963, A critical introduction to some industrial resonance testing techniques, J. of Mech. Sci. 5 (4), pp. 345-367

85. Taylor, G.A., Gaukroger and Skingle, D.R., 1967, MAMA: a semi-automatic technique for exciting the principal modes of vibration of complex structures, R.A.E. (Farnborough), Tech. Report No. 67211

86. Leim, S.D., Jazell, C.R. and Blasko, J.A., 1973, Vibration analysis of circular cylinders by holographic interferometry, J. Sound and Vib., 29, (4), pp. 475-481

87. Burrough, H.L., 1975, Private communication

88. Blow, D.J., 1973, The physical properties of Devcon, C.E.G.B. publication No. RD/L/N 185/73

89. Deb Nath, J.M., 1973, The effect of top ting beams on the natural frequencies of cooling tower shells, C.E.G.B. publication No. RD/L/N 97/73

90. Armitt, J., 1973, The response of cooling towers to wind loading, C.E.G.B. publication No. RD/L/R 1828

91. Haydon, R.E.V. and Winney, P.E., 1974, Personal communication

92. Greville, T.N.E., 1967, 'Mathematical Methods for Digital Computers', (Vol. II, ed. Ralston and Wilf.) Wiley Inc.

93. Wilson, R.R., 1972, VOSTAFo2 - a program for predicting the dynamic behaviour of a structure consisting of beams and plates, C.E.G.B. publication No. RD/L/P 29/72

94. Warburton, G.B., 1964, 'The Dynamical Behaviour of Structures,' Pergamon Press

95. Flügge, W., 1962, 'Stresses in Shells,' Springer-Verlag (Berlin)

96. Herrman, G. and Shaw, J., 1965, Vibration of thin shells under initial shtress, Proc. ASCE, EM5, October

97. Deb Nath, J.M., 1972, Analysis of the vibration of cooling towers, C.E.G.B. publication No. RD/L/N 228/72

98. Adelman, H.M., Catherines, D.S. and Walton, W.C., 1970, Accuracy of modal stress calculations by the finite element method, AIAA J., 8, pp. 462-468

99. Smith, B.L. and Haft, E.E., 1968, Natural frequencies of clamped cylinderical shells, AIAA J., 6, (4) April

100. Forsberg, K., 1964, Influence of boundary conditions on the model characteristics of thin cylindrical shells, AIAA J., 2 (12), pp. 2150-2157

101. Gallagher, R.H., 1966, The development and evaluation of matrix methods for thin shell structural analysis, Report No. 85900-902011, Bell Aerosystems, Buffalo, N.Y., June

102. Dawe, D.J., 1974, Some high-order elements for arches and shells, Conf. on Finite Elements for Thin Shells and Curved Members at University College, Cardiff, May

103. Hellen, T.K., 1970, A computer system for stress analysis, Part I: User's guide, C.E.G.B. publication No. RD/B/N 1761

104. McLeod, R., Node requirements for high-order approximation over curved finite elements, J. Inst. Maths, Applics., 17, pp. 249-254

105. Bogner, F.K., Fox, R.L. and Schmit, L.A., 1967, A cylindrical shell finite element, AIAA J. 5, (4), pp. 745-750

106. Klein, S., 1965, Finite element solution for axisymmetrical shells, J. of the Eng. Mechanics Div., Proc. American Soc. Civil Eng., June, p. 264

107. Wilson, J.M., 1973, DVISOR3: A program to compute the natural frequencies and mode shapes of multi-branched, rigidly connected thin shells of revolution, C.E.G.B. publication No. RD/L/P 18/73

108. Ciarlet, P.F. and Raviart, 1972, General Langrange and Hermite interpolation in R^n with applications to finite element methods, Arch. Rat. Mech. Anal., 46, (3), pp. 177-199

109. Arnold, R.N. and Warburton, G.B., 1949, Flexural vibrations of the walls of thin cylindrical shells having freely supported ends, Proc. Roy. Soc. (A), 197, pp. 238-256

110. Fort, T., 1948,'Finite differences and difference equations in the real domain', Oxford University Press, New York

111. Guyan, R.J., 1965, Reduction of stiffness and mass matrices, AIAA J., 3, (2), p. 380

112. Irons, B., 1965, Structural eignevalue problems: elimination of unwanted variables, AIAA. J., 3, (5), pp. 961-962

113. Henshell, R.D. and Ong, J.H., 1975, Automatic masters for eigen-value economization, Earthquake Engineering and Struct. Dyn., 3, pp. 375-383

114. Mason, V., 1968, Rectangular finite elements for analysis of plate vibrations, J. Sound and Vib., 7, (3), pp. 437-448

115. Thomas, D.L., Personal communication

116. Butlin, G.A. and Leckie, F.A., 1966, A study of finite elements applied to plate flexure, Proc. Sypm. on Numerical Methods, Vibration Problems, at Southampton University, 3, pp. 26-37

117. Kemp, K.O. and Croll, F.G.A., 1976, The rôle of geometric imperfections in the collapse of a cooling tower, The Structural Eng., 54, (1), pp. 33-37

118. Soare, M., 1967, Cooling towers with constructional imperfections, Concrete, November, pp. 396-379

119. Newmark, N.M., 1959, A method of computation for structural dynamics, J. Eng. Mech. Div. (Proc. Amer. Soc. Civ. Engrs.), EM3, 85, pp. 67-94

120. Reinschmidt, K.F. and Narayanan, R., 1975, The optimum shape of cooling towers, Computers and Structures, 5, pp. 321-325

121. Love, A.E.H., 1944, 'A Treatise on the Mathematical Theory of Elasticity', (Fourth Edition), Dover Publications (New York)

ALPHABETICAL LISTING OF AUTHORS

(Only the first author is indexed. The numbers refer to those given in 'REFERENCES'.)

Kraus, H. (62)

Kronrod, A.R. (69)

Leim, S.D. (86)

Love, A.E.G. (121)

MacNeal, R.H. (59)

Martin, D.W. (10, 11)

Mason, V. (114)

McLeod, R. (104)

Mead, D.J. (51, 52, 53, 56)

Merrylees, S.H. (20)

Myklestad, N.O. (27)

Neal, B.G. (31)

Nelson, R.Ll. (5, 72, 73)

Newmark, N.M. (119)

Novozhilov, V.V. (8, 63)

Orris, R.M. (49)

Payne, D.I. (36)

Pendered, J.W. (84)

Percy, J.H. (19)

Pope, R.A. (21)

Prohl, M.A. (28)

Przemieniecki, J.S. (44)

Reissner, E. (26)

Reinschmidt, K.F. (120)

Rockey, K.C. (2)

Schmit, L.A. (7)

Soare, M. (118)

Smith, B.L. (99)

Thomas, D.L. (60, 61, 70, 115)

Timoshenko, S (68)

Tottenham. H. (14)

Traill-Nash (81)

Turner, C.E. (65)

Vlasov, V.Z. (9)

Vronay, D.F. (32)

Wang, Ping-Chun (74)

Warburton, G.B. (94)

Wilkinson, J.H. (75, 77, 78)

Weyl, H. (58)

Williams, J.J. (33, 34)

Wilson, J.M. (107)

Wilson, R.R. (93)

Winney, P.E. (38, 42, 43)

Woodman, N.J. (6)

Yang, T.Y. (41, 66)

Zeinkiewicz, O.C. (4)

BIBLIOGRAPHY

(References that are of general interest but which may not necessarily have a direct bearing on the work reported in the thesis are given below.)

Adelman, H.M. et al., 1976, A method for computation of vibration modes and frequencies of orthotropic thin shells of revolution having general meridional curvature, TND-4972, January, NASA

Ashwell, D.G. and Gallagher, R.H., (Editors), 1976, 'Finite Elements for Thin Shells and Curved Members,' John Wiley Inc.

Bishop, R.E.D. and Johnson, D.C., 1960, 'The Mechanics of Vibration,' Cambridge University Press

Brebbia, C.A., Tottenham, H., Warburton, G.B., et al., 1976, 'Vibrations of Engineering Structures', Computational Mechanics

Dorn, W.S. and McCracken, D.D., 1972, 'Numerical Methods with Fortran IV Case Studies,' John Wiley Inc.

Gibson, J.E., 1975, 'Computating in Structural Engineering' Applied Science Publishers Ltd.

Gibson, J.E., 1965, 'Linear Elastic Theory of Thin Shells,' Pergamon Press

Gourlay, A.R. and Watson, G.A., 1973, 'Computational Methods for Matrix Eigenproblems,' John Wiley Inc.

Gregory, R.T. and Kerney, D.L., 1969, 'A Collection of Matrices for Testing Computational Algorithms,' Wiley - Interscience, 1969

Majid, K.I., 1974, 'Optimum Design of Structures,' Newnes - Butterworth

Newmark, N.M. and Rosenblueth, E., 1971, 'Fundamentals of Earthquake Engineering,' Prentice-Hall Inc.